Deposition of zinc oxide by spray pyrolysis

Fiddes, Alexander James Crawford

Deposition of Zinc Oxide by Spray Pyrolysis

Alexander James Crawford Fiddes

presented for the Candidature of
Doctor of Philosophy

at the University of Durham
in the Department of Physics
1993

Ph.D Abstract

Deposition of Zinc Oxide by Spray Pyrolysis

A.J.C. Fiddes

1993

The objective of this work was to grow doped ZnO by spray pyrolysis at low temperature. This was achieved via the initial objective of growing ZnO in undoped form over a wide range of conditions, in order to understand the growth behaviour of ZnO from $Zn(acac)_2.H_2O$ and to establish the optimum growth procedure at high and low temperature. Various techniques were employed to characterize the films and thus determine the optimum growth conditions (i.e measurement of film thickness, resistivity, Hall coefficient, X-ray diffraction and reflection electron diffraction to name but a few).

With the growth of undoped films it was found that the film properties varied with temperature and moisture content and that the optimum conditions for low temperature growth in a dry ambient were at 200°C and for high temperature growth in a wet ambient at 300°C.

An analysis of the growth behaviour of ZnO was carried out and it was suggested that there were at least four mechanisms leading to the decomposition of the precursor used ($Zn(acac)_2.H_2O$). They were decomposition by *intra*molecular, *inter*molecular, thermolysis and hydrothermolysis processes.

A kinetic analysis demonstrated that evaporation was the dominant process which reduced the efficiency of utilization of $Zn(acac)_2.H_2O$.

The growth of doped ZnO on glass and plastic at low temperature using $InCl_3$ as a dopant yielded conducting films. The results also showed that films obtained using solutions with low concentrations of $Zn(acac)_2.H_2O$ and high concentrations of $InCl_3$ were even more conducting ($\rho \approx 10^{-5}\Omega$m). The morphology of film growth was dominated by the presence of dopant.

High temperature growth of doped ZnO in a wet ambient using $InCl_3$ also yielded conducting films and these were compared with indium, aluminium and gallium doped

films where alternative dopant materials such as $In(acac)_3$, $Al(OPr^i)_3$, $AlCl_3$ and $Ga(acac)_3$ at a variety of different solution concentrations had been used. This was undertaken to discover whether these materials functioned as well as $InCl_3$ in producing low resistivity ZnO. Doped films were characterised using the same techniques as before. Elemental analysis, photoluminescence and optical measurements were also carried out on these films.

The main conclusions were that :

(1) The growth rate of ZnO from $Zn(acac)_2.H_2O$ is heavily influenced by the growth temperature and other conditions.

(2) The film resistivity was influenced by growth temperature. A minimum in the film resistivity was observed when a growth temperature of 300°C was used.

(3) Undoped ZnO films grown below 200°C had a different preferred order to those grown above 200°C.

(4) The best high temperature conditions for the deposition of undoped conducting adherent ZnO lay in the region of 276 - 306 °C.

(5) The best low temperature conditions for the growth of undoped conducting ZnO were in the region of 200°C.

(6) The low temperature growth (175-200°C) of doped ZnO produced films with resistivities of the order of $1\text{-}5\times10^{-5}\Omega m$ and a visible transmittance of 80%. This compares favourably with ZnO:Al and SnO_2 which have also been grown at low temperature.

Deposition of Zinc Oxide by Spray Pyrolysis

Alexander James Crawford Fiddes

Presented for the Candidature of

Doctor of Philosophy

at the University of Durham

in the Department of Physics

1993

Table of Contents **Page**

List of Figures and Tables

Acknowledgements

I wish to thank the following for their technical support :

(1) ICI Plc (Paints and Films) who also sponsored the project.

(2) The mechanical workshop, SEAS.

(3) The electrical workshop, SEAS.

(4) The technicians and departmental superintendent.

(5) The Department Of Applied Physics, The University Of Hull.

(6) The Department Of Geology, The University Of Durham.

(7) The Finance Directorate, Meadowfield.

(8) Dr's A.W Brinkman, K. Durose, and Professor J. Woods.

(9) P. Coates and Dr A. Banister.

(10) My Mother, family and friends.

(11) The Computer Centre, University Of Durham.

(12) The Drawing Office, SEAS.

(13) My fellow students.

Declaration

No part of this work has been previously submitted

for any other degree at any other university

Commercial in Confidence

Intellectual Property Rights -

- University of Durham/ICI PLC

Chapter One

Introduction

It has been known for some time that ZnO can be prepared as a transparent conducting film and consequently it has attracted interest in applications to photovoltaic cells and passive solar heating. ICI have sponsored this and earlier work to find a cheap and efficient method of depositing thin films of ZnO by spray pyrolysis. The earlier work carried out in Durham had used zinc acetate as the precursor and glass as the substrate. The work reported here has concentrated on attempts to grow transparent conducting films on plastic. This required a lower substrate temperature to avoid the decomposition of the plastic. The approach adopted was to investigate a range of precursors prepared in the Department of Chemistry. Most success was achieved with $Zn(acac)_2.H_2O$.

The work reported in this thesis sets out to answer three questions :

(a) Can ZnO be formed by spray pyrolysis below $\approx 300°C$ (the decomposition temperature of zinc acetate) ?

(b) Can it be grown in a thin film form which is both transparent and conducting ?

(c) What is the lowest temperature at which the transparent conducting form can be grown ?

This thesis consists of ten chapters. Chapter two presents a review of the properties, and applications of ZnO.

Chapter three presents a review of spray pyrolysis and the physical and chemical factors influencing the resulting film properties. The chapter ends with a review of earlier work on the spray pyrolysis of zinc oxide.

Chapter four presents a description of the experimental spray pyrolysis kit and and its method of use. The characterisation techniques employed on the films are also

described.

Chapter five (the first results chapter) presents the growth conditions of undoped ZnO films and the results of their characterisation.

Chapter six contains an interpretation of the growth behaviour of ZnO in terms of the decomposition of $Zn(acac)_2.H_2O$ via different routes, and a kinetic analysis of the physical parameters affecting deposition efficiency.

Chapters seven and eight present the description of the conditions for the low temperature and high temperature growth of indium doped ZnO and the results of the characterisation of these films.

Chapter nine contains the description of the conditions for the growth of aluminium, gallium and indium doped ZnO at high temperature.

The last chapter (chapter ten) presents the conclusions, a discussion, some final comments and suggestions for further work.

Zinc oxide is used in a variety of technical applications including porcelain enamels, heat resisting glass, as an activator in vulcanisation, an additive in rubber and plastics, pigments in paints with UV protective and fungicidal properties, as a spacecraft protective coating, as a constituent in cigarette filters and healing ointments, in semiconductors (electro - optic, acousto - optic, acousto - electric), waveguides, and as a transparent conductor. It has also been used as an industrial catalyst and a gas sensor. The broad variability in the applications of zinc oxide is due to the basic properties of zinc oxide in thin film form which depend on the method of preparation. This topic forms the subject matter of this thesis.

This project was funded by ICI PLC and started in October 1988 as a continuation of postdoctoral research by Dr Sener Oktik which began in 1986. The three years were punctuated by meetings at 3 monthly intervals during which progress was reported. Meetings took place at ICI Wilton or Durham University with the staff of ICI Films (Wilton, Teesside) and ICI Paints (Slough) present.

Chapter Two

Review of the Properties of Zinc Oxide Thin Films

2.1 Introduction

This chapter concerns thin films of zinc oxide and their properties. It includes a description of the structure of zinc oxide together with its electronic and optical properties. Applications of zinc oxide are discussed towards the end of the chapter, and in conclusion the material is discussed as a transparent conducting oxide or alternatively as an n - type window layer for a solar cell.

2.2 Structure of Zinc Oxide

Zinc oxide crystallises in the hexagonal wurtzite structure. The mean lattice constants are a = 3.250 Å and c = 5.206 Å . The structure of the unit cell is shown in figure 2.1. The zinc oxygen bond length is 1.992 Å parallel to the c - axis and 1.973 Å in the other three directions of the tetrahedral arrangement of nearest neighbours[1,2].

Figure 2.1 (a) shows the basic unit cell structure and illustrates the tetrahedral arrangement, whereas figure 2.1 (b) is an extended structure showing the c -axis and this structure is used for determining lattice planes in the hexagonal wurtzite system. For the sake of later work presented in the following chapters it is useful to go over the labelling technique for crystal planes for the hexagonal system.

The notation used to describe the hexagonal wurtzite system is based on Miller indices. Their use helps to specify faces and planes within a crystal or space lattice. They specify the orientation of crystal planes relative to the crystal axes without giving the position of the plane in space with respect to the origin.

These indices are based on the intercepts of a plane with three crystal axes, each intercept with an axis being measured in terms of the unit cell dimensions a,b and c along that axis. To determine the Miller indices of a plane the following procedure is used :

1/. Find the numerical intercepts on the three axes.

2/. Take the reciprocal values of these numerical values.

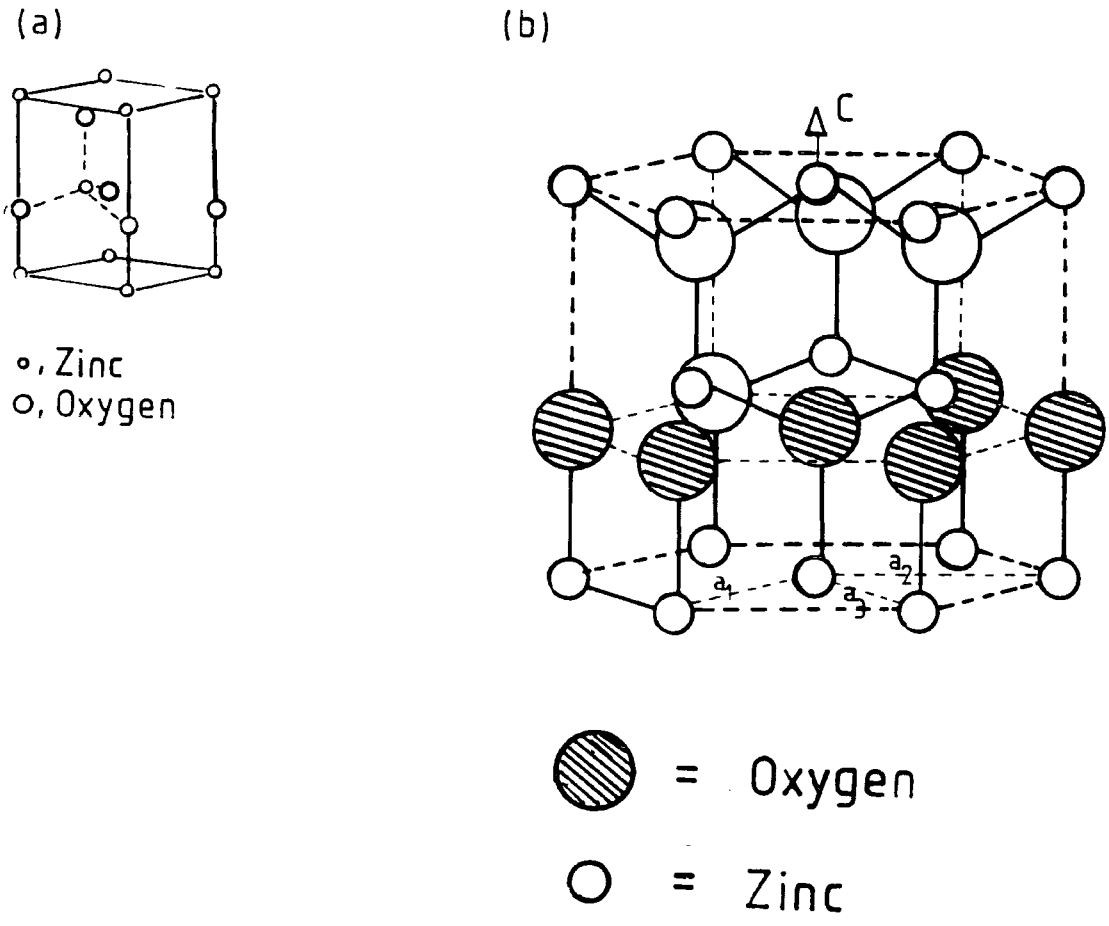

Figure 2.1 Structure of hexagonal wurtzite zinc oxide : (a) unit cell. (b) extended unit cell structure.

3/. Reduce these numerical representations of the intercepts to the smallest integers having the same ratio.

4/. Enclose in parenthesis (hkl).

In order to describe zinc oxide, hexagonal indices can be used based on a four coordinate system with indices (hkil) or a_1, a_2, a_3 and c. This is more suitable for zinc oxide than the three coordinate system because of the source of possible confusion in assigning planes when equivalent planes do not have the same indices. Possible confusion is avoided using the four coordinate system as equivalent planes are indicated by permutations of the first three indices.

For example the three main reflections from the XRD spectrum of a polycrystalline powder sample of zinc oxide using the three coordinate system (hkl) are the (100), (101), and the (002) planes. Under the four coordinate system the labels are the $(10\bar{1}0)$, the $(10\bar{1}1)$, and the (0002). Note that (110) is not equivalent to (101) in the hexagonal structure and this is explicit in the 4 coordinate system where these planes become $(11\bar{2}0)$ and $(10\bar{1}1)$ respectively.

The ASTM card for zinc oxide uses the three indices system. To convert from three to four indices the following formula is used : i = - (h + k) [3]. Table 2.1 shows the ASTM (American Society For Testing And Materials) index for random polycrystalline zinc oxide along with the interplanar spacings, (d_{hkl}) and the reflected intensities from the different planes. Both three and four coordinate labelling systems for zinc oxide planes are included.

Thin film zinc oxide consists of columnar grains and crystallites up to 1μm in average diameter and such films can have a preferred orientation or fibre texture where all crystallites have one particular set of crystallographic planes parallel to the film plane.

2.3 Nonstoichiometry and Defect Structure

When zinc oxide is prepared it is usually as a rather n - type conducting material. The n - type conductivity is caused by an excess of zinc which acts to yield an electron

Crystal plane	d_{hkl}/Å	Peak intensity %
(100)	2.816	71
$(10\bar{1}0)$		
(002)	2.602	56
(0002)		
(101)	2.476	100
$(10\bar{1}1)$		
(102)	1.911	29
$(10\bar{1}2)$		
(110)	1.626	40
$(11\bar{2}0)$		
(103)	1.477	35
$(10\bar{1}3)$		
(112)	1.379	28
$(11\bar{2}2)$		

Table 2.1.ASTM index for random polycrystalline zinc oxide

which is free to move as a carrier in the conduction band. The excess zinc results in a non - stoichiometric material $Zn_{1+\delta}O$ and a degree of structural disorder because of the markedly different ionic radii of zinc and oxygen. Large octahedral interstitial positions exist in zinc oxide into which zinc ions can diffuse. The diffusion rate of zinc in zinc oxide has been found to be higher than that of oxygen. If an absolutely pure stoichiometric single crystal were considered, i.e with no point defects, no impurities, no dislocations, and no grain boundaries, zinc oxide would be an insulator rather than a semiconductor at room temperature. The concentration of the free electrons would be 10^{14} m^{-3} [4] compared to 10^{14} - 10^{25} m^{-3} in semiconductors and up to 8×10^{28} m^{-3} in metals. Figure 2.2 shows the energy band diagram of zinc oxide [2,4].

Also marked on the figure are the energy levels for the excess zinc interstitials ($E_{Zn(i)}$), zinc vacancies ($E_{V(Zn)}$), and oxygen vacancies ($E_{V(O)}$), and their ionization energies. These are examples of native defects and the corresponding native defect energy levels since both are produced by the basic material. The zinc excess can be present in the form of zinc interstitials (Zn_i) or oxygen vacancies (V_o) in the zinc oxide lattice while zinc vacancies (V_{Zn}) imply zinc deficiency. These defects can be singly ionized or doubly ionized and have energies of the order of (E_c - 0.05) eV and (E_c - 0.2) eV if the defect is interstitial zinc , (E_c - 0.5) eV and (E_c - 2.0) eV if the defect is an oxygen vacancy , and (E_v + 0.7) eV and (E_v + 2.8) eV if the defect is a zinc vacancy where E_c is the energy of the bottom of the conduction band and E_v is the energy of the top of the valence band [5,6]. Oxygen vacancies and zinc interstitials act as donors whereas zinc vacancies act as acceptors in thin film zinc oxide. These can be generated thermally by varying the partial pressures of zinc and oxygen and the temperature, according to equations (2.1) and (2.2) :

$$ZnO_{(lattice)} \longleftrightarrow Zn_i + \frac{1}{2}O_2(gas) \tag{2.1}$$

$$ZnO_{(lattice)} \longleftrightarrow Zn_{(lattice)} + V_o + \frac{1}{2}O_2(gas) \tag{2.2}$$

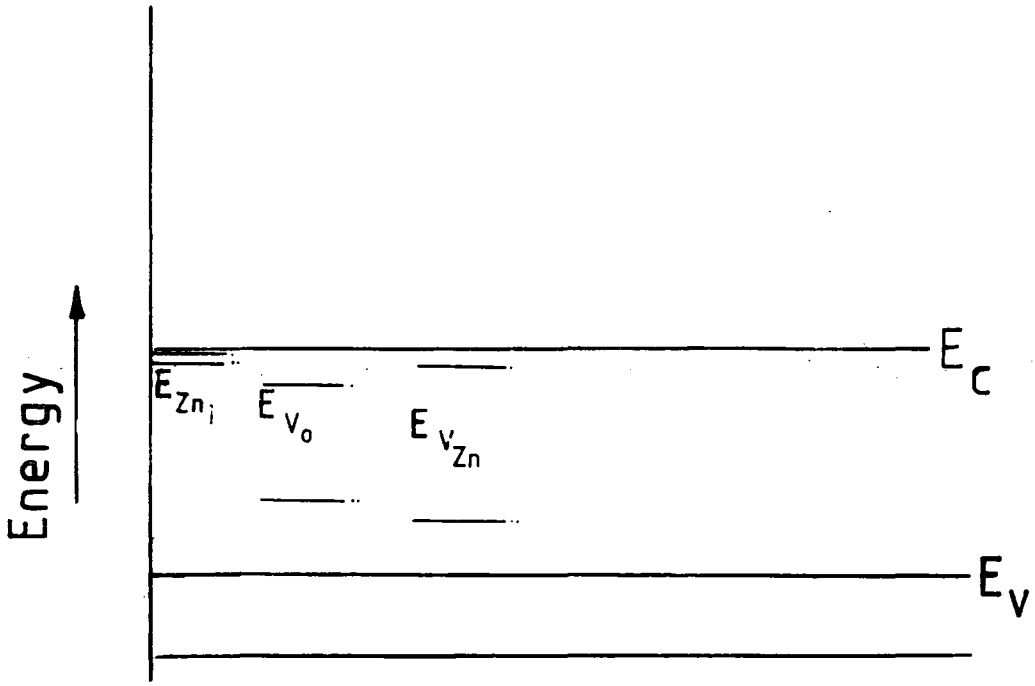

Figure 2.2. Energy band diagram of zinc oxide. E_c = conduction band, E_v = valence band, E_{Zn_i} = energy level for interstitial zinc, E_{V_O} = energy level for oxygen vacancy, $E_{V_{Zn}}$ = energy level for zinc vacancy. • = singly ionized defect :•• = doubly ionized defect.

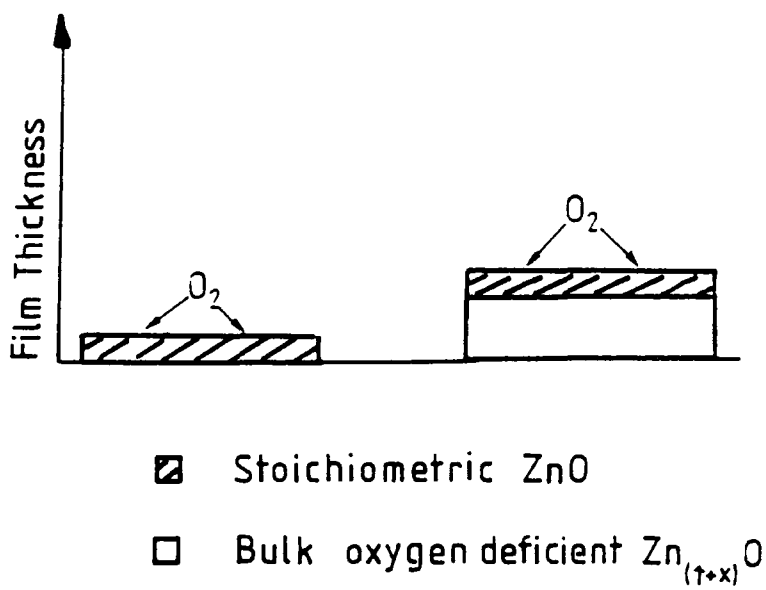

Figure 2.3. Thickness effect. ZnO films have an oxygen rich surface layer which increases resistivity. Films with a smaller thickness are more susceptible.

As native levels are located near the conduction band they can be thermally ionized at room temperature. This process can be described by :

$$Zn_i, V_o \longleftrightarrow Zn_i^+, V_o^+ + e_c \tag{2.3}$$

where e_c is the electronic charge. This represents the concentration of electrons in the conduction band. A concentration of 1 ppm of fully ionized defects generates around 10^{22} electrons per m^3 giving rise to the possibility of changing the electronic properties in a controlled manner.

2.4 Doped Zinc Oxide

Impurities such as trivalent metal cations (M^{3+}) or monovalent halide anions (X^-) can be substitutionally incorporated by a proper doping process [2]. These lead to the formation of impurity point defects and the release of electrons which can contribute to conduction [7] . For example in the case of M = aluminium, gallium or indium, the following equations have been formulated :

$$M_2O_3 \longrightarrow 2M_{\dot{Zn}} + 2O_o + 2e + \frac{1}{2}O_2(gas) \tag{2.4}$$

$$M_2O_3 \longrightarrow 2M_{\dot{Zn}} + 3O_o + V_{Zn}^{'} + e \tag{2.5}$$

for stoichiometric zinc oxide, and

$$M_2O_3 + Zn_i^{\cdot} \longrightarrow 2M_{\dot{Zn}} + 3O_o + Zn_{Zn} + e \tag{2.6}$$

$$M_2O_3 + V_o^{\cdot} \longrightarrow 2M_{\dot{Zn}} + 3O_o + e \tag{2.7}$$

in the case of n - type conducting samples. These reactions lead to an increase in the film conductivity. The solvation energies of some of these processes have been calculated and in the case of aluminium and equations 2.4 and 2.5 the energies were 0.9 and 1 electron volt respectively. For gallium in equation 2.5 the calculated solvation

energy was 1.3 electron volts and for indium in equation 2.5 the energy was 2.3 electron volts [8]. These results suggest that it is energetically more favourable for aluminium to be incorporated onto a zinc site than either gallium or indium.

With halide doping there is also an increase in film conductivity,

$$ZnCl_2 \longrightarrow Zn_{Zn} + 2Cl_o^{\cdot} + V_{Zn}^{'} + e \tag{2.8}$$

$$ZnCl_2 + Zn_i^{\cdot} \longrightarrow 2Zn_{Zn} + 2Cl_o^{\cdot} + e \tag{2.9}$$

and also,

$$ZnCl_2 + V_o^{'} \longrightarrow Zn_{Zn} + 2Cl_o^{\cdot} + e \tag{2.10}$$

The alternative energy levels produced by the addition of these materials are donor impurity levels and are also marked in figure 2.2. Both native and donor impurity levels lie 0.025 - 0.5 eV below the conduction band.

2.5 Parameters Affecting the Resistivity of Zinc Oxide

This section presents some of the film properties that control the resistivity of zinc oxide. The electrical properties of the films are changed by variations in the grain size, the grain boundary barrier height, the doping level and the overall thickness of the films.

2.5.1 Thickness Effect

It has been reported that proportionately thinner films are more resistive [9]. It has also been stated that because of their random structure films 100 nm thick allow a greater proportion of oxygen to be chemisorbed into the film bulk along grain boundaries. It has been suggested that this leads to the formation of traps which deplete the concentration of conduction band electrons.

The possible result of this would be that in thin film form zinc oxide is more stoichiometric and therefore more insulating because oxygen would be able to diffuse through the whole film (see figure 2.3).

However as the film thickness increases this stoichiometric layer becomes confined to the surface since oxygen can no longer diffuse through the entire film. The influence of doping with trivalent metal ions is to reduce the importance of this surface stoichiometric layer as the trap density is much reduced by the free carriers produced according to equations 2.4 to 2.7. It is therefore possible for films to have their electrical properties more or less influenced by the surface properties depending on the conditions of preparation (presence or absence of oxygen) and whether M^{3+} is present or not.

2.5.2 Grain Size and Grain Boundary Barrier Height Effects

In thin films conduction occurs through the grains and is limited by the grain boundary barrier height. The theory of Petritz [10] quotes the film resistivity as being given by :

$$\rho = \rho_g + \rho_s \tag{2.11}$$

where ρ_g and ρ_s refer to the grain boundary resistivity and the resistivity of single crystal - like grains. The grain boundaries are important in several ways. They generally contain fairly high densities of interface states which trap free carriers from the bulk of the grains, scatter free carriers by virtue of the inherent disorder and the presence of trapped charge and may also act as sinks for the segregation of dopant atoms (i.e Al,Ga or In) [11,12]. Interface states may be either intrinsic (related to native ZnO) or extrinsic (related to impurities such as group III metals or group VIII halides)or may result from the adsorption of gases such as oxygen. The density of traps (n_t) (per unit area) determines the maximum amount of charge which can be trapped. Interface charge gives rise to band bending in the bulk of the grain and is the cause of interface barriers. The energy required for a free carrier to cross the barrier is ϕ_B (which is the grain boundary barrier height). Figure 2.4 illustrates the energy band diagram of a granular n - type semiconductor. In the absence of scattering within a single crystal - like grain an electron with energy greater than ϕ_B may cross several grains before colliding with a phonon (lattice vibration). A phonon is an oscillation of the zinc oxide

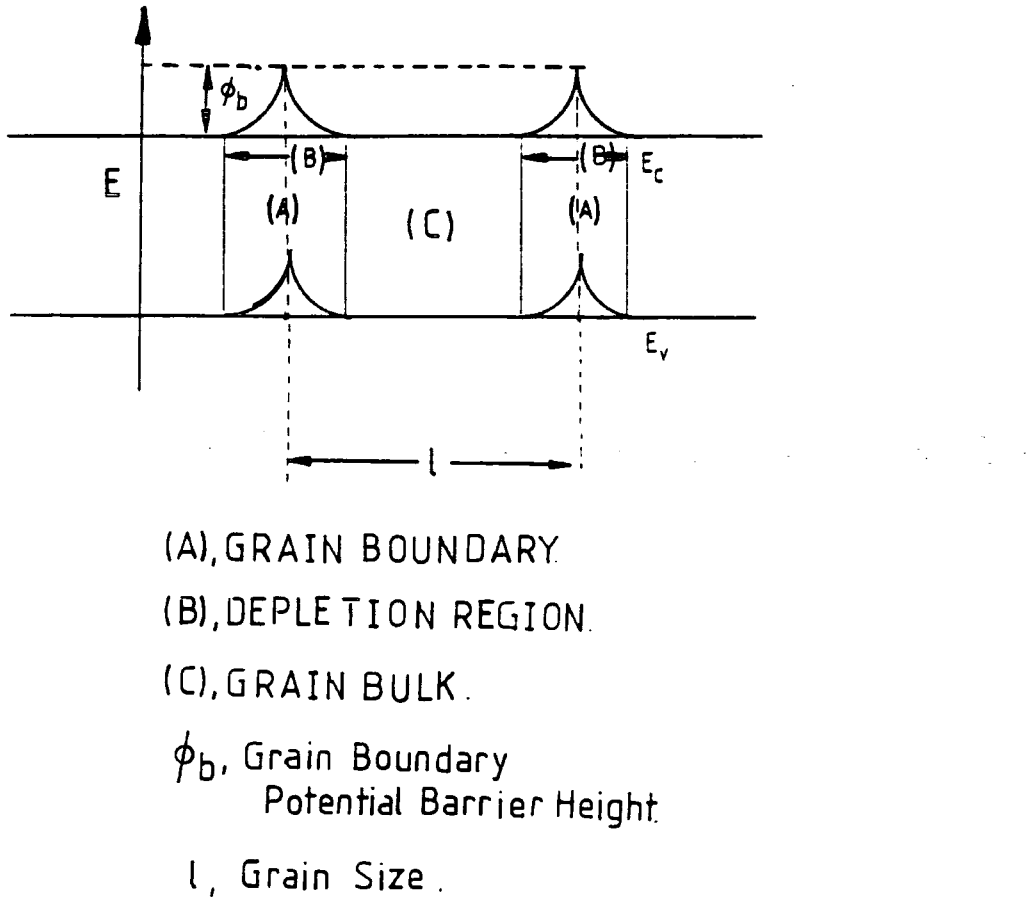

Figure 2.4. The energy band diagram in an n - type granular semiconductor.

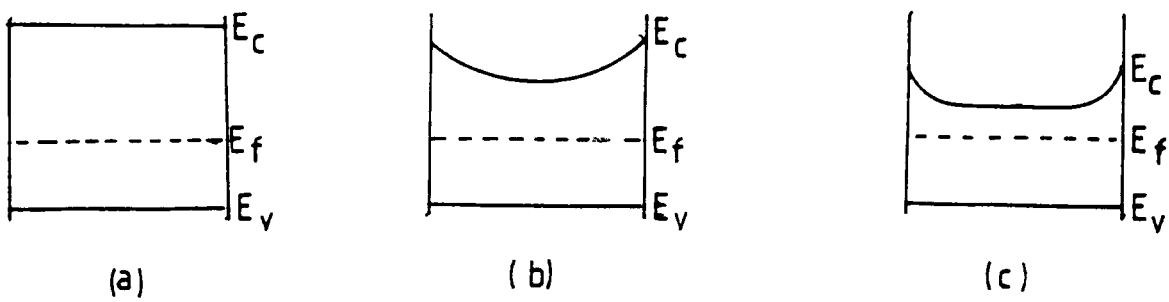

Figure 2.5. The three possible scenarios for a n - type granular semiconductor : (a) $N \leq n_t$, (b) $N \approx n_t$, (c) $N \geq n_t$.

lattice which acts to scatter the electron from its predetermined path [13].

Electrons with energies less than ϕ_B are confined within the potential wells which occur between grain boundaries and are unable to take part in current transport.

If the trap density is high or the bulk doping level low, grains may be completely depleted of free carriers, leading to high film resistivity with a large thermal activation energy.

Three scenarios are possible. The first is a low doping regime in which the doping level is smaller than the trap density and is shown in figure 2.5 (a). In this case the grains are totally depleted resulting in nearly flat conduction and valence bands towards the extremities of the grains. The mobility is not activated and the carrier concentration is dependent on temperature.

In the second case the bulk doping level is comparable with the trap density. This results in the bending of energy bands in the grains causing a depletion layer potential barrier (ϕ_B) at the grain boundaries, which increases with increasing doping level. The mobility is temperature dependent. The carrier concentration is also activated. This scheme is shown in figure 2.5 (b).

The third condition occurs when the dopant level exceeds a critical doping minimum given by :

$$N_c = \frac{n_t}{l} \tag{2.12}$$

where l is the grain size (radius), n_t is the trap density and N_c is the critical doping level [9]. As a result the depletion region is limited to a region near the edges of the grains. The mobility is still temperature dependent while the carrier concentration is independent of temperature (figure 2.5 (c)). The depletion (or grain boundary) barrier height decreases in this highly doped stage.

The conduction mechanisms in microcrystalline zinc oxide involve thermionic emission (i.e. the thermal emission of carriers over the grain boundary potential barrier) and thermal field emission (or tunneling of carriers through the grain boundary potential

barrier in heavily doped samples).

2.6 Optical Properties

The high optical transparency of zinc oxide in the visible and near IR regions of the solar spectrum is a direct consequence of it having a wide bandgap in the range 3.2 - 3.4 eV [1,2,14].

This puts the fundamental absorption edge in the ultraviolet. The bandgap can be varied slightly depending on the conditions of preparation and any added impurities.

The valence bands are p - like (i.e with p - orbital like electron density and parity) in character while the conduction band is s - like.

With undoped zinc oxide the transmission remains high into the infrared region out to long wavelengths (i.e 10 μm). That is the reflectance and absorbance are low and it is only at a wavelength of 20 - 25μm that any features are observed. This is the restrahlen band of the fundamental lattice absorption [2].

When zinc oxide is doped with donors such as aluminium, gallium or indium the free electrons produced when present in high enough concentrations give rise to processes of free carrier absorption and reflection. In the near IR region free carrier absorption becomes important. The optical behaviour can be explained by the Drude Theory (related to the study of conduction in metals) and is essentially governed by free carrier effects. Thus the transmittance decreases while the absorption increases with increasing wavelength beyond the absorption edge.

The maximum in the absorption is called the plasma resonance (λ_p). For wavelengths longer than this the material becomes reflecting. The value of λ_p determines the range over which the ZnO is reflecting. This is due to the presence of free carriers and the resulting ionized impurity scattering which dampens the free carriers and causes the impinging photons to be reflected [15,16].

Two mechanisms operate to influence the absorption edge or bandgap with heavy doping. One is the Moss - Burstein effect which leads to bandgap widening. This is due to the filling of the low lying states in the conduction band with electrons excited

from shallow levels.

The alternative effect is bandgap narrowing which occurs when the impurity donor band merges with the conduction band at a critical doping level. This level may be estimated from the Mott critical density (equation (2.12)). Above this level there is a downward shift of the conduction band along with an upward shift of the valence band. This is due to electron - electron impurity interactions [15–17].

2.7 Applications of Zinc Oxide

A large number of applications have been suggested for thin film ZnO. For example it can be used in surface acoustic wave (SAW) devices and other piezoelectric devices due to its high electromechanical and piezoelectric and optical coupling constants. For optimum performance the properties of the thin film must simulate those of a single crystal. The thin microcrystalline film properties must be carefully controlled with the c - axis either parallel to ((0002) preferred order) or perpendicular ((10$\bar{1}$0) preferred order) to the substrate. The coupling is stronger when the c - axis is perpendicular to the substrate plane and for thin film zinc oxide is only marginally lower than that for single crystals [18].

The surface conductivity of zinc oxide is sensitive to the presence of gases such as NH_3, nitrogen oxides (NO_x), other polyatomic gases (oxygen, hydrogen, carbon monoxide), alcohols and hydrocarbons so that films can be used in gas detection. In some cases zinc oxide is used as a catalyst.

2.7.1 Sensors

Zinc oxide surfaces possess dangling bonds which allow adsorption, physisorption and chemisorption of gaseous species to occur. The change in conductivity can be either due to direct transfer of electrons from the adsorbed gas to the oxide semiconductor or due to a reaction of the adsorbed gas with previously chemisorbed surface oxygen [19,20]. Thus a weak to strong interaction is set up between the zinc oxide film surface and any small molecule on the surface. This allows the transport of electronic charge to or from the zinc oxide surface and may lead to accumulation or depletion of carriers at

the surface. This results in a change in the surface conductivity which can be detected by electrical measurements.

Thus it is the property of the surface in its ability to form bonds with small molecules together with the associated electrical effect which makes zinc oxide an attractive thin film sensor [21]. It is also important to realise that there is reversibility and that when the surface molecules are removed the conductivity returns to its initial value. The response time of the device is dependent on the growth conditions of zinc oxide [22].

2.7.2 Heat Mirror

An interesting application as a heat mirror lies in the property that heavily doped films are reflecting beyond a certain wavelength (λ_p) due to a high concentration of free carriers. Hence heat mirrors allow the temperature of closed spaces to be controlled. They can also act to retain heat in a confined space for use in cold climates [14,23,24]. Heat mirror coatings are useful on the glass envelopes of lamps so that the thermal part of the radiation can be reflected back to the filament while the visible part is transmitted.

2.7.3 n - Type Window Layer for Solar Cells

The major interest in the work reported in this thesis lies in controlling the electrically conducting properties of ZnO. One potential application is as a window layer in certain heterojunction thin film solar cells. The first requirement for an n - type window layer is that it should be reasonably transmitting so that the solar radiation passes through the layer and impinges on the p - type absorber layer. To satisfy this requirement the transparency of the n - type window layer must be high and therefore the material should if possible have a large bandgap. This requirement is fulfilled in the case of zinc oxide.

A typical p - type absorber such as CdTe has a bandgap of 1.5 eV while that of zinc oxide is $\approx$ 3 eV and therefore light will pass through ZnO to CdTe at all energies up to 3 eV and at the same time provide a heterojunction for the separation

of electron - hole pairs. Conductivity and conductivity type are also requirements of n-type window layers where the majority charge carriers are electrons. The absorber material is always p - type in n - type window solar cells and the principle of operation of a solar cell demands that the window material be of opposite majority charge carrier type (so that when light impinges on the p - n junction electron hole pairs are created and are separated by the built-in electric field).

2.7.4 Resistively Heated Coatings

ZnO can be used as a resistively heated coating on a substrate. Then if enough current is passed through, the whole substrate is heated through the dissipation of electrical energy. ZnO possesses good electrical conductivity as well as good chemical stability. Several patents have been issued for an electric resistance device [25–27] based on an electroconductive coating. Doping with indium and gallium was carried out in this work.

One application is on windscreens for the purpose of de - icing (cars, aeroplanes etc.) and as heater elements for bread toasters and room heaters.

Since ZnO films can be made highly conductive while remaining transparent they can be used as coatings on glass to provide the electrodes for liquid crystal and electroluminescent cells, or for smart windows. Our particular interest has been to try to grow conducting films on plastic sheet to avoid problems created by static electricity. This requires a deposition temperature low enough to avoid the thermal decomposition of the plastic.

2.8 Zinc Oxide as a Transparent Conducting Coating

In recent times ZnO films have been deposited by sputtering or CVD techniques. Undoped sputtered films exhibit a strong (0002) preferred orientation, and have a grain size in the range 5 - 30 nm. Films grown by CVD or spray pyrolysis also exhibit a (0002) preferred orientation.

Films grown by R.F magnetron sputtering have had resistivities as low as $10^{-6}\Omega$m and mobilities as high as 120 $cm^2\ V^{-1}\ s^{-1}$ [28]. Film transmittance was of the order

of 85%. Growth using the CVD technique resulted in films having resistivities in the range 10^{-2} - $10^{-4}\Omega$m [29]. Spray pyrolysis using zinc acetate has produced undoped films with resistivities as low as $10^{-5}\Omega$m. The film transmittance was in the range 80% to 90% [29-31].

In attempts to improve the conductivity and stability of the films zinc oxide has been doped with indium, aluminium, boron, silicon or tin [32-35]. The growth techniques used were spray pyrolysis and sputtering. The resulting films were microcrystalline with grain sizes of the order 10 - 80 nm. Preferred orientation tended to be absent when an impurity such as indium or aluminium was added.

With spray pyrolysis using zinc acetate, films have been doped with indium or aluminium. ZnO:In always gave superior results. Typically aluminium doped films have resistivities of the order of 10^{-2} - $10^{-3}\Omega$m, while indium doped zinc oxide in the as - deposited form has a film resistivity of the order $10^{-5}\Omega$m. Annealing aluminium doped films yields an improvement, while for indium doped films little improvement was observed [24]. Film transparency is of the order 85% in the visible region. Bandgap narrowing and widening effects are also observed. In sputtered ZnO:Al the bandgap increases from 3.4 eV to 3.9 eV.

2.9 Other Transparent Conducting Oxide Films

A number of other oxide materials have been investigated or used as conducting coatings, mostly on glass. These include indium oxide, In_2O_3, which has a bandgap between 3.55 and 3.75eV [36,37] and has a resistivity of $2\times10^{-6}\Omega$m with a mobility of 74 $cm^2\ V^{-1}\ s^{-1}$ and a transparency of 90% [38]. Unfortunately, films of In_2O_3 are not particularly stable. The most well known and extensively used transparent conducting oxide is indium tin oxide [39-49]. SnO_2 itself is an n-type semiconductor where the conductivity is caused by oxygen vacancies or chlorine contamination from the starting materials. At best SnO_2 has carrier concentrations of 10^{25} -10^{26} m^{-3} with mobilities in the range 5-30 $cm^2\ V^{-1}\ s^{-1}$ leading to resistivities 10^{-4} - $10^{-5}\Omega$m. In recent years films of indium tin oxide have become commercially available with the

lowest resistivities yet achieved for a transparent thin film. Carrier concentrations are of the order 10^{27} m^{-3} with mobilities in the range 15-40 cm^2 V^{-1} s^{-1}. This leads to film resistivities between $7\times10^{-7}\Omega m$ and $5\times10^{-6}\Omega m$. Other transparent conducting coatings which have attracted considerable attention have been antimony and fluorine doped tin oxide and cadmium stannate. At best all of their resistivities lie in the range 10^{-4} - $10^{-5}\Omega m$, but none, as far as is known, offer the possibility of deposition by spray pyrolysis on to substrates below 200°C.

All these oxides in their undoped state can be produced in a conducting and transparent thin film form. The properties of transparent conducting oxides are summarised in table 2.2. It is also clear that oxygen deficiency or accidental doping results in the release of free electrons to the conduction band resulting in a n - type semiconductor. Most of the films undergo an ageing effect when oxygen diffusion along grain boundaries restores the stoichiometry and the conductivity decreases, accordingly. Doping the films (with donors) has the effect of maximising and stabilizing the film conductivity through the presence of a high concentration of impurity donors rather then relying on oxygen vacancies. However ZnO is very cheap and has many attractive properties.

Summary of the properties of transparent conducting oxides								
	In_2O_3	In_2O_3:Sn	SnO_2	SnO_2:Sb	SnO_2:F	ZnO	ZnO:In	ZnO:Al
Preferred order	$(10\bar{1}0)$ $(11\bar{2}1)$	$(10\bar{1}0)$ $(11\bar{2}1)$			$(20\bar{2}0)$	(0002)	$(10\bar{1}0)$	
Grain size /(nm)	10	40 - 60	20 - 30	60	40	5 - 30	10 - 80	10 - 40
Resistivity /(Ωm)	2×10^{-6}	7×10^{-7} - 5×10^{-6}	10^{-4}- 10^{-5}	5×10^{-6}	5×10^{-6}	10^{-5} - 10^{-6}	10^{-6}	10^{-6}
Mobility /(cm^2 V^{-1} s^{-1})	10 -75	15 - 40	5 - 30	15 - 30		38 - 120	20	22
Carrier concentration /(m^{-3})	10^{25} - 10^{26}	10^{27}	10^{25}- 10^{26}	10^{26}	10^{25} - 10^{26}	10^{26}	10^{26}- 10^{27}	10^{26} - 10^{27}
Bandgap /(eV)	3.55 - 3.75	3.75 - 4.4	3.87 - 4.3	4 - 4.5	3.75 - 4.3	3.31	3.31 - 3.43	3.4 - 3.9
Average transmittance /(%)	90	80 - 92	80 - 90	80 - 90	80 - 90	85	80 - 90	85

Table 2.2. Summary of the properties of common transparent conducting oxides.

2.10 Chapter Two References

(1) Heiland E., Mollwo E., and Stockmann F. , *Sol. Stat. Phys., 8*, 193, (1959).

(2) Hirschwald et al., ed. Kaldis E., Curr. Top. Mater. Sci., 7, 154, North-Holland Publishing Company, (1981).

(3) Barratt C.S., Massalski T.B., Structure of Metals, McGraw - Hill Book Company, (1966).

(4) Hirschwald W., *Acc. Chem. Res.*, 228, (1985).

(5) Gupta T.K., Carlson W.G., *J. Mat. Sci., 20*, 3487, (1985).

(6) Simpson J.C., Cordaro J.F., *J. Appl. Phys., 63(5)*, 1781, (1987).

(7) Choi J.S., Yo C.H., *J. Phys. Chem. Sol., 37*, 1149, (1976).

(8) Mackrodt W.C., Stewart R.F., *J. De Physique*, C6 - 64, (1980).

(9) Major S., Banerjee A. and Chopra K.L., *Thin Sol. Films, 143*, 19, (1986).

(10) Petritz R.L., *Phys. Rev., 104*, 1508, (1956).

(11) Seto J.Y.W., *J. Appl. Phys., 46(12)*, 5247, (1975).

(12) Orton J.W., Powell M.J., *Rep. Prog. Phys., 43*, 1263, (1980).

(13) Sernelius B.F., Berggren K.F., *Phys. Rev., 37 (17)*, 10244, (1988).

(14) Jin Z.C., Hamberg I. and Granqvist C., *J. Appl. Phys., 64(10)* , 5117, (1988).

(15) Jin Z.C., Hamberg I. and Granqvist C., *Appl. Phys. Lett., 51 (3)*, 149, (1987).

(16) Roth A.P., Webb J.B. and Williams D.F., *Phys. Rev. B, 25 (12)*, 7836, (1982).

(17) Major S, Banerjee A. and Chopra K.L., *J. Mater. Res., 1 (2)*, 300, (1986)

(18) Hutson A.R., *Phys. Rev. Lett., 4*, 505, (1960).

(19) Fraser D.B., Cook H.D., *J. Electrochem. Soc., 119*, 1368, (1972).

(20) Seiyama T., Kato A., Fujushi K. and Nagatani. M., *Anal. Chem. , 34*, 1502, (1962).

(21) Nanto H., Minami T. and Takata S., *J. Appl. Phys., 60(2)*, 482, (1986).

(22) Pink H., Treitinger L. and Vite L., *J. Jpn. Appl., 19*, 513, (1980).

(23) Granqvist C., *Phys. Scr., 32*, 401, (1985).

(24) Chopra K.L., Major S. and Pandya K., *Thin Sol. Films, 102*, 1, (1983).

(25) Armour Research Foundation, Illinois, U.S Patent No., 776, 443, (1954)

(26) Philips Electronics, U.S Patent No. 1,119,539, (1965)

(27) Pittsburgh Plate Glass Co., U.S Patent No., 704,793 (1951).

(28) Nanto H., Minami T., Shooj S. and Takata S., *J. Appl. Phys., 55 (4)*, 1029, (1984).

(29) Roth A.P., Williams D.F., *J. Appl. Phys., 52 (11)*, 6685, (1981).

(30) Aranovich J.A., Ortiz A. and Bube R.H., *J. Vac. Sci., 16(4)*, 994,(1979).

(31) Oktik S., Russell G.J., Brinkman A.W. and Woods J., *Properties of Undoped ZnO Films Deposited by Spray Pyrolysis*, (1988).

(32) Streydio J.M., Cossemont D., *J. Cryst. Growth, 72,* 57, (1985).

(33) Major S., Banerjee A. and Chopra K.L., *Thin Sol. Films, 108*, 333, (1983).

(34) Brown H.E., Zinc Oxide - Properties And Applications, International Lead And Research Organisation, NY, (1976).

(35) Minami T., Nanto H., *J. Jpn. Appl. Phys.,24(10)*, L781, (1985).

(36) Muller H.K., *Phys. Stat. Sol., 27*, 723, (1968).

(37) Wickerham C.E., Greene J., *Phys. Stat. Sol. A, 47*, 329, (1978).

(38) Manifacier J.C., Szepessy L., Bresse J.F., Perotin M. and Stuck R., *Mater. Res. Bull., 14*, 163, (1979).

(39) Manifacier J.C., Fillard J.P., *Thin Sol. Films, 77*, 67, (1980).

(40) Pommier R., Gril C. and Marucchi J., *Thin Sol. Films, 77*, 91, (1981).

(41) Haitjema H., Elich J.J. Ph., *Thin Sol. Films, 205*, 93, (1991).

(42) Maudes J.S., Rodriguez T., *Thin Sol. Films, 69*, 187, (1980).

(43) Grozze P., Schmitte F.J., Frank G. and Kostlin H., *Thin Sol. Films, 90*, 309, (1982).

(44) Shanthi E., Dutta V., Banerjee A. and Chopra K.L., *J. Appl. Phys., 51*, 6243, (1980).

(45) Advani G.N., Jordan A.G. and Kluge-Weiss P., *Mater. Sci. Eng., 4*, 99, (1979).

(46) Vossen J.L., *Physics of Thin Films, 9*, 1, (1977).

(47) Haacke G., *Ann. Rev. Mater. Sci., 7*, 73, (1977).

(48) Manifacier J.C., *Thin Solid Films, 90*, 297, (1982).

(49) Dawer Joshi A.L., *J. Mater. Sci., 19*, 1, (1984).

Chapter Three

Review of Spray Pyrolysis

3.1 Introduction

This chapter describes the history and development of spray pyrolysis and the equipment involved (i.e. the basic process and the equipment).

In section 3.2 the applicability of spray pyrolysis for the deposition of a variety of materials is discussed in terms of the chemical nature of the precursor.

In sections 3.3 and 3.4 the physical aspects and chemical aspects of spray pyrolysis are discussed (i.e the influence of deposition parameters and precursor type).

3.2 Spray Pyrolytic Process

A few reviews have been published in this field [1-5] which concentrate on various aspects of spray pyrolysis but which do not form a complete picture of the field. Spray pyrolysis is a process in which a thin film of a technologically or scientifically interesting material is deposited by spraying a solution of a suitable precursor or several precursors in a solvent onto a heated substrate where pyrolysis and solvent vaporisation occur to give the desired material. The chemical reactants are selected such that the products other than the desired compound are volatile at the growth temperature.

The equipment used is outlined in figure 3.1. The spray pyrolysis system consists of a temperature controlled heated deposition platform and a solution atomiser. In some cases one or the other is designed so that a scanning motion is achieved which allows the source of atomized liquid to be spread evenly across the substrate surface.

The solution is fed from a source such as a bottle through pipes to the spray atomiser (see section 4.1 for a full description of the Durham spray kit). The system contains solution and gas lines which connect to the spray atomiser. These lines contain in - line flow and pressure meters and valves (manual or automatic) for the purpose of process control.

In order to carry out spray pyrolysis there is a need for a heated substrate on which to spray along with a temperature controller and a thermocouple probe for temperature

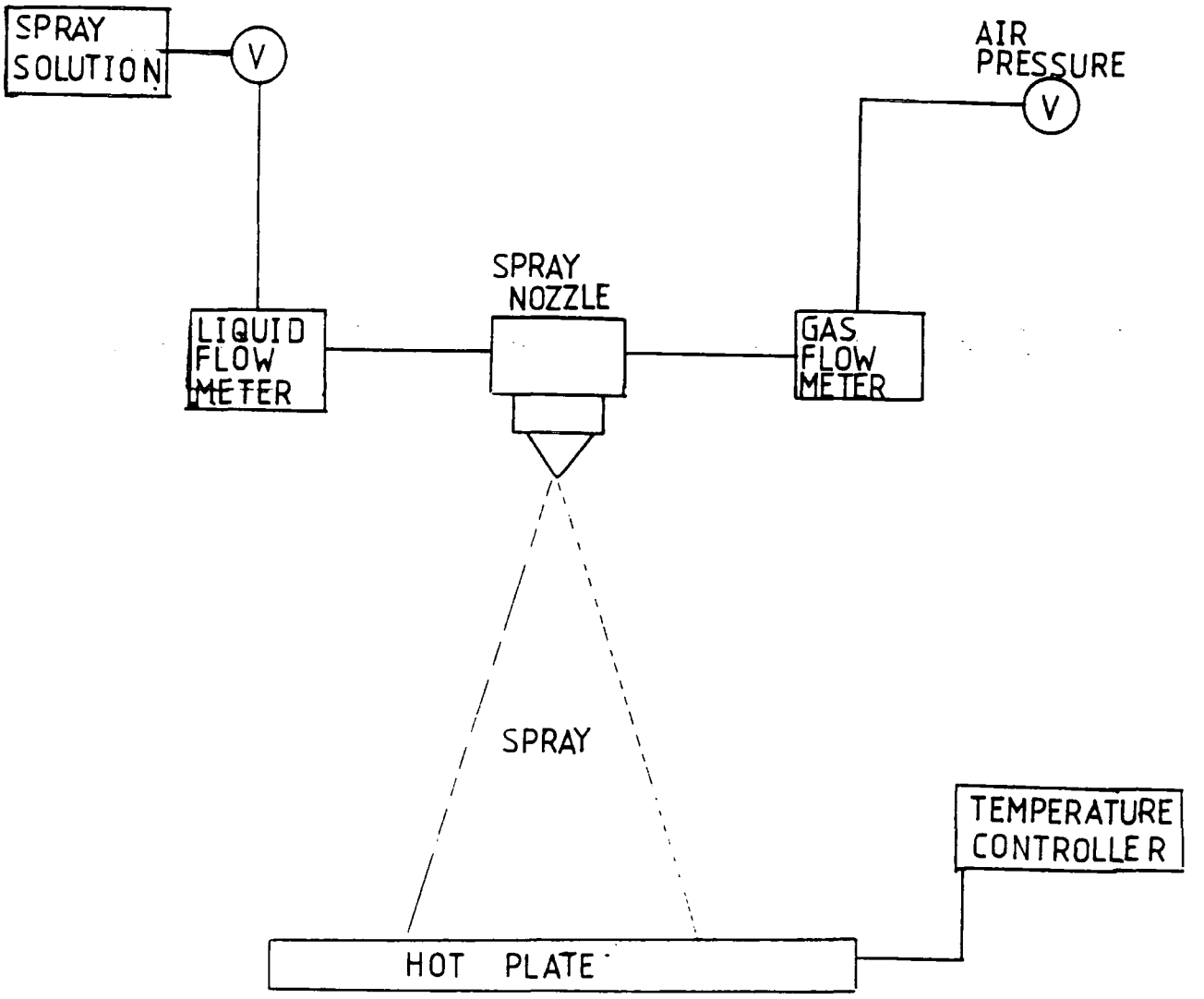

Figure 3.1 Schematic outline of a spray pyrolysis kit showing component parts.

measurement.

There are at least four types of spray guns available.

They are the pneumatic, the airless, the pneumatic airless, and the ultrasonic.

In the pneumatic system atomisation of the solution takes place by the action of compressed air on a fine jet of the spray solution. This jet is broken up by the flow of high pressure gas as shown in figure 3.2, which forces the liquid out of the atomiser through a narrow orifice.

The second type of spray atomiser is the airless or centrifugal type, where atomisation is achieved by forcing the solution directly through a specially designed orifice under high pressure. Using this method the droplets on leaving the atomiser have sufficient velocity to be transported to the substrate without the need for a carrier gas[6].

The third type of spray atomiser is commonly known as the pneumatic - airless and is a combination of (1) and (2). This has the effect of producing a more uniform droplet size[7].

The fourth type of atomiser is the ultrasonic variety in which a solution is shaken violently as a result of which mists are produced which have a very narrow droplet size distribution, the mean size of which is determined by the following equation :

$$d = 0.34\frac{8\pi\gamma}{\rho f^2} \tag{3.1}$$

where γ is the surface tension of the solution, f is the frequency of the ultrasonic transducer and ρ is the density of the solution [8].

3.2.1 Types of Processes Occurring in Spray Pyrolysis

There are at least four main processes that have been described in previous work [9]. Figure 3.3 outlines these processes which are related to the differences in droplet size in the spray as it approaches the substrate. The larger the droplet the greater the likelihood that the solvent will not have evaporated before reaching the substrate. Then the precursor material approaches the substrate as a solute in solvent (i.e as it left

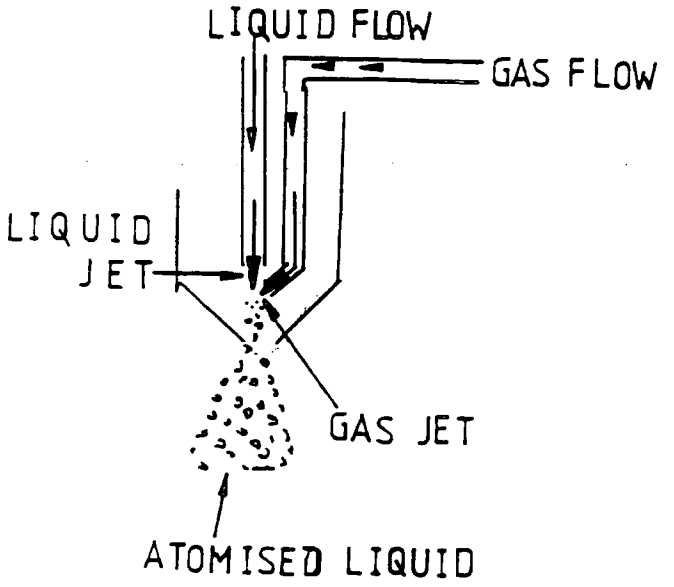

Figure 3.2 Diagram showing the break up of a liquid jet by high pressure gas.

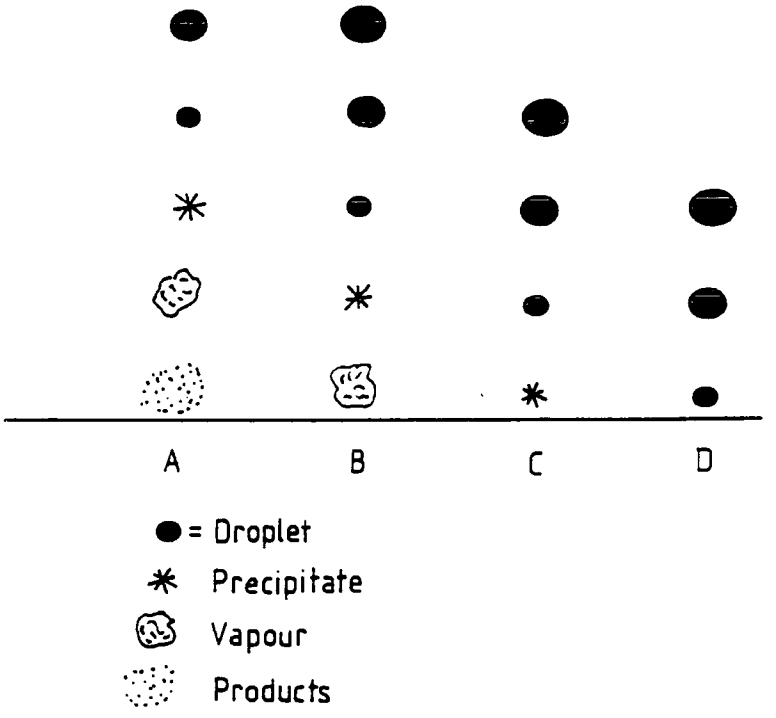

Figure 3.3 Outline of processes occurring during spray pyrolysis including solvent evaporation, precursor precipitation, vapourisation, and decomposition.

the nozzle) in which case the droplet splashes onto the substrate. Precursor pyrolysis occurs before, during and after the final impingement of the droplet on the solvent.

If the droplet sizes are smaller, then a larger proportion of the solvent is vaporised before impinging on the surface, so that the precursor lands as a dry precipitate where decomposition occurs.

For even smaller droplet sizes not only does the solvent vaporise but also the precursor or precursors and these species diffuse to the substrate surface as vapours before undergoing reaction.

Finally for very small droplet sizes all three processes, solvent evaporation, precursor volatilisation and precursor pyrolysis all occur soon after the spray leaves the gun.

Which process predominates also depends on the volatility of the precursors, the solvent, the heating power, and the substrate to spray gun distance and the size of droplet produced. Varying any one of these parameters while holding the rest constant should produce shifts in the relative proportion of these processes.

3.3 The Application of Spray Pyrolysis to the Deposition of Different Classes of Material

Spray pyrolysis is one of a number of ways of depositing thin films of a range of materials, including metals, oxides, sulphides and compounds of more than one anion and/or cation. Where the material is an oxide the stoichiometry can be controlled by controlling the composition of the ambient (i.e oxygen and water content).

The film materials which have been produced from various precursors are summarised in Appendix 1 which gives details of the precursors, solvents and growth temperatures used and comprehensive references are included.

3.3.1 Metallic Films

The deposition of palladium, ruthenium and platinum has been carried out from the acetylacetonate complexes in butanol. The growth temperatures ranges were 300 - 350°C (Pd), 380 - 400°C (Ru), and 340 - 380°C (Pt). The noble metals are more stable

than their oxides which may explain why the decomposition of the acetylacetonates yields the metal and not the metal oxide.

3.3.2 Metal Oxides

Metal oxide films are the most commonly produced materials to be deposited by spray pyrolysis from their chlorides and include SnO_2, In_2O_3, In_2O_3:Sn and undoped and doped ZnO.

3.3.2.1 Tin Oxide

The most commonly used precursors for tin oxide are summarised in appendix 1 along with their typical solvents. For the most part these are all moisture sensitive liquids and include tin tetrachloride, tin dichloride, ammonium hexachlorostannate, tin dichloro - diacetate, tetrabutyltin, tin difluoride and tin tetrabromide. The solvents used have been mixtures of water and alcohol, water and HCl, butyl acetate and pure alcohol. The addition of alcohol to aqueous solutions tends to decrease the surface tension and so increase their volatility. This results in smaller droplet sizes and a reduction in the thermal shock as droplets impinge on the substrate [10]. The decomposition of $SnCl_4$ also gives off HCl which is poisonous although additions of HCl have been shown to improve the structural quality of the films.

Typical dopants used to increase the conductivity of SnO_2 have been NH_4F to produce SnO_2:F films, and $SbCl_3$ for SnO_2:Sb as reported on in chapter 2. The range of deposition temperatures used varied from 220°C to 600°C.

3.3.2.2 Indium Oxide and Indium Tin Oxide

In the past there have been only a small number of indium precursors available. $InCl_3$ is the most commonly used source for the growth by spray pyrolysis of In_2O_3. $In(acac)_3$ has also been used. The solvents are water - alcohol mixtures or the pure alcohols (methanol, ethanol, propanol and butanol) or butyl acetate. $In(acac)_3$ has been used in acetylacetonate. Water mixtures are safer than pure alcohol mixtures but are also less volatile, unless alcohols of a high molecular weight are used. Acetylacetonate and butanol are the most involatile, and methanol and butyl acetate the most volatile.

Typical growth temperatures have been in the range 480°C - 500°C for pure In_2O_3 and 450 - 500°C for ITO. Both $In(acac)_3$ and $InCl_3$ are more thermodynamically stable than the corresponding tin compounds and this has restricted the lower temperature limit for successful precursor decomposition and film formation of indium containing materials. The optical and electrical properties are dependent on the Sn/In ratio in ITO.

The deposition of In_2O_3 would seem to be energetically less favourable compared to the deposition of SnO_2. A discussion of the deposition of ZnO by spray pyrolysis is deferred until the end of the chapter.

3.3.2.3 Other Materials

Other materials which have been deposited by spray pyrolysis are listed in the appendix. They include the oxides of some of the elements of groups III and IV and the technologically important chalcogenides such as PbS, ZnS and the ternary alloys. Chalcopyrite films such as $CuInSe_2$ have been produced for solar cells. Photoconductive films of PbS and superconducting films of Yttrium Barium Copper Oxide have also been put down by the spray pyrolytic method.

Studies of the spray pyrolysis of a few materials (i.e ITO, SnO_2, CdS) have been carried out for the most part with metal chlorides, nitrates, acetates and acetylacetonates. The chlorides of most metals can be decomposed to form metal films or oxides at growth temperatures between 200 and 600°C. The addition of a sulphur, selenium or tellurium precursor to a solution of the appropriate metal chloride gives rise to the sulphide, selenide or telluride as long as growth occurs in an oxygen - free ambient.

There are three types of system available i.e. water based, solvent based and mixed solvent - water based.

Most nitrates and acetates dissolve in water while some chlorides can be dissolved in all three systems. Deposition from water based systems is limited by the boiling point but is safer than solvent based systems. The acetylacetonates are restricted to non aqueous systems and offer the possibility of being deposited at lower temperatures.

However these solvents may be toxic and flammable although the precursors are safer to handle. Chlorides are generally more available than acetylacetonates and are also cheaper. The chlorides are more likely to undergo hydrolysis (many are moisture sensitive and hygroscopic) especially if water is present, whereas the acetylacetonates are more likely to either thermolyse or hydrolyse.

Various types of materials have been used, the most common being the chlorides, usually in water. The growth temperatures are high (300°C - 600°C) but in some cases growth at temperatures as low as 175°C has been achieved. Chlorides of copper and cadmium have been shown to give better results than the corresponding acetates, but the acetate of zinc gives better results than the chloride.

This shows the anomaly among the precursor materials as to which precursor type will yield the better film. It is not the chemical make up which matters but the physico - chemical properties and these must be evaluated in each individual case using analytical techniques such as thermogravimetry, mass spectroscopy and differential scanning calorimetry. These techniques applied to precursors help to establish the vapour pressure, boiling point, melting point and decomposition temperature and possibly the decomposition pathway.

The choice of the source material must satisfy a number of essential conditions in that it should be stable at room temperature and not be susceptible to long term decomposition. It should not oxidise in air. It should have a decomposition temperature as low as possible but still higher than the boiling and melting temperature. However the growth temperatures should be sufficient to fulfil the energetics of film growth.

The growth of sulphur containing materials is easier to achieve than their selenium or tellurium analogues due to decreasing instability, which is a disincentive to working with these materials.

At the heart of spray pyrolysis is the atomisation process. Its principal effect is to produce a high ratio of surface to mass in the liquid phase, resulting in a high evaporation rate leading to the production of a finely divided product with unique

properties of particle size and density.

3.4 Physical Aspects of Spray Pyrolysis

Droplet size, velocity and the overall geometry and dynamics of the spray are determined by the flow rates of the bulk solution as it enters the atomiser (nozzle) or the flow rate of the carrier gas in the case of pneumatic atomisation.

Lampkin [11] concluded from the results of his work that the droplet size and velocity should be minimal for the growth of uniform films.

Difficulties to achieving this are (a) an off centre nozzle, (b) blocked nozzle, (c) mechanical wear of the nozzle, and (d) bubbles in the flow line. These are overcome by careful design (air tight fittings, joints) of the spray system and constant re-adjustment, repair, and if necessary replacement. It is also better if the entire system is built from corrosion-free materials such as stainless steel or teflon.

It will be appreciated that the droplet size and velocity and the droplet temperature will influence which of the four processes can occur as outlined in section 3.2.1. Attempts have been made to produce uniform momentum by applying an electric field between the substrate and atomiser in order to produce better films and the application of an electric field has been shown to have some beneficial effects [11]. The use of a corona discharge in which the aerosol droplets are transported in an electric field to the substrate has been demonstrated by Siefert [12] and deposition efficiencies as high as 80% were reported. Conducting ITO and SnO_2 were produced in this way.

Ultrasonic atomisation has been adopted in preference to pneumatic atomisation since it produces a smaller, more uniform droplet size (3 - 5 μm as opposed to 5 - 50μm) and the variation in the droplet size is smaller (see section 3.1). The narrower distribution helps to reduce growth variations resulting from droplet size effects while smaller droplets aid the efficiency of solvent evaporation. This releases more energy for precursor decomposition and film formation. Effective gas entrainment of the spray also aids the growth uniformity as does a high carrier gas flow rate which serves to control the geometry of the spray between atomiser and substrate. This has the effect

of causing the spray droplets to approach the substrate in a reproducible way.

At very high flow rates however, lateral turbulence at the substrate surface can sweep away droplets, resulting in a reduced growth rate and thinner films. The amount of solution sprayed will define the overall thickness of the film.

When film growth is temperature activated there is a maximum precursor delivery rate to the substrate above which the growth rate will no longer increase (e.g for SnO_2 from $SnCl_4$).

When the precursor delivery rate is excessive there is the possibility that impinging droplets may interfere with the film growth. Film surfaces will be rougher and transparency and film conductivity will also be decreased. The number of nucleation sites will be higher and this may lead to increased film disorder, misorientation and defects. Adatom mobility is also affected adversely by the spray. With the growth for example of $CuInSe_2$ from a solution containing the relevant precursors at a rate of 7 cm^3 min^{-1}, films consisted of the chalcopyrite phase while a higher flow rate of 11 cm^3 min^{-1} yielded films consisting of the sphalerite phase. Clearly the flow rates of materials of mixtures of precursors leading to the formation of ternary materials can determine which phase is obtained. High flow rates in the deposition of this material result in sulphur deficiency.

However spray pyrolysis has the disadvantage that it has a low efficiency of deposition (a few percent). The reasons for this are that blowing the aerosol stream towards the substrate gives rise to a ram point which deflects the gas flow sideways. Therefore a large fraction of the droplets will be carried out of the coating region. The convection forces coming off the substrate also tend to keep the aerosol away from the substrate. The film growth rate has also been boosted through the use of a corona discharge [12,13].

Albin and Risbud [14] proposed a nucleation growth model for CdS deposition. It was stated that initially a droplet impinges on the substrate and begins to spread and flattens out to form a ring. As the droplet is spreading, the solvent evaporates leaving behind a $CdCl_2$ - thiourea precipitate which then undergoes pyrolysis to form CdS.

This process repeats itself many times and droplets containing precursor overlap resulting in a pinhole free film [14].

3.5 The Effect of Growth Conditions on Spray Pyrolysed Films

The following sections present a review of the different variables that are operative during the growth of films by spray pyrolysis. It is not exhaustive and reflects the past understanding of the process.

3.5.1 The Effect of Growth Temperature on Growth Rate and Film Properties

The choice of substrate temperature influences film adhesion, visible transmittance, film morphology, structure and the electrical properties. The study of the spray pyrolysis of different materials has led to the identification of the general growth behaviour and other influences that affect growth. The growth behaviour is largely determined by the chemicals and solvents used. With SnO_2, growth from $SnCl_4$ for a constant amount of precursor sprayed led to an exponential increase in the growth rate as the temperature increased [1–5]. Thus the growth of SnO_2 is temperature activated at low temperatures (the growth rate is temperature limited) while at higher temperatures the growth becomes diffusion limited (governed by the rate of precursor arrival). The growth rate of ITO using $InCl_3$ and $SnCl_4$ was found to increase linearly with temperature [1–5].

In contrast, growth of ZnO from zinc acetate and CdS from $CdCl_2$ both show higher rates of deposition at lower temperatures. This would suggest that the deposition is controlled by evaporation and convection (i.e mass transport to the substrate diminishing as the growth temperature increases).

It has been suggested that growth rates at low temperatures are erroneously high due to the incorporation of impurities. This has been put down to low precursor decomposition rates and low byproduct diffusion rates away from the substrate, but no firm evidence has been presented to support this. At higher temperatures these two processes are rapid and thinner films result.

Film adhesion breaks down when low growth temperatures are used possibly due to a lack of energy available for strong intra-film and film-substrate bonding. Solvent from the process may also lead to the film cracking.

Film morphology is affected by temperature and film surfaces are usually smoother at intermediate temperatures, above and below which the surfaces become rough. Film roughness has also been found to increase with increasing film thickness [12,15]. The choice of growth temperature also determines whether the resulting film is amorphous or crystalline. For example deposition of SnO_2 from $SnCl_4$ has yielded amorphous films between 200°C and 350°C. Above this temperature the deposits were crystalline.

For $CuInS_2$ growth substrate temperatures below 250°C produced amorphous deposits. As the growth temperature was increased the crystallinity improved gradually. The growth temperature can also affect the preferred orientation of the films. In the deposition of CdS films at substrate temperatures ranging from 285 - 450°C the XRD intensity of the (0002) increased as the growth temperature increased. At a temperature of 450°C the (0002) plane had become dominant [16].

In a more recent X -ray diffraction study of CdS films grown by spray pyrolysis, the degree of preferred order of the (0002) plane was found to vary with growth temperature. An increase in this orientation takes place between 375°C and 460°C. Therefore preferred order develops and changes with growth temperature [14].

There are other examples of a change in the preferred orientation with growth temperature. Tin oxide films grown at 350°C possessed a $(20\bar{2}0)$ preferred order. However as the growth temperature was increased the preferred order changed to $(11\bar{2}0)$. Increasing the temperature yielded films having a random orientation of crystallites.

A change in the growth temperature can affect the lattice type of a material. For CdS growth a variation in the crystal structure was observed with changes in the growth temperature. Both the cubic zincblende and the hexagonal wurtzite structure were found in sprayed CdS films. The relative proportion of each type of structure is a function of the growth temperature and between 375°C and 460°C the hexagonality

increases to 90% (see references to CdS in appendix 1).

Grain size and grain growth were also affected by growth temperature. As the growth temperature was raised from 240°C to 450°C the grain size increased markedly (see references to CdS in appendix 1).

When very low growth temperatures are used, and when the precursors are thermodynamically stable with respect to decomposition to the related oxide, contamination by anionic species such as chloride may result. The latter has been detected in concentrations as high as 40% in the CdS films grown from $CdCl_2$ [17].

Auger analysis of sprayed CdS and ZnO films showed a higher surface concentration of chloride compared to the bulk as a result of spray cooling effects [18,19]. Chloride is a recrystallisation flux and films deposited using chlorine containing precursors at lower temperature may have larger grain sizes [20].

3.5.2 Growth Ambient

The atmosphere in which spray pyrolysis takes place has an influence on the properties of the sprayed film. Spraying non - oxide films in air may give rise to oxidation of the film material. Oxygen can be incorporated in the film itself or can be absorbed at grain boundaries. This may affect the electrical properties of the films as oxygen often gives rise to surface trapping states [21].

In order to minimize the oxygen content in non - oxide films, oxygen free nitrogen was used in the growth of ternary chalcopyrites. This approach does not work for CdS [22.23]. Correspondingly the use of an N_2 ambient in the growth of oxide films has the effect of producing an oxygen deficiency.

3.5.3 Substrate Effects

When spray pyrolysis of a material is undertaken on a crystalline substrate it has been shown that the overlayer can be crystalline as well. This can occur for CdS growth on several substrates (i.e CdTe , Al_2O_3 and SiO_2). The CdS was (0002) oriented [17]. On the other hand on amorphous substrates it is likely that initially the film growth will also be amorphous but that with increasing film thickness the films become crystalline.

Growth rates of the same material may in addition differ when different substrates are used. This was found to be the case for CdS and $CuInS_2$ growth [24]. This is due to the different sticking coefficients of the coalescing material on the different substrate orientation.

The sticking coefficient is a measure of the probability that clusters of material remain on the substrate and contribute to the overall film thickness rather than evaporating and leaving the substrate.

3.6 Chemical Aspects

3.6.1 Main Source Precursors

As already outlined in section 3.2 the types of materials used are inorganic salts such as chlorides, nitrates, and acetates and the acetylacetonates and the alkoxides. The requirements for a suitable precursor have already been outlined and they rule out pyrophoric materials such as $Zn(Et)_2$, $In(Me)_3$, and $Al(Pr^i)_3$ which are too reactive. The precursor used affects the film quality and the right precursor can be found only by trial and error (e.g the example of cadmium chloride and acetate) by spraying over a range of different growth temperatures and under different conditions.

3.6.2 Dopants

The addition of a dopant precursor to the main precursor is made to enhance the resultant film properties in a beneficial way through the incorporation of impurity species into the film. The addition of indium to ZnO films for example improves the film conductivity [25], and in small quantities (0.5 atomic percent) improves the film transparency, but in larger quantities reduces it (4 atomic percent) [26]. The addition of dopant can also result in a shift in the bandgap at high doping levels when the semiconductor becomes degenerate.

Dopant impurities can also act as a flux for grain growth. Indium and chlorine act in such a way in CdS, as does Sb in SnO_2. Dopant impurities can also influence the preferred order and crystallinity of deposited films.

Dopants can also confer chemical resistance to a film. Additions of $AlCl_3$ to solu-

tions of $CdCl_2$ and thiourea mixtures achieve this through the segregation of Al_2O_3 at grain boundaries in CdS [1,20,27].

3.6.3 Cation : Anion Ratio

Variations in the cation to anion ratio in the spray solution can have an influence on the stoichiometry, preferred orientation, crystallinity and the microstructure of the films.

In the growth of CdS it has been observed that excess sulphur increases the conductivity. Improvements in optical transmission have also been observed [28].

In the growth of stoichiometric $CuInSe_2$ excess selenium is required, and the relative atomic ratios in the solution are 1:1:2.3, indicating that the rate of selenium evaporation is higher [29]. Adjustment of the cation to anion ratio may be necessary when attempting the growth of films of the same stoichiometry at different temperatures. For example the spray pyrolysis of ZnCdS at 450°C yields cadmium rich films, whereas at 200°C the films are approximately stoichiometric [30]. It has also been reported that the Cd:S ratio in the spray solution affects the preferred order in the films obtained [31].

3.6.4 Precursor Strength

There are also trends to be observed when solutions of different concentrations are used to spray a specific film material. The use of weaker solutions obviously means that film growth takes longer, but the advantages are that the film surfaces are smoother, and the films are more transparent. Grain size is usually larger when weaker solutions are used, compared with concentrated solutions, since there are fewer individual clusters nucleating on the surface, and it is also possible for individual clusters to grow out. However an excess of solvent may affect the film structure detrimentally.

3.6.5 Solvents

The function of the solvent is to dissolve a precursor or precursors, and enable them to be transported to the substrate. It must then evaporate off leaving the precursor(s) to decompose. The use of zinc acetate in different solvents resulted in different

growth rates of ZnO. The use of different solvents also changed the film resistivity and transmission[32].

Zinc acetate sprayed in methanol gave the least resistive films ($\rho \approx 5\times10^{-5}\Omega$m) overall. The use of zinc acetate in water gave films having resistivities of 0.018 Ωm [32]. Oxygen containing solvents can work to oxidise films during film growth and where polar solvents are involved ionization and/or decomposition of precursors may occur. Non - polar solvents such as toluene will not interact strongly with the precursors, and consequently the behaviour of precursors in such solvents will be more predictable than that in polar solvents.

3.7 Review of the Spray Pyrolysis of ZnO

Zinc oxide has been grown by spray pyrolysis for many years. One of the first investigations was by Nobbs and Gillespie who used zinc acetate as a precursor at a substrate temperature of 550°C [33]. They measured the spectral transmission, film thickness and film conductivity. The films were undoped and highly resistive. Nuikura used $Zn(NO_3)_2$ as a precursor, again the films were undoped and highly resistive [34]. Aranovich et al. [35] also grew ZnO using $ZnCl_2$ and $Zn(acetate)_2$ at temperatures between 300°C and 400°C. The optical quality of the films grown using zinc acetate [18,36] was better. The substrates used were either Corning glass or alkali glass. In the seventies there were relatively few attempts to grow zinc oxide using spray pyrolysis. In the eighties a much larger number of attempts were made to grow ZnO in a more controlled way. The dark resistivity in the as-deposited state was around 0.1 Ωm while annealing in hydrogen reduced the film resistivity to $10^{-4}\Omega$m. More recently zinc nitrate was used to make ZnO films for photoelectrochemical cells. The films had a transmission of 90% to 95% in the visible region and a bandgap of 3.2 eV. Their resistivity decreased to $10^{-3}\Omega$m after annealing [37]. ZnO has also been grown in an undoped form on InP by Eberspacher. After annealing the resistivity varied from 6-$8\times10^{-5}\Omega$m with a transmission of approximately 85% [38]. In the field of doped ZnO attempts have been made to produce ZnO:Al and ZnO:In by adding $InCl_3$ or $AlCl_3$ to

the spray solution. The resulting film resistivities were of the order of $10^{-4}\Omega$m - $10^{-5}\Omega$m for ZnO:In and $10^{-2}\Omega$m for ZnO:Al with an average transmittance of 85% [24,25]. The carrier concentrations for ZnO:In films were typically 10^{25} m^{-3} while for ZnO:Al films the typical concentrations were 10^{23} m^{-3}. Spray pyrolysis of ZnO generally produces films that in the as-deposited state are slightly inferior to sputtered layers. However spray pyrolysis is cheaper, easier to use, and safer and faster than sputtering when an atmospheric pressure based system is used. The different methods of producing zinc oxide are compared in section 3.8.

ZnO has also been deposited on p-type substrates to produce solar cells. ZnO/CdTe junctions are one example and have been prepared by Aranovich et al. [35]. The cell efficiency was typically 8.8%. The CdTe was single crystal and the precursors used were zinc acetate and zinc chloride. Optimum results were obtained at 460°C. The as-deposited resistivity was $10^{-1}\Omega$m for undoped films and 10^{-3} - $10^{-5}\Omega$m for annealed undoped and indium doped films.

Tomar and Garcia [39] produced an all sprayed ZnO/$CuInSe_2$ solar cell using zinc chloride and zinc acetate. The optimum substrate temperature was 375°C. The zinc oxide layer which was undoped had a resistivity of $10^{-3}\Omega$m. The efficiency was only 2% however.

A more serious attempt to use ZnO as an n-type layer for a solar cell was made at Stanford, where ZnO/InP solar cells were made with efficiencies of 14%. The InP was single crystal [40].

Work in Durham on the spray pyrolysis has been sponsored by ICI Plc and had been in progress since 1986. The first investigations used zinc acetate and zinc chloride at a growth temperature of 400°C.

The as-deposited films had resistivities of 0.5 MΩm which after annealing fell to $10^{-4}\Omega$m. The film transparency was 90%.

Later work concentrated on zinc acetate and indium chloride. Typically the films had resistivities of the order $1.3\times10^{-5}\Omega$m with carrier concentrations of 10^{26} m^{-3} and

mobilities of 19 $cm^2\ V^{-1}\ s^{-1}$ [41].

This programme has continued with the use of zinc acetylacetonate ($Zn(acac)_2$ or $Zn(acac)_2.H_2O$) since this offered the prospect of growth at a lower temperature where the nitrate, acetate, and chloride required higher growth temperatures to promote pyrolysis.

In parallel with the present study, work was carried out by P.D. Coates and A.J. Banister (Department of Chemistry) to synthesise, characterize, and purify new low temperature precursors for the deposition of zinc oxide films in conjunction with the Applied Physics Group in a three year programme. They successfully synthesised the derivatives $Zn(acac)_2.H_2O$ and $Zn(acac)_2$.2,6 Lutidine which were found to be of higher purity than the forms commercially available. These were used for the deposition of ZnO in the Applied Physics Group. $Zn(formate)_2$ was also prepared and used by the Department of Chemistry to produce ZnO. This latter material has the advantage in that it can be sprayed in water whereas $Zn(acac)_2$ is used in alcohol.

3.8 Other Methods of Depositing Films

There are of course various other methods of depositing thin films of zinc oxide. These include CVD and MOCVD which involve the transport of highly volatile organometallic materials in a suitable gas. The zinc containing material is frequently dimethyl or diethyl zinc and the carrier gas hydrogen. The reactants are transported into a heated chamber where thermolysis of the zinc -carbon bond occurs, typically at substrate temperatures in the range 200 - 500°C.

The substrates are often sapphire, and the growth is epitaxial and single crystal. Typical additions to promote the reaction are H_2O, N_2O, or CO_2.

Another important technique is sputtering which has been used extensively. The film material to be deposited is formed as a target. Bombardment of this target from an appropriate plasma results in the ejection of atoms which travel through the plasma and condense onto the substrate to form a thin film.

Sputtering involves the formation of high energy clusters of a critical size diffusing

across the surface and coalescing. The particles carry enough energy to aid recrystallisation of the film material , thus increasing the orderliness of the film. Lateral mobility of condensing particles is known to enhance film properties [42]. The high energy particles have a strong influence on the substrate surface causing roughness, penetration, and imperfections.

3.9 Chapter Three References

(1) Mooney J.B., Radding S.B., *Ann. Rev. Mater. Sci., 12*, 81, (1982).

(2) Chopra K.L., Kainthla R.C., Pandya D.K. and Thakoor A.P., *Physics Of Thin Films, 12*, 167. (1982).

(3) Albin D.S., Risbud S., *Advanced Ceramic Materials, 2(3a)*, 243, (1987).

(4) Pulker H.K., Coatings On Glass, Thin Films Science And Technology, 6, Elsevier, (1984).

(5) Ortiz A., Garcia F.J., *Prog. Cryst. Growth Chara., 17*, 171, (1988).

(6) Marshall W.R. Jr, *Atomisation and Spray Drying, 2(50)* Chemical Engineering Monograph, (1954)

(7) Muirhead J., Science and Technology Of Surface Coatings, 248, Academic Press, eds. Chapman B.N., Anderson J.C., (1974).

(8) Tian Quan - Liu, Osamu Sakurai, Noboyasu Mizutani, *J. Mat. Sci.*, 21, 3698, (1986).

(9) Viguie J., Spitz *J. Electrochem. Soc., 122(4)*, 585, (1975).

(10) Kim H., Laitinen H.A., *J. Am. Ceram. Soc., 58*, 23, (1975).

(11) Pommier R., Gril C., Marucchi J., *Thin Sol.* Films, 77, 91, (1981).

(12) Shanthi E., Banerjee A., Dutta V., Chopra K.L., *Thin Sol. Films, 88*, 93, (1983).

(13) Siefert W., *Thin Sol. Films, 121*, 275, (1984).

(14) Aranovich J.A., Ortiz A., Bube R.H., *J. Vac. Sci., 16(4)*, 994, (1979).

(15) Albin D.S., Risbud S.H., *Thin Sol. Films, 147*, 203, (1987).

(16) Rajaram P., Thangaraj R., Sharma A.K. and Agnihotri O.P., *Sol. Cells, 14*, 123, (1985).

(17) Marucchi J., Perotin M., Oudeacoumar, Bougnot J. and Saveli M., 13^{th} IEEE Photov. Spec. Conf., Washington DC, 298, (1978)

(18) Aranovich J.A., Ortiz A., Bube R.H., *J. Vac. Sci., 16(4)*, 994, (1979).

(19) Ma Y.Y., Bube R.H. and Fahrenbruch A.L., *Appl. Phys. Lett., 30(8)*, 423, (1977).

(20) Grayson M., Encyclopaedia Of Semiconductor Technology, 570, Wiley, New York, (1984).

(21) Micheletti F.B., Mark P., *Appl. Phys. Lett., 10(4)*, 136, (1967).

(22) Cheng C.H., Jones K.A., Shirreffs B.F. and Geib K., *J. Electrochem. Soc., 131(2)*, 440, (1984).

(23) Gorska M., Beaulieu R., Loferski J.J. and Roessler B., *Sol. Energ. Mater., 1*, 313, (1979).

(24) Chamberlain R.R.,*Am. Ceram. Soc. Bull., 45(8)*, 698, (1966).

(25) Streydio J.M., Cossemont D., *J. Cryst. Growth, 72*, 57, (1985).

(26) Major S., Banerjee A., Chopra K.L., *Thin Sol. Films, 108*, 333, (1983).

(27) Thakoor A.P., Chopra K.L., Raj B., *Thin Sol. Films, 83,* 231, (1981).

(28) Bougnot J., Perotin M., Marucchi J., Sirkis M., Savelli M., 12*th* IEEE Photovoltaic Spec. Conf., NY, (1976).

(29) Loferski J.J., Case C., Kwietniak M., Sarro P.M., Castener L., and Beaulieu R., *Appl. Surf. Sci., 22/23,* 645, (1985).

(30) Reshamwala, Hsu W.B., Burton L.C. and Singh V.P., 3^{rd} EC Photovoltaic. Solar Energy Conf., Carres, 787, (1980).

(31) Chamberlain R.R., Skarman J.S., *J.Electrochem. Soc., 113(1),* 86, (1966).

(32) Guillemoles J.F., Vedel J., Livicot D. and Cowache P., 10^{th} European Photovoltaic Solar Energy Conf. And Exhibition, Lisbon, Portugal, 8 - 12 April, (1991).

(33) Nobbs J., Gillespie F.J., *J. Phys. Chem. Solid, 31(10),* 2353, (1970).

(34) Nuikura I., Watanabe H. and Wada M., *Jpn. J. Appl. Phys.,, 12(5),* 657, (1973).

(35) Aranovich A.L., Golmayo D., Fahrenbruch A.L. and Bube R.H., *J. Appl. Phys., 51,* 4260, (1980).

(36) Fahrenbruch A.L., Aranovich A.L., Courreges F., Chynoweth T. and Bube R.H., *13^{th} IEEE Photov. Spec. Conf.,* (1979).

(37) Bahadur L., Hamdani M., Koenig J.F. and Chartier P., *Solar Energy Materials, 14,* 107, (1986).

(38) Eberspacher C., Fahrenbruch A.L. and Bube R.H., *Thin Sol. Films, 136,* 1, (1986).

(39) Tomar M.S., Garcia F.J., *Thin Sol. Films, 90,* 419, (1982).

(40) Eberspacher C., Fahrenbruch A.L. and Bube R.H., Conf. Proc. 17^{th} IEEE Photov. Spec. Conf., Kissimmee, U.S.A., (1984).

(41) Oktik S., Russell G.J., Brinkman A.W. and Woods J., *Properties of undoped films deposited by spray pyrolysis,* (1988).

(42) Nanto H., Minami T., Shooj S. and Takata S., *J. Appl. Phys., 55 (4),* 1029, (1984).

Chapter Four

Experimental Details

4.1 Introduction

This chapter contains the experimental details of the deposition of undoped and doped zinc oxide and includes a description of the apparatus used and the deposition procedures.

The choice and preparation of substrates and precursor solutions are then described. Finally the techniques used to characterize ZnO thin films and the underlying principles are outlined together with a description of the equipment used and the practical aspects of applying the technique to ZnO.

4.2 Spray Apparatus

The first films were grown using a manually operated spray system. This was later modernised into an automated system driven by a control unit when the conditions for successful film growth of undoped films had been established. Doped ZnO was grown using the automated system.

The manual and the semi-automatic spray systems used in this project were based on a pneumatic piston pump and spray gun that were made and marketed by Wagner Spray systems (Germany). The atomisation of the spray was a combination of centrifugal and pneumatic methods. The rest of the system was manufactured in the University workshops.

The pump was supplied and driven by high pressure oxygen-free nitrogen gas at the start of the project but later with compressed air after the installation of an air compressor. The gun was supplied with three lines. They were:

(1) A connection from the pump to the gun for the supply of pressurised solution to the gun and resulting in the centrifugal/pneumatic atomisation of the solution into a fine spray.

(2) A N_2 gas line for the gas shroud for the entrainment and pneumatic atomisation of the spray.

(3) A gas supply to operate a pneumatic valve on the spray gun to switch the solution flow on and off.

The main component besides the spray pump and gun was the substrate table which included motors that allowed it to move in a trochoidal motion (simultaneous translational / rotational motion) under the spray to aid thickness uniformity. The substrate heating (4×450W) was supplemented by separate heating lamps (in - flight heating) hung above and on either side of the substrate table. These were initially each powered by 750W tungsten lamps. The power output to the lamps was controlled (and therefore the temperature) by a Eurotherm 818 temperature controller which monitored the temperature on the substrate by means of a Pt - Rh thermocouple probe which was placed in close proximity to the substrates. The probe was calibrated using boiling water.

The substrates in the majority of cases were 5 3×1 inch alkali glass slides. The other components were the feed bottles that contained the precursor solution together with an in - line filter to sieve out undissolved material in the precursor solution large enough to cause blockages in the spray gun. The spray gun was fitted with a 0.007 in swirl type centrifugal pressure nozzle.

Figure 4.1 shows a schematic diagram of the manual spray system. The substrate top, spray gun and optical in-flight heating were all enclosed in a spray cabinet made of stainless steel while the pump and gas and flow control system (including the pump and the feed bottles) were in a separate enclosure. Access to both was through hinged doors (initially glass but changed to stainless steel afterwards). There were air intakes in the sides of the spray cabinet and twin exhaust outlets to extract the byproducts through carbon filters out of the spray area. Gas flow was switched on and off and the flow directed using Whitey manual valves marked by circles on the figure. The exact flow rate was controlled by pressure regulators and measured by flowmeters. The nitrogen gas could in this way be made to pass through a water bubbler or a drying column or straight from the bottle so that film growth could be carried out in one of

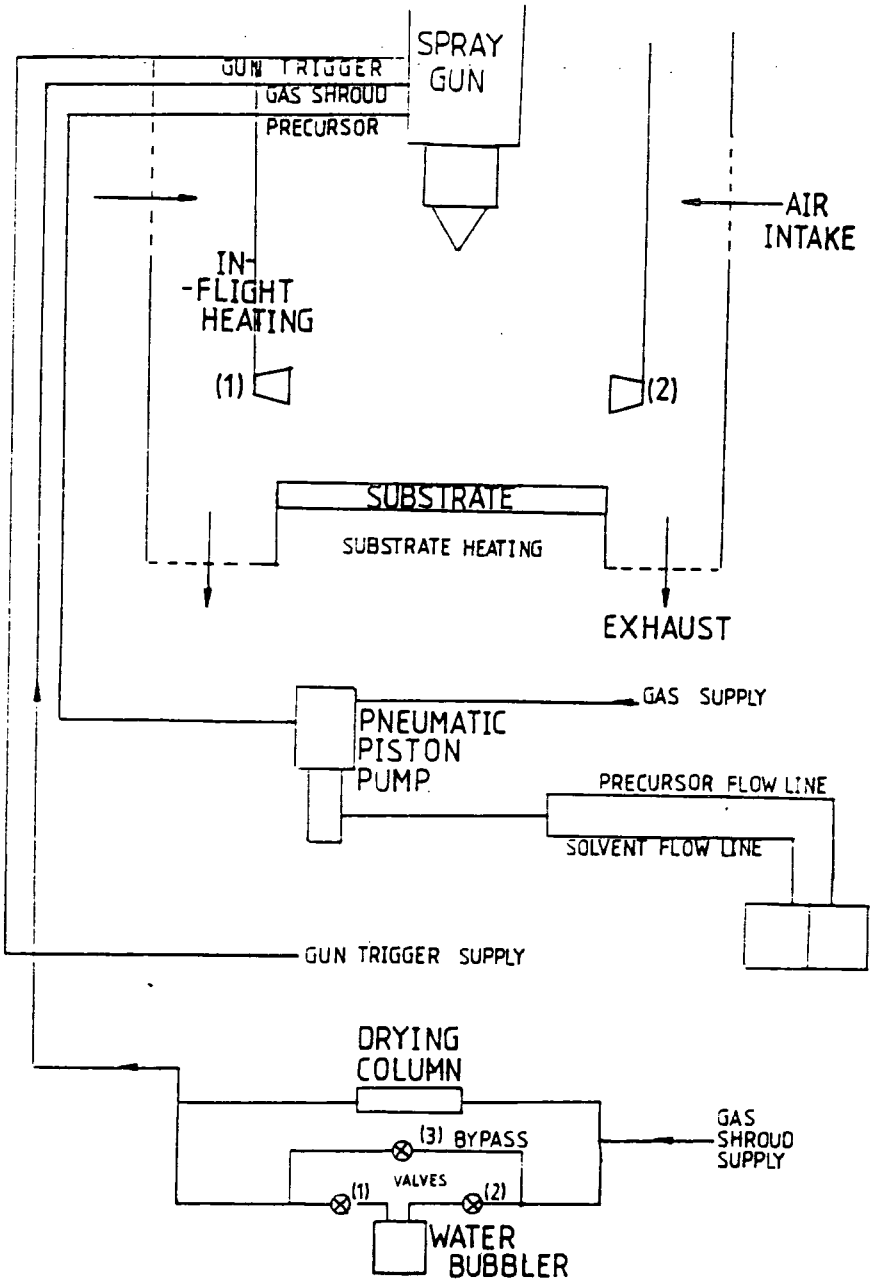

Figure 4.1 Schematic diagram of the manual spray kit.

three ambients (i.e water saturated, dry, or variable moisture content/ as - supplied). Solution flow was controlled by varying the gas pressure to the pneumatic piston pump using in - line flowmeters. Solutions were taken up by the pump from the feed bottles during deposition of ZnO through $\frac{1}{4}$ in PVC piping.

In March 1990 the spray kit was modernised. This involved the addition of two major components. They were the controller system (University) and a bank of remotely controlled pneumatic valves (Valeader Pneumatics). The kit also included air actuated bellows valves (Nupro - Teesside Valve) for the control of the flow of liquids and gases and for the activation and deactivation of the spray gun. In this work, solution and gas flows through the spray system were controlled by the controller system through direct electrical connections to a bank of solenoid actuators that in turn operated air actuated valves as shown in figure 4.2. In particular the flow of nitrogen shroud gas could be controlled automatically and remotely so that it could be made to pass through a water bubbler, a drying column or pass through as a gas of variable moisture content straight from the gas bottle. Therefore film growth could be carried out in the presence of a saturated gas shroud or a dry gas shroud or as an as-supplied gas shroud. The controller was designed so that the path of the solution and gas could be chosen by switches. Switches on the logic controller allowed the choice of gas shroud to be made. When a switch was changed the circuitry inside the controller translated into several electrical pulses which were sent to the bank of solenoid actuators. These actuators, when triggered by an electrical pulse, either opened or closed one or more air actuated valves and allowed a high pressure gas supply to trigger the air actuated bellows valves.

The spray system was also fitted with safety interlocks which were linked from various key parts of the apparatus to the controller.

The circuitry in the logic controller was designed so that there were three possible conditions. The first condition was that spraying would not be permitted with heating on unless both sets of doors to the spray enclosure were closed and the extract was switched on.

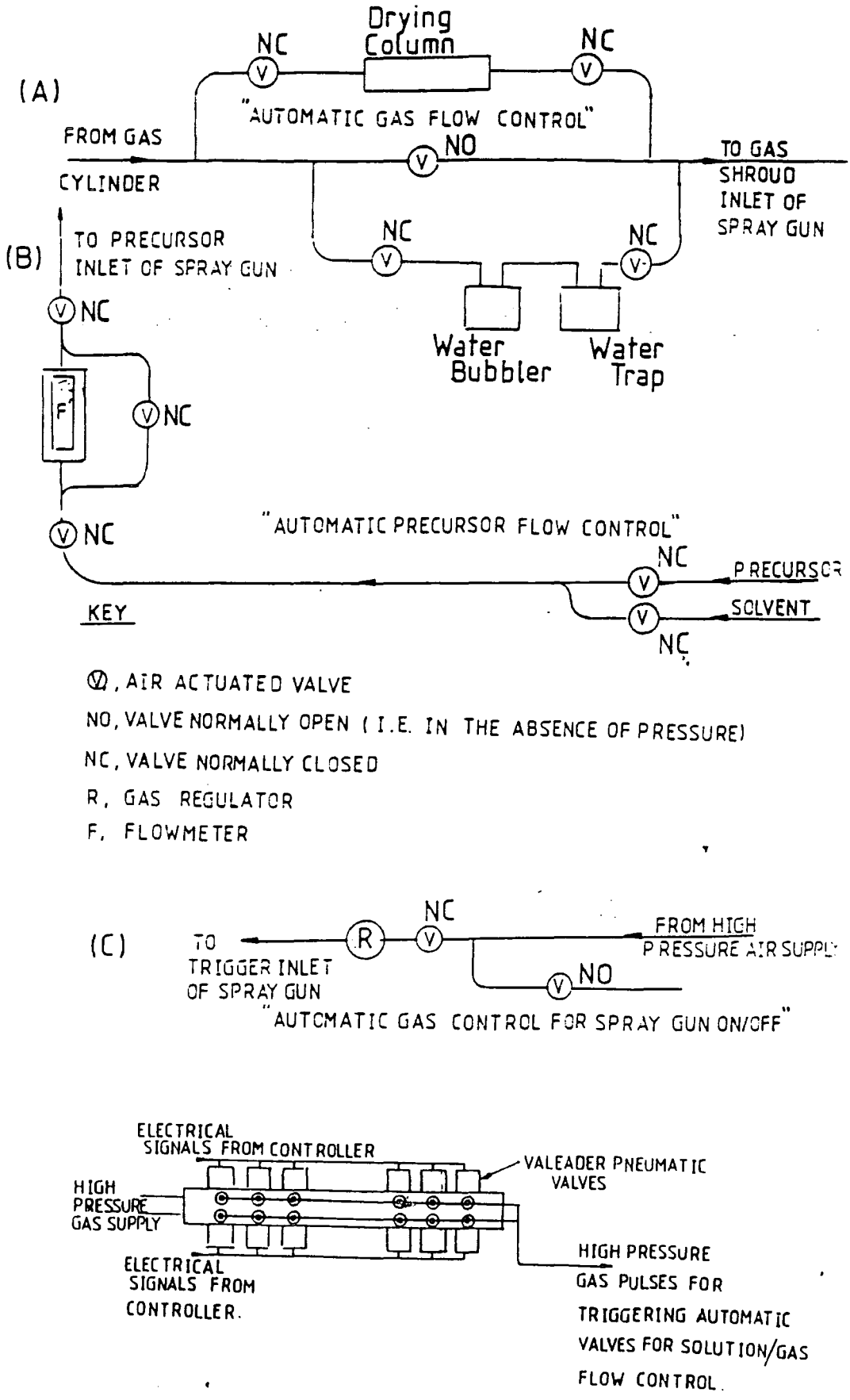

Figure 4.2 Schematic outline of the valve system in the automated spray kit.

The second condition was that spraying was not permitted with the doors open unless the heating was off.

The third condition was that heating with the doors open was not permitted unless the spray was switched off.

Other safety features included the flooding of the substrate heating lamps with nitrogen to prevent overheating and oxidation of the lamp contacts, which would result in the burn out of the lamps and a reduction in the possible working life. This was also a precaution against the build up of flammable alcohol vapours and their mixing with oxygen.

All gas and solution flows were monitored using in - line flowmeters and $\frac{1}{4}$ in PVC and stainless steel tubing.

The controller also incorporated the Eurotherm temperature controller and the control for the lateral and rotational movement for the deposition /substrate platform.

4.3 Operating Conditions - Manual System

The nitrogen supply to the manual kit was split to supply the pump for the pressurisation of precursor solution and the nitrogen gas shroud for the pneumatic atomisation and entrainment of the spray. The pressures used were 2 bar in both cases while the pressure to the spray gun trigger was 10 bar. The gas and the solution flows were 140 l min^{-1} for the nitrogen shroud and 40 - 50 cm^3 min^{-1} for the precursor flow. The flows of gas and precursor solution are shown in table 4.1.

This system was used for the growth of undoped zinc oxide. The choice of whether to use a wet or dry gas shroud was made manually. When a wet ambient was used the water bubbler was filled with approximately 120 g of water.

The operational steps were as follows :

(1) The first step was to switch on the nitrogen gas shroud to the spray kit from the gas bottle having cleaned out the pipelines using pure alcohol.

(2) The shroud gas was passed either through the water bubbler or the drying column. Where the water bubbler was used approximately 120 g of water was employed.

OPERATING CONDITIONS - MANUAL SPRAY KIT			
Location in spray system	Pressure/(bar)	Flow/(cm^3 min^{-1})	Fluid
N_2 pressure to gas shroud intake of spray gun	2	140,000	N_2
Air pressure to pneumatic pump	2	static	N_2
Air pressure to spray gun trigger	10	static	N_2
Solution pressure to precursor intake of spray gun	-	40 - 50	alcohol

Table 4.1 Summary of the operating conditions for the manual spray kit.

The required volume of precursor in a special bottle was attached to the feed line into the pneumatic pump. A bottle of pure solvent was also fitted on - line to the pump through an alternative route.

(3) Once the integrity of the system had been demonstrated the substrates were loaded on the substrate/deposition platform and the thermocouple placed alongside. In most cases five 3×1 in glass slides were used as shown in figure 4.3.

(4) The substrate heater was then switched on and the temperature controller allowed to automatically raise the substrate temperature to a setpoint value (± 2°C) by controlling the tungsten lamps via feedback from the thermocouple. The N_2 supply to the substrate heaters was switched on.

(5) At this point the gas flow to the gas shroud was also switched on and the spraying of pure solvent was initiated. This had the effect of lowering the substrate temperature initially (by approximately 70°C) and it was necessary to wait while the temperature controller restored equilibrium.

(6) After the system had stabilized at the desired temperature, the pure solvent was switched off and replaced by the precursor containing solution. The motors producing the lateral and rotational motion of the deposition platform were switched on.

(7) During the deposition of the thin film, checks were made on the gas and precursor solution pressures and flow where necessary. A stopwatch was normally used to measure the duration of the film growth. The thermocouple temperature was also monitored. The substrate temperature fluctuated by ± 10°C.

(8) When the appropriate volume of precursor had been sprayed the spray gun was switched off as were the temperature controller and the heating system. The motors for producing lateral and rotational growth were also switched off.

(9) The deposited films were removed from the spray cabinet and were allowed to cool down in a closed container under a flow of nitrogen.

(10) The substrate holder was cooled down using the nitrogen gas shroud.

(11) If the gas shroud to the spray gun passed through the water bubbler to produce

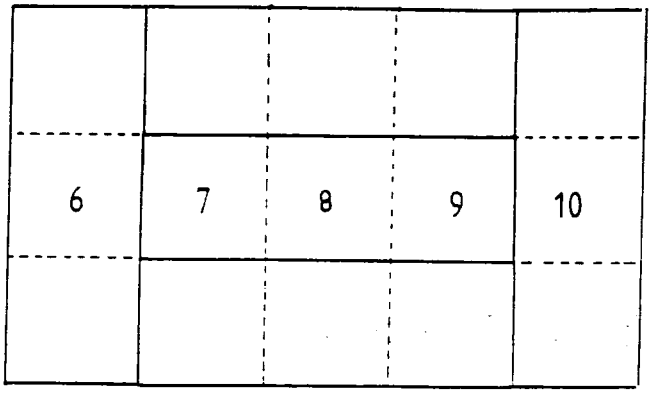

Figure 4.3 Diagram showing the substrate arrangement.

OPERATING CONDITIONS - AUTOMATIC SPRAY KIT			
Location in spray system	Pressure/(bar)	Flow/(cm^3 min^{-1})	Fluid
N_2 pressure to gas shroud intake of spray gun	2	85.000 - 90.000	N_2
Air pressure to pneumatic pump	5.5	static	air
Air pressure to spray gun trigger	6.0	static	air
Solution pressure precursor intake of spray gun	15 - 18	50	alcohol
N_2 gas supply to substrate heater	$\leq$0.5	$\approx$0	N_2

Table 4.2 Summary of the operating conditions for the automatic spray kit.

a film deposited in a wet ambient then the water left over was weighed out so that the ratio of $Zn(acac)_2.H_2O$ to H_2O could be estimated.

4.3.1 Operating Conditions - Automated System

The operating procedures used with the automated kit are shown in table 4.2. Extra nitrogen supplies were needed for the pneumatic valves and for the flooding of the substrate heaters . Typical N_2 pressure to the whole system was about 6 bar. The gas source was split up to supply the following :

(a) The gas shroud for the pneumatic atomisation and entrainment of the spray from the spray gun.

(b) The gas supply to the pneumatic pump for the pressurisation of precursor on its route to the spray gun.

(c) The bank of pneumatic valves for the control of the air actuated valves.

(d) The flooding of the substrate heater to cool lamps and to flush out oxygen.

The 2 bar pressure of gas to the pump resulted in the precursor solution being pressurised to surplus of 15 - 18 psi. The resulting precursor solution flow was always in the region 40 - 50 $cm^3\ min^{-1}$. This is high in spray pyrolysis where 2 - 20 $cm^3\ min^{-1}$ is more normal.

The choice of a high flow rate system was made due to difficulties with spray tips. The tip used (0.007 in diameter swirl-type tip) in all experiments was chosen for its block-free reliability and its relatively low flow rate compared with industrial paint spray systems.

The sequence of operations for depositing a film was essentially similar to that in the manual system. The differences were that the films were taken out immediately after deposition and cooled externally in a flow of oxygen free nitrogen. In the automatic system pure solvent was sprayed directly onto the films at full heat. After precursor flush out the spray was switched off remotely from the controller. The substrate heating was kept on along with the gas shroud to purge the systems of alcohol vapour. This was carried out for 2 - 3 minutes. After this the substrate heating was turned off and

the films were allowed to cool under a flow of dry nitrogen whether the original growth had been carried out in dry or wet nitrogen. When the temperature reading from the thermocouple on the substrate platform was 50°C or lower the films were removed from the substrate, labelled and stored in plastic coplin jars. A higher turnover of runs was achieved after automation of the kit.

4.4 Substrates and Materials

In most runs the substrates used were microscope slides. They contained alkali ions (mostly sodium) as the ESCA spectrum in figure 4.4 shows. Diffusion of these ions into the film could be detrimental to film conductivity. However diffusion between film and substrate is only significant at temperatures above 420°C [1].

The glass slides were cleaned rigorously in the following sequence. The steps are outlined as follows together with the action of treatment on the substrates.

(a) Agitation in $HNO_{3\ (aq)}$ for 30 minutes. This leaches alkali ions from the substrate surface.

(b) Reflux in trichloroethane. This acts to remove dirt and grease from the substrate surface.

(c) Agitation in caustic alkali for 30 minutes. This acts to chemically degrade any persistent organic residues attached to the substrate surface.

(d) Agitation in propan-2-ol for 30 minutes. This acts to remove residues of all previous materials and also leaves the substrate surface stain free and uniformly clear and smooth.

(e) Reflux in propan-2-ol for 24 hours. This is a higher temperature version of the cleaning process in (d).

This procedure was found to give uniformly clean, clear and smooth substrates. As stated earlier one of the major objectives of the work was to deposit films on plastic. That most commonly used was Upilex provided by ICI Plc, the monomer structure of which is shown in figure 4.5.

This type of material is called a polyimide and decomposes at temperatures above

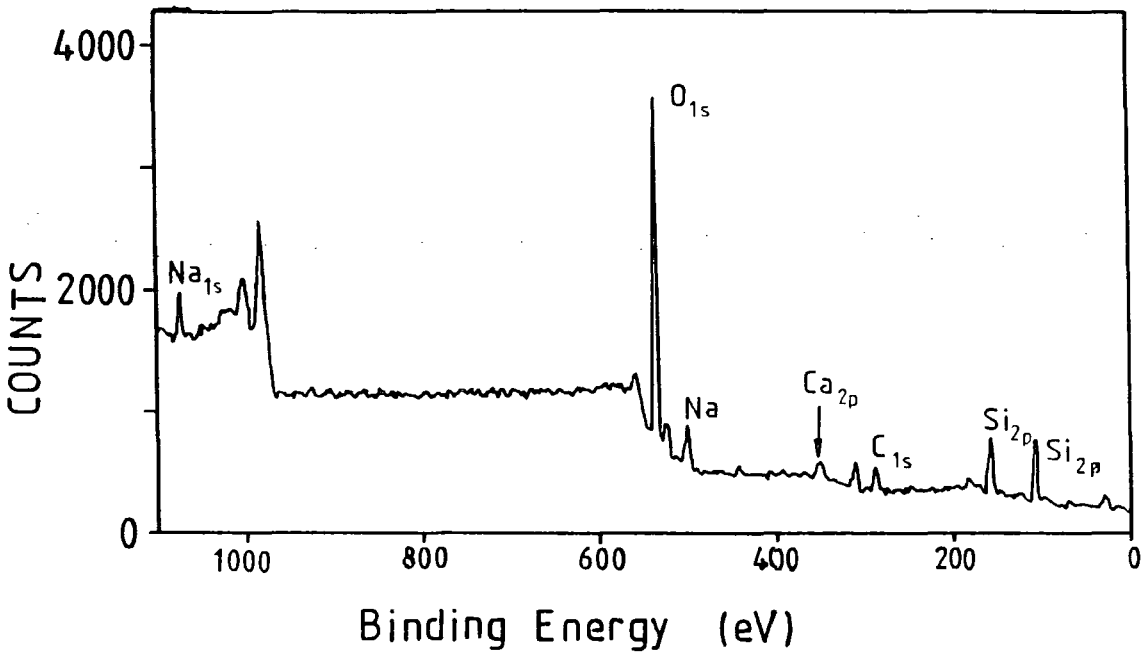

Figure 4.4 ESCA spectrum of the substrate material (glass slides).

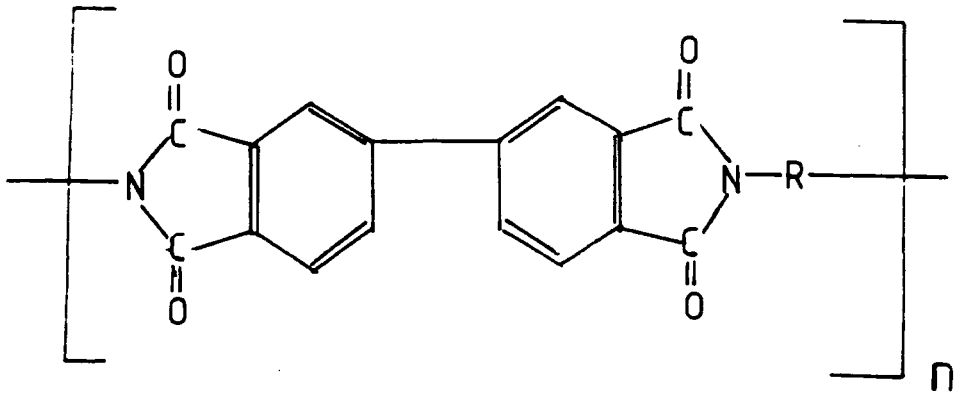

Figure 4.5 Chemical structure of Upilex polyimide.

600°C. It is also insoluble in organic solvents and resistant to virtually all chemicals. The surface roughness of the Upilex is less than 3 nm. No cleaning treatments were carried out prior to its use as a substrate material as attempts to do so did not improve the film quality.

4.5 Choice of Precursors

In previous work on the growth of zinc oxide by spray pyrolysis in Durham the precursors used were $ZnCl_2$ (melting point 237°C) and zinc acetate (melting point 283°C), and of these two materials the acetate gave the superior results. However the stability and volatility of both these materials meant that growth temperatures below 270 - 300°C did not give ZnO films with acceptable film properties. Since the aim was to produce conducting zinc oxide at low temperature a variety of other precursors was investigated in cooperation with the Chemistry Department. Of them $Zn(acac)_2$ was chosen because of its lower stability (decomposition temperature 191°C) and higher volatility (melting point 125°C). However the work of Coates and Banister [2] showed that $Zn(acac)_2$ polymerizes to form a complex material which is insoluble in solvents. Banister and Coates demonstrated that a monohydrate adduct of $Zn(acac)_2$ was stable as a monomer and readily soluble in organic solvents. Therefore $Zn(acac)_2.H_2O$ (molecular weight 281 g) prepared in Chemistry was adopted. The solvent used was propan-2-ol in AnalaR or reagent grade. Precursor solutions were thoroughly filtered before use.

4.6 Characterisation Techniques

4.6.1 Adhesion of Films to Substrate

This was a simple qualitative test introduced to see whether ZnO films were adherent to their substrate. Sellotape was applied to the ZnO film surface, then pulled away firmly and quickly in one stroke. Examination of the tape and the film surface was required to see if any film material had come away with the tape and if significant damage had been caused in the film. This test was found to be reliable and was used on both undoped and doped ZnO films.

4.6.2 Visual Appearance of ZnO Films

All films were examined by eye for their transparency, colour, smoothness and the uniformity of these qualities. The optical transmission of a number of films was measured as a function of wavelength using a Perkin Elmer Spectrophotometer. The transmission spectrum was analysed as described in appendix 2 to obtain values of refractive index, extinction and absorption coefficients.

4.6.3 Film Thickness

The thickness of the films was measured using a profilometer. This required the formation of a step across which the stylus of the profilometer could be drawn. The step was produced by etching in dilute HCl.

The measurement of the step was made using a Tencor alphastep 200 stylus profilometer. The principle of the instrument relies on a stylus traversing the step and recording the change in height. The principle of operation of the machine is shown in figure 4.6. Any number of measurements were made ranging from 5 up to 12 depending on the sample. From these measurements an average can be calculated together with an estimate of the error.

Each of the five substrate slides was labelled and divided in 1 in^2 sections as shown in figure 4.3. The variation in thickness across the substrate was assessed by comparing the thicknesses of areas 7, 8 and 9 and of areas 6, 8 and 10. Thicknesses from the central area, 8, were used to generate ln(thickness) vs. 1/T plots.

The surface morphology of the films was examined in a Cambridge Instruments S600 scanning electron microscope in the secondary emission mode [3].

4.6.4 Surface Roughness

A surface roughness measurement was made on some samples using the Tencor alphastep 200 stylus profilometer.

The instrument takes readings as it moves along the surface and calculates an average value.

Consider for example a journey from point A to D (figure 4.7) on a theoretical

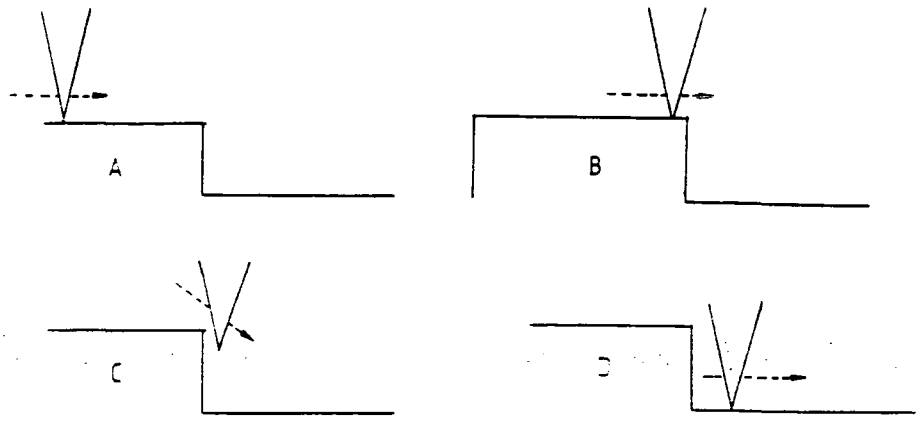

Figure 4.6 Principle of operation of an alphastep profilometer.

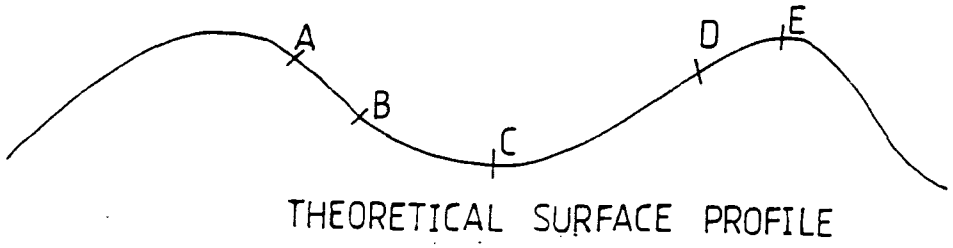

Figure 4.7 Theoretical profile of a film surface.

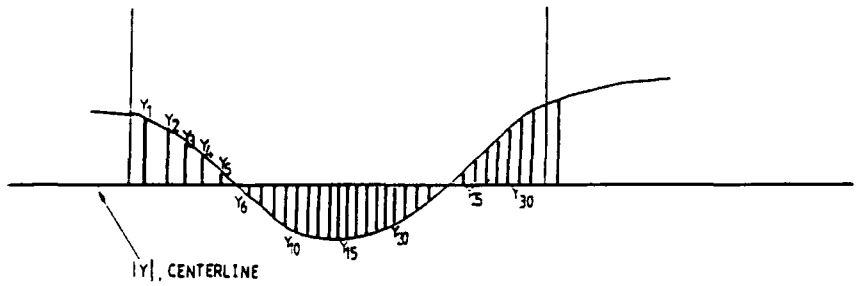

Figure 4.8 Representation of the alphastep measurement as the stylus traverses the film surface.

rough film surface. The stylus traverses from A to B recording a decrease in the height and continues to do so until C when for a short distance the film surface is effectively flat. However the film surface rises again and for each successive reading through the stylus a relative increase is recorded individually. A, B C, and D are called profile heights. Together they form a surface profile.

In order to calculate surface roughness the alphastep 200 software/hardware combination measures the profile heights without any reference in one case. The sum of those profile heights is taken and divided by their number. The result is labelled |Y|. This is called the centreline on the cross section through the rough film surface and represents an average. The software also measures the profile heights relative to the first point on the screen which acts as zero. Y_1 to Y_n are the values of the subtraction product of profile heights measured using the first measured point of the scan as the reference and |Y| as the centreline. The profile of the points is summed together and divided by n, giving the surface roughness, R_a,

$$R_a = \frac{y_1 + y_2 + y_3 + ... + y_n}{n} \tag{4.1}$$

where y_1 to y_n are the absolute values of Y_1 to Y_n. The measurement is shown in figure 4.8.

$$y_1 - y_n = profileheight - |Y| \tag{4.2}$$

4.6.5 Crystal Structure

The crystal structure of the films was assessed by reflection high energy electron diffraction (RHEED) and X-Ray diffraction (XRD). A comprehensive review of these techniques is available [4-6]. RHEED studies were carried out in a JEM 120 transmission electron microscope (TEM). The technique was used to assess the crystallinity and the degree of preferred orientation of crystallites. This technique samples the first few monolayers. The technique is non-destructive and characterisation takes only a few minutes.

Figure 4.9(a) is the form of a diffraction pattern observed for a polycrystalline sample of ZnO [4,7] with no preferred orientation. The pattern consists of a set of continuous concentric semi-circles. The next example of a pattern (Figure 4.9(b)) demonstrates the existence of preferred order as determined by the build up of intensity in short arcs rather than complete semicircles. Figure 4.9(c) is an idealised pattern taken from a material with a highly preferred order. Crystallinity was assessed by the examination and comparison of one spectrum with another to identify relative changes in the structure.

XRD studies were carried out using a Philips diffractometer with a Ni source and radiation with $\lambda = 1.7902$Å. The technique was used to identify the material deposited, assess the degree of preferred order and to calculate grain sizes. The radiation penetrates films microns thick and any information obtained is an average of the entire film material. Only those planes parallel to the substrate surface contribute to diffraction intensities.

The diffractometer recordings were used to confirm the presence or absence of zinc oxide by comparison of peak positions with the ASTM (American Society for Testing and Materials) index for a pure polycrystalline ZnO sample.

The comparison between the intensities of the peaks in the ASTM index for polycrystalline ZnO and that of thin film zinc oxide yields a measure of the preferred orientation of crystallites as an average of the entire film thickness. This is done by calculating the relative intensities for reflection from planes with identifiable Miller indices assigning a relative intensity of 100% to the most intense peak in the spectrum. Any relative difference in peak intensity or change in the order of peak intensity from reflection by ZnO planes when compared to the ASTM index for ZnO indicates a relative deviation from being totally polycrystalline. The grain size can also be measured by comparing the full-width half maximum of the main peak in the XRD spectrum of a ZnO film with that measured from several XRD spectra of single crystal GaAs recorded at different detector sensitivities [4,6].

The line width of the GaAs peak is taken as being representative of the instru-

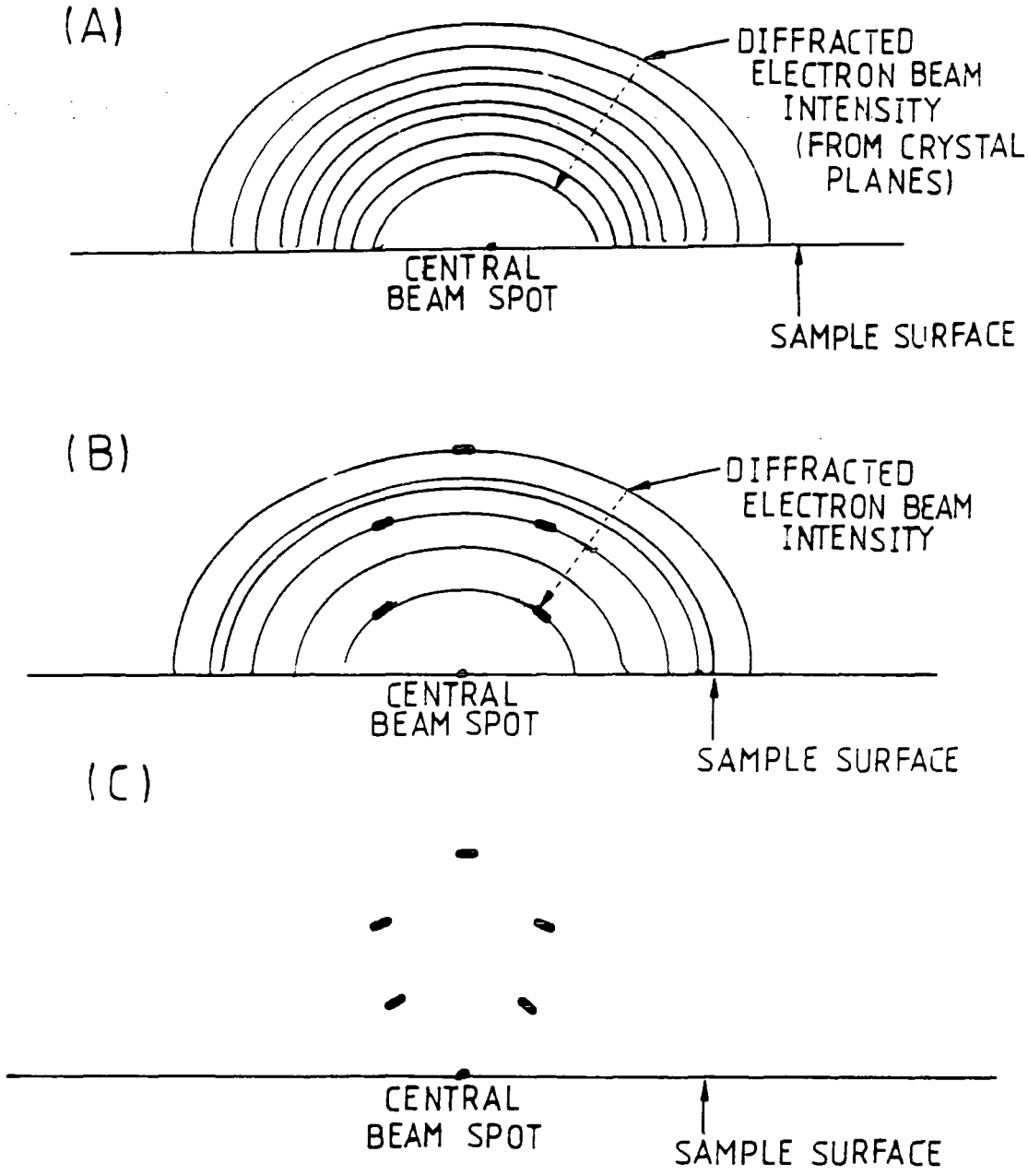

Figure 4.9 Idealised RHEED patterns for a randomly oriented sample (a), a sample with some preferred order superimposed on a background of randomly oriented crystallites (b), and a sample with a high degree of preferred order (c).

mentation broadening, on the assumption that GaAs is a near perfect crystal (infinitely thin line - in practice GaAs line widths are of a finite width).

The measurement of grain size using this method assumes that line broadening due to lattice strain is absent. The formulae are as follows :

$$\beta = \sqrt{B^2 - b^2} \tag{4.3}$$

and

$$\epsilon = \frac{\lambda}{\beta cos\theta} \tag{4.4}$$

where β is the broadening factor, b is the full width half maximum of the peak in the single crystal GaAs, B is the full width half maximum of the main peak in the spectra of ZnO films. These are all measured in radians. λ is the wavelength of the x-ray radiation, θ is the angle between the beam and the sample and ϵ is the grain size.

4.6.6 Electrical Measurements - Four Point Probe van der Pauw Technique

The resistivity of ZnO films was generally measured using the van der Pauw technique [8] and for the more conducting samples the Hall coefficient, carrier concentration and mobility were also measured.

Van der Pauw showed that the resistivity and Hall coefficent of a thin layer of a known thickness but arbitrary shape can be measured by applying four ohmic contacts (labelled A, B, C, D) of negligible size anywhere on the outermost edges of the sample. It is preferable that the contacts are equally spaced and of equal size and that the film is uniform in thickness and composition and free of pinholes as shown in figure 4.10.

To obtain the resistivity four resistances must be measured, namely $R_{AB,CD}$, $R_{BC,DA}$, $R_{CD,AB}$, $R_{DA,BC}$. The first pair of subscripts refer to the current terminals and the second pair to the voltage terminals. In all cases as the current is passed through one pair of terminals the voltage is measured across the opposite pair of terminals.

The formula for the resistivity measurement is given by :

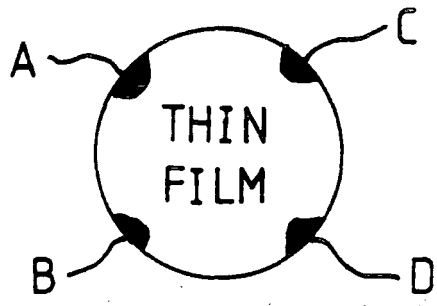

Figure 4.10. Diagram showing the ideal sample for four point probe van der Pauw resistivity and Hall measurements.

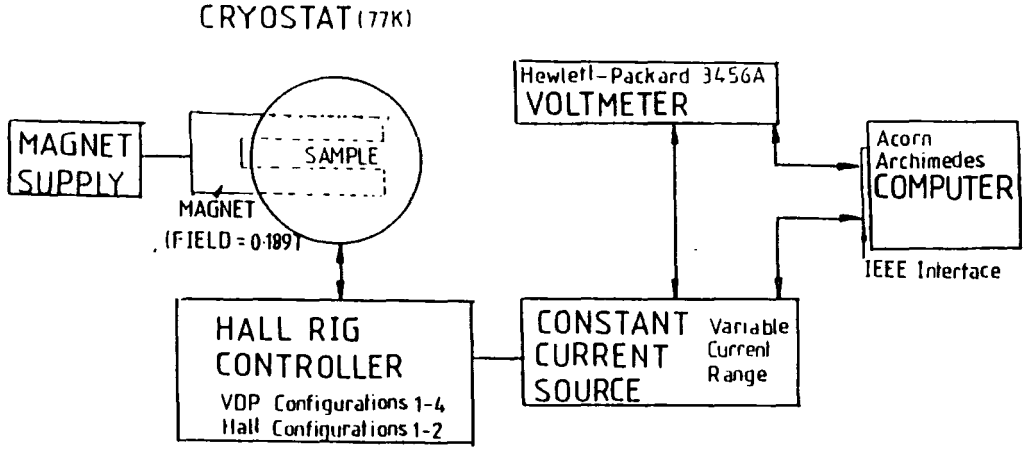

Figure 4.11. Diagram showing the outline of the Hall and resistivity measurement apparatus.

$$\rho = \frac{\pi d}{ln2} \frac{R_{AB,CD} + R_{BC,DA}}{2} f\left(\frac{R_{AB,CD}}{R_{BC,DA}}\right) \tag{4.5}$$

where d is the film thickness, $R_{AB,CD}$ and $R_{BC,DA}$ are the adjacent resistances, f is a function of the ratio of the two adjacent resistances and is equal to 1 if $R_{AB,CD} = R_{BC,DA}$. Function f satisfies the relation

$$\frac{R_{AB,CD} - R_{BC,DA}}{R_{AB,CD} + R_{BC,DA}} = \frac{f}{ln2} arcosh \frac{exp\frac{ln2}{f}}{2} \tag{4.6}$$

Replacing $R_{AB,CD}$ with $R_{CD,BA}$ and $R_{BC,DA}$ with $R_{DA,BC}$ gives a second value of ρ (4.7). The mean of the two is the best value.

$$\rho = \frac{\pi d}{ln2} \frac{R_{CD,BA} + R_{DA,BC}}{2} f\left(\frac{R_{CD,BA}}{R_{DA,BC}}\right) \tag{4.7}$$

The Hall coefficient is determined from the change in resistances $R_{AB,CD}$ or $R_{BC,DA}$ with a change in the magnetic field perpendicular to the plane of the sample ΔB.

$$R_H = \frac{d}{\Delta B} \Delta R_{AB,CD} \tag{4.8}$$

In fact the system used to measure the electrical properties was automated. The components in the system were an Archimedes computer, a constant current source, an overall controller, and a magnet and a power supply and is shown schematically in figure 4.11. The microcomputer controlled a constant current source, the magnet power supply and a bank of reed relays designed to configure the system for each of the required measurements. There were four resistivity and two Hall configurations. Voltages were measured using a Keithley digital multimeter and communicated to the computer over an IEEE bus. The system was capable of providing programmed constant currents in the range 10^{-1} - 10^{-5} A (subject to sample resistance) and variable magnetic fields up to 0.189 T.

The sample was placed in a cryostat which could be evacuated down to 10^{-4} mm Hg and cooled to liquid nitrogen temperatures. Manual measurements were also made

independently of computer control.

4.6.7 Optical Transmittance Measurements

Measurements of optical transmittance were made using a Perkin - Elmer Lambda 19 VIS/NIR Spectrophotometer. This is a computer driven system capable of measuring transmittance in the wavelength range 175 nm to 3.2μm. The spectrophotometer is a double beam double monochromator type with a tungsten source for producing visible and near infrared radiation.

The beam is split into two beams, one is directed to the ZnO sample while the other passes through a blank control (a piece of the substrate material i.e a blank slide). The path lengths over which the split beams travel are equal. The detector then compares the intensity of the two beams and calculates a transmittance for the film with respect to the substrate. Since the comparison between the sample and reference beams is made simultaneously, the instrument compensates for beam fluctuations.

The calculation of the optical constants, n and k, and the absorption coefficient from an experimental transmission curve is described in appendix 2.

The absorption coefficient α (ν) for a direct gap semiconductor is given by

$$\alpha = A^*(h\nu - E_g)^{0.5} \tag{4.9}$$

where E_g is the bandgap value, h is Planck's constant, and ν is the frequency of the incident light and A* (the Richardson constant) is given by

$$A^* = \frac{q^2(2m_h^* m_e^*)/(m_h + m_e)^{1.5}}{nch^2 m_e^*} \tag{4.10}$$

Thus the bandgap of ZnO may be obtained from the extrapolated intercept on the horizontal axis of a plot of α versus $\sqrt{h\nu}$ [9].

4.6.8 ESCA - X-Ray Photoelectron Spectroscopy

X-ray photoelectron spectroscopy was carried out at ICI Wilton by the Surface Analysis Group using a V.G Scientific instrument. XPS is a technique whereby a specimen is irradiated in ultra high vacuum by monochromatic X-rays [10]. This gives rise

to the emission of photoelectrons from the surface of the specimen which are analysed by an energy dispersive technique to provide a spectrum of electron intensity versus electron binding energy. Peaks observed in the spectrum are due to electrons which have been ejected from core levels of atoms and have characteristic energies allowing elemental analysis of the material under study. The technique is sensitive to all elements except hydrogen and analyses to a depth of 1-5 nm. The ejected electrons are detected and counted using a multi channel analyser.

The typical detection limit of any element was 0.2-0.5 atomic percent. The radiation used was Al $K_{\alpha 12}$ which has an energy of 1487 eV.

4.6.9 Photoluminescence

Photoluminescence emission spectroscopy was carried out in the Department of Applied Physics, Hull University. A schematic diagram of the experimental apparatus is shown in figure 4.12. Photoluminescence provides a non-destructive technique for the analysis of semiconductors, and gives information on free and bound excitons. It is normally applied to single crystal specimens and is suitable to identify centres responsible for the shallow donor and acceptor species by which the electrical properties are usually controlled. Measurements at low temperatures (2K) are required to obtain good resolution.

The excitation was provided by a 5W Spectra Physics argon ion laser which was focussed on to the sample with lens L_1. The emission was then passed through a mechanical chopper and focussed with lens L_2 onto the entrance slit of a SPEX monochromator. This had a focal length of 1m and a 1μm blazed grating with 1800 lines/mm. The monochromator was controlled using a SPEX compudrive system linked to a Victor computer and could be scanned using speeds from 0.002 A/s to 160 A/s. The light dispersed through the monochromator was detected using an S20 Hamamatsu photomultiplier. The output from the photomultiplier was fed through a Brookdeal amplifier and a phase sensitive amplifier (PSD) which was referenced to the chopper and then displayed on the Victor computer system. The wavelength accuracy of the SPEX system

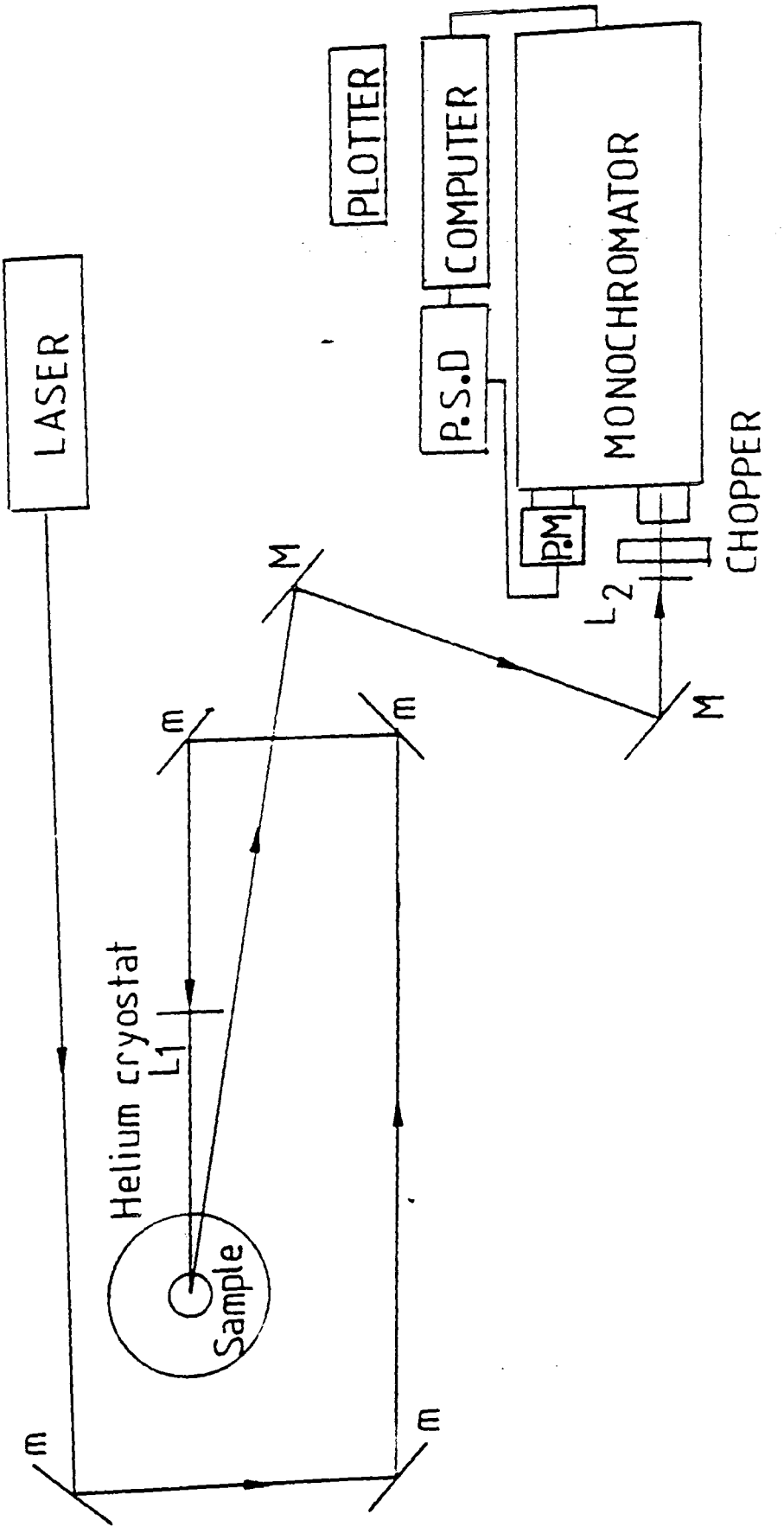

Figure 4.12. Outline of the photoluminescence apparatus used at Hull University.

was less than $1\mathring{A}$, verified by passing the laser line through the monochromator.

Chapter Four References

(1) Albin D.S., Risbud S.H., *Thin Sol. Films, 147*, 203, (1987).

(2) Coates P., Priv. Comm., (1992).

(3) Practical Scanning Electron Microsopy, eds., Goldstein J.I., Yokowitz H., Plenum Press, (1975)

(4) Russell G.J., *Prog. Cryst. Growth Chara., 5*, 291, (1983).

(5) Klug H.P., Alexander L.E., X - Ray Diffraction Procedures, Wiley, NY, (1974).

(6) Cullity, Elements Of X - Ray Diffraction, Wesley, (1979).

(7) Scherer A., Inal O.T., *Thin Sol. Films, 119*, 413, (1984).

(8) Van der Pauw L.J., *Phil. Res. Rep., 13(1)*, 1-9, (1958).

(9) Pankove J.I., Optical Processes in Semiconductors, Prentice - Hall, (1971).

(10) Carlson T.A., Photoelectron And Auger Spectroscopy, Plenum Press, (1975).

Chapter Five

Deposition and Characterisation of Undoped Zinc Oxide Films

5.1 Introduction

The initial plan of the research described in this thesis was to study the preparation of undoped films of ZnO deposited by spray pyrolysis using $Zn(acac)_2.H_2O$ dissolved in isopropyl alcohol. A water soluble precursor would have been preferable but despite extensive work in the Chemistry Department no such precursor was found. The main objective of this first part of this work was to establish the experimental conditions for the preparation of uniform undoped transparent films with as low a resistivity as possible. This involved a study of the ways in which adhesion, film thickness, crystallographic texture and resistivity varied with the preparative conditions. These aspects are described in the present chapter and form the basis for a discussion of the mechanism by which a layer grows as the droplets of spray impinge on the substrate. This discussion forms the subject matter of the following chapter.

5.2 Film Deposition

This part of the research involved the growth of undoped zinc oxide in twenty-four growth experiments which were carried out in order to investigate the influence of deposition conditions on the film properties. In the majority of cases $Zn(acac)_2.H_2O$ was the precursor used. The conditions of ZnO deposition are described below. The facility to introduce water vapour into the spray via the nitrogen gas shroud on the spray head was provided because the notion that hydrolysis can occur in spray pyrolysis is discussed in the literature, see for example [1]. An indication that hydrolysis is important in $Zn(acac)_2.H_2O$ spray pyrolysis is given by the work of Kamata [2],[3].

The system was also equipped with a substrate heater and a pair of tungsten lamps positioned above the substrate. This secondary or in-flight heating provided auxiliary power allowing substrate temperatures as high as 400°C to be achieved [4]. The maximum temperature achievable in the absence of in-flight heating was 336°C.

It was also speculated that in-flight heating might influence the quality of deposits by assisting solvent evaporation while the droplets are in transit.

ZnO films were grown under four different sets of conditions, namely with and without in-flight heating, and in wet or dry ambients.

All combinations of heating and wet/dry conditions were investigated by spraying 700 cm^3 of 0.1M $Zn(acac)_2.H_2O$ in isopropyl alcohol at temperatures between 96°C and 396°C. The experiments performed in this sequence are listed in table 5.1 and the assessment of the films is presented in section 5.3. Measurements of the resistivity of these films are also described and since as-deposited films tended to be fairly insulating, a series of annealing trials in a reducing atmosphere were carried out. An additional set of experiments was performed to investigate the effect of spraying different volumes of precursor solution at the same rate. 100 cm^3, 200 cm^3, 400 cm^3 and 700 cm^3 of 0.1M solution were used in standardized spray conditions i.e in a wet ambient with in-flight heating at 306°C. The results are presented in section 5.4.

Finally a series of depositions was performed using the alternative precursor $Zn(acac)_2$.2,6 lutidine. This precursor was used to assess the importance of coordinated water in the pyrolysis process and the results of this work are presented in section 5.5.

Films were grown on a group of five glass slides as described in section 4.3.5.

5.3 Study of Film Properties as Influenced by Heating Mode and Water Vapour

5.3.1 Introduction

In this section the results of the study of the influence of substrate temperature, heating mode, and water vapour on the properties of ZnO films deposited using $Zn(acac)_2.H_2O$ are presented.

5.3.2 Film Adhesion

All films grown below 200°C in a dry ambient were non-adherent to the substrate, the entire layer peeling away during a sellotape test. These films were grainy in appearance but were transparent. The films grown at 216°C and above in a dry ambient were

Table 5.1 Summary of film deposition conditions investigated using $Zn(acac)_2.H_20$.
(a) Deposition in a dry ambient.

Growth temperature /(°C)	Heating arrangement
96	Substrate/In-flight
126	Substrate/In-flight
126	Substrate
156	Substrate/In-flight
156	Substrate
216	Substrate/In-flight
216	Substrate
276	Substrate/In-flight
276	Substrate
336	Substrate/In-flight
336	Substrate
396	Substrate/In-flight

(b) Deposition in a wet ambient.

Growth temperature /(°C)	Heating arrangement
126	Substrate/In-flight
126	Substrate
156	Substrate/In-flight
156	Substrate
216	Substrate/In-flight
216	Substrate/In-flight
276	Substrate/In-flight
306	Substrate/In-flight
336	Substrate/In-flight
336	Substrate/In-flight

completely adherent to the substrate and were clear and transparent, being colourless or light pink to the eye. The inclusion of in-flight heating or water vapour had no obvious effect on these film properties except that deposition at higher temperatures in a wet ambient led to a brownish tinge.

5.3.3 Film Thickness

It was necessary to exercise some caution in using film thickness measurements to calculate deposition rates since in the manually operated kit variations in the flow rate of the precursor were observed. This was caused by blocking of an in-line filter in the precursor flow line which was avoided to some extent by cleaning the filter after each run. After this procedure was adopted the average run time was 16 $\pm$3 minutes. This variation meant that the interpretation of the thickness data in terms of deposition rate was somewhat uncertain. However as the same amount of precursor was used in all the experiments the film thickness gives an indication of reactant utilization. This assumes that the rate of arrival of precursor at the substrate does not significantly influence the percentage utilization of reactants. This assumption is acceptable where growth occurs in a dry ambient if the delivery rate does not become excessive. However where growth occurs in a wet ambient it has to be remembered that the water was delivered via the gas shroud. As a result, for experiments of different durations the ratio of $Zn(acac)_2.H_2O$ to H_2O will have varied, but since the molar ratio for an average run was 1:10 it is probable that water was always in excess.

Film thicknesses were measured as a function of substrate temperature and Arrhenius plots for log(thickness) vs 1/T(K), figures 5.1 and 5.2, were used to determine whether thermally activated processes were involved during growth. For films grown in a dry ambient the film thickness was found to be independent of the heating mode and decreased steeply from 1.0μm to 0.3μm with increasing substrate temperature in the range 126°C-216°C but at higher temperatures remained invariant at approximately 0.3μm up to to the maximum temperature used.

The variation in the thickness with changing substrate temperature suggests that

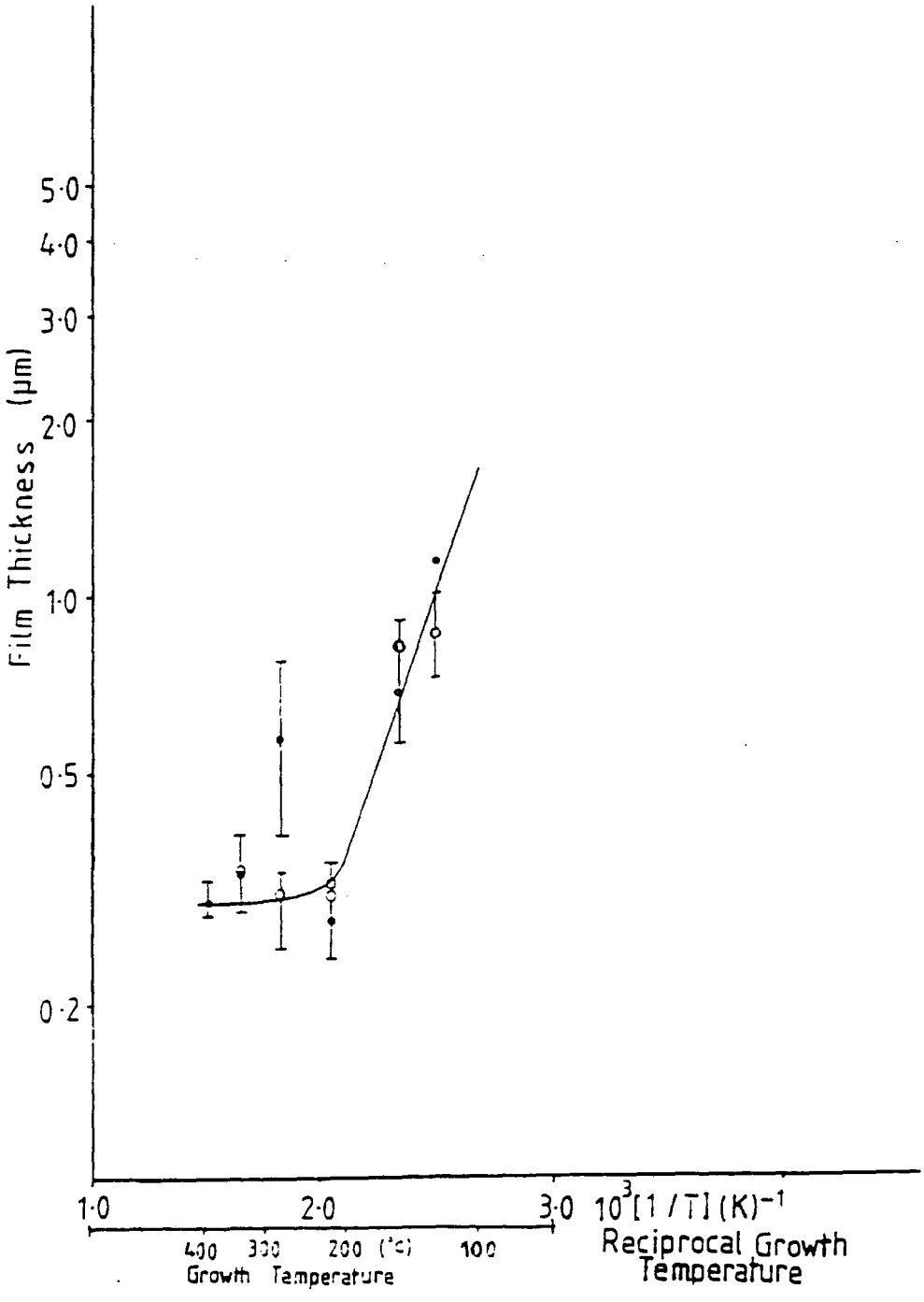

Figure 5.1. Variation of zinc oxide film thickness with substrate temperature when grown in a dry ambient. Symbols: ● = growth with substrate and in-flight heating; O = growth with substrate heating.

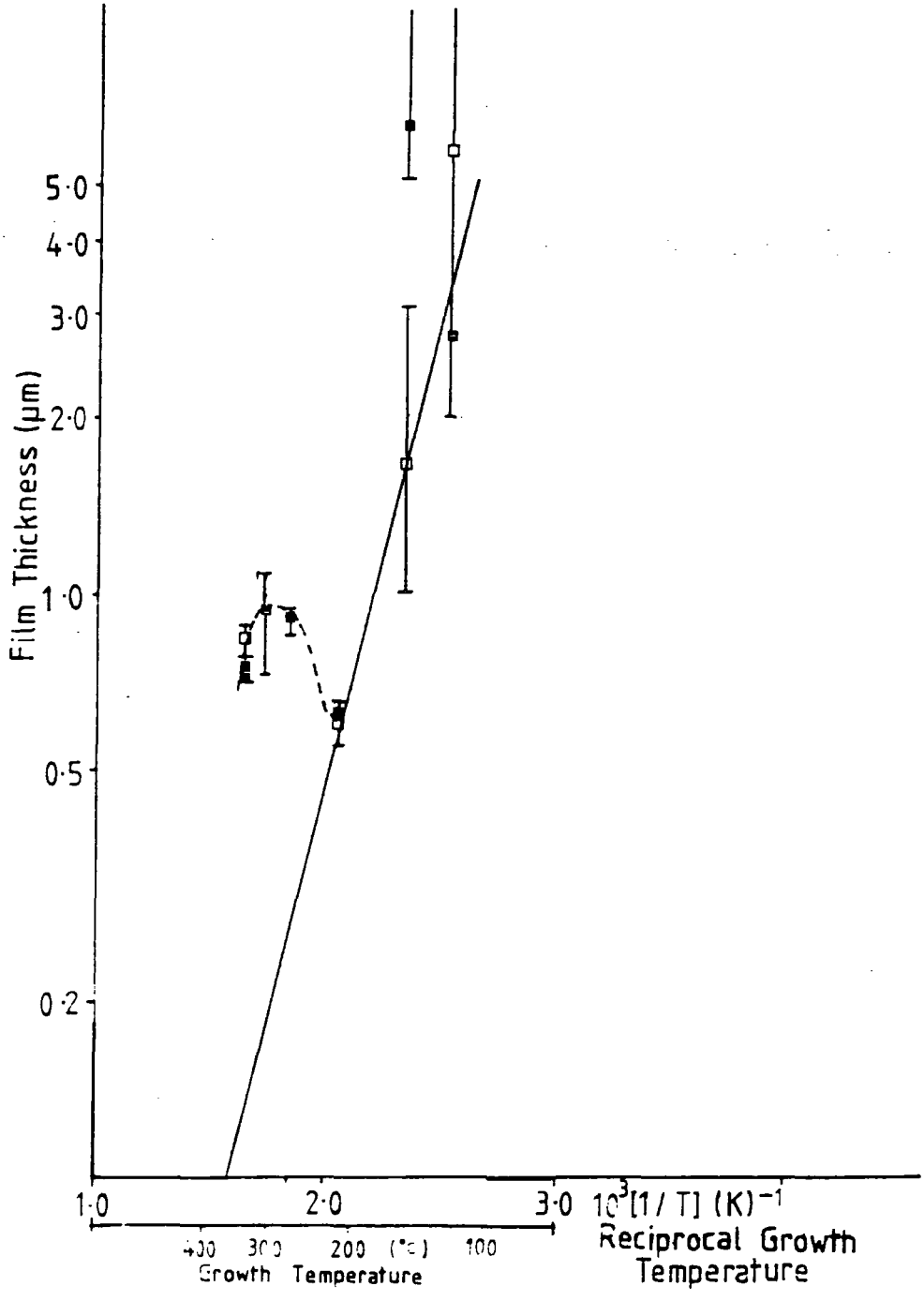

Figure 5.2. Variation of zinc oxide film thickness with substrate temperature when grown in a wet ambient. Symbols: ■ = growth with substrate and in-flight heating; □ = growth with substrate heating.

there are two regimes. The first, between 126°C and 216°C where the thickness is changing, and the second from 216°C to 396°C where the thickness is invariant. The point at 276°C in figure 5.1 represents an unusually high reactant utilisation. Each point in the graph is the average of 10 step height measurements and the error bars represent the spread of the values. The point at 276°C is therefore genuinely anomalous and was ignored in interpreting the data.

For films grown in a wet ambient the film thickness was again found to be independent of the heating mode used. As with films grown under dry conditions, the film thickness decreased with increasing temperature (from about 5μm to 0.6μm) in the temperature range 126°C to 216°C. Above 216°C the film thickness did not vary greatly as a function of substrate temperature. All of the films deposited between 216°C and 336°C had thicknesses in the range 0.6μm -1.0μm and there was a slight maximum at 306°C.

Overall, the films deposited in a wet ambient were 40 to 90% thicker than their dry counterparts, indicating the degree to which water enhances the decomposition of the precursor. The influence of water was more marked at the lower temperature. The main discussion of the dependence of film thickness on growth temperature will be reached in the next chapter when the mechanistic aspects of the decomposition of $Zn(acac)_2.H_2O$ to ZnO have been described.

5.3.4 Surface Morphology

The surface morphology of zinc oxide films was assessed by scanning electron microscopy. Films grown at the lower deposition temperatures (i.e less than 200°C) were often but not always cracked as shown in Figure 5.3 which is a micrograph of a film grown at 156°C under wet conditions. However the appearance of cracking was independent of the presence of water and of the heating mode used. Since the occurrence of this feature depended on the deposition temperature the likely cause of the cracking must be due to the effect of excess solvent.

Other important features of figure 5.3 are spherical artefacts approximately 0.5-

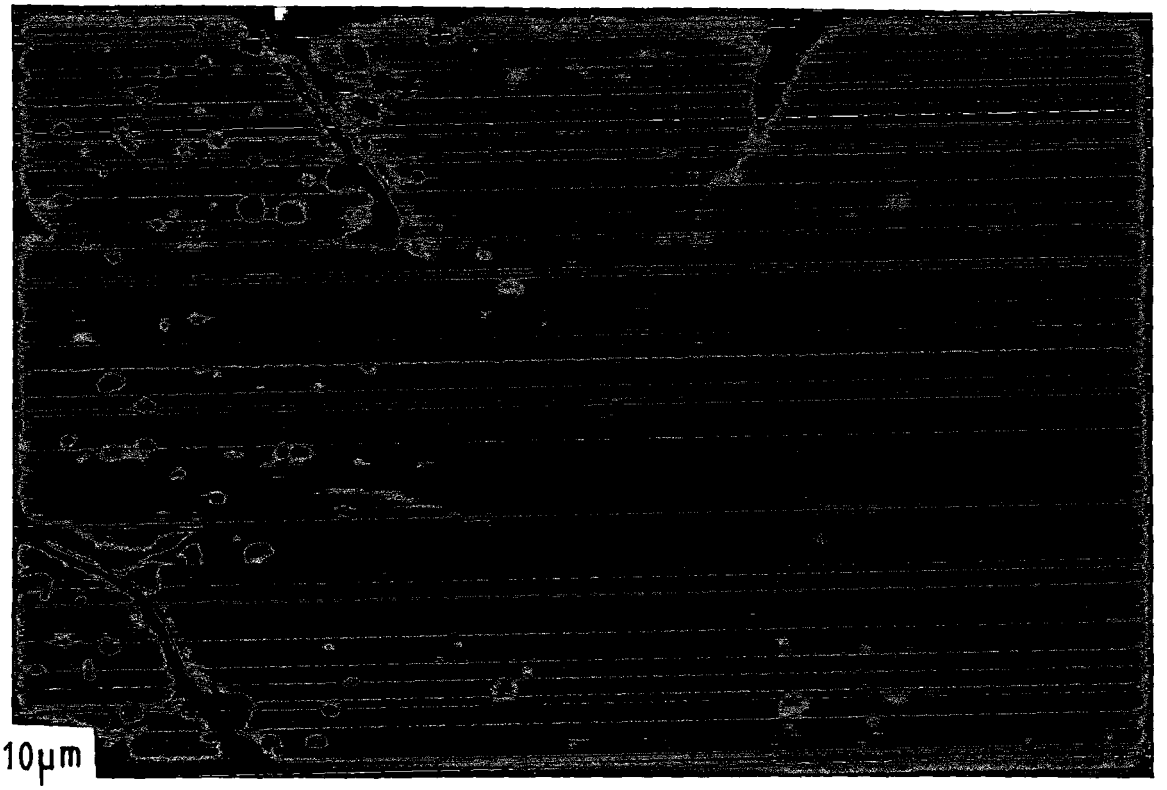

Figure 5.3. Secondary emission micrograph of the surface of a zinc oxide film grown at 156°C in a wet ambient with in-flight heating.

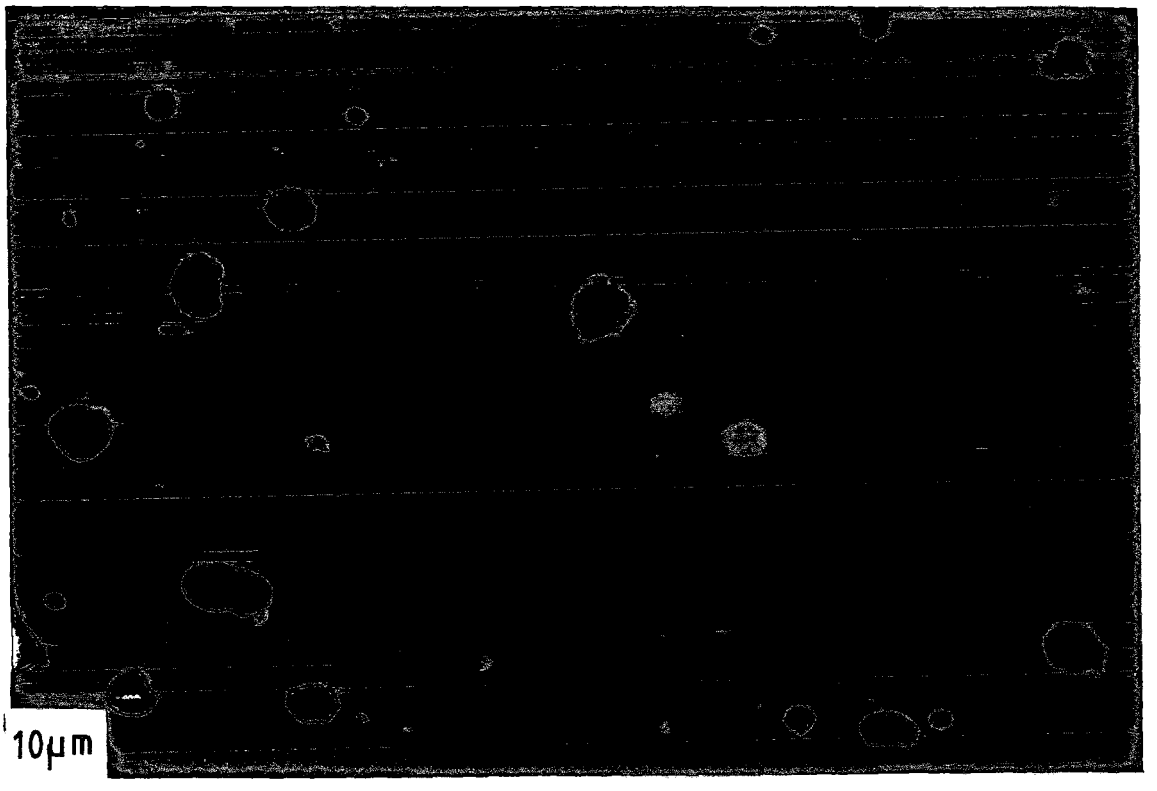

Figure 5.4. Secondary emission micrograph of the surface of a zinc oxide film grown at 156°C in a dry ambient with in-flight heating.

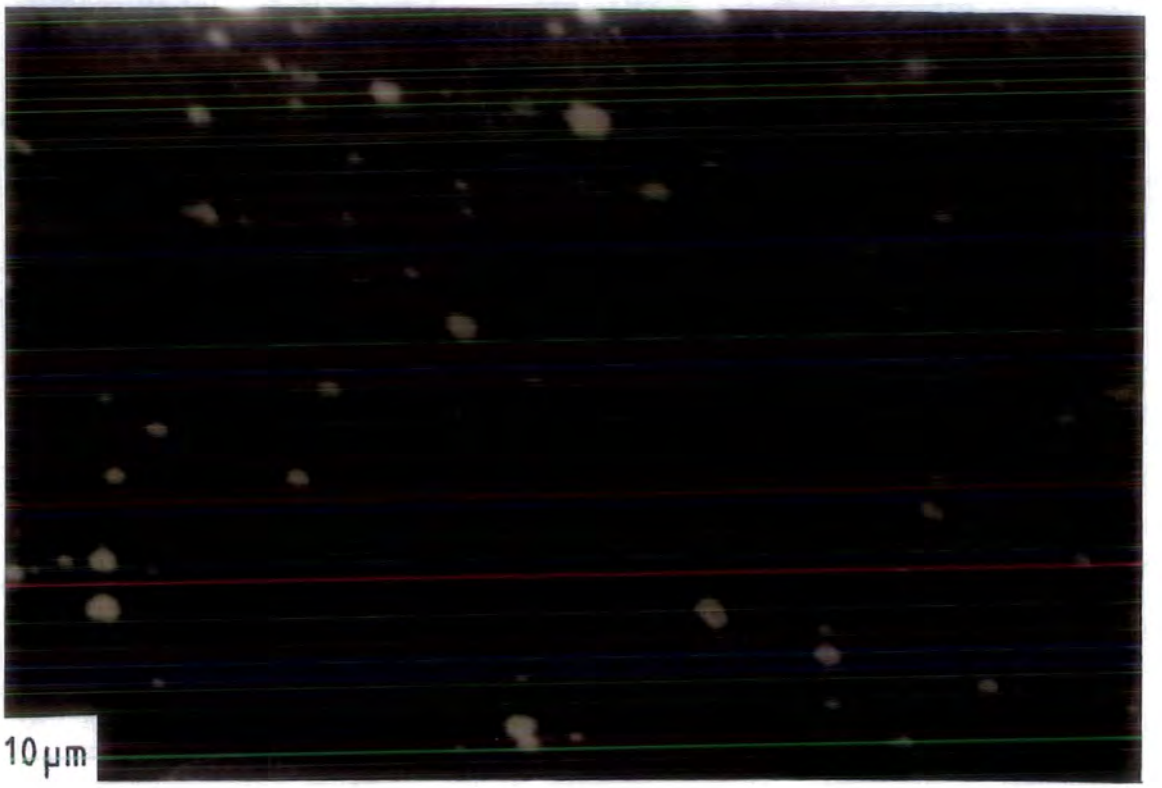

'igure 5.5. Secondary emission micrograph of the surface of a zinc oxide film grown at 216°C in a dry mbient with in-flight heating.

3μm in diameter which appear bright under secondary imaging conditions. EDAX analysis showed that the composition of the spherical features was the same as that of the ZnO film i.e only zinc could be detected. The spherical features were observed in approximately equal densities on films deposited under dry and wet conditions regardless of heating mode. For example figure 5.3 of a film grown under wet conditions (156°C) shows a density of 8×10^{11} spheres per m^2 while figure 5.4 of a film grown under dry conditions (156°C) shows a density of 2.6×10^{11} spheres per m^2. Some 93% of the spheres in figure 5.4 were 0.3-3μm in diameter with the balance having diameters in the range 4-6μm. Cracking was not observed in this film. Films grown at higher temperatures had a rather smaller density of spheres with somewhat smaller diameters. There was a slight suggestion that the spheres were larger when dry conditions were used. Another type of feature observed, shown in figure 5.3, was disc like marks 10-20μm in diameter in the plane of the film. These features have been observed by other workers [5],[6] and have been attributed to large solvent containing droplets bursting on the substrate. Such features were rarely observed.

At high magnification it was possible to observe the background morphology of the films themselves, as opposed to that of the spray artefacts. It was common to observe sub-micron roughness as shown for example in figure 5.5 for films deposited at 216°C. For films deposited at temperatures below 200°C there was no particularly strong dependence of surface roughness on temperature although slightly smoother morphologies were obtained at higher deposition temperatures.

5.3.5 Thickness Uniformity

5.3.5 (a) Thickness Uniformity in the Central Portion

Uniformity within a defined region refers to the flatness of the film surface at that particular level of magnification or scale. Eight to ten values of the film thickness were taken on each film. The results of the percentage variation of the thickness of the films from the average value from the central 1 inch^2 section of the substrate (section 4.6.3) as a function of deposition conditions are plotted in figures 5.6 and 5.7.

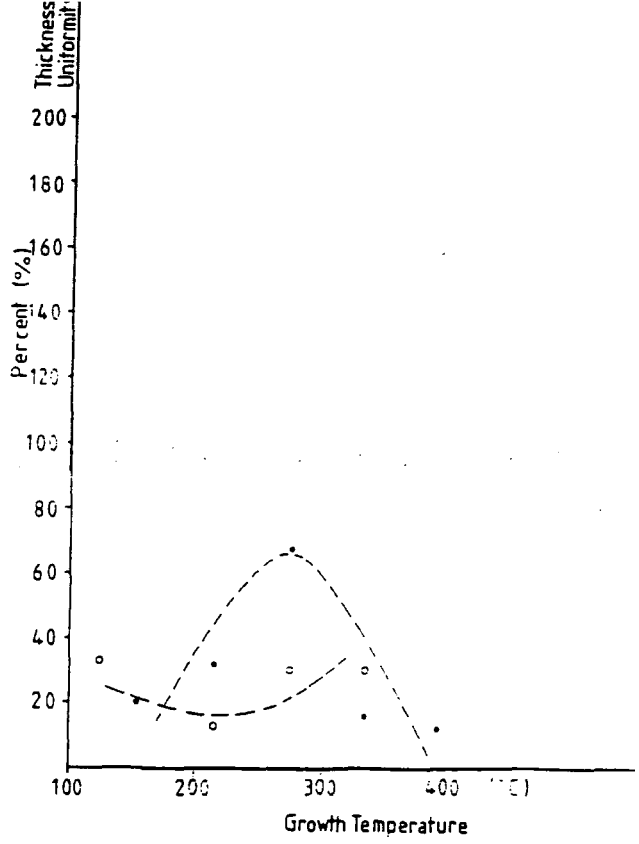

Figure 5.6. Dependence of the thickness uniformity in the centre of zinc oxide films on growth temperature when carried out in a dry ambient. Symbols: ● = growth with substrate and in-flight heating; ○ = growth with substrate heating.

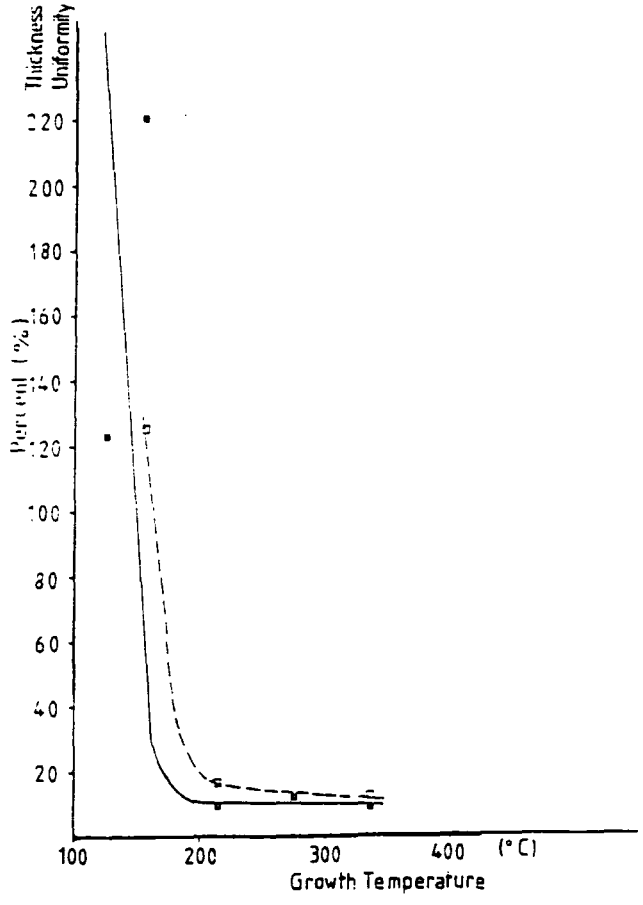

Figure 5.7. Dependence of the thickness uniformity of zinc oxide films on growth temperature when carried out in a wet ambient. Symbols: ■ = growth with substrate and in-flight heating; □ = growth with substrate heating.

Figure 5.6 shows that for films grown in a dry ambient the uniformity of the films varies from 10% to 33% over the temperature range investigated. In-flight heating had a marginally beneficial effect at the higher temperatures.

The variation of uniformity with deposition conditions when water was present was markedly different as shown in figure 5.7. At substrate temperatures below 200°C the variation in the thickness was of the order 120% - 200%. From substrate temperatures of 200°C up to 336°C the film uniformity was invariant at about 10%.

The most uniform films were grown at high temperatures whether dry or wet conditions were employed. A typical minimum variation in the thickness was 16% for a film grown in a dry ambient at 336°C with in-flight heating and 9% for a film grown in a wet ambient with in-flight heating at the same temperature. The breakdown in the film uniformity below 200°C when water is present in the spray correlates with the breakdown in film adhesion and onset of translucency and is associated with the onset of the low temperature reaction regime outlined in section 5.3.2.

5.3.5 (b) Thickness Uniformity from Edge to Centre of ZnO Film

The areas of film under study from which measurements were taken are outlined in section 4.6.3.

With a dry ambient the variation in the thickness uniformity from the edge to the centre of the substrate decreased from 40% to 16% as the deposition temperature was raised from 126°C to 400°C. The absence of in-flight heating generally acted to degrade uniformity especially at low temperatures where its use appeared to improve uniformity by a factor of two. However at high temperatures (336°C) films grown with and without in-flight heating were equally uniform.

For films grown in a wet ambient the percentage variation in the thickness varied from 24% when a growth temperature of 216°C was used to 15% when growth was carried out at 336°C. Measurements on films grown below 200°C were not possible due to their lack of adhesion to the substrate. There was no systematic difference between films grown with and without in-flight heating.

5.3.6 Microscopic Surface Roughness

Microscopic surface roughness was measured in the central 1 inch^2 section of the substrate using the alphastep profilometer. This is a different measurement from that of thickness uniformity (5.3.5(a)) since it is measured on a different scale. The results of surface roughness measurements carried out on undoped zinc oxide grown in dry and wet conditions are plotted in figures 5.8 and 5.9. The results point to a difference in the influence of varying the substrate temperature depending on whether in-flight heating was present or not.

With in-flight heating in a dry ambient, surfaces became smooth as the substrate temperature was raised. The surface roughness number decreased from 440 nm to 110 nm as the growth temperature was raised from 126°C to 396°C. However where in-flight heating was omitted surfaces became steadily smoother with a reduction in the substrate temperature. For example a roughness of 305 nm for a film grown at 336°C was reduced to 120 nm for one grown at 126°C.

Films grown in a wet ambient where in-flight heating was excluded were smoother at lower substrate temperatures. Films grown at 336°C had a surface roughness of 365 nm whereas a film grown at 156°C had a roughness of 160 nm. Thus the trend of ZnO films to become increasingly rough as the growth temperature was increased in the absence of in-flight heating was common to growth behaviour whether water was present or not.

In contrast ZnO films grown in a wet ambient with in-flight heating were comparatively very smooth when deposition took place above 200°C. The roughness ranged from 85 to 160 nm which is slightly better than the films deposited in dry conditions using in-flight heating at 336°C. Measurement of surface roughness for films grown below 200°C temperature were difficult to make due to the nonadherence of the ZnO material to the substrate although a film grown at 156°C had a roughness of 450 nm. This indicates a major increase in film roughness below 200°C and this is consistent with other findings in the chapter.

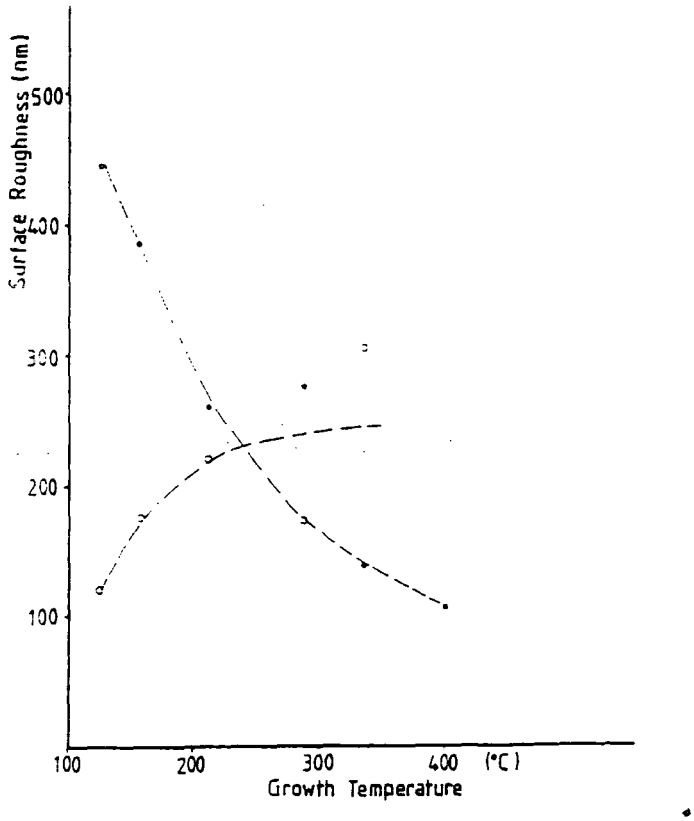

Figure 5.8. Variation of zinc oxide film roughness with growth temperature and heating mode when carried out in a dry ambient. Symbols: ● = growth with substrate and in-flight heating; ○ = growth with substrate heating. (The points at 276°C are anomalous).

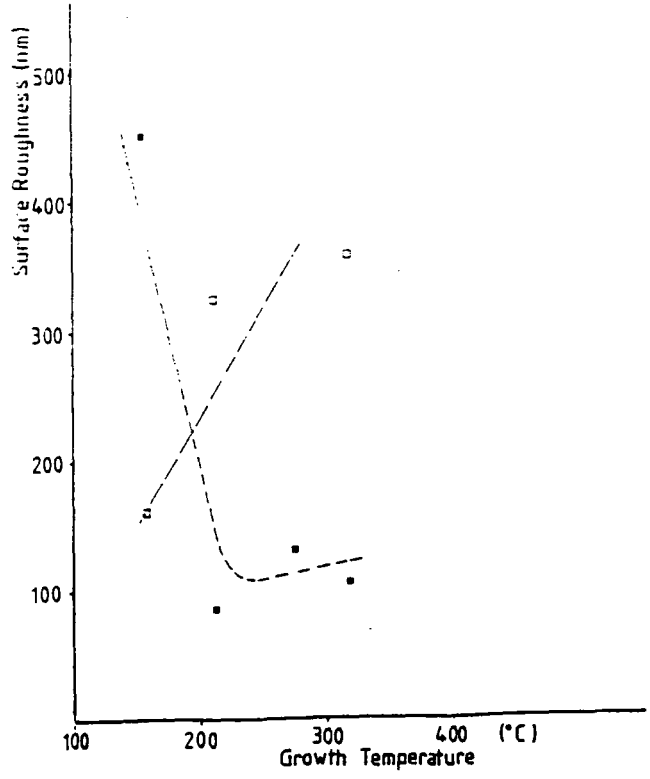

Figure 5.9. Variation of zinc oxide film roughness with growth temperature and heating mode when carried out in a wet ambient. Symbols: ■ = growth with substrate and in-flight heating; □ = growth with substrate heating. (N.B. Substrate temperatures above 336°C could not be achieved when water vapour was included).

5.3.7 Discussion of Morphology, Uniformity and Roughness Phenomena

(a) Surface Morphology

The high density of spherical artefacts observed in figures 5.3 and 5.4 for films grown at low temperature is probably caused by the drying and pyrolysis of spray droplets in the spray cloud prior to impinging on the film surface. This effect leads to the formation of dried ZnO powder. Several papers report deliberate attempts to produce ZnO powders using a suitable zinc compound such as zinc acetate or zinc acetylacetonate. These experiments gave spherical particles having diameters of 150 nm when zinc acetate was used and 21-35 nm when $Zn(acac)_2.H_2O$ was used. The particles were produced through the evaporation and pyrolysis of larger particles of the precursor which decreased in size as a result of these processes [7],[8]. Convection caused by hot gases rising off the substrate would tend to carry spray droplets away from the substrate area. The use of high substrate temperature implies that there is heating at the substrate and in the spray. This would lead to the evaporation of the $Zn(acac)_2.H_2O$ or freshly formed ZnO from the substrate area. Under these conditions spheres would decompose.

Cracking in the film was only observed in films grown below 200°C and was due to the effect of excess solvent on the film during and after growth. The cracking occurs in cases where the film has shrunk after deposition. This is due to the effect of desolvation from the film. Therefore it is certain that in some circumstances the film grows in a solvent medium.

It is probable that large droplets impinging on the film surface caused the splash marks observed in the low temperature film in figure 5.4 but that at increasingly higher temperatures these vaporise more completely along with the smaller ones. These marks on the surface of ZnO films have been observed before with the explanation that they originate from large droplets impinging on the substrate surface before desolvation occurs [5],[6].

Smoother morphologies were obtained with increasing temperature. Smoother

morphology in the high temperature films could be due to the fact that the diameters of the spray droplets were smaller when higher deposition temperatures were used. The incorporation of smaller decomposed precursor particles would lead to more uniform increase in the film thickness.

The improvement in the morphology could also be caused by a chemical effect of better precursor pyrolysis and film growth.

SEM studies show that below 200°C the film quality breaks down at microscopic and macroscopic levels. Low temperature films are discontinuous to the eye as well as by SEM and nonadherent to the substrate. These facts point to a lower temperature limit to the process yielding usable films. However above 200°C films are relatively smooth, continuous, transparent, and adherent.

(b) Thickness Uniformity in Central Region

The results point to the maintenance of good thickness uniformity in the central region of zinc oxide films when the growth temperature fell below 216°C as long as dry conditions were used. This can be attributed to the volatility of the zinc acetylacetonate-propan-2-ol precursor-solvent system across the whole temperature range, and the convective and evaporative effects. This leads to the effects of parameters controlling the temperature dependence of thickness uniformity being constant down to the lowest growth temperatures used. Thus over a large temperature range the same relative distribution of film material occurs across the substrate.

At high temperatures (336°C) generally in-flight heating contributed a significant fraction of its output to the substrate and helped maintain a steady constant temperature on the surface. It also preheated the spray to some extent and decreased the cooling influence of the spray on the substrate. It is also possible that in-flight heating enhanced the mobility of species on the film surface hence increasing re-evaporation.

Where films have been grown in a wet ambient below 200°C the inclusion of water produced extremely rough surfaces on this scale. It has already been stated that water decomposes $Zn(acac)_2.H_2O$ at low temperature [2,3] and that in spray pyrolysis thicker

films are obtained when water is included in the growth conditions. Rapid reaction at the surface increases the variation in thickness over the central 5 cm^2. The presence of water would also decrease evaporation and convection effects thus leading to an increased amount of material staying on the substrate surface.

(c) Thickness Uniformity from the Edge to the Centre of the Substrate

It is likely that the cause of the improved uniformity at high growth temperatures (336°C) was due to the influences of convection and evaporation from the heated substrate and a more uniform temperature distribution across the substrate leading to a more even distribution of material. Convection and evaporation at the substrate limit the amount of material building up in one place. At substrate temperatures below 300°C films grown with in-flight heating were more uniform than those grown in its absence. Therefore in-flight heating must in some way impart enough energy to the substrate to produce enough convection to fan the spray cloud out over a wider area and improve the uniformity of the temperature profile across the substrate.

At substrate temperatures above 300°C the overall effect of the energy present in the spray leads to comparable results whether in-flight heating is present or not. This suggests that the overall temperature generated on the substrate surface produces a uniform temperature profile across the substrate whether in-flight heating was present or not.

(d) Surface Roughness

The importance of the influence of water and in-flight heating on surface roughness is illustrated in figures 5.8 and 5.9. In-flight heating at high substrate temperatures (336°C) preheats the spray and film surface. Thus considerable desolvation of the spray droplets occurs when it is included with the result that the droplets are smaller and hotter on their approach to the substrate. This will reduce the thermal shock caused by cool liquid droplets impinging on the substrate. Some of the precursor will vapourise. In-flight heating increases the degree of re-evaporation from the film and increases the mobility of species on the surface. This would act to even out any inhomogeneities on

the film surface since evaporation from high points such as hills and spikes is greater than that from relatively smoother surfaces. The rate of evaporation is dependent on the radius of curvature of a section of the film. The roughness of films grown under these conditions increases at lower substrate temperatures (216°C). This increase is due to precursor particles landing on the film surface and remaining there without further movement due to a reduction in the rate of surface diffusion and re-evaporation. In-flight heating effectively removes the majority of the solvent before the precursor reaches the substrate but does not supply enough energy at low temperature to the substrate to produce smooth surfaces through the processes of diffusion and re-evaporation.

If in-flight heating is not used at high substrate temperatures (336°C) less pre-heating occurs and larger cooler droplets approach the substrate and cause disorder at the film surface through the cooling influence of unheated liquid landing on the film surface and through lower surface mobility. Less desolvation occurs compared to deposition with in-flight heating. The result is inhomogeneous film growth. Surface mobility and other processes which act to smooth out local inhomogeneities are suppressed. The shift towards lower temperatures sees a steady decrease in film roughness for films grown without in-flight heating. It is likely that spray droplets contain more solvent when they impinge on the film so that the dissolved zinc precursor they contain spreads out over a wide area of the substrate. This leads to films having a smoother morphology. Thus the relationship between surface roughness and thickness of films grown without in-flight heating under dry conditions is opposite to that observed for films grown with in-flight heating and expected from previous work [9].

At high substrate temperatures the influence of in-flight heating is to provide extra heat energy which drives off the solvent and then quite possibly causes the the vapourisation of the zinc chemical precursor. However at low temperatures it is likely that the drying of the majority of large spray droplets gets no further than the formation of a dried particle which is more difficult to incorporate in to the film in a non disruptive way.

5.3.8 Structural Characterisation

In this section the results of the structural characterisation of undoped ZnO by Reflection High Energy Electron Diffraction (RHEED) and by X-ray-Diffraction (XRD) are presented and discussed. RHEED is a surface sensitive technique whereas XRD takes an average of the entire film structure. Where appropriate the results are compared with the ASTM index card for zinc oxide (Table 2.1) which gives the intensities from planes for a random polycrystalline sample. A description of the zinc oxide lattice is given in chapter 2.

5.3.8.1 Surface Structure by RHEED

RHEED provides information on the crystal orientation, perfection and the degree of preferred orientation of crystallites at the surface of a thin film.

The results of the preferred orientation determination for films grown under the different sets of conditions are shown in table 5.2. Films grown at temperatures below 200°C were too rough to allow RHEED analysis (except for one film grown at 96°C) The electron diffraction patterns taken from the surfaces of zinc oxide films grown at 336°C and 396°C in a dry ambient are shown in figures 5.10 to 5.12.

Films grown in a dry ambient above 200°C have a preferred orientation of crystallites. However this appears to have degraded at 400°C. Figure 5.11 has been indexed with reference to the reflections due to the main preferred orientation. Preferred orientation is determined by finding the indices of the most intense peak perpendicular to the shadow of the substrate surface as shown on figure 5.11.

Most of the films including that in figure 5.12 showed a $(11\bar{2}2)$ preferred orientation with varying degrees of background randomness indicating that at least on the surface this is the dominant plane. This effect on the diffraction pattern is very pronounced since in a random polycrystalline sample of ZnO $(11\bar{2}2)$ is one of the least intense lines according to the ASTM card for ZnO.

The pattern obtained for the film grown at 96°C in a dry ambient with in-flight heating consists of continuous rings which indicates that the film had a totally random

Zinc oxide films grown in a dry ambient		
Growth temperature/°C	Heating arrangement	Surface preferred orientation
96	Substrate/In-flight	None; random polycrystalline
336	Substrate only	$(11\bar{2}2)$ strong pref. order
336	Substrate/In-flight	$(11\bar{2}2)$ strong pref. order
396	Substrate/In-flight	$(11\bar{2}2)$ pref. order
Zinc oxide films grown in a wet ambient		
Growth temperature/°C	Heating arrangement	Surface preferred orientation
216	Substrate/In-flight	(0002) pref. order/random polycrystalline
276	Substrate/In-flight	$(11\bar{2}2)$ pref. order
306	Substrate/In-flight	$(11\bar{2}2)/(10\bar{1}1)$ pref. order
336	Substrate/In-flight	$(11\bar{2}2)$ pref. order

Table 5.2. Summary of the surface preferred orientations of zinc oxide films grown under different conditions using $Zn(acac)_2.H_2O$.

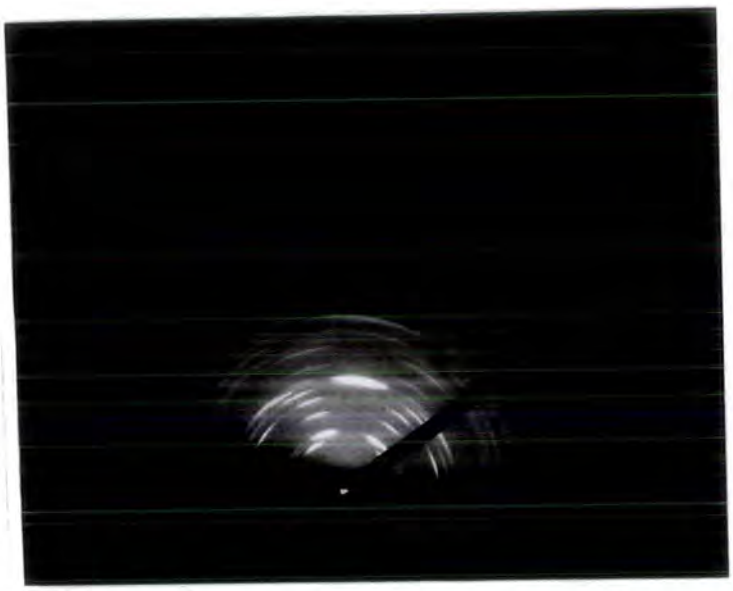

Figure 5.10. RHEED pattern from a zinc oxide film grown at 336°C in a dry ambient.

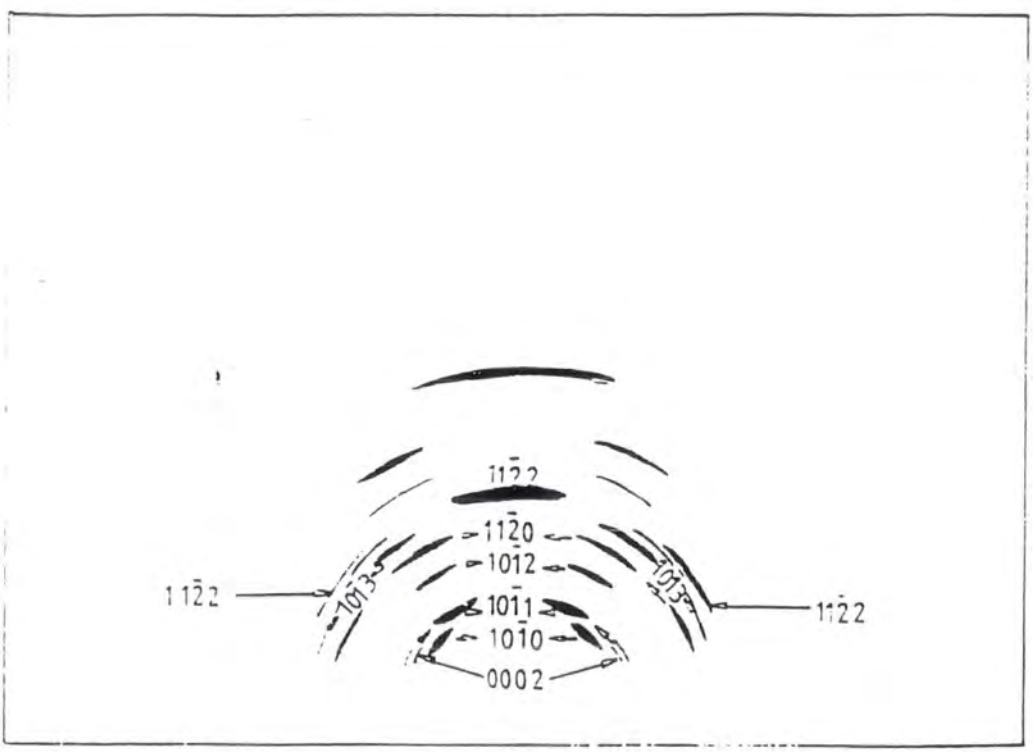

Figure 5.11. RHEED pattern as shown in figure 5.10 identifying reflections from crystal planes by their Miller-Bravais indices.

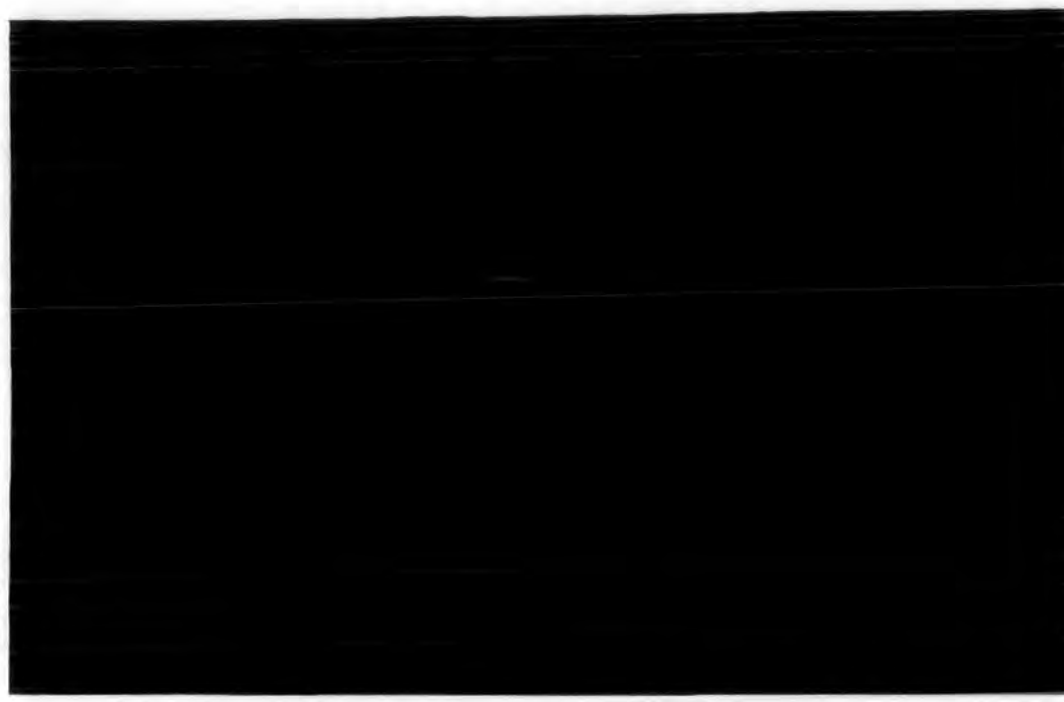

Figure 5.12. RHEED pattern from a zinc oxide film grown at 396°C in a dry ambient.

orientation of crystallites.

Films grown at 336°C using both heating modes possessed the highest degree of preferred orientation. The pattern from a film grown with in-flight heating is shown in figure 5.10 and is indexed in figure 5.11. It consists of arcs with one arc of particularly high intensity along a line perpendicular to the shadow of the substrate edge. This arc corresponds to the $(11\bar{2}2)$ plane. The other arcs in the pattern line up around the axis of the main arc at definite angles, as mentioned earlier in the section. These correspond to other planes within the crystallites at angles to the main preferred plane. Where there is sufficient preferred orientation and film order it is possible to measure the angle between the central arc and the subsidiary arcs. These measured angles can be compared with the angles between planes in the unit cell of ZnO which are calculated using the following formula :

$$cos\phi = \frac{h_1h_2 + k_1k_2 + \frac{1}{2}(h_1k_1 + h_2k_1) + \frac{3}{4}\frac{a^2}{c^2}l_1l_2}{\sqrt{(h_1^2 + k_1^2 + h_1k_1 + \frac{3}{4}\frac{a^2}{c^2}l_1^2)(h_2^2 + k_2^2 + h_2k_2\frac{3}{4}\frac{a^2}{c^2}l_2^2)}}$$

The letters h,k, and l together with their numerical subscripts represent the Miller indices of the two sets of planes. The planes of ZnO can either be represented by a three index (hkl) or a four index (hkil) notation as outlined in section 2.2.1. The four index system is generated from the three index system and is used to distinguish between non-identical planes with the same hkl values [10]. $Cos\phi$ represents the angle between the two planes in question. Agreement between the angles calculated from the above formula and the angles measured from the pattern shown in figure 5.11 was found. For example the angle between the (0002) and the $(11\bar{2}2)$ planes calculated from the above formula was 65° while the measured angle from the pattern between the same two planes was the same notwithstanding experimental error. The angle between the $(10\bar{1}0)$ and the $(11\bar{2}2)$ calculated from the above formula was 42° and the measured value from the pattern was 45°.

In this way it was possible to confirm that the reflections in figure 5.11 were due to the films being $(11\bar{2}2)$ oriented. Films grown at 396°C in a dry ambient with in-flight

heating had a $(11\bar{2}2)$ orientation with the pattern containing only arcs consistent with this. This was superimposed on rings indicating that a proportion of the crystallites are lying at all angles. The pattern from the film is shown in figure 5.12. The arcs themselves are unbroken and of an even intensity indicating that the grain size is small.

RHEED patterns from films grown in a wet ambient with in-flight heating indicate that the films become ordered at growth temperatures in the region of 200°C and that the degree of ordering increases with increasing growth temperature up to about 276°C but that any further substantial increase in the temperature results in a loss of the order.

It is also clear that a change in the identity of the preferred orientation occurs on increasing the substrate temperature from 200°C to 300°C. The preferred order changes from (0002) to a mixture of $(11\bar{2}2)$ and $(10\bar{1}1)$ to $(11\bar{2}2)$ as the substrate temperature increases.

Generally films grown with water in the gas shroud had a weaker degree of preferred orientation than ones grown in dry conditions and were more likely to contain crystallites with their axes pointing in random directions indicating greater disorder.

In addition to RHEED studies on the as-grown film surfaces, a series of diffraction patterns were taken from a ZnO film that was successively etched in dilute aqueous HCl to investigate how the structure of the film varied with depth. The depth profiling was calibrated using an alphastep surface profilometer.

The ZnO film chosen was grown in a dry atmosphere with in-flight heating at 336°C and was approximately 300 nm thick. The pattern from the unetched surface showed the expected $(11\bar{2}2)$ preferred orientation. The surface structure after the removal of 50 nm of material showed that the arcs were similar but slightly broader. The preferred order was still $(11\bar{2}2)$ after removing a total of 100 nm. The pattern was no different from that after 50 nm had been removed. However 150 nm below the original surface some randomisation of the crystallites had occurred but the $(11\bar{2}2)$ preferred orientation was still strong. The pattern obtained approximately 300 nm below the

surface indicated that further randomisation had occurred but that $(11\bar{2}2)$ was still the preferred orientation.

These results suggest that the ZnO film is nucleated both randomly and with some degree of $(11\bar{2}2)$ order. As the film thickened the preferred orientation strengthened at the expense of the randomly oriented crystallites. The XRD results presented in the next section were interpreted with this in mind.

5.3.8.2 Bulk Averaged Film Structure

X-ray diffraction was used to investigate the composition and crystallographic texture of the films. All of the peaks observed were attributed to ZnO and indexed by comparison with the ASTM index data card for that material. No additional peaks due to impurities, reaction intermediates or unreacted precursor material were observed for films grown under wet or dry conditions even at temperatures as low as 96°C.

Table 5.3 summarises the intensity data obtained for the ZnO films compared with the ASTM intensity data for a random polycrystalline sample of ZnO. Table 5.4 compares the surface orientations of films as obtained by RHEED with the bulk averaged orientations of the films as obtained by XRD. The films characterised were those grown with in-flight heating. Figure 5.13 shows a typical X-ray diffractogram obtained from a ZnO film grown at 336°C under dry conditions. The structure of the films was found to depend on the growth temperature. A film grown at 96°C in a dry ambient had a completely random orientation of crystallites. Films grown at 126°C and 156°C possessed a strong (0002) preferred orientation that decreased as the temperature of the substrate was progressively raised. The prominence of the $(10\bar{1}1)$ plane also increased in this temperature range. At a growth temperature of 216°C it was found that films grown in a dry ambient showed a $(10\bar{1}1)$ preferred orientation when in-flight heating was excluded from the growth conditions and a (0002) preferred orientation when in-flight heating was included. Thus the presence of in-flight heating caused a change in the preferred order. When growth was carried out at 336°C the $(10\bar{1}1)$ plane was still the preferred plane while at the highest growth temperature

Table 5.3. Summary of the results from X-ray diffraction. The intensity data from a polycrystalline ZnO sample (a) are compared with the intensity data from ZnO films grown under various conditions using $Zn(acac)_2.H_2O$ (b)-(e).

	(a) Intensity data for polycrystalline zinc oxide							
Crystal plane	$(10\bar{1}0)$	(0002)	$(10\bar{1}1)$	$(10\bar{1}2)$	$(11\bar{2}0)$	$(10\bar{1}3)$	$(11\bar{2}2)$	Preferred Order
d_{hkl}/Å	2.816	2.602	2.476	1.911	1.626	1.477	1.379	None ; random
Peak intensities/%	71	56	**100**	29	40	35	28	polycrystalline
Growth temperature/°C	(b) Intensity data for zinc oxide films grown in a dry ambient with in-flight heating							
96	100	**100**	88	20				None ; random
126	11	**100**	13	9		13		(0002)
156	12	**100**	23	12				(0002)
216	26	**100**	50		9			(0002)
336		40	**100**	18			27	$(10\bar{1}1)$
396	20	80	**100**			23		$(10\bar{1}1)/(0002)$
	(c) Intensity data for zinc oxide films grown in a dry ambient with substrate heating only							
216	16	14	**100**	12	8	7.5		$(10\bar{1}1)$
	(d) Intensity data for zinc oxide films grown in a wet ambient with in-flight heating							
126	12	**100**	24			8.5		(0002)
156	20	**100**	45			23		(0002)
216	40	24	**100**	10				$(10\bar{1}1)$
306	15	35	**100**					$(10\bar{1}1)$
336	24	17	**100**	7				$(10\bar{1}1)$
	(e) Intensity data for zinc oxide films grown in a wet ambient with substrate heating only							
216	21.4	13	**100**	10	8	6	27	$(10\bar{1}1)$

Zinc oxide films grown in a dry ambient		
Growth temperature/°C	Surface preferred orientation	Bulk averaged preferred orientation
96	Random polycrystalline	Random polycrystalline
336	$(11\bar{2}2)$	$(10\bar{1}1)$
396	$(11\bar{2}2)$	$(10\bar{1}1)/(0002)$
Zinc oxide films grown in a wet ambient		
Growth temperature/°C	Surface preferred orientation	Bulk averaged orientation
216	(0002)	$(10\bar{1}1)$
306	$(11\bar{2}2)$	$(10\bar{1}1)/(0002)$
336	$(11\bar{2}2)$	$(10\bar{1}1)$

Table 5.4. Summary and comparison of surface and bulk averaged preferred orientations in zinc oxide films produced under various conditions.

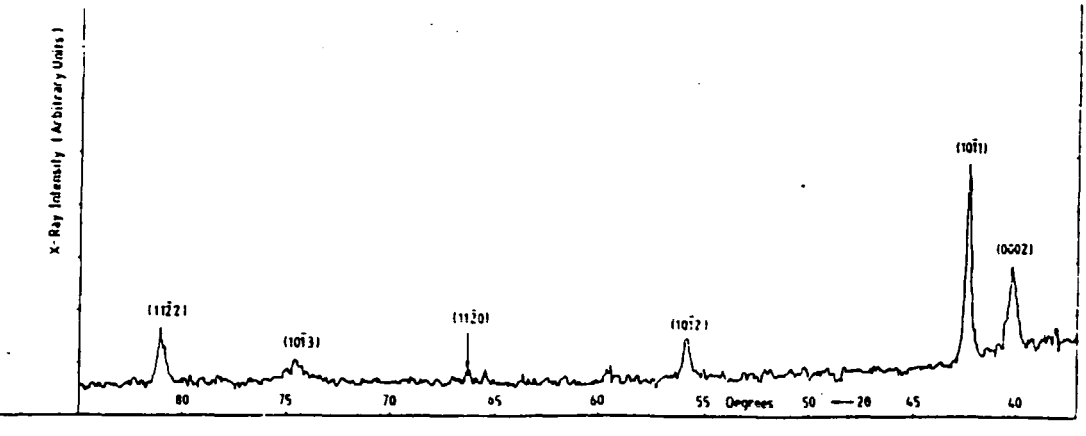

Figure 5.13. X-ray diffractogram showing principal peaks of zinc oxide from a film grown at 336°C in a dry ambient with in-flight heating.

of 396°C the proportion of $(10\bar{1}1)$ was relatively lower, the (0002) orientation having become strong once more. However, the most profound change in the preferred order occurred at about 216°C.

For films grown in a wet ambient at 126°C and 156°C the (0002) orientation was preferred with the dominance of the (0002) plane being greater at the lower temperature. There was also a profusion of peaks corresponding to minor orientations. The most commonly observed planes were the $(10\bar{1}2)$, $(10\bar{1}3)$, $(11\bar{2}2)$, and the $(11\bar{2}0)$. Films grown in a wet ambient at 216°C and above all had $(10\bar{1}1)$ preferred orientation regardless of heating mode, indicating a change in the most favourable crystal orientation.

At growth temperatures above 216°C all films showed a $(10\bar{1}1)$ preferred orientation. The highest degree of preferred orientation was observed in the ZnO films grown at 336°C, where available data suggests films grown in a wet ambient possessed a slightly higher degree of orientation than their counterparts grown in a dry ambient.

The effect of the addition of water is to randomise the orientation of crystallites at 126°C and 156°C. Otherwise the most profound influence on the preferred orientation is substrate temperature.

For films grown in a dry ambient annealing improved the preferred order. This effect was accentuated in films grown below the annealing temperature. Annealing the films grown in a wet ambient led to a slight increase in the preferred order.

5.3.8.3 Grain Size Studies on Zinc Oxide

Grain sizes were calculated from X-ray diffraction peak widths using the method outlined in section 4.6.5. In all cases the peak used for this measurement corresponded to the preferred orientation for that film. The results are plotted against substrate temperature in figures 5.14 and 5.15 for growth in dry and wet ambients. The results show that grain sizes in zinc oxide films grown at 156°C and below in a dry ambient with in-flight heating were in the range 11-23 nm. At temperatures of 216°C and above the grain size was fairly constant 35 nm. The observation that an increase in the grain size occurs over a narrow temperature range indicates a temperature activated process

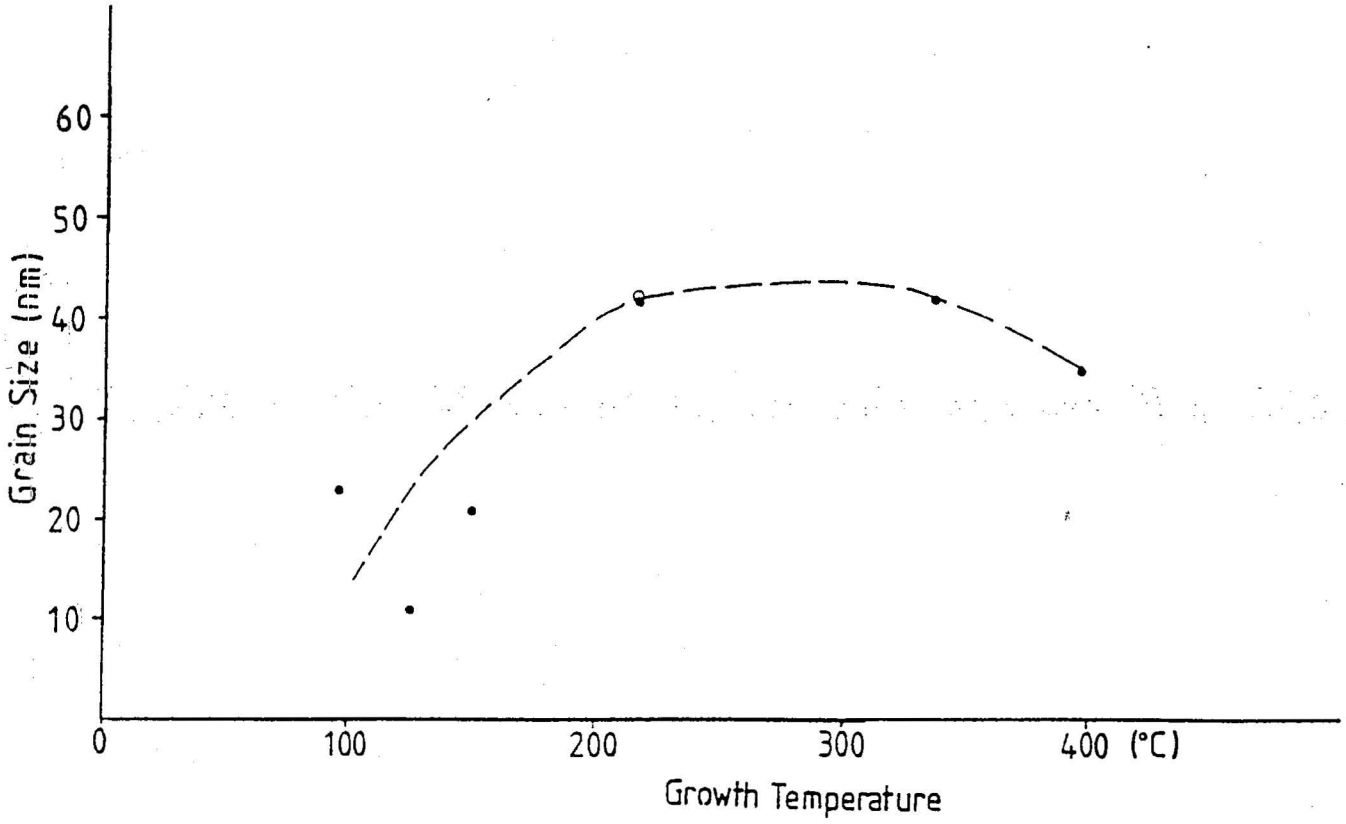

Figure 5.14. Variation of the zinc oxide grain size with growth temperature when carried out in a dry ambient. Symbols: ● = growth with substrate with substrate and in-flight heating; ○ = growth with substrate heating.

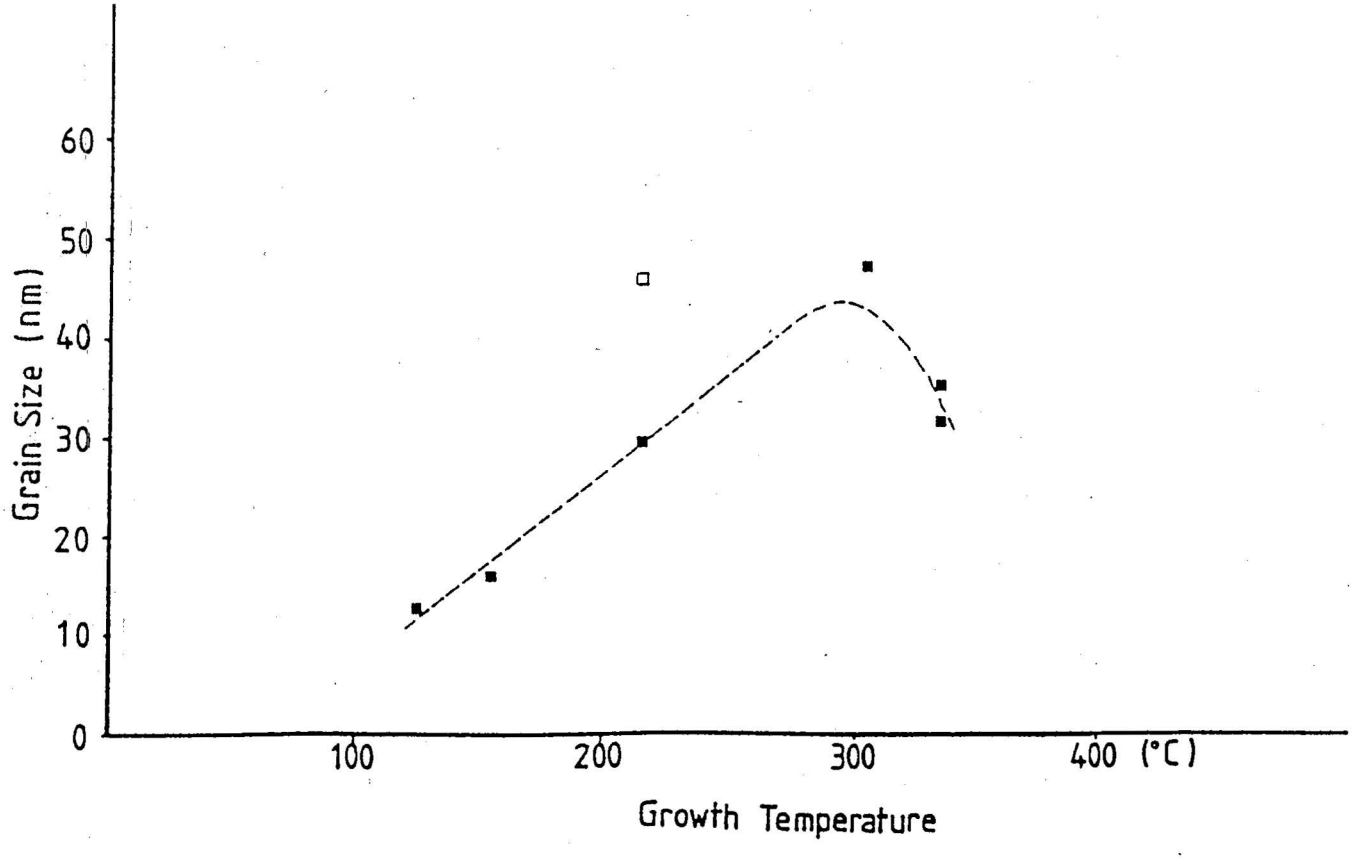

F'igure 5.15. Variation of the zinc oxide grain size with growth temperature when carried out in a wet ambient. Symbols: ■ = growth with substrate and in-flight heating; □ = growth with substrate heating.

the full effects of which are reaped within a 50°C increase in temperature.

When film growth was carried out in a wet ambient with in-flight heating the grain size increased from 13 nm at a growth temperature of 216°C to values within the range 35 - 45 nm at growth temperatures of 306°C and above. The effect of annealing had no influence on the grain size in films grown at 336°C and above but increased it in films grown at 216°C. The same trend was observed in films grown in a wet ambient.

To summarise, the grain size of ZnO films grown under wet and dry conditions increases rapidly with growth temperature to a plateau at 200°C - 400°C with some slight indication of smaller grains being associated with the highest temperature used.

5.3.8.4 Discussion of Structural Studies and Crystallographic Texture

(a) Preferred Orientation

An important point to draw out of the work is the commonality of the surface preferred orientation of $(11\bar{2}2)$ in high temperature films as determined by RHEED. This extends to a depth of approximately 300 nm below the film surface in one case and is therefore not a surface effect and shows that films have approximately the same structure regardless of the type of heating used. Where water is included in the growth conditions the $(10\bar{1}1)$ intensity is nearly as strong as the $(11\bar{2}2)$. Another important point to draw out of the work is the increase in the preferred order in the deposited films as the growth temperature was increased from 96°C up to higher temperatures. The presence of water also acts to increase the randomness of the orientation of crystallites of minor planes and is probably a consequence of the relatively higher deposition rate of ZnO in the presence of water, so that when the film is growing more rapidly the orderliness of the growth of crystallites breaks down. However the intensity of the main preferred orientation is only slightly affected. The change in preferred orientation from (0002) to $(11\bar{2}2)$ and $(10\bar{1}1)$ as the growth temperature was raised from 216°C to 276°C is likely to be due to a change in the kinetics and thermodynamics of the growth process. The (0002) preferred orientation is a common one in ZnO films, which have been grown by a whole host of workers [5,11–17] using the techniques of sputtering, CVD, spray

pyrolysis, and MOCVD at temperatures ranging from 150°C to 400°C.

The main differences between the films grown in wet and dry conditions at 216°C are the relative randomness of crystallites in the film where water is included in the growth conditions when both essentially possess a (0002) preferred orientation. This again is due to a higher deposition rate which in this case favours the growth of ZnO at all angles with respect to the main preferred orientation.

X-ray diffraction results indicate that the way the film is deposited changes below 200°C. This is shown by the changes in the preferred order and grain size. The difference in the film quality was especially apparent when films were grown with water present. The results also indicate that in many films the preferred order in the bulk of the film is different from that on the surface as demonstrated by comparing the results from RHEED and XRD. The electron diffraction patterns taken from a ZnO film that was etched down successively showed that the $(11\bar{2}2)$ surface orientation persisted down to at least 150 nm below the film surface for a film grown at 336°C in a dry ambient. The XRD technique averages the whole film structure and gave an averaged orientation of this particular film of $(10\bar{1}1)$. This is different from the orientation as determined by RHEED. It can be concluded therefore that a gradual change occurred in the way the film grew. At first the ZnO was being deposited on glass but after some time the coverage of ZnO on the glass was complete and ZnO then began to grow on itself. Thus the conditions of the film growth changed. The surface of the glass slide is amorphous and so any initial deposit is likely to be relatively disordered.

However as the coverage of the surface increased and the film thickened, the ZnO adopted a more ordered structure. This led to the fastest growing planes dominating the growth and becoming the preferred orientation. This dominant plane was found to be $(11\bar{2}2)$ using RHEED. Although the RHEED results are self consistent the XRD data obtained from the same films indicate that the dominant bulk averaged preferred orientation at higher temperature was not $(11\bar{2}2)$ but $(10\bar{1}1)$. This was unexpected since the RHEED - step etching experiments showed that there was no evidence of a change

from one preferred orientation to another at the surface. In almost every case XRD showed film growth occurred initially with the $(10\bar{1}1)$ plane as the preferred choice. Thus this plane must have had some affinity with the glass substrate surface. Growth could be envisaged as occurring along vertical and horizontal planes. Vertical growth occurred along the $(10\bar{1}1)$ plane with Si-O-Zn bonds ensuring good adhesion. When there was insufficient energy to activate the glass surface for bonding then adhesion broke down. Lateral growth occurred along the (0001) and the $(000\bar{1})$. However as the film thickened the preferred growth parallel to the substrate surface became the $(11\bar{2}2)$.

An alternative to the explanation of the temperature dependence of preferred orientation would be based on a deposition mechanism in which platelets of ZnO are generated above the substrate and become incorporated into the film. If these platelets were hexagonal in shape with their c-axes perpendicular to their major faces then these would cover a surface to give a (0002) oriented film. This would occur below 200°C. Above 200°C this theory requires that the shapes of crystallites formed should change i.e that the crystallites formed should adopt different habit planes.

(b) Grain Size

The main point to come out of the grain size calculations is the comparatively small grain size obtained at growth temperatures below 200°C. At low temperatures not only is there not enough energy for adhesion between film and substrate and cohesion within the film itself, but additionally there is insufficient energy for appreciable grain growth. Overall a typical value of grain size in films grown above 200°C in this work was 40 nm. This compares with a quoted range of 20-90 nm for films grown by the spray pyrolysis of zinc acetate at 400°C-450°C [6],[16],[18] and with the sizes of ZnO powder particles obtained using $Zn(acac)_2.H_2O$ as a precursor i.e 21-35 nm [8]. Owing to the larger amounts of material deposited at lower temperatures, film growth is more rapid and as a result relatively little energy is available for grain growth since relatively larger amounts of precursor are being decomposed and solvent driven off. At higher temperatures the grain size is larger because there is no shortage of energy in the growing film. This

difference in the grain size between films grown above and below 200°C coincides with a change in crystal habit and agrees with the results from preferred orientation. From the results of the laser Doppler measurements it was found that the mean average droplet radius in the spray was 3μm. This corresponds to a mass of 9×10^{-15}kg or $1.6\times10^{-18}m^3$ of ZnO. Since the mass of an average grain was 2×10^{-19}kg, or $10^{-23}m^3$ it is apparent that around 5×10^4 grains were formed from each $Zn(acac)_2.H_2O$ containing droplet. It can be envisaged therefore that as desolvation and precursor pyrolysis occur the ZnO forms into a very large number of spherical particles that are built into the film to become crystallites and grains. The fact that the grains are small in size relative to the volume of ZnO contained in one droplet suggests that crystal habit is masked more readily at low temperature.

(c) Thickness Effects

A number of films were grown at 306°C from different volumes of 0.1M precursor solution (100 cm^3, 200 cm^3, 400 cm^3, and 700 cm^3) in order to investigate how their properties varied with thickness. The substrate temperature of 306°C was chosen because the earlier work had shown that the quality of films grown was very good.

Measured film thicknesses as a function of volume of precursor sprayed are plotted in figure 5.16. The results show that there is a direct proportionality between the thickness of film material deposited and volume of precursor solution sprayed under these growth conditions.

The surface roughness (R_a) also increased with film thickness. It varied from 40 nm for a film 0.091μm thick to 590 nm for a film 0.941μm thick.

XRD spectra of films grown at 306°C in wet conditions with in-flight heating from different volumes of 0.1M precursor solution were also recorded. Generally speaking, the degree of preferred orientation increased with increasing film thickness. The film with the highest degree of order was grown from 400 cm^3 of solution, the second largest volume used. The film grown from the 700 cm^3 had a relatively lower degree of preferred order. Most films exhibited the $(10\bar{1}1)$ preferred orientation.

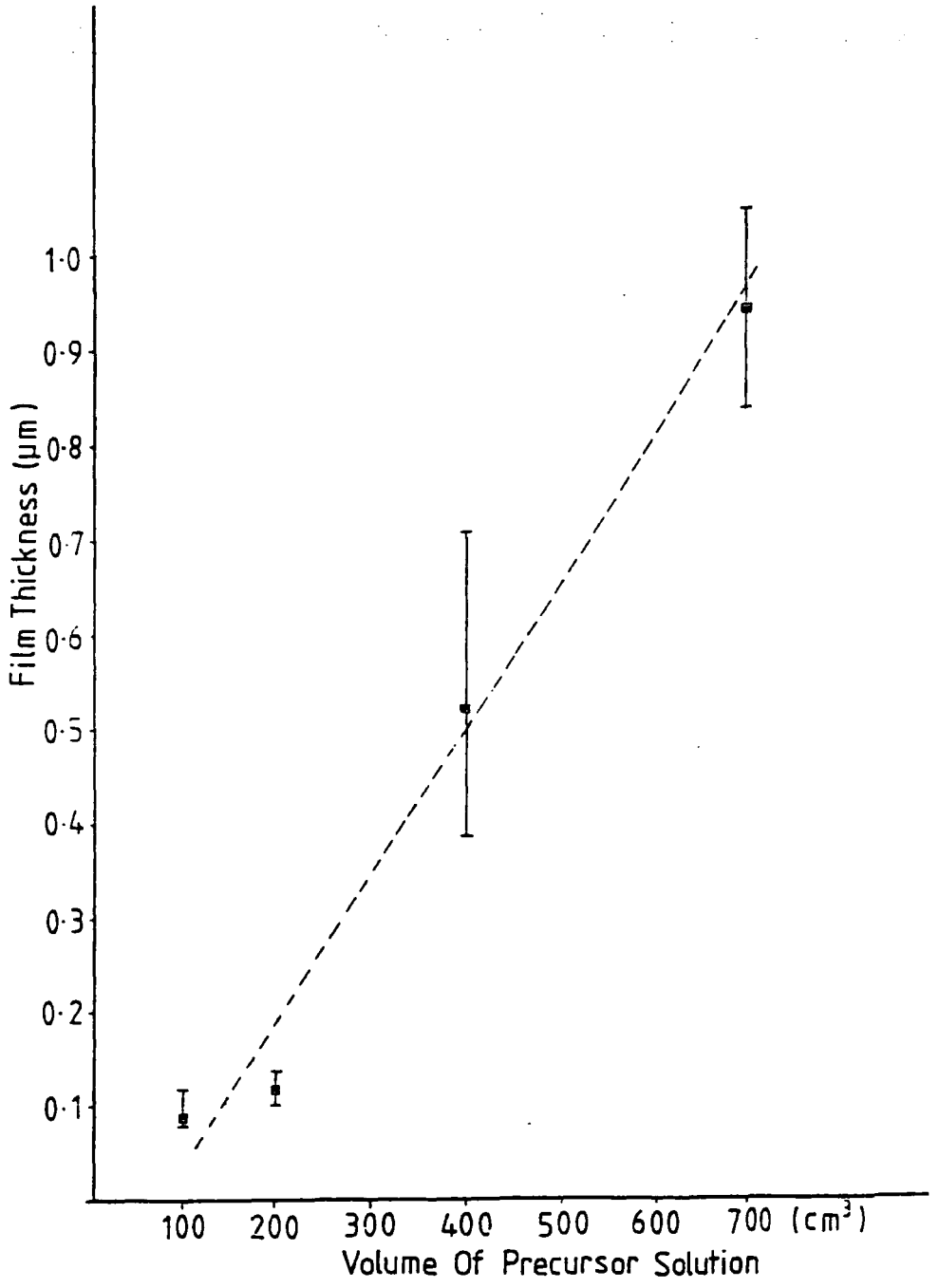

Figure 5.16. Variation of zinc oxide film thickness with volume of precursor solution sprayed under constant deposition conditions. Symbol: ■ = growth at 306°C in a wet ambient with in-flight heating.

Grain sizes were calculated from X-ray diffraction peak widths for these films taken from the peak representing the preferred orientation. The grain sizes increased from approximately 27 nm to 42 nm as the spray volume increased from 100 cm^3 to 700 cm^3. The film thickness increased from 0.091μm to 0.941μm in the same range. These results indicated that grains grew in the timescale of the experiments (0-15 minutes) even though fresh precursor and solvent were arriving at the film surface.

From the thickness measurements it is apparent that the effects of desorption of established film material from the substrate surface with spray time, and possible densification of film material do not alter the proportionality which exists between the amount of precursor sprayed and the film thickness. Therefore it is possible to say that once material has been incorporated into the film it is not lost due to re-evaporation. The results might also suggest that the density of atomic packing in the film does not change with spray time i.e no voids are incorporated in the film.

The fact that surface roughness is relatively low for thin films and much higher for thicker films indicates that either the amount of surface disorder or the degree of facetting increased with thickness.

A relationship between the overall film thickness and the surface roughness has been developed which is based on statistical analysis [9]. If it is assumed that the zinc precursor decomposes and sticks where it lands on the substrate without subsequent surface diffusion on the substrate, then statistical fluctuations in the local film thickness will result. The average deviation in the film thickness δd from the average thickness t is given by the Poisson probability distribution of a random variable. The relationship between δ d and t is given by

$$\delta d = c\sqrt{t}$$

Thus this equation predicts that the surface roughness of a film increases with the square root of the film thickness. However this equation and the thinking behind it cannot account for the extreme roughness of these films. The thickest film, for example, was of 0.941μm and had a roughness of 590 nm. If the square root relationship were

obeyed then the roughness would be less than 100 nm. The thinnest film of 0.091μm had a roughness of 40 nm and according to the square root relationship a roughness approximately 10 nm would be expected. Therefore the film surfaces are rougher than expected. This could be explained by the reactivity of the precursor in the presence of water and a lack of diffusion at the surface. Differences in growth rates between grains having the preferred orientation and other grains with different orientations, would also affect the roughness. If there was a constant difference in growth rates then the roughness would increase linearly with thickness. The experimental data support this mechanism.

5.4 Films Grown Using $Zn(acac)_2$.2,6 Lutidine

Two zinc oxide films were grown from this precursor. The first film grown at 216°C in a dry ambient with no in-flight heating was clear and transparent with no surface speckle. The second film grown at 336°C in a wet ambient with in-flight heating had a dark brown tint. Both films were adherent to their substrates.

The properties of films deposited from $Zn(acac)_2$.2,6 lutidine were not very different from those of films deposited using $Zn(acac)_2.H_2O$. The film grown from the monohydrate adduct under identical preparation conditions at 216°C had a $(10\bar{1}1)$ bulk averaged preferred orientation whereas the film grown from the lutidine adduct had a (0002) preferred order. Films grown at 336°C under identical deposition conditions from the monohydrate and lutidine adducts both had the $(10\bar{1}1)$ preferred orientation. Grain size measurements indicated that similar results were obtained from both precursors when film growth was carried out under identical conditions of a dry ambient and no in-flight heating. This indicates that grain growth is not significantly limited by the presence of byproducts related to 2,6 lutidine which might have acted to cause discontinuities between planes. Therefore 2,6 lutidine must break off the $Zn(acac)_2$ parent molecule and volatilize away without appreciable decomposition or incorporation into the film.

5.5 Resistivity of Zinc Oxide Films

Film resistivity has been measured for both as-deposited and annealed ZnO films. Films were annealed at 375°C for 30 minutes in a reducing atmosphere of 600cm^3 min^{-1}. The composition of the reducing gas was 20% hydrogen with oxygen free nitrogen. The effect of annealing the zinc oxide films was to drive off oxygen, leading to a zinc excess in the films which promoted n-type conductivity.

5.5.1 Resistivity of As-Deposited Films

The results of the resistivity measurements for as-deposited films grown in dry and wet ambients are plotted as the logarithm of the resistivity against growth temperature in figure 5.17. The resistivity of films grown in a dry ambient with in-flight heating was dependent on the growth temperature. Resistivities of films grown at the lowest temperatures used were very high ($9\times10^3\Omega$m at 156°C) but decreased sharply until about 200°C. Above 200°C the resistivity varied only slowly with temperature reaching a shallow minimum of 1 Ωm at 336°C. The increase at higher temperatures was only slight (i.e 1.13 Ωm at 396°C). A similar trend for the variation of film resistivity with growth temperature was observed for films grown in a dry ambient without in-flight heating.

When growth was carried out in a wet ambient the resistivities of films grown at 126°C and 156°C with and without in-flight heating were too high to measure by any available technique. These films had resistivities in excess of $10^4\Omega$m. However when growth was carried out at temperatures above 216°C with in-flight heating the resulting resistivities fell to values from 1.0 to $2.5\times10^{-2}\Omega$m.

In summary, films grown in a dry ambient below 200°C were more conductive than those grown in a wet ambient. At high temperature, films grown in a wet ambient were twenty times more conducting than those grown in a dry ambient. Films grown at 216°C in both wet and dry ambients were comparable in resistivity.

5.5.2 Resistivity of Annealed Films

Annealing films in a reducing atmosphere led in general to a reduction in the

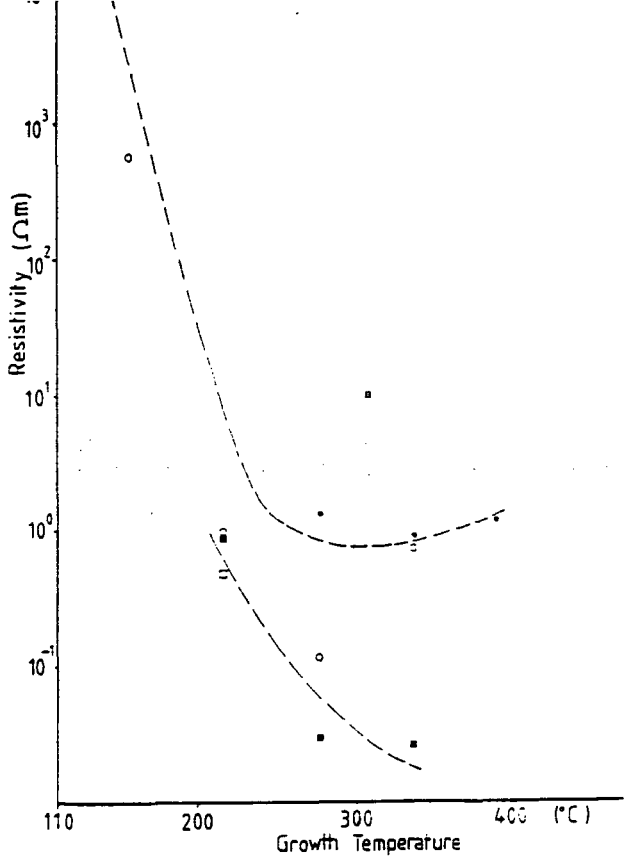

Figure 5.17. Variation of zinc oxide film resistivity with substrate temperature, ambient and heating mode. Symbols: ● = growth in a dry ambient with substrate and in-flight heating; ○ = growth in a dry ambient with substrate heating; ■ = growth in a wet ambient with substrate and in-flight heating; □ = growth in a wet ambient with substrate heating.

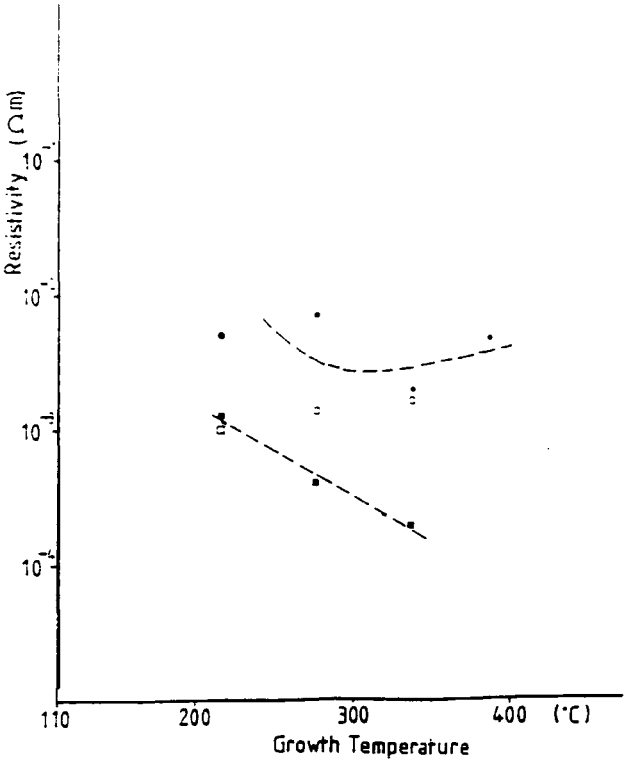

Figure 5.18. Variation of annealed zinc oxide film resistivity with substrate temperature, ambient and heating mode. Symbols: ● = growth in a dry ambient with substrate and in-flight heating; ○ = growth in a dry ambient with substrate heating; ■ = growth in a wet ambient with substrate and in-flight heating; □ = growth in a wet ambient with substrate heating.

resistivity by about 2 orders of magnitude.

Measurements of films grown in a dry ambient with in-flight heating are presented in figure 5.18. The resistivities of annealed films were roughly independent of the growth temperature and were about $3\times10^{-3}\Omega$m. With dry ambients and no in-flight heating annealed resistivities were slightly lower at $1.5\times10^{-2}\Omega$m.

Annealing films grown under wet conditions using substrate and in-flight heating produced resistivities close to $10^{-3}\Omega$m regardless of the growth temperature. Surprisingly however, when substrate heating only was used the lowest resistivities were achieved after annealing films grown at temperatures of 276 and 336°C (see figure 5.18).

5.5.3 Discussion

The main points to draw out of these results are that the resistivity is very large when growth occurs below 200°C and relatively low when growth occurs above 200°C. The lowest resistivities are achieved under wet conditions.

Clearly there is a relation between growth conditions and electrical properties. Such a relation has been observed before by workers using spray pyrolysis, MOCVD, and CVD to deposit zinc oxide [5],[11],[12],[19].

The low temperature films are relatively disordered and discontinuous, consisting of small grains. These features would inhibit the current flow. For example, potential barriers associated with intergrain boundaries reduce the mobility of charge carriers while carrier depletion in the bulk of the grains may also limit the conductivity.

Another factor relates to the geometry of grain packing, that is the relationship between crystallites and grains in the films and the presence or absence of intergranular phases. This type of inhomogeneity relates especially to powders which are similar to thin films in their electrical behaviour. In this case current is constrained to flow in non-uniform patterns and irregular routes and pathways for geometric reasons because the grains are not in intimate contact. Normally, in a thin film the grains are in intimate contact. However it is probable that the low temperature films contained intergranular regions comprising highly disordered and highly resistive zinc oxide. This may in part

be due to the small growth rate of the grains leading to a proportion of the zinc oxide accumulating outside the grains. Thus the potential barrier to charge transfer from grain to grain will be high. The effective resistances of these grains will be governed by the resistance of the grain to grain contact resistances.

In the low temperature films it is also possible that there were areas where grain to grain contact was not total. Thus not all intergranular regions will allow conduction from grain to grain and this will result in complex and resistive preferred pathways for current flow. Of course, for conduction to occur a complete chain of these conducting pathways is necessary. The conduction mechanisms in ZnO powders and polycrystalline films have been reviewed by Orton and Powell [20].

At high substrate temperatures the grain size increased and the films were cohesive and crystalline. There was probably little or no intergranular phase since the grains were in intimate contact. At temperatures above 200°C the growth rate of grains was higher increasing the possibility of most of the zinc oxide being incorporated into the grains leading to the elimination of intergrain phases. Thus there is the likelihood that the grain boundaries will consist of a narrow region where there is discontinuity between planes but otherwise good intimate contact, and the barrier between the grains to current transport will be lower and carrier transport will be less inhibited. Hence the film conductivity will be close to that of the conductivity of the grains. Due to the continuity of the films there would also be a larger number of complete conducting links through the film which would be more conductive as a result. It is probable that a high degree of preferred order in a film leads to an increase in the number of conducting pathways from one side of the film to the other. At growth temperatures in the region of 276°C-336°C the benefits of the growth conditions on the structural and electrical properties of the ZnO films were fully realised. Both grain size and preferred orientation were optimized. Another strong possibility is that the films contained an excess of zinc in the form of either oxygen vacancies and /or zinc interstitials (i.e were partially reduced in the as - grown condition).

Experiments on films of different thicknesses show that the top surface of the zinc oxide film was often of a different stoichiometry from the bulk and contained more oxygen. This surface layer can be up to 100 nm thick and was more resistive than the bulk [20]. In films where the entire film thickness is not much more than the thickness of the surface layer the resistivity will be higher than for a thicker film grown under the same conditions. This is due to either a lower carrier concentration or higher potential barriers at grain boundary interfaces since an increased amount of oxygen reduces the number of carriers. This explanation could account for the lower resistivities of films grown in wet ambients above 200°C since they are appreciably thicker. This thickness effect evidently outweighs the effect of preferred order which favours the thinner films.

The deposition of undoped zinc oxide using other techniques has yielded films possessing both higher and lower resistivities compared to this work. Spray pyrolysis of solutions of zinc acetate [5,6,21,22] at 360°C produced as-deposited films with resistivities in the range 1-100 Ωm which after hydrogen annealing fell to values in the range 10^{-2} - 10^{-4} Ωm.

ZnO films produced by activated reactive evaporation had resistivities of the order $8\times10^{-6}\Omega$m [23].

ZnO films produced by sputtering had very low resistivities in the range 10^{-5} - 10^{-6} Ωm [11,24]. CVD [25], MOCVD and photo-MOCVD [14] have produced layers with resistivities of $2\times10^{-4}\Omega$m, $10^{-1}\Omega$m and $10^{-2}\Omega$m. The influence of UV radiation on the growing film surface led to an improvement in the film conductivity by an order of magnitude.

The lowest resistivity obtained in the present work was $2.5\times10^{-2}\Omega$m for an undoped as-deposited film grown at 336°C in a wet ambient with in-flight heating present. After an annealing treatment the resistivity fell to $2\times10^{-4}\Omega$m. Thus the results of the present work compare favourably with previous work.

5.6 Chapter Five References

(1) Sears W.M., Gee M.A., *Thin Sol. Films, 165*, 265, (1988).

(2) Kamata K., Hirotsugu H., *Chemistry Letters*, 2021, (1984).

(3) Kamata K., Matsumoto S., *J.Ceram.Soc., 89 [6]*, 337, (1981).

(4) Cumberbatch T.J., Barden P.E., and Durrant J., *Thin Sol. Films 167*, 169, (1988).

(5) Aranovich J., Ortiz A. and Bube R.H., *J. Vac. Sci. Technol., 16(4)*, 994, (1979).

(6) Eberspacher C.,Fahrenbruch A.L. and Bube R.H., *Thin Sol. Films, 136*, 1, (1986).

(7) Tian Quan Liu, Osamu Sakurai, Nobuyasu Mizutani and , Masanori Kato, *J. Mat. Sci., 21*, 3698, (1986).

(8) Kamata K., Matsumoto S. and Otsuka N., *J. Chem. Soc. Japan [Pure Chemistry Section], 12*, 1715, (1983).

(9) Maissel L.I., Glang R., Handbook of Thin Film Technology, 8-41, McGraw-Hill Book Company, (1983).

(10) Barrett C.S., Massalski T.B., Structure Of Metals, McGraw-Hill Book Company, 615, (1966).

(11) Nanto H., Minami T., Shooj S. and Takata S., *J. Appl. Phys., 55 (4)* , 1029, (1984).

(12) Shimuzu M., Kamel H., Tanizawa M. and Shiosaki T., *J. Cryst. Growth, 89*, 365, (1988).

(13) Ghandi S.K., Field R.J. and Shealy J.R., *Appl. Phys. Lett., 37 [5]*, 449 ,(1980).

(14) Shimuzu M., Katayama T., Shiosaki T. and Kawabata A., *J. Cryst. Growth, 99*, 399, (1990).

(15) Shimuzu M., Katayama T., Tanaka Y. and Shiosaki T., *J. Cryst. Growth, 101*, 171, (1990).

(16) Major S., Banerjee A. and Chopra K.L.,*Thin Sol. Films, 108*, 333, (1983).

(17) Cossement D., Streydio J.M, *Journal Of Crystal Growth, 72*, 57, (1985).

(18) Major S., Banerjee A. and Chopra K.L,*J. Mater. Res. 1,[2]* , 300, (1986).

(19) Roth A.P., Williams D.F.,*J.Appl.Phys.52 (11)*, 6685, (1981).

(20) Orton J.W., Powell M.J.,*Rep.Prog.Phys., 43*, 81,(1980).

(21) Woods J., Russell G.J., Brinkman A.W. and Oktik S., *Preparation And Evaluation Of Thin/Thick Film Photovoltaic Devices*, Department Of Applied Physics, University Of Durham, (1987).

(22) Guillemoles J.F., Lincot D., Cowache P. and Vedel J., 10^{th} European Photovoltaic Solar Energy Conference And Exhibition, Lisbon 8-12 April, (1991).

(23) Brodie D.E., Singh R., Morgan J.H., Leslie J.D., Moore L.J., and Dixon A.E. , *Proc. $14^{t}h$ IEEE Photovoltaic Specialists Conf.*, San Diego, CA, 1980, 468.

(24) Webb J.B., Williams D.F., and Buchanan M., *Appl. Phys. Lett.*, 39, 640, (1981).

Chapter Six

Kinetics and Mechanism of the Deposition of ZnO from $Zn(acac)_2.H_2O$

6.1 Introduction

One of the first objectives of the work was to try to understand the processes which affect the variation of ZnO film thickness with growth temperature. This chapter therefore is concerned with the interpretation of the deposition behaviour of ZnO from $Zn(acac)_2.H_2O$ as a function of growth temperature and moisture content in the spray. The kinetic and mechanistic aspects of the decomposition of $Zn(acac)_2.H_2O$ to ZnO film are discussed in section 6.3 and this culminates in some detailed modelling of the spray process in section 6.4. The modelling highlights the most important physical features of the spray pyrolysis process.

6.2 Undoped ZnO Film Thickness Measurements

The results of thickness measurements on zinc oxide films grown in dry and wet ambients were described in chapter 5 and were shown in figures 5.1 and 5.2 as plots of ln(film thickness) versus reciprocal growth temperature.

To summarise, the film thickness increased progressively as the growth temperature decreased below 200°C in a dry ambient. Above 200°C the film thickness was virtually constant.

In a wet ambient the growth behaviour below 200°C was similar to that in dry conditions, except that the rate of change of growth rate with temperature and the resultant film thicknesses were larger. Above 200°C, the decrease in film thickness with increasing temperature was arrested and the film thickness went through a maximum at 306°C and then began to decrease with increasing growth temperature thereafter. Overall films grown with a wet ambient were thicker than those grown in a dry ambient.

6.2.1 Dependence of ZnO Film Thickness on Growth Temperature and Moisture

The variation of ZnO film thickness with growth temperature under both wet and dry conditions is produced by the physical properties of the spray droplets and their evaporation from the substrate area and the kinetics and mechanism of the decomposition of $Zn(acac)_2.H_2O$. The growth behaviour observed here at temperatures below 200°C (i.e film thickness decreasing with increasing growth temperature) is consistent with previously reported experience in the spray pyrolysis of other materials [1],[2]. However the change in the temperature dependence of growth above 200°C suggests that there is more than one mechanism for conversion of $Zn(acac)_2.H_2O$ to ZnO. In figure 6.1 the results of film thickness in a dry ambient versus reciprocal temperature are replotted.

The equation of the thick continuous line for growth between 100°C and 200°C is

$$t \simeq t_o exp\left(\frac{-E}{RT}\right) \tag{6.1}$$

with $t_o = 1.8 \times 10^{-9}$ m and E = -21 KJ mol^{-1}. This represents the low temperature route for the decomposition of $Zn(acac)_2.H_2O$ to ZnO (curve (1)). This line was extrapolated above 200°C and values obtained were then subtracted from the experimentally determined film thicknesses. This gave rise to another set of points connected with the broken line in figure 6.1 (curve 3) corresponding to the high temperature route for the decomposition of $Zn(acac)_2.H_2O$ to ZnO. Thus the spray pyrolysis of $Zn(acac)_2.H_2O$ involves two different growth mechanisms which operate over different but overlapping temperature ranges. The activation energy associated with the low temperature process was -21 KJ mol^{-1}, whereas that of the high temperature portion was +24 KJ mol^{-1}. These two values represent overall process energies that include the different chemical (i.e precursor decomposition) and physical (solvent evaporation) effects occurring during spray pyrolysis. The processes occurring at high temperature have a net positive activation energy showing that whatever processes are taking place are temperature

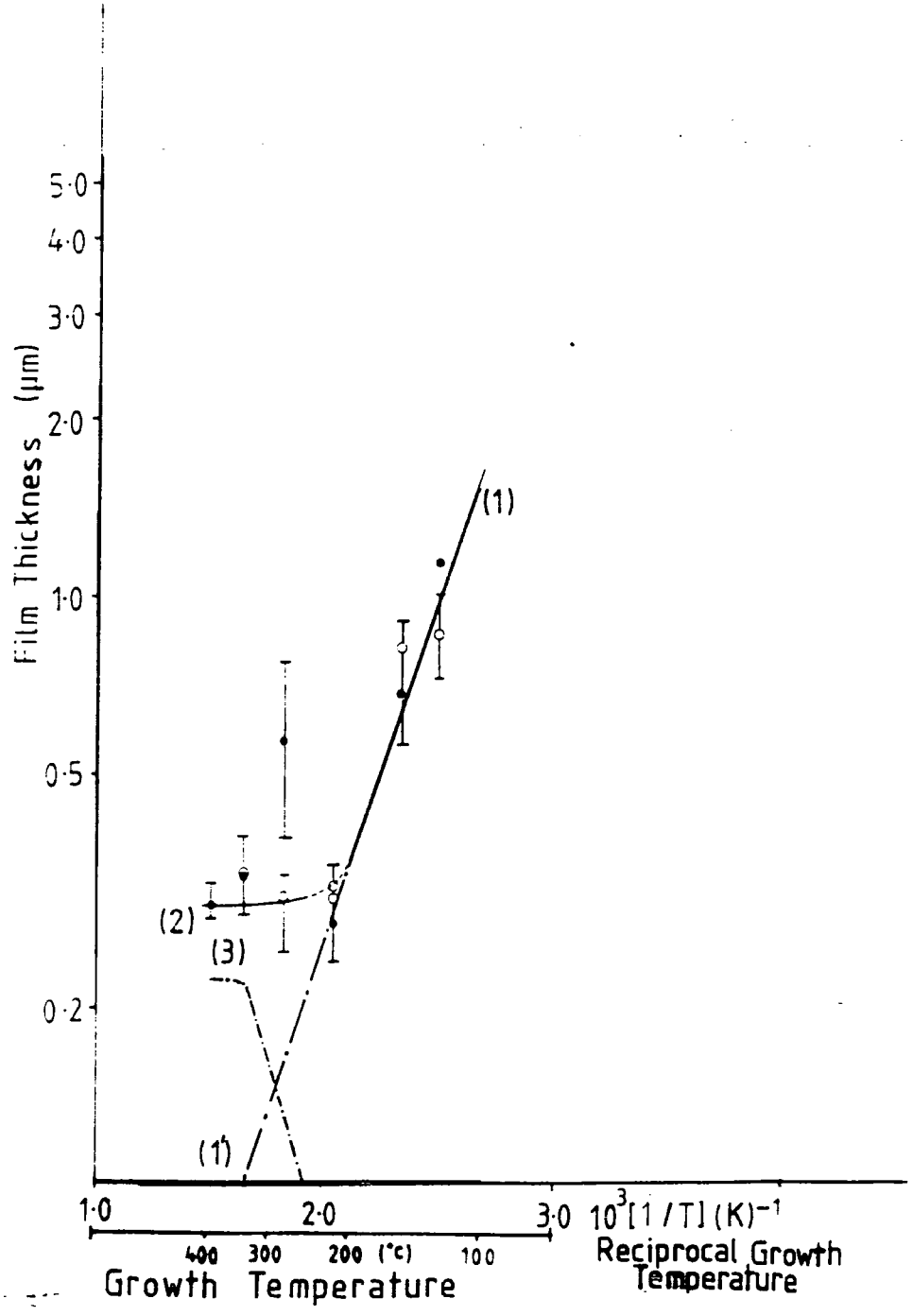

Figure 6.1. Variation of the zinc oxide film thickness with substrate temperature when grown in a dry ambient. Symbols: ● = growth with substrate and in-flight heating; ○ = growth with substrate heating. Low temperature growth (1), high temperature growth (2) and extrapolated low temperature growth (1') and thermolysis mechanisms (3-calculated).

activated. In this respect spray pyrolysis resembles CVD where the growth rate is also temperature activated. This type of behaviour has been reported for the growth of ZnO from $Zn(Et)_2$ [3],[4] where film growth rate is either diffusion limited or, at higher temperatures, kinetically limited. The low temperature growth however is temperature deactivated (negative activation energy) and resembles the spray pyrolysis of CdS from $CdCl_2$ [5] and ZnO from $Zn(acetate)_2$ [6].

Growth in a wet ambient is rather similar. Thickness measurements are replotted in figure 6.2. The extrapolation and subtraction procedure emphasises the change in growth behaviour at 200°C. The net effects of the higher temperature processes are also CVD-like as shown on curve 7 (which is the yield from the high temperature thermohydrolysis), and the low temperature growth mechanisms are again temperature deactivated. Below 200°C the characteristic is well described by equation 6.1 with slope and intercept values of E = -30 KJ mol^{-1} and $t_o = 3.4\times10^{-10}$ m (curve (4) figure 6.2). By subtracting the line for dry growth from that for wet growth below 200°C it was possible to assess the effects of a hydrolysis mechanism. This led to line 6 in figure 6.2 the constants of which are E = -36 KJ mol^{-1} and $t_o = 3.36\times10^{-11}$. If the effects of low temperature dry decomposition, low temperature hydrolysis and high temperature dry decomposition are subtracted from the high temperature wet thickness line a considerable yield of ZnO is left unaccounted for where the film thickness increases with growth temperature before flattening off at 300°C. Therefore there must be a fourth mechanism, or a variant of a previously mentioned mechanism or mechanisms (hydrothermolysis) which are more efficient because water is present.

6.3 Decomposition Mechanisms of $Zn(acac)_2.H_2O$

The structure of $Zn(acac)_2.H_2O$ is shown in figure 6.3 below. The zinc atom is coordinated to three different molecules through five bonds. Two of the molecules are acetylacetonate $C_5H_7O_2$ groups while the third is water. All bonding is between zinc and oxygen. The molecule has a square pyramidal shape. The Zn-OH_2 bond is the weakest.

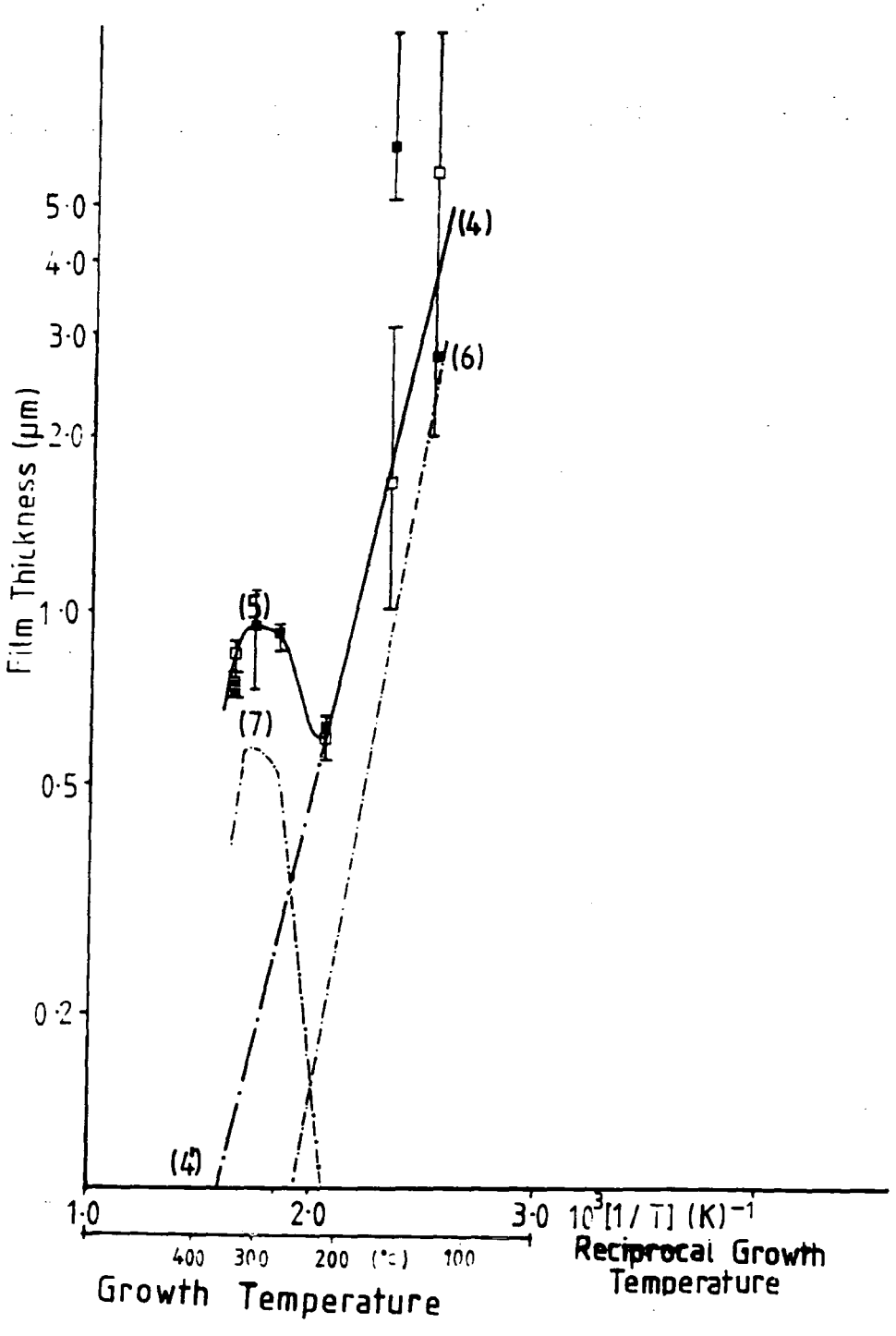

Figure 6.2. Variation of the zinc oxide film thickness with substrate temperature when grown in a wet ambient. Symbols: ■ = growth with substrate and in-flight heating; □ = growth with substrate heating. Low temperature growth (4), and high temperature growth (5). Calculated curves for variation of the zinc oxide yield with growth temperature by low temperature hydrolysis (6) and high temperature thermohydrolysis (7) mechanisms.

Figure 6.3. Chemical structure of the zinc acetylacetonate monohydrate molecule.

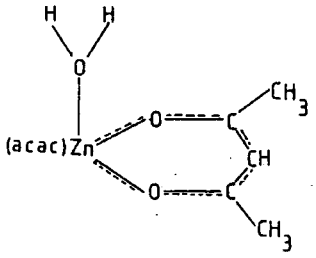

The molecule should consist of formal single and double bonds but due to electronic delocalisation, the bonds between Zn, $C_{2,3,4}$, and $O_{1,2}$ atoms are approximately equal[5]. The relative strengths of the interatomic bonds are listed in table 6.1.

Table 6.1. Summary of the bond energies between carbon, oxygen, hydrogen and zinc

Bond Energies							
Bond	C-C	C-O	C-H	Zn-O	O-H	C=C	C=O
KJ mol^{-1}	345	357	411	276	460	602	798

Thus the thermodynamic ordering of the breaking of single bonds is Zn-O then C-C, C-O, C-H, O-H, and the order for the breaking of double bonds is C=C then C=O. However this does not take into account the possible steric and kinetic effects that might outweigh thermodynamic considerations. Consequently, certain decomposition pathways involving a series of bond-breaking and bond- forming events that represent the lowest energy route in theory might not be the pathways to decomposition actually observed.

It is also useful to know the electronegativities of individual atoms as this determines which atoms have either positive or negative charges in any particular molecule. The electronegativity gives a measure of the electron withdrawing power of an atom and in a molecule helps to establish the relative distribution of electon density and therefore the partial charges on atoms. When atoms of low electronegativity are bonded to atoms of high electronegativity, electron density is shifted to atoms of higher electronegativity (higher electron withdrawing power) from adjoining atoms. As a result atoms with a high electron density have a partial negative charge while adjoining atoms will have

partial positive charges. In some mechanistic steps decomposition takes place when an atom in a molecule with a partial charge of one sign attacks an atom in another molecule with a partial charge of opposite sign. This is called nucleophilic attack if the atom being attacked has a partial positive charge. The electronegativities of atoms involved in the decomposition mechanisms of $Zn(acac)_2.H_2O$ to ZnO are shown in table 6.2.

Table 6.2. Summary of the electronegativities of elements

Atom Electronegativities				
Atom	C	H	O	Zn
Electronegativity	2.5	2.2	3.44	1.65

These figures imply that oxygen has the highest electron withdrawing power and zinc the lowest. The order of preference for nucleophilic attack on the basis of these figures alone would be Zn, H, C, and O.

6.3.1 Films Grown in a Dry Ambient

Mechanistic work on $Zn(acac)_2.H_2O$ using DSC, TG, and DTA has shown that it can decompose in at least three different ways in the spray process. Firstly the molecule may suffer pyrolysis, the bulk decomposition temperature of which is 191°C[6]. Secondly, Coates and Banister[7] have shown that decomposition can occur at temperatures below 191°C via an *intra*molecular hydrolysis due to the presence of coordinated water in the monohydrate. Finally, Kamata has shown that the mixing of water with $Zn(acac)_2.H_2O$ yields zinc oxide [8], suggesting an *inter*molecular hydrolysis.

(a) *Intra*molecular Mechanism

It is probable that for growth below 200°C the route to ZnO is the intramolecular one although this has been estimated to be only 3-4% efficient [7].

From figure 6.1 (deposition in a dry ambient) it is evident that a rapid decrease occurs on increasing the growth temperature from 100°C to 200°C, and as the extrapola-

tion of the low temperature curve shows, the yield from the intramolecular route alone has become negligibly small (0.08μm) by a substrate temperature of 396°C. Larger thicknesses were obtained between 100°C and 200°C than at higher temperatures due to physical effects (evaporation and convection). The preferential loss of precursor from the substrate before decomposition will be discussed in section 6.3.

In the intramolecular route to decomposition it is probable that the oxygen atom (with partial negative charge) in coordinated water attacks the $Zn(acac)_2.H_2O$ at the carbonyl carbon C_2 in a nucleophilic process (i.e at atoms with partial positive charge).

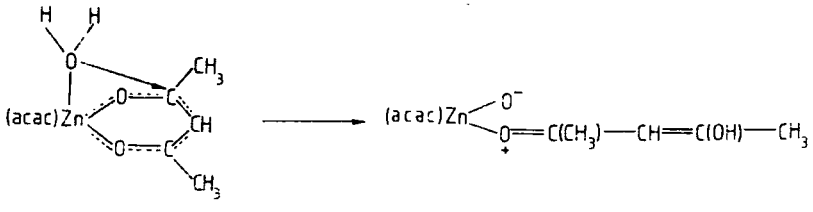

Figure 6.4. First step in the *intra*molecular route to the decomposition of $Zn(acac)_2.H_2O$ to ZnO

Figure 6.4 corresponds to nucleophilic attack at the carbonyl atom which would have a partial positive charge, by the oxygen atom of the water molecule. This attack results in the cleavage of the carbon-oxygen adjacent bond to the zinc central atom, the formation of a bond between C_2 and the oxygen atom of the coordinated water molecule, and the formation of carbon - carbon and carbon oxygen double bonds. This leaves a $Zn(acac)O^-$ coordinated to a $C_5H_7O_2$ molecule which from an electronic standpoint is self-sufficient. This is an exothermic step the heat of reaction being $\sim$-700 KJ mol^{-1}. Cleavage of the bond joining this electronically self-sufficient molecule to the $Zn(acac)_2^-$ molecule is shown in figure 6.5. This step is nominally endothermic since it involves the breaking of a Zn-O bond. However it is probable that the energy change is smaller than the full Zn-O bond energy, due to the electronic stability of the $C_5H_7O_2$ molecule.

Figure 6.5 Second step in the *intra*molecular route to the decomposition of $Zn(acac)_2.H_2O$ to ZnO.

For the decomposition of $Zn(acac)O^-$ it is probable that the following steps take place as shown in figure 6.6(a) :

(I) the cleavage of a zinc-oxygen bond, (II) the breaking of a carbon-hydrogen bond, (III) the breaking of a carbon-oxygen bond, (IV) the formation of an oxygen-hydrogen bond, (V) the formation of a carbon-carbon double bond.

This is an endothermic step with a heat of reaction of approximately +330 KJ mol^{-1}.

Figure 6.6(a). Third step in the *intra*molecular route to the decomposition of $Zn(acac)_2.H_2O$ to ZnO.

(b). Fourth step in the *intra*molecular route to the decomposition of $Zn(acac)_2.H_2O$ to ZnO.

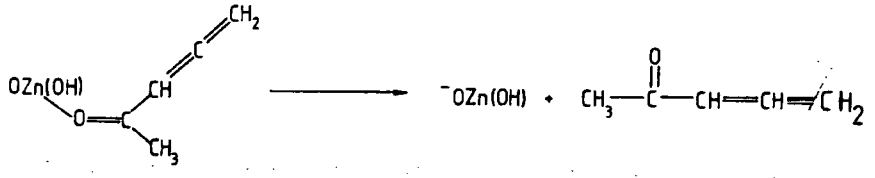

Figure 6.6(b) shows the decomposition of $^-OZn(OH)OC(CH_3CHCCH_2)$. The $Zn(OH)O^-$ species formed on the surface of the film are presumably able to migrate to a site on the film where incorporation could occur.

The byproduct C_5H_6O probably remains on the substrate for a relatively short time before volatilizing away. The heat of reaction is again likely to be endothermic

but less than the zinc oxygen bond energy ($\sim$+276 KJ mol^{-1}).

The reaction could either occur in the spray itself or at the substrate. If the reaction occurred in the spray then the resulting film would have a powdery surface due to the fallout of the ZnO formed in the spray. Spray artefacts on film surfaces were observed and might indicate that some prereaction does occur (section 5.3.4 and 5.3.7).

(b) Thermolysis Mechanism

As the growth temperature is raised beyond 200°C the thermolysis process is likely to occur more readily and the intramolecular route is less likely to contribute to the overall yield of ZnO.

From the work of Ohrbach, MacDonald and Politycki [9],[10],[11] it appears that the thermolysis of $Zn(acac)_2.H_2O$ involves the stepwise removal of both acetylacetonate groups. It is possible to make suggestions as to the likely type and sequence of fragmentation and the identity of the fragments from the published works. However the decomposition mechanism of $Zn(acac)_2.H_20$ in a solvent environment such as in spray pyrolysis might not exactly parallel the mechanism as determined by the study of reaction products (in the vapour phase) by mass spectroscopy.

It is assumed that since the H_2O ligand is relatively weakly coordinated to the zinc atom, the H_2O is rapidly detached at high temperatures and does not necessarily lead to the break-up of the entire molecule.

There are three possible routes to the loss of the first acetylacetonate group:

The first route involves the loss of the complete ligand as shown below.

$$Zn(acac)_2^+ = Zn(acac)^+ + (acac)^{\cdot} \qquad (6.2)$$

Bond energy calculations suggest that this is an endothermic process with two Zn - O bonds being broken, the heat of reaction being $\sim$+552 KJ mol$-$1.

The second possible route to the loss of the first acetylacetonate group involves: the breaking of a Zn-O bond at (I) in figure 6.7, the cleavage of a carbon-carbon bond at (III), the formation of a carbon oxygen double bond at (II),

This route is endothermic, the heat of reaction being $\sim$+180 KJ mol^{-1}.

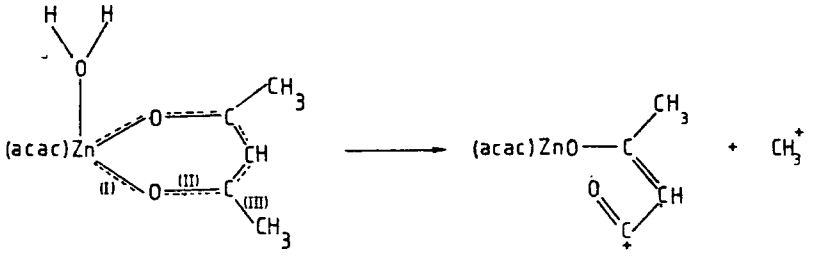

Figure 6.7. First step in the second and third fragmentation routes leading to the loss of the first acetylacetonate group.

However, to accomplish the loss of the rest of the first acetylacetonate group a further step occurs. This involves a rearrangement of the remainder of the first acetylacetonate fragment as shown in figure 6.8. requiring the cleavage of a Zn-O bond at (I), and the formation of a carbon oxygen double bond at (II), the transfer of an electron pair from bond (III) to bond (IV).

This step is exothermic with a heat of reaction of $\sim$-165 KJ mol^{-1}.

Figure 6.8. Final step in the second fragmentation route leading to loss of the first acetylacetonate group.

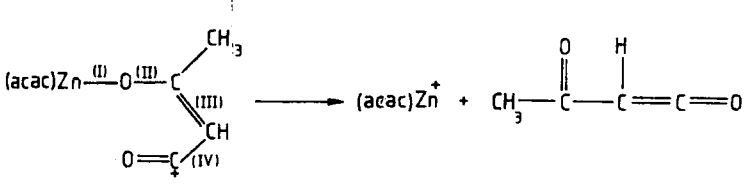

The third route begins with the fragmentation of the $Zn(acac)_2.H_2O$ molecule according to the step outlined in figure 6.7. This is followed by a rearrangement in which a carbon-oxygen double bond is formed at (I) and an electron pair is transferred from bond (II) to bond (III) as shown in figure 6.9(a). This step is exothermic with a heat of reaction of -440 KJ mol^{-1}. This is followed by the loss of two CH_2CO molecules in consecutive steps as outlined in figures 6.9(b) and 6.9(c).

Figure 6.9(a). Second step in the third fragmentation route leading to the loss of the first acetylacetonate group.

(b). Third step in the third fragmentation route leading to the loss of the first acetylacetonate group.

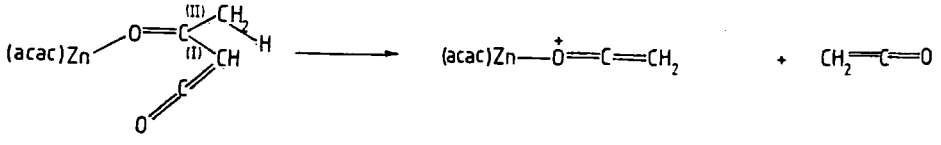

(c). Final step in the third fragmentation route leading to the loss of the first acetylacetonate group.

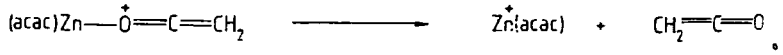

Initially (figure 6.9(b)), the molecules of $Zn(C_4H_4O_2)$ break up to form $Zn(C_2H_3O)$ and CH_2CO molecules. This is an endothermic step (heat of reaction $\sim$+88KJ mol^{-1}) involving the cleavage of the carbon-carbon single bond at (I), a hydride transfer from C_1 to C_3 and the formation of a carbon-carbon double bond at (II).

The final step towards the loss of the first acetylacetonate group involves the further loss of CH_2CO molecules with the subsequent release of the $Zn(acac)^+$ molecules as shown in figure 6.9(c). A zinc oxygen bond is severed in this step. However the coordinated molecule is electronically stable and therefore the heat of reaction is less than the zinc oxygen bond energy.

It is possible to envisage the remaining $Zn(acac)^+$ group becoming coordinated to th ZnO film surface as O-Zn-O-$Zn(acac)^+$.

The fragmentation of the remaining acetylacetonate ligand can go by two separate routes as shown in figure 6.10.

Figure 6.10. Only step in the first fragmentation route leading to the loss of the second acetylacetonate group.

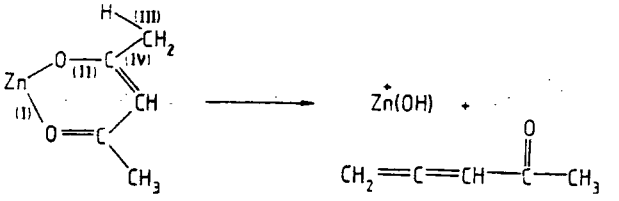

The first route involves the cleavage of the zinc oxygen bond at (I), the cleavage of the C-O bond at (II), the cleavage of the C-H bond at (III), the transfer of the free hydrogen atom to the oxygen at (I), and the formation of a carbon-carbon bond at (IV), leading to the formation of a $Zn(OH)^+$ and a $CH_2CCHCOCH_3$ byproduct. This step is endothermic ($\sim$+330 KJ mol^{-1}). The $Zn(OH)^+$ species gives an approximate idea of the identity of the product of this reaction. Such a species may not be stable or long-lived. $Zn(OH)^+$ would probably decompose rapidly to ZnO.

The second possible breakdown mechanism for the loss of the second acetylacetonate group is shown in figure 6.11 and equation 6.3. Initially it involves: the cleavage of a carbon-carbon single bond at (I) and the cleavage of a carbon-hydrogen bond at (II) followed by the formation of a carbon-hydrogen bond at (III), to yield $ZnOCCH_2CH_3$ and CH_2CO. This step is endothermic ($\sim$+350 KJ mol^{-1}).

Figure 6.11. First step in the second fragmentation route to the loss of the second acetylacetonate group

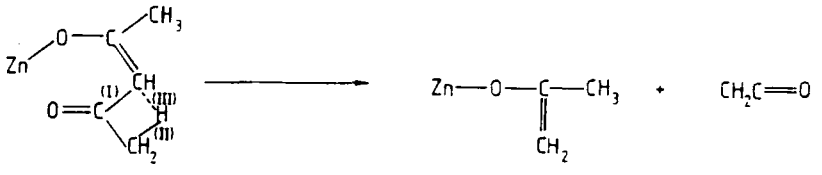

$$Zn(C_5H_7O_2) = Zn(C_3H_5O) + CH_2CO \qquad (6.3)$$

The second step in the final fragmentation of the second acetylacetonate ligand involves: the breaking of a carbon-oxygen bond at (I), the breaking of a carbon-hydrogen bond at (II), the formation of an oxygen-hydrogen bond at (III), the formation of a

carbon-carbon single bond at (IV), as shown in Figure 6.12. This step is exothermic ($\sim$-37 KJ mol^{-1}).

Figure 6.12. Final step in the second fragmentation route leading to the loss of the second acetylacetonate group

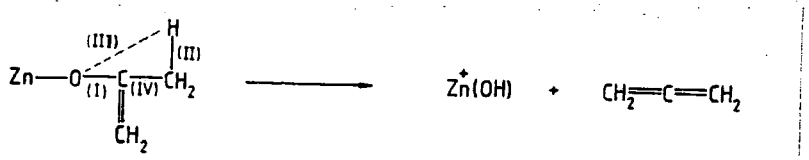

The overall equation is :

$$Zn(C_3H_5O) = Zn(OH)^+ + CH_2CCH_2 \qquad (6.4)$$

Again the final zinc containing product could be described only generally by the $Zn(OH)^+$ species. It probably decomposes to ZnO or reacts with another hydroxyl group to form $Zn(OH)_2$. The nature of the byproducts ensures that they volatilize away since they are hydrocarbon species of low molecular weight.

6.3.2 Films Grown in a Wet Ambient

The presence of water in the spray means that hydrolysis identical to that reported by Kamata [11] can occur. (This has been shown to occur at temperatures as low as 25°C). There are then two decomposition mechanisms which can lead to the formation of ZnO. The intramolecular mechanism, involving water coordinated within the hydrated molecule, and conventional hydrolysis resulting from the addition of water to the spray. Thus the deposition efficiency is in principle enhanced in the presence of H_2O. It was observed that the intramolecular mechanism depended on the presence of water to detach the acetylacetonate groups. The results suggest that the additional hydrolysis decomposition mechanism is more efficient in yielding ZnO from $Zn(acac)_2.H_2O$ than the intramolecular mechanism up to 200°C. At higher growth temperatures the spray process becomes significantly more efficient than would be expected from the three known mechanisms.

Two possible pathways for the intermolecular hydrolysis of $Zn(acac)_2.H_2O$ are outlined in figures 6.13 to 6.14. The water molecules could attack $Zn(acac)_2.H_2O$ at

carbon (C_2) (fig.6.13) or at zinc (fig.6.14). The step in figure 6.13(a) shows that the action of nucleophilic attack by water at carbon (C_2) results in the cleavage of a carbon-oxygen bond at (I) and a hydride transfer from water to C_2. The step is exothermic ($\sim$-240KJ mol^{-1}).

Figure 6.13(a) First step in the first route to the *inter*molecular hydrolysis of $Zn(acac)_2.H_2O$

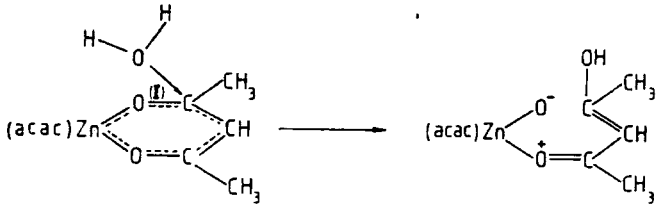

(b) Second step in the first route to the *inter*molecular hydrolysis of $Zn(acac)_2.H_2O$

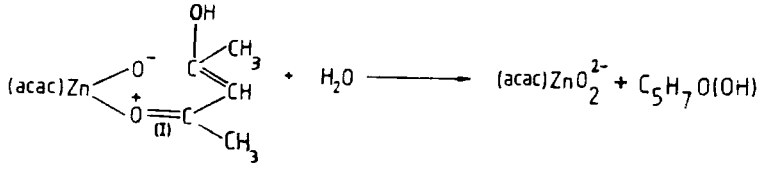

Figure 6.13(b) shows the cleavage of a carbon-oxygen bond at (I) leading to the removal of the first acetylacetonate ligand. The steps in figures 6.13(a) and (b) are repeated for the removal of the second acetylacetonate ligand. This leads to the formation of ZnO_4H_n where n = 1 - 4. The second route to decomposition via attack at zinc by oxygen in H_2O is shown in figure 6.14. The steps of this second route are : the cleavage of a zinc-oxygen bond at (I), the formation of a carbon-oxygen bond at (II) and the formation of a carbon-carbon double bond at (III). This process may be repeated until the first acetylacetonate group is removed. The second step to the removal of the first group is shown in figure 6.14(b) and involves the cleavage of a zinc-oxygen bond at (IV).

The loss of the second acetylacetonate group occurs through a repeat of the steps shown in figures 6.14(a) and (b).

Figure 6.14(a) Initial step of the second route to the *inter*molecular hydrolysis of $Zn(acac)_2.H_2O$

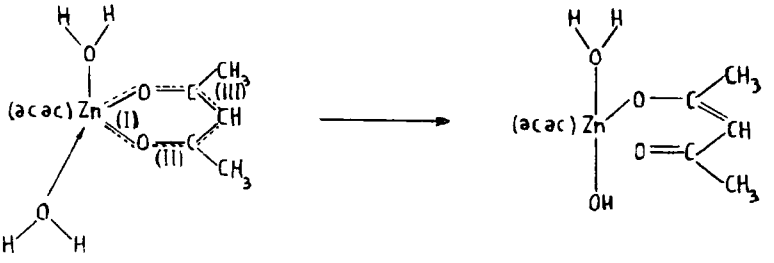

(b) Second step of the second route to the *inter*molecular hydrolysis of $Zn(acac)_2.H_2O$

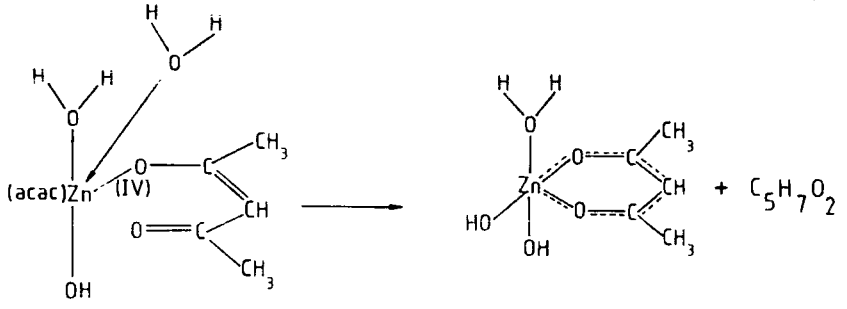

The steps have a heat of reaction of $\sim$-650 KJ mol^{-1}. The resulting species formed is $Zn(OH_2)(OH)_4^{2+}$. It is possible that the solvent plays a role in the decomposition of $Zn(acac)_2.H_2O$. This could occur as a consequence of the stabilization of ionic species through the delocalisation of charge over a cloud of solvent molecules surrounding the decomposing precursor. It is also possible that solvent molecules coordinate to fragments of $Zn(acac)_2.H_2O$.

The rate of the *intra*molecular mechanism is significant at low temperatures and when water is present the hydrolysis mechanism is further enhanced. At high temperatures the thermolysis becomes more important as more energy is available and as both the coordinated and the externally added water are driven off more rapidly by evaporation. If it may be assumed that the *intra*molecular and thermolytic processes are independent of added water, then the net contribution of hydrolysis to the decomposition of $Zn(acac)_2.H_2O$ is determined from the difference between wet and dry characteristics (figure 6.2).

The resulting line falls steeply as growth temperature increases indicating that this decomposition is very temperature sensitive. In fact this mechanism could serve to en-

hance the *intra*molecular mechanism at low temperatures (100°C), but at temperatures higher than 200°C the results indicate that it is beneficial to have weakly bound water coordinated directly to the precursor. This does not account for the large thicknesses obtained at high growth temperatures. This is likely to be due to an enhanced variant of thermolysis (hydrothermolysis).

The heats of reaction indicate that the low temperature processes are exothermic (intramolecular -94 to -370 KJ mol^{-1}, hydrolysis -1000 KJ mol^{-1}) and that the high temperature processes are endothermic +291 to 900 KJ mol^{-1}. The activation energies indicate that the low temperature processes are deactivated by an increase in temperature which would tend to agree with the interpretation of the values of the heats of reaction (exothermic), which suggest that exothermic reactions are suppressed by increasing reaction temperature. The pre-exponential factors are very small in magnitude for processes occurring at low temperature (for processes that are exothermic with negative activation energies) and considerably larger for high temperature processes. This might indicate that the collision frequency of $Zn(acac)_2.H_2O$ with other molecules of the same formula or with solvent molecules increases as the growth temperature increases. Such collisions can lead to the decomposition of $Zn(acac)_2.H_2O$ through the concentration of energy in particular bonds or the activation of the entire molecule. This can be called the transition state. From it the molecule can either lose energy again to surrounding molecules without breaking up, or can be decomposed to the products. In the spray it is likely that molecules of $Zn(acac)_2.H_2O$ undergo many collisions before decomposition, perhaps in order to gain enough energy to decompose, since individual steps are endothermic.

The *intra*molecular route is a 3 step process, the thermolysis a 2 - 8 step process and intermolecular hydrolysis a 4 step process. The thermolysis is the most complex and yet offers more pathways than the others. As for the hydrothermolysis-thermolysis occurring at high temperatures it can only be presumed that water acts in some way to increase the rate of individual steps and perhaps lower the overall heat of reaction.

It is probable that the decomposition through the thermolysis mechanism involves the activation of zinc precursor molecules through multiple collisions, whereas mechanisms involving water molecules need only collide with one to undergo hydrolysis or not at all if the coordinated water is responsible for decomposition. In conclusion the decomposition of $Zn(acac)_2.H_2O$ is complicated and requires further work, but it is apparent that the decomposition mechanism does affect the film structure indirectly (through the increased reaction efficiency at lower temperatures) and possibly directly through surface reactions and a change in the mechanism for films grown in a dry ambient.

To summarise:

(1) Zinc oxide film growth is governed by three main decomposition routes: the *intra*molecular hydrolysis route, the thermolytic route and the *inter*molecular hydrolytic route.

(2) The *intra*molecular route leads to the decomposition of $Zn(acac)_2.H_2O$ between growth temperatures of 100°C and approximately 276°C, the thermolysis mechanism between 191°C and higher temperatures and the hydrolysis mechanism at growth temperatures between 100°C and 200°C. There are one or more possible pathways for these decomposition routes but it is not known which are favoured.

6.4 Spray Modelling

This section outlines the physical aspects (i.e the processes of desorption and evaporation) of spray pyrolysis using kinetic modelling.

The aim of the modelling is to elucidate the main factors affecting the process and to make a comparison between theory and the experimental data. Two models have been considered. The first assumes that the $Zn(acac)_2.H_2O$ (or simply $Zn(acac)_2$) arrives above the growing film surface and that some of the precursor is converted to ZnO and some is vented off. It is therefore possible to define two rate constants at which these processes occur and write an equation for the rate of change of precursor

concentration on the substrate. In the second model, the precursor is assumed to form a reactive intermediate (which could be for example $Zn(OH)_{1/2}$ ZnO_2^{2-} or ZnO_4H_n where n = 1 - 4 which then decomposes to form the ZnO.

6.4.1. First Model

If R (mol s^{-1}) is the rate of arrival of precursor at the substrate and k_{ZnO} is the rate of decomposition of $Zn(acac)_2$, k_{evap} is the rate at which precursor leaves the substrate without decomposing and $[Zn(acac)_2]$ is the concentration of the precursor in the spray, then the following equation can be written for the rate of change of $[Zn(acac)_2]$ under the assumptions of model 1

$$\frac{d[Zn(acac)_2]}{dt} = R - k_{ZnO}[Zn(acac)_2] - k_{evap}[Zn(acac)_2] \tag{6.5}$$

The rate of formation of ZnO is

$$\frac{d[ZnO]}{dt} = k_{ZnO}[Zn(acac)_2] \tag{6.6}$$

where [ZnO] is the concentration of ZnO on the substrate. The exact value of k_{ZnO} will depend on the temperature and the presence of water and which of the intramolecular or thermolytic or hydrolytic mechanisms are operating as indicated by the experimental data presented in section 6.3.2. The magnitude of k_{evap} will also be influenced by the substrate temperature and should increase as the growth temperature increases.

Under steady state conditions the surface concentration of the zinc precursor remains constant and

$$\frac{d[Zn(acac)_2]}{dt} = 0 \tag{6.7}$$

and

$$R - k_{ZnO}[Zn(acac)_2] - k_{evap}[Zn(acac)_2] = 0 \tag{6.8}$$

Defining a mean rate constant k_{ave} by the following expression

$$k_{ave} = k_{ZnO} + k_{evap} \tag{6.9}$$

then equation 6.8 can be rewritten as

$$[Zn(acac)_2] = \frac{R}{k_{ave}} \tag{6.10}$$

which can be used to obtain information about the spray process. The relative magnitudes of k_{ZnO} and k_{evap} can vary in three different ways, $k_{ZnO} > , = , < k_{evap}$. Inserting $k_{ZnO} = k_{evap}$ in equations 6.9 and 6.10 gives

$$[Zn(acac)_2] = \frac{R}{2k_{ZnO}} \tag{6.11}$$

Combining equations 6.6 and 6.11 gives the following expression for the formation of ZnO

$$\frac{d[ZnO]}{dt} = 0.5R \tag{6.12}$$

and integrating leads to

$$[ZnO] = 0.5Rt \tag{6.13}$$

giving the amount of ZnO deposited after a spray time t. It indicates that when the rate of evaporation equals the rate of decomposition of precursor to ZnO then half of the material is deposited. When $k_{ZnO} \gg k_{evap}$ equation 6.10 can be written as

$$[Zn(acac)_2] \simeq \frac{R}{k_{ZnO}} \tag{6.14}$$

Substitution into equation 6.6 gives

$$\frac{d[ZnO]}{dt} \simeq R \tag{6.15}$$

indicating that the rate of conversion to ZnO is nearly equal to the rate of arrival of $Zn(acac)_2.H_2O$ and therefore,

$$[ZnO] \simeq Rt \tag{6.16}$$

indicating that the process is efficient and that most of the precursor is converted to ZnO on the substrate.

The third condition sets the rate of evaporation of the precursor as greater than the rate of decomposition of precursor to ZnO, which is more similar to our experimental situation than the other two cases. Then,

$$k_{evap} \simeq k_{ave} \tag{6.17}$$

and

$$[Zn(acac)_2] \simeq \frac{R}{k_{evap}} \tag{6.18}$$

and the rate of change of concentration of ZnO is given by

$$\frac{d[ZnO]}{dt} \simeq \frac{Rk_{ZnO}}{k_{evap}} \tag{6.19}$$

or on integrating

$$[ZnO] \simeq \frac{Rtk_{ZnO}}{k_{evap}} \tag{6.20}$$

Therefore the amount of zinc oxide deposited in this case will depend on the ratio of the rate of decomposition of precursor to ZnO to the rate of evaporation of precursor from the substrate but will always be less than half the arrival rate.

Rate constants are Arrhenius type expressions of the form

$$k = A_a exp\left(\frac{-E_a}{RT}\right) \tag{6.21}$$

where A is a constant and E_a is the activation energy. The pre-exponential factor is the number of collisions between reactant molecules per unit time and the E_a is the energy required to initiate a reaction. This means that the expressions for the rates of formation of ZnO and evaporation from the substrate can be written in the following way

$$k_{ZnO} = A_{ZnO} exp\left(\frac{-E_{ZnO}}{RT}\right) \tag{6.22}$$

$$k_{evap} = A_{evap} exp\left(\frac{-E_{evap}}{RT}\right) \tag{6.23}$$

The ratio of k_{ZnO} to k_{evap} is then given by

$$\frac{k_{ZnO}}{k_{evap}} = \frac{A_{ZnO}}{A_{evap}} exp\left(\frac{E_{evap} - E_{ZnO}}{RT}\right) \tag{6.24}$$

Equations 6.20 and 6.24 can be combined to give

$$[ZnO] \simeq Rt \frac{A_{ZnO}}{A_{evap}} exp\left(\frac{E_{evap} - E_{ZnO}}{RT}\right) \tag{6.25}$$

Taking the logarithm of this expression gives

$$ln[ZnO] \simeq ln\left(Rt \frac{A_{ZnO}}{A_{evap}}\right) + \left(\frac{E_{evap} - E_{ZnO}}{RT}\right) \tag{6.26}$$

A plot of ln(thickness) versus reciprocal growth temperature then has a slope equal to

$$\left(\frac{E_{evap} - E_{ZnO}}{R}\right)$$

This expression applies when the rate constant for the evaporation of precursor from the substrate k_{evap} is greater than the magnitude of the rate constant for the decomposition of $Zn(acac)_2.H_2O$.

Thus if E_{evap} is greater than E_{ZnO} then the slope will be positive and if E_{evap} is less than E_{ZnO} then the slope of the curve will be negative. These two regimes

are drawn out in figure 6.1 and are similar to those marked (1) and (3). However the interaction of chemical processes makes separate effects difficult to disentangle.

6.4.2 Second Model

The second model envisages a process in which some of the precursor at the substrate can be converted to an intermediate that decomposes to ZnO and some can evaporate directly from the substrate unchanged.

Therefore there are three processes at work with three rate constants : (k_{evap}), the rate of decomposition of $Zn(acac)_2.H_2O$ to the intermediate ($k_{Zn(O_xH_y)}$), and the rate of conversion of the intermediate to ZnO (k_{ZnO}).

The rate of change of the precursor concentration is

$$\frac{d[Zn(acac)_2]}{dt} = R - k'_{Zn(O_xH_y)}[Zn(acac)_2] - k'_{evap}[Zn(acac)_2] \qquad (6.27)$$

In the steady state

$$R - k'_{ave}[Zn(acac)_2] = 0 \qquad (6.28)$$

where

$$k'_{ave} \simeq k'_{Zn(O_xH_y)} + k'_{evap} \qquad (6.29)$$

In the steady state the rates of change of concentration of $Zn(O_xH_y)$ and ZnO are

$$\frac{d[Zn(O_xH_y)]}{dt} \simeq k'_{Zn(O_xH_y)}[Zn(acac)_2] - k'_{ZnO}[Zn(O_xH_y)] = 0 \qquad (6.30)$$

and

$$\frac{d[ZnO]}{dt} \simeq k'_{ZnO}[Zn(O_xH_y)] = 0 \qquad (6.31)$$

so that

$$\frac{d[ZnO]}{dt} \simeq k'_{Zn(O_xH_y)}[Zn(acac)_2] \qquad (6.32)$$

From equation 6.29

$$R \simeq (k'_{evap} + k'_{Zn(O_xH_y)})[Zn(acac)_2] \tag{6.33}$$

or

$$[Zn(acac)_2] \simeq \frac{R}{k'_{ave}} \tag{6.34}$$

which is the same as

$$[Zn(acac)_2] \simeq \frac{R}{\left(k'_{evap} + k'_{Zn(O_xH_y)}\right)} \tag{6.35}$$

Therefore,

$$\frac{d[ZnO]}{dt} \simeq \left(\frac{k'_{Zn(O_xH_y)}R}{k'_{ave}}\right) \tag{6.36}$$

Integrating this expression gives

$$[ZnO](t) \simeq \left(\frac{k'_{Zn(O_xH_y)}Rt}{k'_{ave}}\right) + constant \tag{6.37}$$

with the condition

$$k'_{evap} > k'_{Zn(O_xH_y)} \tag{6.38}$$

then equation 6.28 becomes

$$R - k'_{evap}[Zn(acac)_2] = 0 \tag{6.39}$$

and substitution into equation 6.37 leads to

$$[ZnO](t) \simeq \frac{\left(k'_{Zn(O_xH_y)}\right)k'_{evap}[Zn(acac)_2]t\Big)}{k'_{ave}} \tag{6.40}$$

If

$$k'_{Zn(O_xH_y)} \simeq k'_{evap}$$

then

$$[ZnO](t) \simeq \frac{\left(k^{2'}_{Zn(O_xH_y)}[Zn(acac)_2]t\right)}{k'_{ave}} \tag{6.41a}$$

$$[ZnO] \simeq \frac{\left(k^{2'}_{evap}[Zn(acac)_2]t\right)}{k'_{ave}} \tag{6.41b}$$

Substituting for the rate constants with expressions in terms of the activation energies and pre-exponential constants gives the expression

$$[ZnO] \simeq \frac{\left(A_{evap}exp\frac{(-E_{evap})}{kT}\right)^2[Zn(acac)_2]t}{\left(A_{evap}exp\frac{(-E_{evap})}{kT} + A_{Zn(O_xH_y)}exp\frac{(-E_{Zn(O_xH_y))}}{kT}\right)} \tag{6.42}$$

A plot of ln(thickness) versus reciprocal temperature if these conditions applied would have a slope of

$$\frac{(-E_{evap})}{(-E_{evap} + E_{Zn(O_xH_y)})}$$

6.5 Discussion

In the spray pyrolysis process the solvent has to be driven off before the spray reaches the substrate for the deposition of films of an acceptable quality. Above 200°C for 0.1M solutions of $Zn(acac)_2.H_2O$ the large majority of solvent aerosol is driven off before it reaches the substrate surface. However in films grown below 200°C solvent impinges on the film surface. This has been shown in sections 5.2.4 and 5.2.7 to destroy and degrade film cohesion and surface morphology. If there is enough energy for the solvent to evaporate then the $Zn(acac)_2.H_2O$ will also evaporate to some extent and the rate of evaporation of both solvent and precursor increase as the growth temperature increases. In addition to this there then follows the decomposition of the precursor by one of the three routes described in section 6.3. Therefore the deposition characteristic depends not only on the efficiency and temperature range of the decomposition mechanisms themselves but also on the evaporation characteristics of the solvent and precursor. At growth temperatures below 200°C these reactions may to a certain extent occur in the liquid phase and the kinetic energy of the molecules will be low.

Above 200°C it is more likely that the reactions take place in the gas phase and at the film surface.

The maximum possible yield of the ZnO film thickness if all the precursor used were converted to ZnO would be 100μm. In fact the experimentally determined thickness was in the range 0.3-10μm. This means that the majority of the zinc precursor evaporates or is deflected through hydrodynamic effects. Thus the spray process fits the condition of k_{evap} greater than k_{ZnO} and spray pyrolysis is dominated by precursor effects. Thus from 100°C to 400°C there is a general trend of decreasing film thickness with increasing growth temperature and the rate of evaporation increases with respect to the rate of decomposition. However the rate of decomposition varies with temperature as the mechanism changes with temperature, and the presence or absence of water. Thus the rate of decomposition of the precursor under dry conditions should be larger at high temperature since the *intra*molecular mechanism, as determined by Coates and Banister[7] is only 3-4 % efficient. At high temperature the decomposition through the thermolysis mechanism is expected to be more efficient because the mechanism does not rely on the presence of H_2O. However the evaporation rate is still significant and the result is an overall decrease in ZnO film thickness with substrate temperature. From the theoretical interpretation of the spray pyrolysis process it is clear that the changes in slope as the temperature increases indicate a change in the sum (E_{evap} - E_{ZnO}). The slope of the experimental plot of ln(thickness) versus reciprocal temperature plot for films grown in a dry ambient indicates that E_{ZnO} is always greater than E_{evap} but the change in the slope between the temperature ranges 100°C - 200°C and 200°C - 400°C implies that a change occurs in the mechanism of decomposition of ZnO at about 200°C. This coincides with the change from the *intra*molecular to the thermolysis mechanism. This change in the dominant mechanism is reflected in the changes which were observed in the structural properties (i.e the bulk preferred orientation changes from (0002) to $(10\bar{1}1)$ and the electrical and optical properties. The slope of the plot above 200°C is approximately zero indicating that here E_{evap} - $E_{ZnO} \simeq 0$.

When water is present the effect is to introduce an additional mechanism to increase the rate of decomposition relative to the rate of evaporation. The presence of water not only increases the yield of ZnO but also changes the slope of the ln(thickness) versus reciprocal temperature plot for films grown in a wet ambient. This indicates a change in the sign of the activation energy, with the activation energy for evaporation being greater than that for process of decomposition . The presence of the water leads to the decomposition of the precursor along a lower energy route compared to straight thermolysis where the need for the breaking of bonds through collision and activation is replaced by the benefit of water catalysed hydrolysis.

6.6 Summary and Conclusions

Decomposition of ZnO from $Zn(acac)_2.H_2O$ occurs by four different routes. These are: 1/ *intra*molecular mechanism, a low temperature route where the coordinated water is responsible for the hydrolysis of $Zn(acac)_2.H_2O$. The mechanism is exothermic.

2/the thermolysis mechanism, a high temperature route where the only means of the decomposition of the zinc precursor are by the cleavage of bonds through the concentration of energy. This is likely to be aided by a high collision frequency among molecules. This is an endothermic mechanism.

3/ *inter*molecular mechanism, a low temperature mechanism where the hydrolysing agent is external. The mechanism is exothermic.

4/ an unknown mechanism, dependent on the onset of thermolysis and therefore a high temperature mechanism. It probably involves portions of the thermolysis aided by the water hydrolysis, lessening the reliance on purely thermal activation. The overall controlling factor is re-evaporation from the substrate across the temperature range studied.

Chapter Six References

(1) Chopra K.L., Kainthla R.C., Pandya D.K. and Thakoor A.P., *Physics of Thin Films, 12,* 167, (1982).

(2) Albin D.S,, Risbud S.H.,*Thin Sol. Films, 147,* 203, (1987).

(3) Roth A.P., Williams D.F.,*J. Appl. Phys., 52,* 6685, (1981).

(4) Shimuzu M.,Kamel H.,Tanizawa M. and Shiosaki T.,*J. Cryst. Growth, 89,* 365, (1988).

(5) Chow L.W., Lee Y.C. and Kwok H.L.,*Thin Sol. Films, 81,* 307, (1981)

(6) Aranovich J.,Ortiz A. and Bube R.H, *J. Vac. Sci Technol.,16(4),* 994, (1979).

(5) Shibata S.,Ohta M.,*J. Molec. Struc., 77,* 265, (1981).

(6) Charles R.G., Pawlikowski M.A.,*J. Phys. Chem., 62,* 440, (1958)

(7) Coates P., Priv. comm., University of Durham. (1992).

(8) Kamata K., Hosono H., Maeda Y. and Miyokawa K., *Chemistry Letters* , 2021, (1984).

(9) MacDonald C.G., Shannon J.S., *Aust. J. Chem.,19,* 1545, (1966).

(10) Ohrbach K.H., Radhoff G., and Kettrup A., *Thermochemica Acta, 67,* 189, (1983).

(11) Polytycki A., Hieber K., Science and Technology of Surface *Coatings*, Academic Press, ed. Chapman B.N., Anderson J.C., , NATO, (1974).

Chapter Seven

Deposition and Characterisation of Doped Zinc Oxide Grown at Low Temperature

7.1 Introduction

Since one of the prime objectives of the project was to deposit transparent conducting coatings on plastic our approach had been first to determine whether good quality films could be put down by spray pyrolysis in the range 150°C - 200°C. As it has been demonstrated, as described in chapter five, that this could be best done under dry conditions with substrate heating only, the next requirement was to improve the conductivity of such films by doping with a suitable donor impurity. $InCl_3$ was chosen for this because earlier work [1,2] had shown it to be the most effective. The growth of In doped ZnO films at low temperature forms the subject of this chapter. Other dopants have been investigated but proved less efficient. Experiments on these will be described later in chapter 9.

7.2 Growth of Doped Films

Growth of indium doped zinc oxide was initially carried out at 200°C. Three different concentrations of zinc precursor were used. They were 0.1M, 0.05M, and 0.02M solutions of $Zn(acac)_2.H_2O$ in propan-2-ol. Solutions were doped with either 3 atomic percent (at.%) or 6 atomic percent of $InCl_3.3H_2O$ and in all cases 700 cm^3 of solution was sprayed, on the glass substrate.

After these trials proved successful further experiments were standardised and all spray runs were carried out using 0.02M $Zn(acac)_2.H_2O$ doped with 6 atomic percent of $InCl_3.3H_2O$. Deposition was then carried out in the range 100°C-200°C on glass and on Upilex^R plastic supplied by ICI Plc. Upilex is a polyimide material and is described in detail in section 4.4. The spray times varied from 15 to 19 minutes. Thicker zinc oxide was also grown from a larger volume of solution (2.1 litres) when spray times varied from 41 minutes to 50 minutes.

7.3 Physical Properties of Films Grown at Low Temperature

7.3.1 Visual Appearance and Adherence of Films to Their Substrate

All films grown at low temperature in a dry ambient were adherent to the substrate, and those grown at 200°C from lower concentrations (0.02M) of $Zn(acac)_2.H_2O$ were smooth, clear, and speckle-free. The films grown from the highest concentrations (0.1M) of zinc precursor possessed a speckled surface but were otherwise clear and transparent.

The combined use of the highest zinc precursor concentration and highest dopant concentration led to films with the least transparency and highest roughness.

7.3.2 ZnO Film Thickness

The thicknesses of films grown solely from 700 ml of 0.02M solutions of $Zn(acac)_2.H_2O$ containing $InCl_3$ were roughly independent of dopant concentration at 200 nm. Thicknesses did vary with growth temperature (see figure 7.1) and with zinc precursor concentration, figure 7.2. Results are plotted in figure 7.1 for growth between 150°C and 200°C from 700 cm^3 of precursor solution. The film thicknesses varied from 0.43μm to 0.165μm over the temperature range 150°C to 200°C. The thicknesses of films grown using 2.1 litres of precursor solution are also plotted against growth temperature in figure 7.1 and are not appreciably dependent on temperature. The thicknesses of films deposited on Upilex^R plastic varied from 0.360μm to 0.550μm in the temperature range 175°C and 200°C. Clearly the nature of the substrate had little effect on the thickness of films grown at 200°C.

The relative insensitivity of the film thickness to dopant concentrations and temperature at these low temperatures is somewhat surprising. It suggests that the $InCl_3$ was in fact influencing the deposition of $Zn(acac)_2.H_2O$ by controlling the availability of nucleation sites and opposing evaporative effects during the growth of ZnO. The net effect is that the growth rate is influenced by the decomposition of $InCl_3$ which sets in by 200°C (see section 7.4).

The results from the preliminary doping trials are plotted as film thickness against the concentration of $Zn(acac)_2.H_2O$ in figure 7.2 for films grown at 200°C from solutions

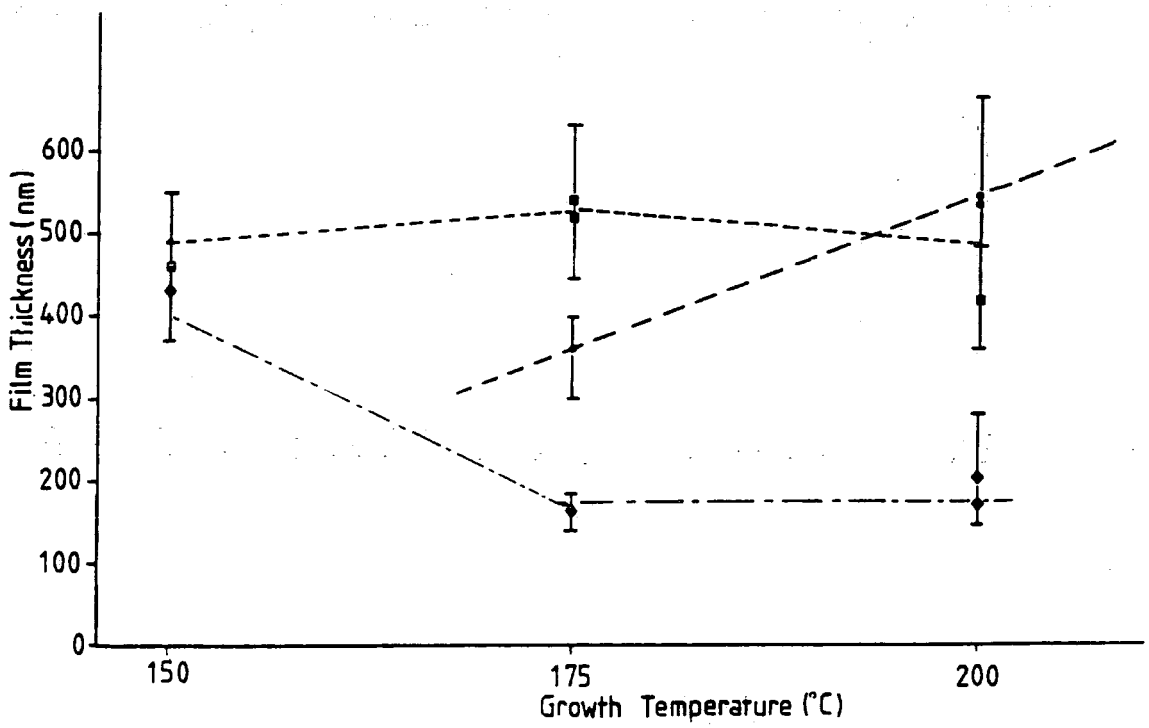

Figure 7.1. Variation of the zinc oxide film thickness versus growth temperature using 0.02M solutions of $Zn(acac)_2.H_2O$ doped with 6 atomic percent of $InCl_3$; Symbols : ■ = growth using 2.1 l of solution and glass substrates ; ◆ = growth using 700 cm^3 and glass substrates ; ● = growth using 2.1 l and plastic substrates.

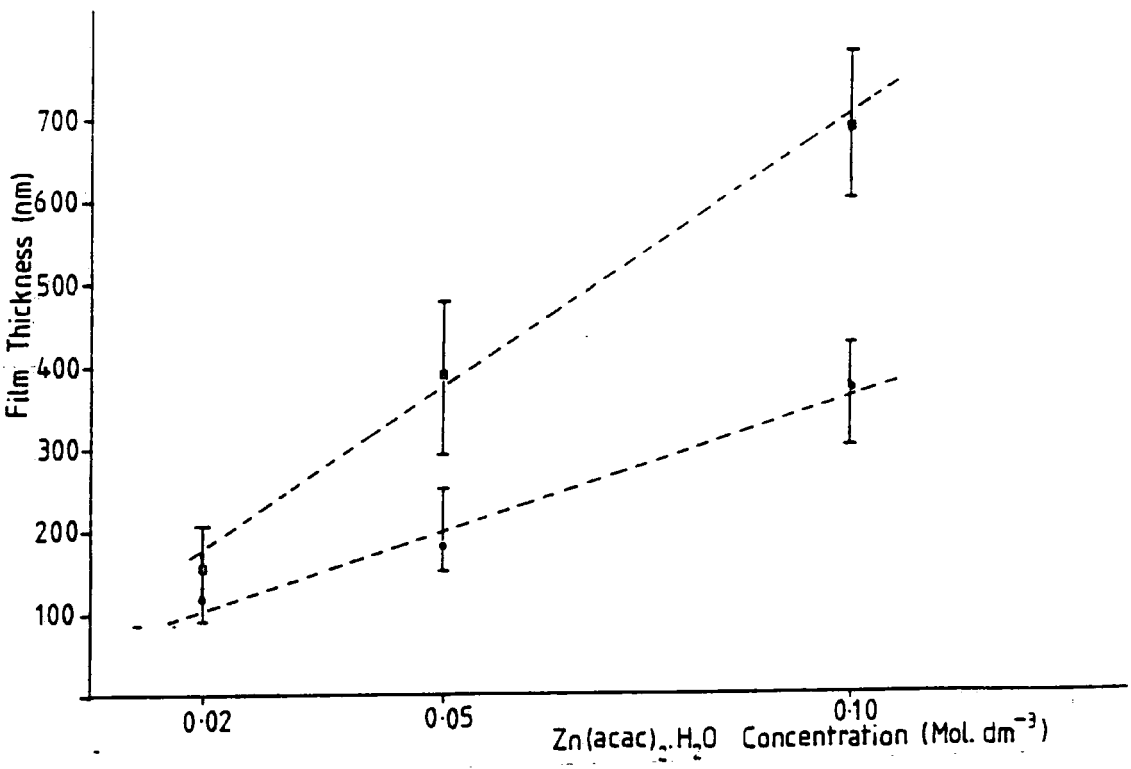

Figure 7.2. Variation of the zinc oxide film thickness versus precursor concentration and $InCl_3$ doping level; Symbols : ● = growth using solutions doped with 3 atomic percent of $InCl_3$; ■ = growth using solutions doped with 6 atomic percent of $InCl_3$.

doped with 3 and 6 atomic percent $InCl_3$. The thickness of ZnO deposited increased as the $Zn(acac)_2.H_2O$ concentration was increased from 0.02M to 0.1M. The film thickness also varied with the dopant concentration, i.e since doubling the $InCl_3$ concentration increased film thickness by a factor of 1.4 at a precursor concentration of 0.02M and by nearly a factor of 2 at 0.1M.

7.4 Indium Concentration in Zinc Oxide Films

The concentration of indium present in ZnO films was determined using ESCA, and spectra for films grown at 150°C and 200°C are shown in figures 7.3 and 7.4. They show the lines due to the various electronic energy levels of zinc, oxygen, indium and chlorine and carbon identified by their binding energies. The indium and chlorine contents are detectable by the lines due to the In_{3d} and Cl_{2p} electronic shells. The main difference between the two spectra is the presence of the Cl_{2p} in the film grown at 150°C.

The measured concentrations of indium and chlorine in the films are plotted as a function of growth temperature in figure 7.5 for an original solution doping concentration of 6 atomic percent of $InCl_3.3H_2O$. The indium concentration in the films did not vary significantly with growth temperature. The chlorine concentration in contrast decreased from approximately 3 atomic percent to below 0.5 atomic percent as the growth temperature was increased. The results obtained from films grown at 150°C and 175°C would suggest that the $InCl_3$ is not decomposed since the atomic ratio of indium to chlorine is 1 : 3 in this range. However by 200°C the amount of chlorine present is insignificant confirming that $InCl_3$ is decomposing and the chlorine is evaporating.

Depth profiling using ion beam thinning of one film grown at 200°C under otherwise identical conditions showed that the concentration of indium varied between 0.9 to 1.2 atomic percent from the surface down to a depth of 0.24μm. The concentration of chlorine in the film was always below 0.5 atomic percent. Figure 7.6 shows a plot of the concentrations in the film of a selection of elements found in both ZnO and alkali glass. The figure shows how the concentration of zinc and indium increased on going from the surface to the bulk, whereas the amount of carbon and oxygen

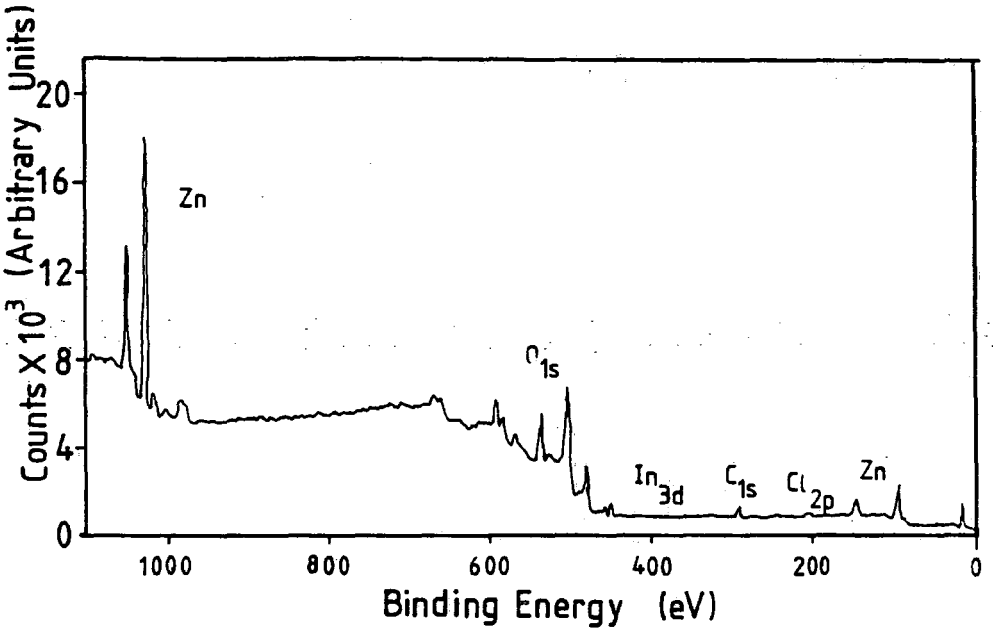

Figure 7.3. ESCA spectrum from a film grown at 150°C using 2.1 l of 0.02M $Zn(acac)_2.H_2O$ solution dop with 6 atomic percent of $InCl_3$.

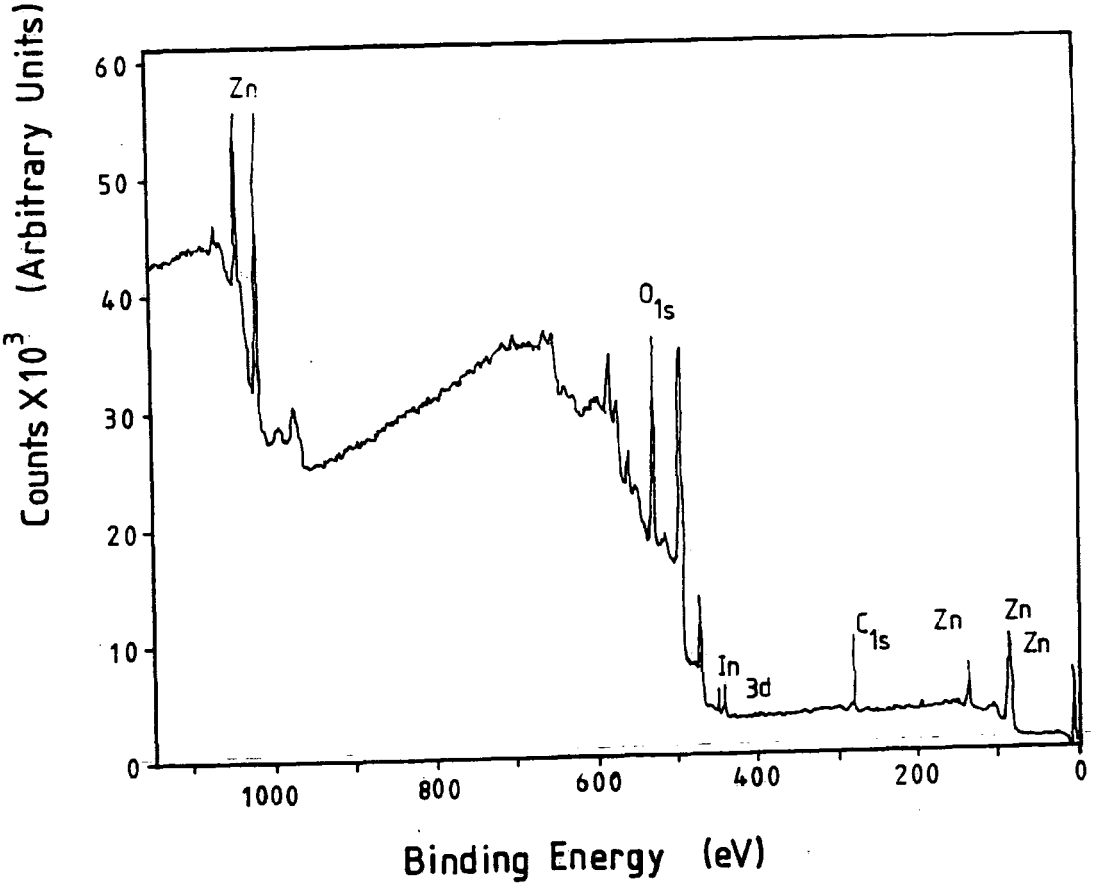

Figure 7.4. ESCA spectrum from a film grown at 200°C using 2.1 l of 0.02M $Zn(acac)_2.H_2O$ solution doped with 6 atomic percent of $InCl_3$.

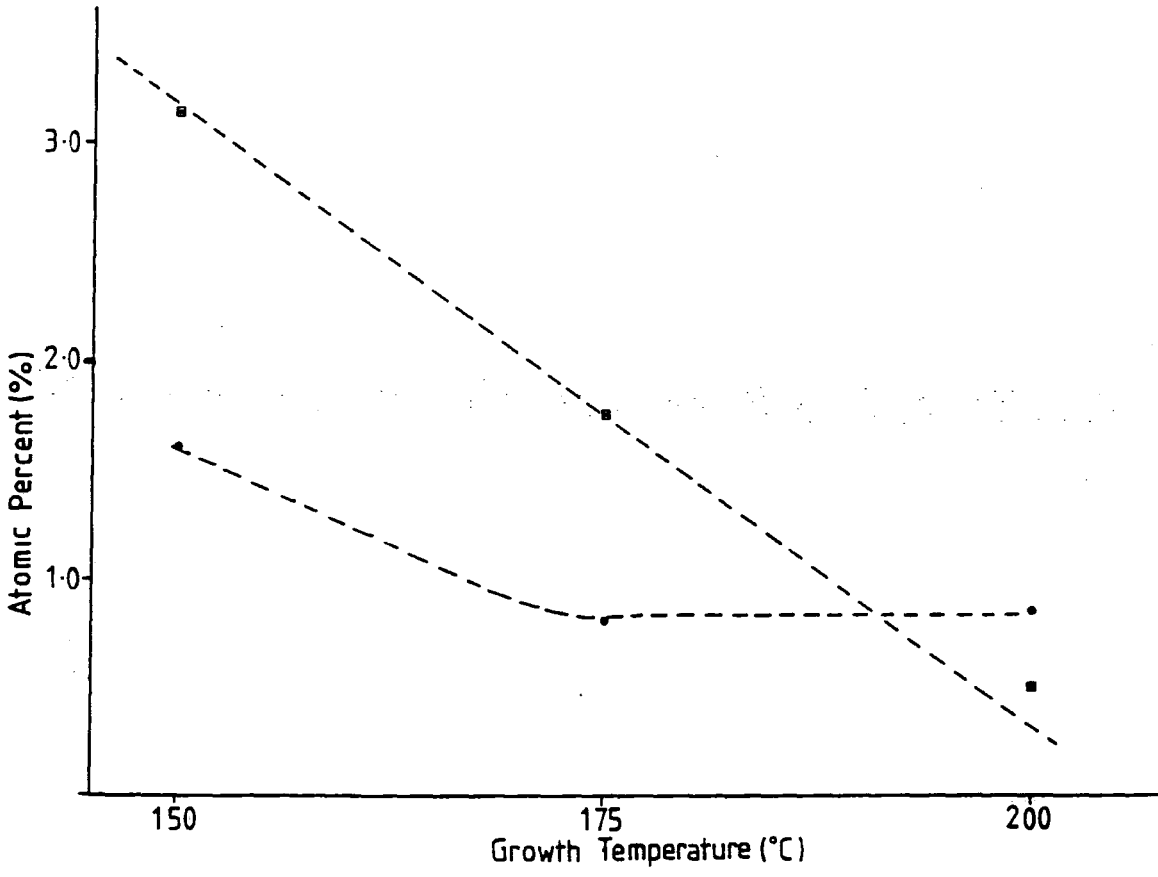

Figure 7.5. Concentration of indium and chlorine in doped zinc oxide films versus growth temperature : Symbols : ● = indium ; ■ = chlorine.

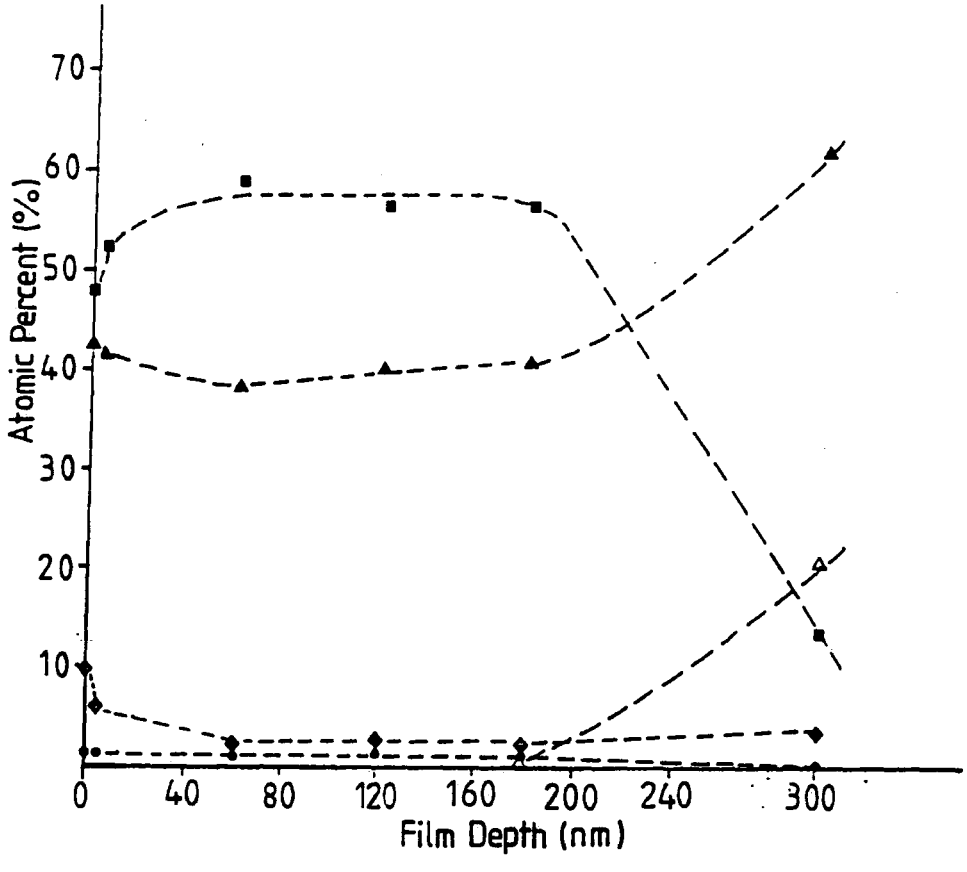

Figure 7.6. Concentration of film and substrate constituents versus film depth ; Symbols: ■ = zinc ; ▲= oxygen ; ● = indium ; Δ= silicon ; ◆ = carbon.

decreased. The concentration of silicon was low until the substrate was reached. At the substrate the zinc concentration fell to zero and the concentration of silicon and oxygen increased suddenly. The results suggest that the films contain an excess of zinc (in the form of zinc interstitials or oxygen vacancies) but that they are more stoichiometric at the surface. The total film depth was approximately 0.25μm as shown by the analysis technique indicating approximately zero indium concentration after the removal of 0.3μm of film material. This result demonstrates the uniformity of the doping process. The penetration depth of XPS is 1-5 nm and the quoted sensitivity is 0.2-0.5 atomic percent.

7.5 Structural Characterisation of Doped Films

Films grown at 200°C from the lower concentrations of zinc precursor had better morphology due to a lower growth rate.

Increasing the dopant concentration also increased the roughness and disorder in the films at grain boundary interfaces. Films grown at lower temperatures had good morphology in the range 175°C to 200°C, but at 150°C the morphology became severely degraded suggesting that film order breaks down abruptly. This might have been caused by a change in the rate of evaporation from the substrate (section 7.3), a change in the mechanism of film formation, or due to undecomposed $InCl_3$.

7.5.1 Surface Structure by RHEED

The surface structure of most films has been examined in RHEED. Diffraction patterns could not be obtained from very thin films suggesting that they were amorphous and that a minimum thickness was required for a crystalline structure to be established on glass (amorphous) substrates.

The observed surface preferred orientations of low temperature doped films are summarised in table 7.1. The results show that most films exhibited some degree of orientation, but on three different planes depending on the conditions of deposition and with substrate temperatures of 175°C and higher.

Figure 7.7 is a pattern taken from a film grown in a dry ambient doped with 3

Doped ZnO grown at 200°C in a dry ambient		
$Zn(acac)_2.H_2O$ concentration / mol dm^{-1}	$InCl_3$ concentration / (At. %)	Surface preferred orientation
0.02 M	3	$(10\bar{1}1)$
0.02 M	6	(0002)
Doped ZnO grown at 200°C in a wet ambient		
0.02 M	3	$(11\bar{2}2)$
0.02 M	6	random
Doped ZnO grown at 200°C in a dry ambient		
0.05 M	3	$(10\bar{1}1)$
0.05 M	6	(0002)
0.1 M	3	(0002)
0.1 M	6	$(10\bar{1}1)$

Table 7.1. Summary of the surface preferred order of doped ZnO films grown at 200°C.

	(a) Intensity data for polycrystalline Zinc Oxide							
Crystal plane	$(10\bar{1}0)$	(0002)	$(10\bar{1}1)$	$(10\bar{1}2)$	$(11\bar{2}0)$	$(10\bar{1}3)$	$(11\bar{2}2)$	Preferred Order
d_{hkl}/Å	2.816	2.602	2.476	1.911	1.626	1.477	1.379	None : random
Peak intensities/%	71	56	**100**	29	40	35	28	polycrystalline
Dopant concentration/ (atomic percent)	(b) Intensity data for films grown from 0.02M $Zn(acac)_2.H_2O$ in a dry ambient							
3	20	20	**100**	26	16	18		$(10\bar{1}1)$
	(c) Intensity data for films grown from 0.02M $Zn(acac)_2.H_2O$ in a wet ambient							
3	**87**	25	**100**	25				$(10\bar{1}1)/(10\bar{1}0)$
	(d) Intensity data for films grown from 0.05M $Zn(acac)_2.H_2O$ in a dry ambient							
3	12	41	**100**	23		13		$(10\bar{1}1)$
6		48	**100**	53		36		$(10\bar{1}1)/(10\bar{1}2)$
	(e) Intensity data for films grown from 0.1M $Zn(acac)_2.H_2O$ in a dry ambient							
3	15	60	**100**	25		25	20	$(10\bar{1}1)/(0002)$
6	25	**100**	30	10	6	14		(0002)/random

Table 7.2. Summary of the XRD intensity data for doped ZnO grown at 200°C.

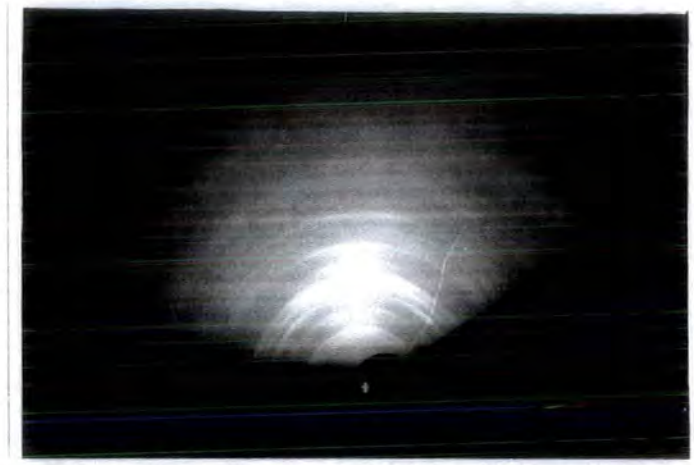

Figure 7.7. RHEED pattern from a film grown at 200°C in a dry ambient from 700 cm^3 of 0.02M $Zn(acac)_2.H_2O$ doped with 3 atomic percent of $InCl_3$.

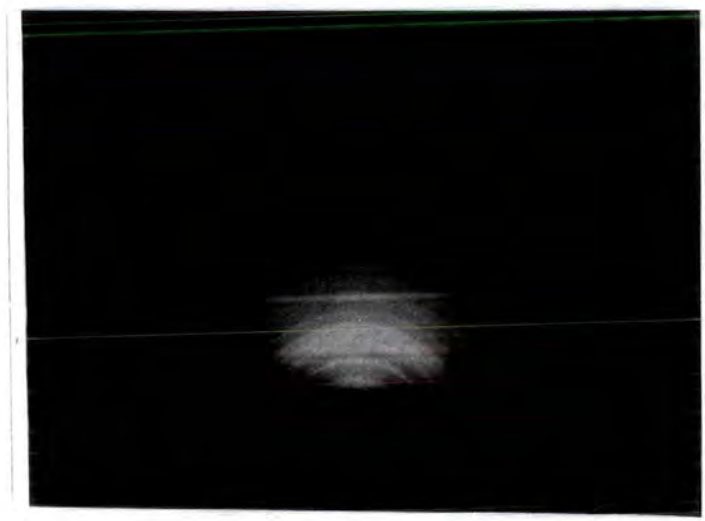

Figure 7.8. RHEED pattern from a film grown at 200°C in a dry ambient from 700 cm^3 of 0.02M $Zn(acac)_2.H_2O$ doped with 6 atomic percent of $InCl_3$.

atomic percent of $InCl_3.3H_2O$. It consists of one central arc corresponding to a $(10\bar{1}1)$ preferred orientation with a set of arcs of varying angular length lying off the central arc at specific angles. The pattern suggests that the film has a preferred orientation superimposed on an almost totally random array of crystallites oriented at different angles to the substrate plane.

In contrast figure 7.8 is a pattern taken from a film grown in a dry ambient doped with 6 atomic percent of $InCl_3.3H_2O$. The pattern consists of continuous rings (corresponding to reflections from planes that are oriented over 180°) indicating that this film has a (0002) preferred orientation but a more random background. Figures 7.7 and 7.8 taken together indicate that increasing the dopant concentration leads to the randomisation of the film structure and a decrease in the degree of preferred order.

A similar but more pronounced effect was observed with films grown in a wet ambient. Figure 7.9 and figure 7.10 are patterns taken from films grown in a wet ambient doped with 3 and 6 atomic percent of $InCl_3.3H_2O$. In figure 7.9 $(11\bar{2}2)$ is the preferred orientation and figure 7.10 shows clearly that here the crystallites were randomly oriented.

7.5.2 Bulk Averaged Structure by XRD

X-ray diffraction was used to investigate the crystallographic texture of doped films. All peaks observed were attributed to zinc oxide by comparison with the ASTM card for a random polycrystalline powder sample of ZnO and were indexed accordingly. Table 7.2 summarises the intensity data obtained for doped ZnO films grown at low temperature and makes a comparison with the intensity data for a random polycrystalline sample. Table 7.3 compares the surface orientations as obtained from RHEED with the bulk averaged orientations as obtained by XRD. Examination of table 7.3 shows that the surface bulk preferred orientation was the same in some films but not in others. No explanation for this could be found. However with growth of thicker films at temperatures of 175°C and above, the surface orientation was $(11\bar{2}2)$ as against the bulk preferred order of $(10\bar{1}1)$. Figure 7.11 shows the pattern obtained from a film de-

Figure 7.9. RHEED pattern from a film grown at 200°C in wet ambient from 700 cm^3 of 0.02M $Zn(acac)_2.H_2O$ doped with 3 atomic percent of $InCl_3$.

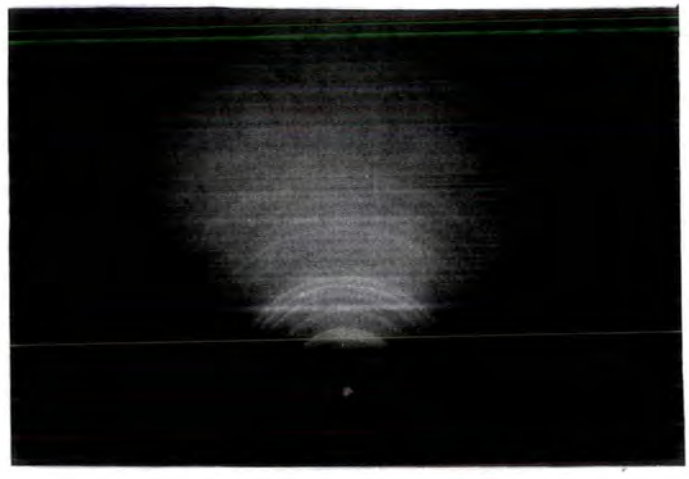

Figure 7.10. RHEED pattern from a film grown at 200°C in a wet ambient from 700 cm^3 of a 0.02M solution of $Zn(acac)_2.H_2O$ doped with 6 atomic percent of $InCl_3$.

Doped ZnO grown at temperatures between 150°C and 200°C		
Growth temperature/°C	Surface preferred orientation	Bulk preferred orientation
150 (glass substrate)	random	$(10\bar{1}1)$
175 (glass substrate)	$(11\bar{2}2)$	$(10\bar{1}1)$
175 (plastic substrate)		(0002)
200 (glass substrate)	$(11\bar{2}2)$	$(10\bar{1}1)$
200 (plastic substrate)	$(11\bar{2}2)$	(0002)

Table 7.3. Comparison of the surface and bulk averaged preferred order in films grown between 150°C and 200°C.

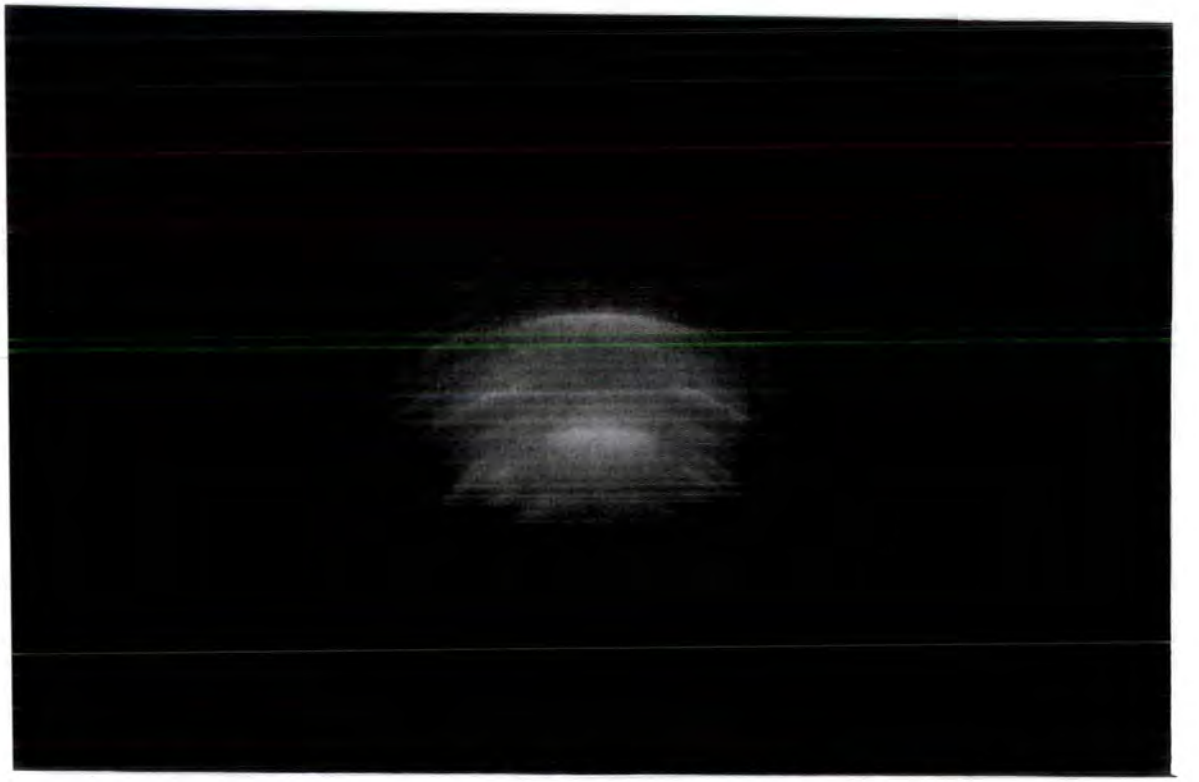

;ure 7.11. RHEED pattern from a film grown at 200°C using 2.1 l of 0.02M $Zn(acac)_2.H_2O$ doped with atomic percent of $InCl_3$ on a plastic substrate.

posited on plastic at 200°C. This film had a $(11\bar{2}2)$ preferred orientation as can be seen by the intense centralised reflection from this plane. The rest of the pattern consists of fewer arcs of narrower width and dimension which in some cases are composed of spots. This would suggest that the crystallites are large and irregularly shaped and are aligned in clusters around well defined axes with little misorientation. Structurally films deposited on plastic are not very different therefore from those deposited on glass.

7.6 Grain Size Studies

Grain sizes were measured from the full width half maximum of the preferred orientation reflection as determined by XRD. Grain sizes were small and varied from 20 nm to 50 nm over all the concentrations studied. The addition of too much $InCl_3$ (6 *at.*%) tended to decrease the grain size, whereas a higher zinc precursor concentration had the opposite effect.

The points plotted in figure 7.12 show the grain sizes in films deposited on glass and plastic. It is apparent that grain size increased as the growth temperature was increased for both types of film, but that the grain size was larger when plastic was used. For growth on glass the grain size reached its maximum at 175°C while on plastic the grain size rose with increasing temperature. This suggests that grain growth on plastic is temperature activated, while that for films grown on glass at temperatures higher than 175°C may be restricted by evaporation, or a high rate of nucleation leading to the formation of smaller grains. The results suggest that larger nuclei are formed on the substrate surface when plastic is used. This may be due to a better lattice match and chemical bonding between the film and the substrate when the substrate is plastic since the latter has a crystalline surface. This will improve order on the growing layer and encourage larger grains.

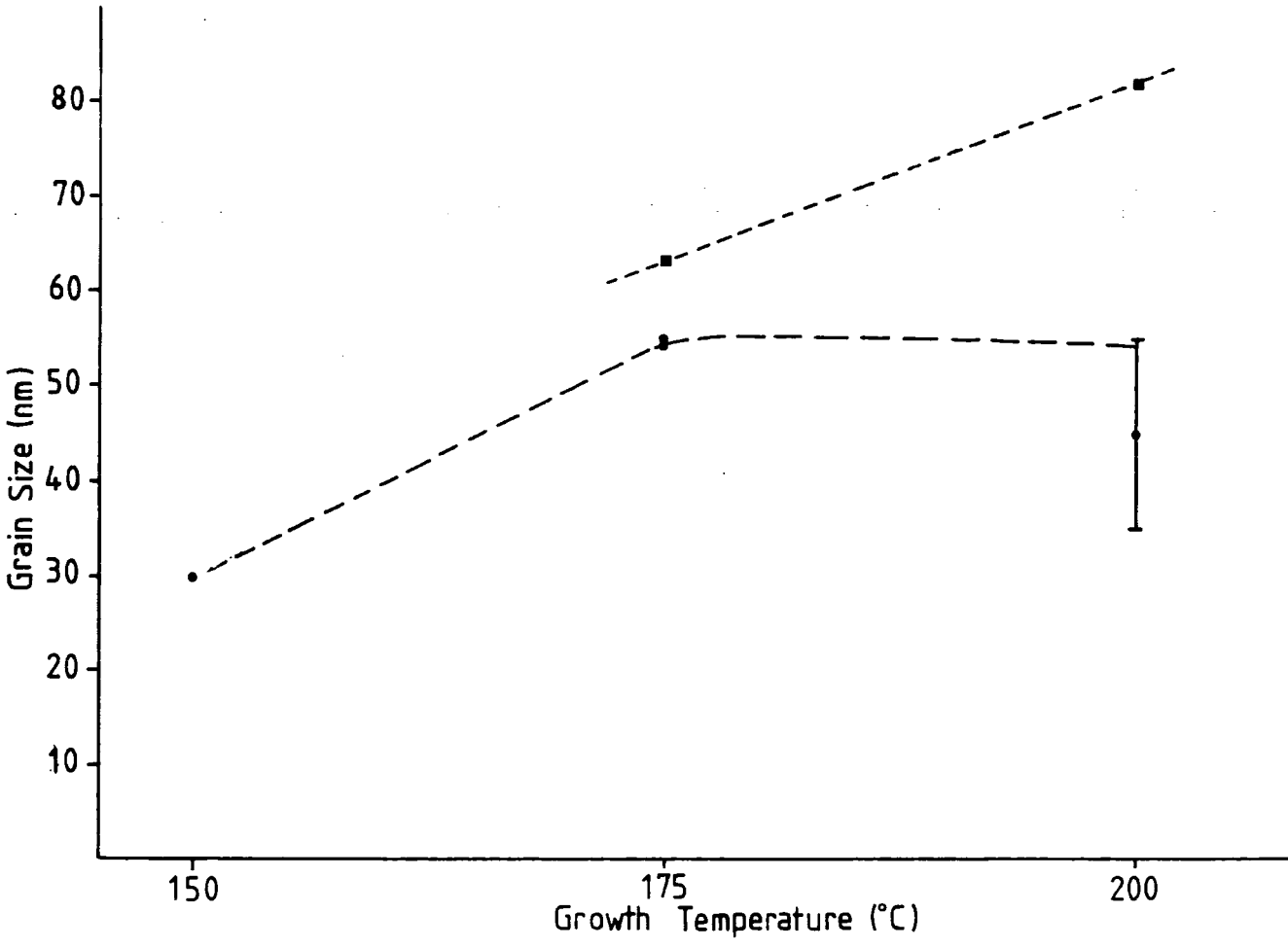

Figure 7.12. Variation of grain size with growth temperature for films grown on glass and plastic : Symbols: ● = growth from 2.1 l of 0.02 M $Zn(acac)_2.H_2O$ on glass : ■ = growth from 2.1 l of 0.02M $Zn(acac)_2.H_2O$ on plastic.

7.7 Discussion of Structural Studies and Crystallographic Texture

Trends revealed by the structural study can be summarised as follows. The use of weaker solutions resulted in the randomisation of film structure. The influence of water in the gas shroud was to increase the randomness of crystallite orientation, and increasing dopant concentration removed the necessary conditions for preferred order.

The influence of dopant in increasing the film thickness was described in section 7.4. The increase in growth rate probably creates sufficient disorder at the grain boundaries so as to degrade film quality.

The preferred orientation was found to be variable, suggesting that the dominance of a particular preferred orientation was sensitive to small effects when film preparation conditions were changed slightly. In most films the surface preferred order was either $(10\bar{1}1)$ or (0002). Some agreement was found between the results of preferred orientation as determined by RHEED and XRD for films grown at 200°C. This indicates that the preferred plane does not change during growth and that the thermodynamic and kinetic factors affecting which preferred plane is the fastest growing and has the lowest surface energy do not change. Therefore the argument that the surface does not correspond to the true preferred order does not need to be invoked. The only comparable work to produce zinc oxide films at low temperatures involved MOCVD which yielded films having a (0002) preferred orientation [3].

When a larger volume of precursor (2.1l) was sprayed the surfaces were all $(11\bar{2}2)$ preferred orientation while the bulk was either $(10\bar{1}1)$ or (0002). The use of lower precursor concentrations and the presence of dopant resulted in the altering of the preferred plane so that the $(10\bar{1}1)$ was sometimes observed. This could be due to a shift in the utilisation of energy available at the substrate from precursor decomposition to film formation, since there is less precursor to decompose per unit time. This results in slower film growth and allows the thermodynamic and kinetic effects of growth to decide which is the preferred orientation rather than mass effects. There are similarities between these results and those presented in in section 5.3. It will be remembered that

when an undoped film was successively etched, RHEED patterns taken at each stage indicated that the $(11\bar{2}2)$ preferred orientation was preserved. This was put down to different etch rates along different planes leading to a false picture of the true structure of the film. However this did not explain why the untouched surface orientation was different from the bulk. That the bulk preferred order is retained down to temperatures as low as 150°C in some films, indicated that even if the surface is relatively degraded as a result of a decrease in temperature, the bulk still retains order. The constant growth rate over the temperature range 150°C to 200°C would also act to support the idea that the films are growing to the same degree of perfection whether the preferred plane is the same or not. This indicates that the employment of lower concentration solutions results in the lowering of the temperature limit of ZnO films possessing crystalline order. Finally it is worth noting that these low temperature films are crystalline in contrast to those of SnO_2 which are amorphous when grown using spray pyrolysis at 220°C [4].

7.8 Electrical Properties

Comprehensive electrical measurements were carried out on films grown from solutions doped with 3, 4.5 and 6 atomic percent in a sequence grown at 200°C in a dry ambient using 0.02M $Zn(acac)_2.H_2O$. The variation of resistivity with solution dopant concentration is shown in figure 7.13 indicating that saturation occurs beyond a solution doping level of 4.5 atomic percent. Film resistivity varied from 1×10^{-2} to $\simeq 5\times10^{-4}\Omega$m with increasing concentration of $InCl_3.3H_2O$. The corresponding carrier concentrations obtained from Hall measurements were of the order 10^{25} - 10^{26} m^{-3}.

The resistivities for films grown at 200°C using different concentrations of $Zn(acac)_2.H_2O$ and $InCl_3.3H_2O$ are plotted in figure 7.14. The resistivity of doped ZnO films increased from $10^{-3}\Omega$m to 0.01 Ωm as the concentration of zinc precursor was increased from 0.02M to 0.1M when the solution dopant concentration was 6 atomic percent, indicating that a larger proportion of the dopant material is electrically active in the film when the growth rate is reduced. This is of course achieved at lower precursor concentrations and at higher solution dopant concentration.

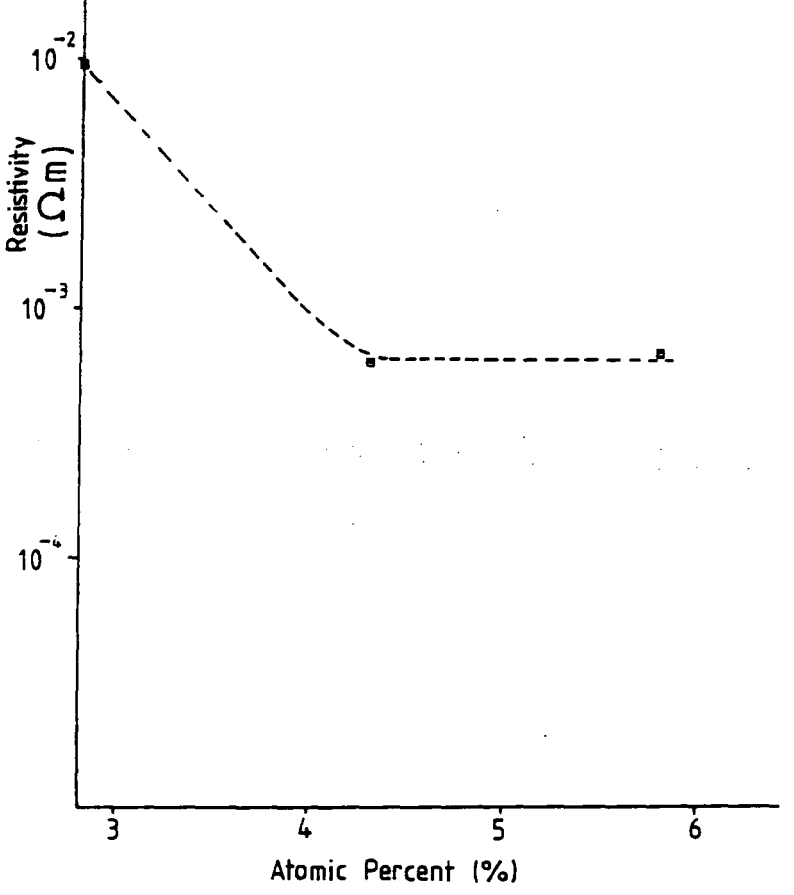

Figure 7.13. Variation of the film resistivity versus $InCl_3$ concentration ($Zn(acac)_2.H_2O$ concentration 0.02M) for film growth at 200°C.

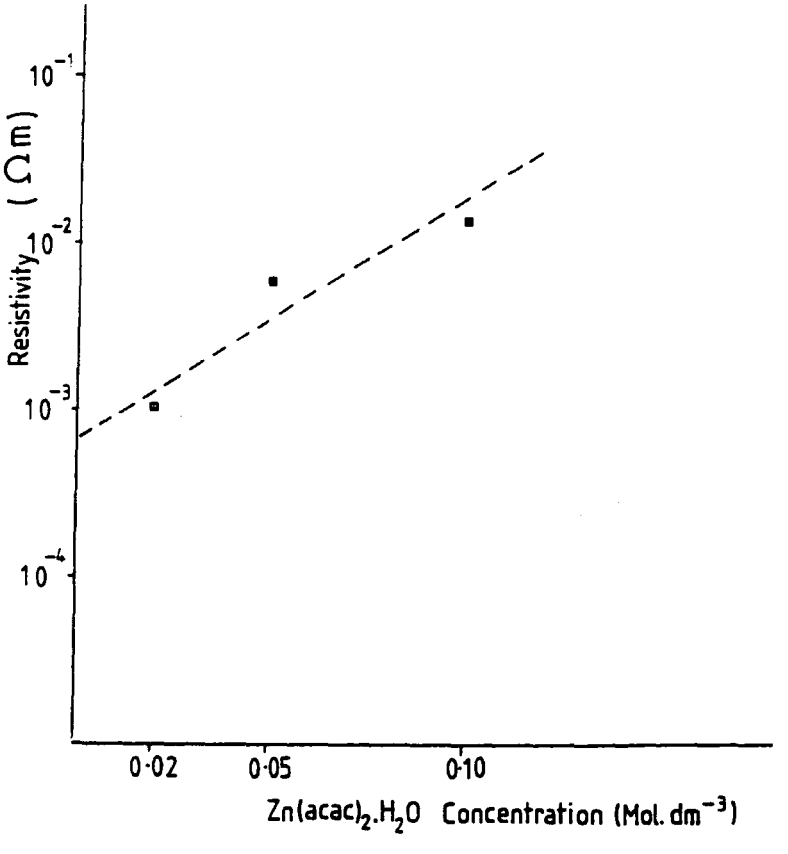

Figure 7.14. Resistivity of films grown at 200°C from 700 cm^3 of different concentrations of $Zn(acac)_2.H_2O$ and doped with 6 atomic percent of $InCl_3$.

The resistivities of doped films grown between 150°C and 200°C using 700 cm^3 of 0.02M $Zn(acac)_2.H_2O$ doped with $InCl_3$ decreased dramatically with substrate temperature. At 150°C the resistivity of the layers could not be measured, but when growth was carried out between 175°C to 200°C the resulting film resistivities fell to between 2.6-3.4$\times 10^{-3}\Omega$m and 0.5-1.0 $\times 10^{-3}\Omega$m.

A similar pattern was observed with thicker doped films grown from a larger volume of precursor, except that resistivities were lower. In the range 175°C - 200°C resistivities were of the order $10^{-4}\Omega$m. In some samples resistivities as low as $10^{-5}\Omega$m were obtained on glass and $5\times 10^{-5}\Omega$m on plastic. Below a substrate temperature of 175°C the film resistivity increased and with films grown at 150°C was $6\times 10^{-2}\Omega$m. This is attributed to the reduced decomposition of $InCl_3.3H_2O$ and incorporation of the indium in an electrically inactive form into the lattice as confirmed by the ESCA measurements reported in section 7.4.

Between growth temperatures of 175°C and 200°C evaporation would prevent any excess of dopant from being incorporated into the film while there is still enough energy available for the formation of electrically active species derived from indium and chlorine. These conclusions are backed up by the results of elemental analysis and thickness data discussed above (section 7.3.2, 7.4.). The structural data suggest that the smaller grain size (30 nm) in films grown at 150°C compared with 60 - 80 nm in films grown at 175°C and 200°C influences the film conductivity much more than any changes in preferred order which are relatively slight. Mobilities and carrier concentrations of the doped films varied from 6 $cm^2\ V^{-1}\ s^{-1}$ to 20 $cm^2\ V^{-1}\ s^{-1}$ and from $5\times 10^{24}\ m^{-3}$ to $3\times 10^{26}\ m^{-3}$.

Whereas the lowest resistivity of one film grown at 200°C was of the order $10^{-5}\Omega$m, comparable resistivities of ZnO:Al and SnO_2 films deposited onto polyester foil using the sputtering technique were of the order 5 - 6 $\times 10^{-6}\Omega$m and $5\times 10^{-5}\Omega$m respectively [5],[6], while sputtered In_2O_3:Sn grown at $\approx$ 150°C had a resistivity of $2\times 10^{-6}\Omega$m [7]. The growth of amorphous SnO_2 at 220°C using spray pyrolysis yielded films with a

resistivity of $10^{-4}\Omega$m [4].

7.9 Optical Properties

Since our prime interest in this project was to grow conducting transparent films of ZnO, the next objective after determining how to grow conducting layers was to measure their transmission, and this was done on films grown at 175°C and 200°C from 2.1 litres of 0.02M $Zn(acac)_2.H_2O$ containing 6 atomic percent of $InCl_3$. Plots of transmittance versus wavelength are shown in figures 7.15 and 7.16. They demonstrate that the film transmittance is of the order 80 % to 95 % in the visible and near infrared regions (550 nm to 1000 nm), but in both samples the transmittance falls off at wavelengths beyond 1000 nm decreasing from 80 % to between 10 and 20% at 3000 nm when free carrier absorption becomes significant. The transmission spectra are analysed and discussed in more detail in the following chapter. Earlier films grown from different concentrations of zinc precursor were also transmitting, typically by about 70% to 85 % in the visible region (400 nm - 900 nm). The transmittances of comparable transparent conducting oxides such as ZnO:Al and SnO_2 are of the order 83 % and 76 % respectively [5],[6] in the visible. Low temperature sputtered In_2O_3 has an average transmittance of 78% [7]. Spray pyrolysed indium doped zinc oxide grown at high temperature can have average transmittances of 85% [1] or 92 % [2]. Low temperature zinc oxide again compares favourably with previous work.

Photoluminescence measurements at 2K undertaken at Hull were made on three films grown from $Zn(acac)_2.H_2O$ solutions doped with 6 atomic percent of $InCl_3.3H_2O$. the films were grown on glass at 175°C and 200°C and on plastic at 200°C

All these films gave broad bands indicative of deep centre emission, a typical example of which is shown in figure 7.17. The intensity of emitted radiation was greatest for both films grown at 200°C which both gave comparable intensities, indicating that the quality of the films on plastic was as good as that of the films grown on glass. The spectra consisted of a broad band centred at 550 nm which is associated with substantial impurity related deep centre emission. The bands for each sample displayed rather

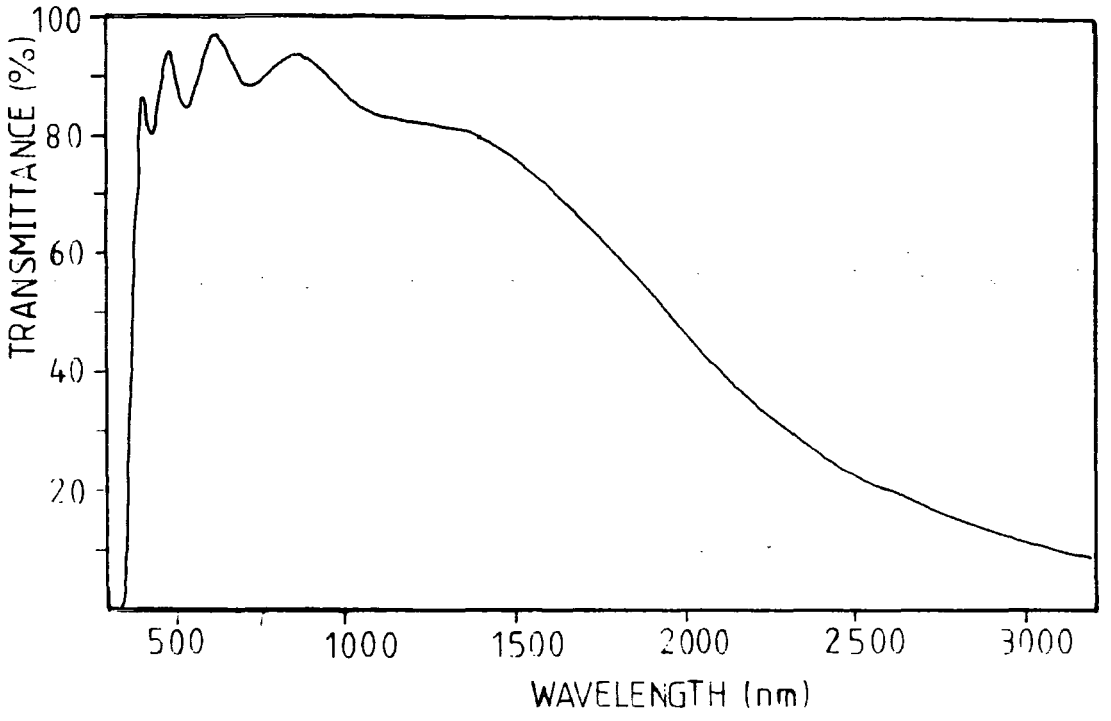

Figure 7.15. Variation of the transmittance with wavelength for a doped film grown at 175°C from 2.1 l of 0.02M $Zn(acac_2.H_2O$ between 0.3 μm to 2.5 μm.

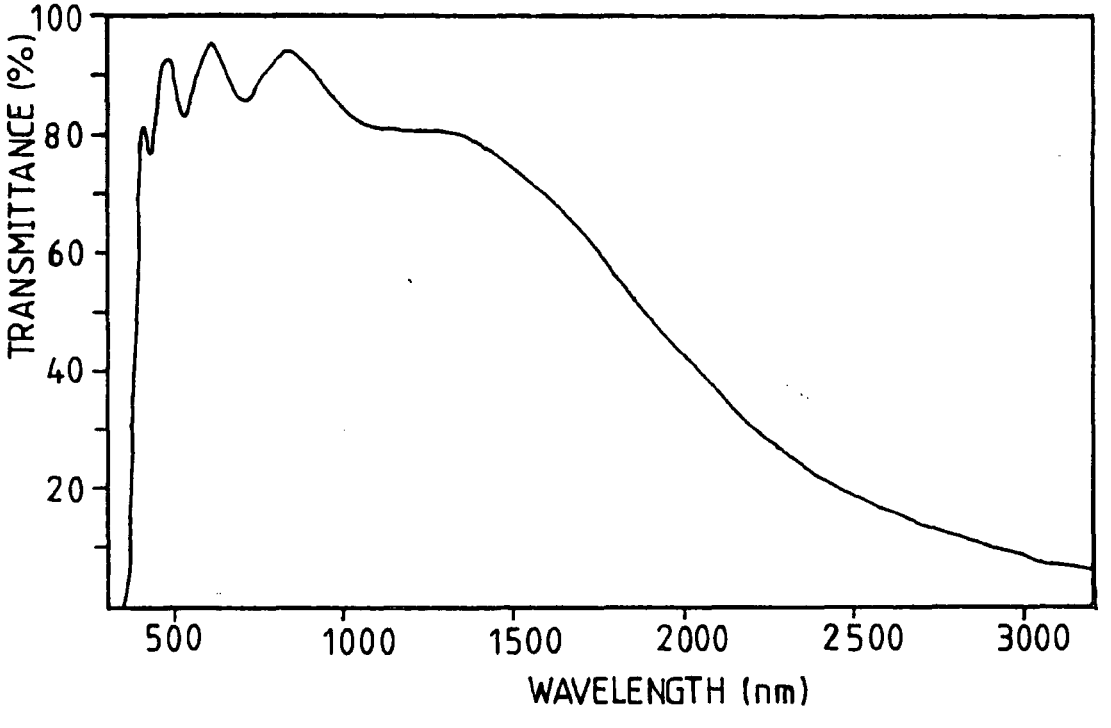

Figure 7.16. Variation of the transmittance with wavelength for a doped film grown at 200°C from 2.1 l of 0.02M $Zn(acac)_2.H_2O$ between 0.3 μm to 2.5 μm.

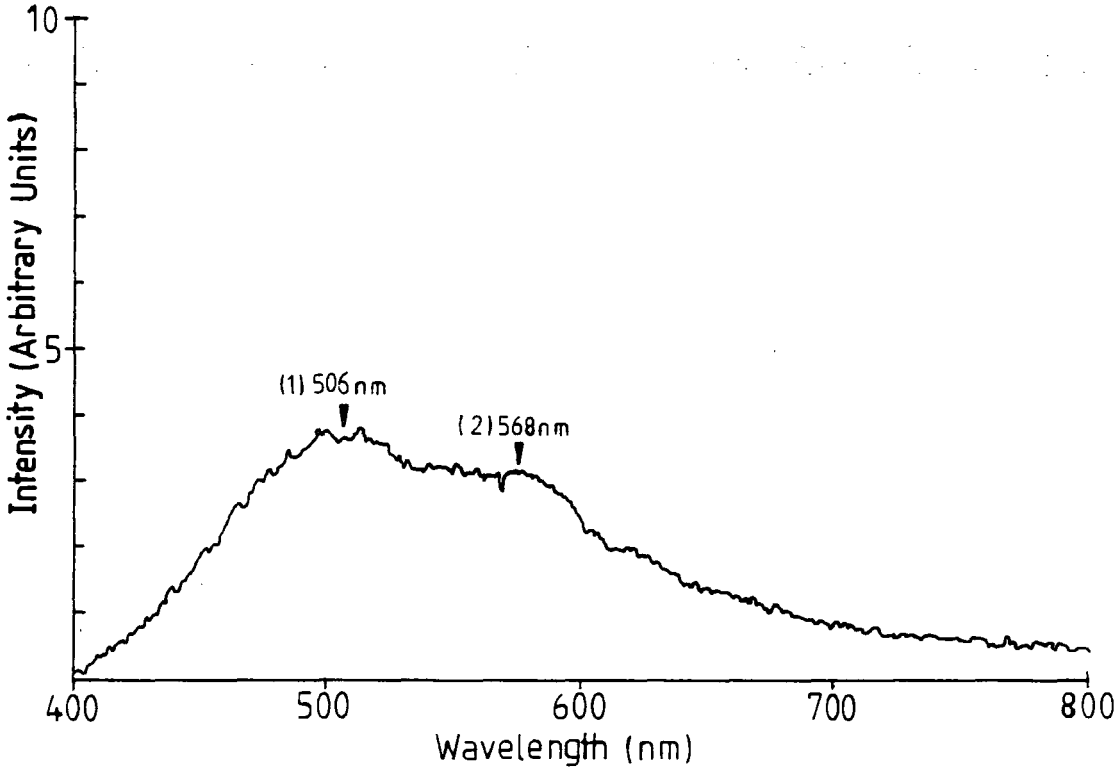

Figure 7.17. Photoluminescence spectrum of the film grown at 200°C on glass.

diffuse structure with secondary peaks at 506 and 568 nm. but better crystallinity would be necessary for any detail to be observed. The green blue emission in ZnO at 510 nm has long been known, but the origin is uncertain. It is usually found when zinc is present in excess.

7.10 Discussion of Electrical and Optical Properties

The characterisation of doped films using these techniques gave the following important results. Firstly the film resistivity is lower when using low concentrations of zinc precursor and high concentrations of dopant. The growth of ZnO from weak solutions using high doping levels has the effect of increasing the incorporation efficiency of $InCl_3.3H_2O$. Under normal circumstances the thicker films with the higher degree of preferred orientation might be expected to be more conducting. However this was not found to be the case and the thinner films with the random structure were more conductive. What matters is the degree to which the dopant $InCl_3.3H_2O$ is incorporated into the film in an electrically active form. The use of stronger zinc precursor solutions seems to prevent this. Therefore the two elements appear to be in competition to become incorporated into the film.

The results of resistivity measurements on films grown between 150°C and 200°C using 700 cm^3 and 2.1 litres of precursor show that the effect of decreasing growth temperature is to increase film resistivity. The thicker films grown from the larger volume of solution are more conductive. The efficiency of the doping process is constant between 175°C and 200°C in that the resistivity is fairly constant as are the structure and In concentration in the films. Below 150°C the concentrations of indium and chlorine have built up to higher levels and the resistivity is considerably higher. From ESCA it is clear that $InCl_3$ does not decompose efficiently at these growth temperatures. The change in electrical properties could be related to the result of the compositional analysis in that towards lower temperatures one would expect to see a decrease in evaporation and also in decomposition of $InCl_3.3H_2O$. Bulk structural properties are not significantly degraded at the lowest temperatures and cannot therefore be responsible

but the degradation of film surfaces might contribute to the observed changes.

The optical transmission of films grown at 175°C and 200°C was similar, with a high transmittance in the visible region of the electromagnetic spectrum and a low transmittance in the IR region. This changeover is gradual. A high transmittance in the visible region (500 nm - 800 nm) is what would be expected at longer wavelengths than the bandgap since only radiation having energies higher than the bandgap value would lead to absorption.

The optical behaviour in the near IR and the IR could be due to either free carrier absorption or reflection processes due to high carrier concentrations (10^{24} - 10^{26} m^{-3}).

7.11 Summary

All films grown at temperatures as low as 150°C were adherent to their substrate even weeks after their initial growth. Most were highly transmitting in the visible and near infrared region. The low temperature growth of doped zinc oxide produces films with resistivities of the order $10^{-5}\Omega m$ and visible transmittances of 90% at growth temperatures of 175°C to 200°C. This compares favourably with ZnO:Al and SnO_2 which have also been grown at temperatures to which plastics and foils are resistant.(ITO cannot be deposited at such low temperatures).

The use of low concentrations of $Zn(acac)_2.H_2O$ and high $InCl_3$ dopant concentrations made this possible as these produce the conditions necessary for the formation of a conducting film at low growth temperatures.

Relatively large grain sizes and a high degree of preferred order were also observed in the most conducting films but were not a necessary requirement for a conducting film, suggesting that a high doping level was the dominant factor.

Thinner films were less conductive than thicker films and have a random structure. Thicker films were more ordered due to the survival of the fastest growing planes and therefore the development of a stronger preferred order.

Doped ZnO can also be grown on a plastic substrate resulting in a film slightly less conductive ($5\times10^{-5}\Omega m$) than a film deposited on glass under identical conditions.

Films grown on plastic had a different structure and significantly larger grain size. This is attributed to substrate effects, in that the plastic used had a crystalline oriented surface while the glass did not. Clearly conducting zinc oxide can be grown on a wide range of substrates and materials that cannot withstand high temperatures.

Growth of doped ZnO below 175°C led to the formation of films that were not suited to the application of a transparent conducting oxide. They had higher resistivities and lower transmittances. However they were very adherent to their substrates and might be used as hard antistatic coatings.

7.12 Chapter Seven References

(1) Major S., Banerjee A. and Chopra K.L., *Thin Sol. Films, 108,* 333, (1983)

(2) Guillemoles J. F., Lincot D., Cowache P. and Vedel J., *10th European Photovoltaic Conference And Exhibition*, Lisbon, Portugal, 8 - 12, (1991).

(3) Shimuzu M.. Kamel H., Tanizawa M. and Shiosaki T., *J. Cryst. Growth, 89*, 365, (1988).

(4) Jousse D., Constantino C. and Chambouleyron I., *J. Appl. Phys., 54(1)*, 431, (1983).

(5) Jin Z., Granqvist C., *Appl. Opt., 26 (16)*, 3191, (1987).

(6) Stjerna B., Granqvist C., *Appl. Opt., 29 (4)*, 447, (1990).

(7) Granqvist C., Hamberg I., *J. Appl. Phys., 60 (11)*, R123, (1986)

Chapter Eight

Deposition of Doped Zinc Oxide at High Temperature Using $InCl_3$ as a Dopant Precursor

8.1 Introduction

Having established the conditions for the successful growth of transparent conducting films on plastic, which required substrate temperatures of 200°C or less, the next objective was to prepare the best films on glass where the restriction on the substrate temperature was removed. In this $InCl_3$ was again used as the source of donor dopant. Accordingly films were grown with in-flight heating in a wet ambient, since preliminary investigations, coupled with the work reported in the preceding chapter, showed that thicker and crystallographically better films were deposited under these conditions.

8.2 Appearance and Thickness of Films

All the films were continuous, transparent and free from surface speckle. For deposition at 276°C the lightly doped films were light green and with increasing $InCl_3$ dopant concentration the films became dark brown and slightly opaque. However the tints of films grown at 306°C varied from light green to green and to dark brown. The adhesion of all films with one exception was very good.

The thickness of the films grown at 276°C and 306°C as a function of the atomic percent of dopant in the spray solution is shown in figure 8.1. Clearly the addition of $InCl_3$ to the spray solution reduced the thickness of the films compared with undoped ones grown at these temperatures (0.91 μm, 276°C; 0.94 μm, 306°C). Films grown at 276°C were generally thinner than those grown at 306°C. The thickness of the films grown at the higher temperature varied from 0.35 μm for growth from solutions containing 0.5 atomic percent to 0.78 μm for growth from solutions containing 6 atomic percent. The suppression of thickness varied from 20% to 63% compared to an undoped film. The presence of small amounts of $InCl_3.3H_2O$ reduced the growth rate significantly. However the thicknesses of films grown from the most concentrated solutions were comparable with those of undoped films.

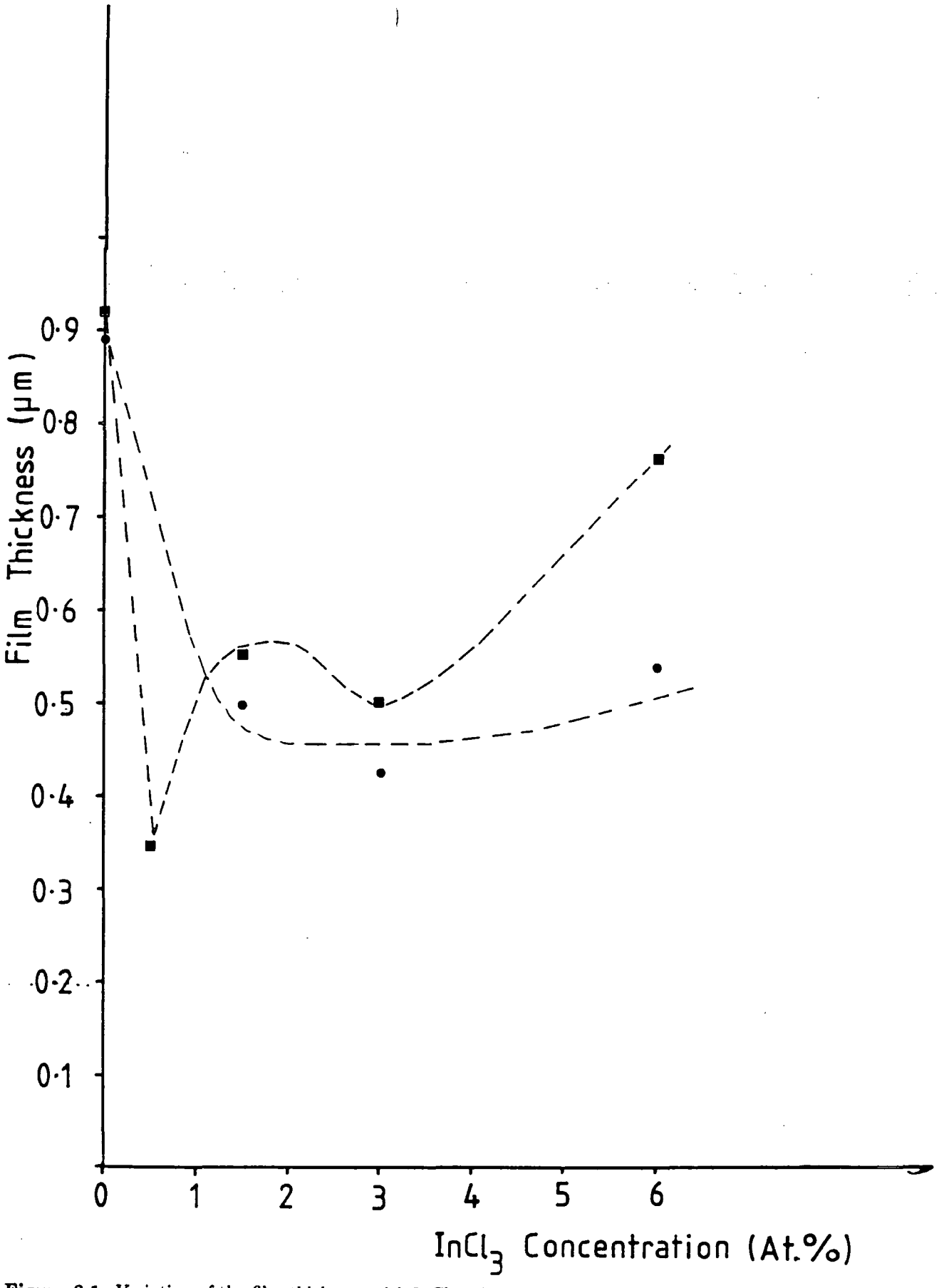

Figure 8.1. Variation of the film thickness with $InCl_3$ solution concentration for film growth at 276°C (●) and 306°C (■) in a wet ambient with in - flight heating from 700 cm^3 of 0.1M $Zn(acac)_2.H_2O$.

A number of films were analysed for indium and chlorine content using ESCA at ICI Wilton. The films tested were those grown at 306°C from solutions containing 3 and 6 atomic percent of $InCl_3.3H_2O$ and at 276°C from a solution containing 6 atomic percent. Figure 8.2 shows the ESCA spectrum from 0 to 700 eV for the layer grown at 306°C from a solution containing $\simeq$ 3 atomic percent of indium. The In_{3d} peak can be seen at 480 eV and it was estimated that some 1 atomic percent of indium had been incorporated in the film. Chlorine is also present in this film as shown by the Cl_{2p} peak at 200 eV. The estimated atomic concentrations of the various species in the different films are listed in table 8.1. Rather more indium was incorporated at the lower temperature.

This is in contradiction to previous work on doped zinc oxide [1] where the incorporation of indium was found to increase with increasing growth temperature.

The elemental analysis indicates that both indium and chlorine were incorporated into films grown at 306°C, and that saturation occurred when solution concentrations above 3 atomic percent were used.

This compares with a higher level of indium and no chlorine at all found in the film grown at 276°C from a 6 atomic percent $InCl_3$ doped solution. The incorporation efficiency of $InCl_3$ was of the order 30% to 60%. This can be compared with the deposition efficiency of $Zn(acac)_2.H_2O$ which varies from 0.35% to 1%. $InCl_3$ is very much less volatile than $Zn(acac)_2.H_2O$. The saturation observed at a growth temperature of 306°C was not a solubility limit however since the incorporation efficiency of indium increased as the growth temperature decreased. This indicated that the incorporation is controlled by evaporation and is not a temperature activated process.

8.3 Structural Characterisation

This section outlines the results from the structural characterisation by X-ray diffraction and RHEED of films grown at 276°C and 306°C from solutions doped with $InCl_3.3H_2O$. Most films showed some degree of preferred orientation and table 8.2 is a summary of these preferred orientations as obtained from the examination of the film

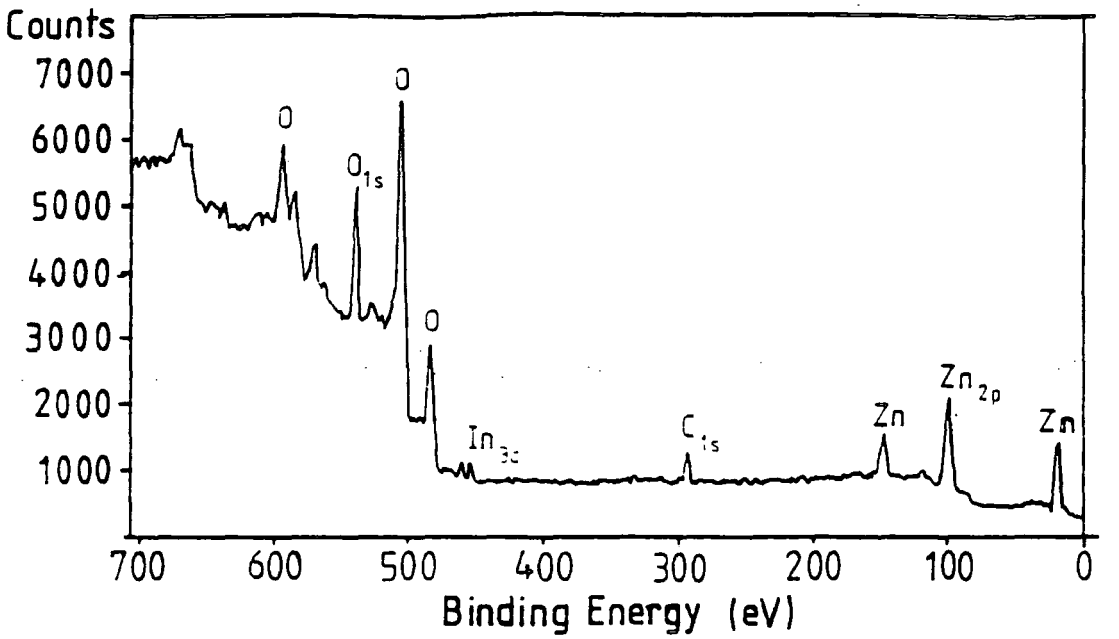

Figure 8.2. ESCA spectrum of doped zinc oxide grown at 306°C from a 3.0 atomic percent $InCl_3$ doped solution.

Composition of $InCl_3$ doped ZnO films (at.%)						
	Film composition (a) at the surface					
	(b) after slight etching					
Growth temperature	$InCl_3$ *soln*	Zinc	Oxygen	Indium	Carbon	Chlorine
276°C	6	40 a	42 a	1.6 a	17 a	≤ 0.5 a
		37 b	41 b	1.4 b	20 b	≤ 0.5 b
306°C	3	38 a	40 a	0.9 a	21 a	≤ 0.5 a
		33 b	42 b	1.1 b	22 b	1.4 b
306°C	6	37 a	43 a	1.1 a	19 a	≤ 0.5 a
		32 b	43 b	1.1 b	22 b	≤ 1.4 b

Table 8.1. Summary of the elemental composition of In-doped ZnO grown at high temperature.

Comparison of the surface and bulk averaged preferred order		
(a) Doped ZnO grown at 306°C in a wet ambient with in-flight heating		
Dopant concentration	Surface preferred orientation	Bulk averaged preferred orientation
0	$(11\bar{2}2)$	$(10\bar{1}1)$
0.5	$(11\bar{2}2)$	$(10\bar{1}1)/(11\bar{2}2)$
1.5	$(11\bar{2}0)$	$(10\bar{1}1)$
3.0	$(11\bar{2}2)/(10\bar{1}1)$	$(10\bar{1}1)$
6.0	$(11\bar{2}2)/(11\bar{2}0)$	$(10\bar{1}0)/(11\bar{2}0)$
(b) Doped ZnO grown at 276°C in a wet ambient with in-flight heating		
Dopant concentration	Surface preferred orientation	Bulk averaged preferred orientation
0	$(11\bar{2}2)$	$(10\bar{1}1)$
1.5	$(10\bar{1}1)/(11\bar{2}2)$	$(10\bar{1}1)$
3.0	$(10\bar{1}1)/(10\bar{1}0)$	$(10\bar{1}1)$
6.0	$(11\bar{2}2)/(11\bar{2}0)$	$(10\bar{1}1)$

Table 8.2. Summary and comparison of the surface and bulk averaged preferred orientations for In-doped ZnO films grown at high temperature.

(a) Intensity data for polycrystalline zinc oxide								
Crystal plane	$(10\bar{1}0)$	(0002)	$(10\bar{1}1)$	$(10\bar{1}2)$	$(11\bar{2}0)$	$(10\bar{1}3)$	$(11\bar{2}2)$	Preferred Orientation
d_{hkl}/Å	2.816	2.602	2.476	1.911	1.626	1.379	1.379	None : random
Peak intensities/(%)	71	56	100	29	40	35	28	polycrystalline
(b) Intensity data for doped films grown at 306°C in a wet ambient with in-flight heating								
Dopant concentration/(at.%)								
0	12	35	**100**					$(10\bar{1}1)$
0.5	15	5	**100**		10		24	$(10\bar{1}1)/(11\bar{2}2)$
1.5	21	42	**100**	15		9	10	$(10\bar{1}1)$
3.0	20		**100**				11	$(10\bar{1}1)$
6.0	**100**	8	44		21			$(10\bar{1}0)/(11\bar{2}0)$
(c) Intensity data for doped films grown at 276°C in a wet ambient with in-flight heating								
1.5	32		**100**		6			$(10\bar{1}1)$
3.0	7	6	**100**				7	$(10\bar{1}1)$
6.0	36		**100**				5	$(10\bar{1}1)$

Table 8.3. Summary of the XRD intensities from In-doped ZnO grown at high temperature.

surface by RHEED and the bulk by XRD. A summary of the reflected peak intensities from XRD spectra is included in table 8.3.

Electron diffraction patterns were taken from a series of films grown at 306°C from solutions containing 0.5, 1.5, 3 and 6 atomic percent of $InCl_3.3H_2O$. The pattern from an undoped film grown under identical conditions had a random structure as shown by long and diffuse arcs. When a small amount of dopant was added to growth solutions (0.5 atomic percent) the lengths of the arcs decreased considerably and they became less diffuse as seen by examination of the edges of the arcs (figure 8.3). This pattern closely resembled one obtained from an undoped film grown at 336°C in a dry ambient (section 5.3.8, figure 5.10).

Thus the film became more ordered with this addition. The sharpness of the arcs suggests that the grains were in more intimate contact and that there was not very much intergranular material present.

With 1.5 atomic percent of $InCl_3.3H_2O$ the film structure became more randomised (though not to the same extent as the undoped film) since the arcs lengthened and were more diffuse compared to those shown in figure 8.3 for the film grown from a 0.5 atomic percent doped solution. Thus the crystallites were not so well aligned with respect to the main preferred orientation. This may possibly be due to an increase in the grain boundary volume and an increase in disorder between grains.

Films grown from solutions containing 3 atomic percent of $InCl_3.3H_2O$ gave patterns where the arcs were now more or less spread out over 180° and are better described as rings suggesting that the crystallites were randomly oriented at all possible angles and over most orientations. However there was still a maximum in intensity along the 90° line of the pattern indicating that certain orientations were still preferred. The rings were broken and consisted of areas of sharpness and diffusivity among the general intensity of the background ring. Such a pattern is indicative of irregularly shaped grains.

Films grown from solutions containing 6 atomic percent of $InCl_3.3H_2O$ showed

Figure 8.3. RHEED pattern from a film grown at 306°C from a 0.5 atomic percent $InCl_3$ doped solution.

increased randomness of crystallites and the presence of more planes indicated by the spread of lines in the X-ray spectrum, visible out to high 2θ values measured along the 90° direction from the central beam spot. A preferred orientation still occurred in this material superimposed on a totally random background. The pattern consisted of broken rings consisting of particles again indicative of large irregularly shaped grains.

The surface structure of films grown at 276°C from solutions doped with 1.5, 3, and 6 atomic percent was very similar to that of films grown at 306°C. Once again a low concentration of $InCl_3$ led to a preferred orientation which became more diffuse as the dopant concentration was increased. However at this lower temperature the evidence was that the crystallites were smaller in size and their shape less affected by increasing the doping than at 306°C.

As table 8.2 shows, most of films grown at 306°C had a $(11\bar{2}2)$ preferred surface orientation except for the film grown from a solution containing 0.5 atomic percent. Increasing the dopant level to 1.5 atomic percent led to films having a $(11\bar{2}0)$ preferred orientation. Films grown from 3 and 6 atomic percent $InCl_3$ doped solutions also had some additional slight $(10\bar{1}1)$ and $(11\bar{2}0)$ order. Films grown at 276°C had a $(11\bar{2}2)$ preferred order when no dopant was present and a mixture of $(10\bar{1}1)$ and $(11\bar{2}2)$ major orientations when the growth solution contained 1.5 atomic percent. The preferred order changed to $(10\bar{1}1)$ and $(10\bar{1}0)$ as the solution doping level was raised to 3 atomic percent. At the highest doping level used (6 atomic percent) the preferred order was a mixture of $(11\bar{2}2)$ and $(11\bar{2}0)$. These two particular planes do not normally give high intensity reflections in fully random polycrystalline samples (i.e. they are low intensity reflections in the ASTM index), so that the influence of an increasing level of dopant is to increase the number of major orientations. The $(11\bar{2}0)$ and $(10\bar{1}0)$ orientations were not previously observed in undoped films and occurred solely as a result of the presence of $InCl_3$.

It must be remembered that the surface structure extends some way below the surface as demonstrated from results presented in chapter 5. Thus electron diffraction of

these films gives an indication of how the films grew once they have became established on the film surface.

The preferred orientations of these films as determined by XRD are summarised in table 8.2 and compared with those obtained using RHEED. The majority of the films had a $(10\bar{1}1)$ preferred orientation (showing that these films possessed approximately the same structure as undoped films). The most heavily doped film had a $(10\bar{1}0)$ preferred order. Again this orientation occurred purely as a result of the presence of the dopant.

The films grown at 276°C all had $(10\bar{1}1)$ orientations thus indicating that the dopant was present throughout the film.

8.3.1 Grain Size Measurements

The grain sizes of films grown from doped solutions at 276°C and 306°C are plotted in figure 8.4 as a function of dopant concentration. The grain size was not very different and varied from 32 nm up to 45 nm when the growth temperature of 306°C was used and from 35 to 55 nm when the growth temperature was 276°C.

The general trend was of an initial reduction in the grain size when 0.5 atomic percent of $InCl_3$ was used in spray solutions followed by a gradual increase as the dopant concentration was increased from 0.5 to 3.0 atomic percent.

8.3.2 TEM Studies on Doped Zinc Oxide

TEM was carried out on two samples from films grown on cleaved rocksalt substrates at 276°C from a 3 atomic percent $InCl_3$ doped solution and at 306°C from a 0.5 atomic percent $InCl_3$ doped solution. (The NaCl substrates were subsequently dissolved away in water). TEM showed similar polycrystalline diffraction patterns at both temperatures and that for growth at 306°C is shown in figure 8.5. Micrographs of individual grains were also taken and for the 306°C film is shown in figure 8.6. The micrographs demonstrate that the crystallites are randomly oriented in all directions but a higher proportion are oriented along the $(10\bar{1}0)$ and $(10\bar{1}1)$ growth axes.

This can be compared with the result from growth on glass as shown in table

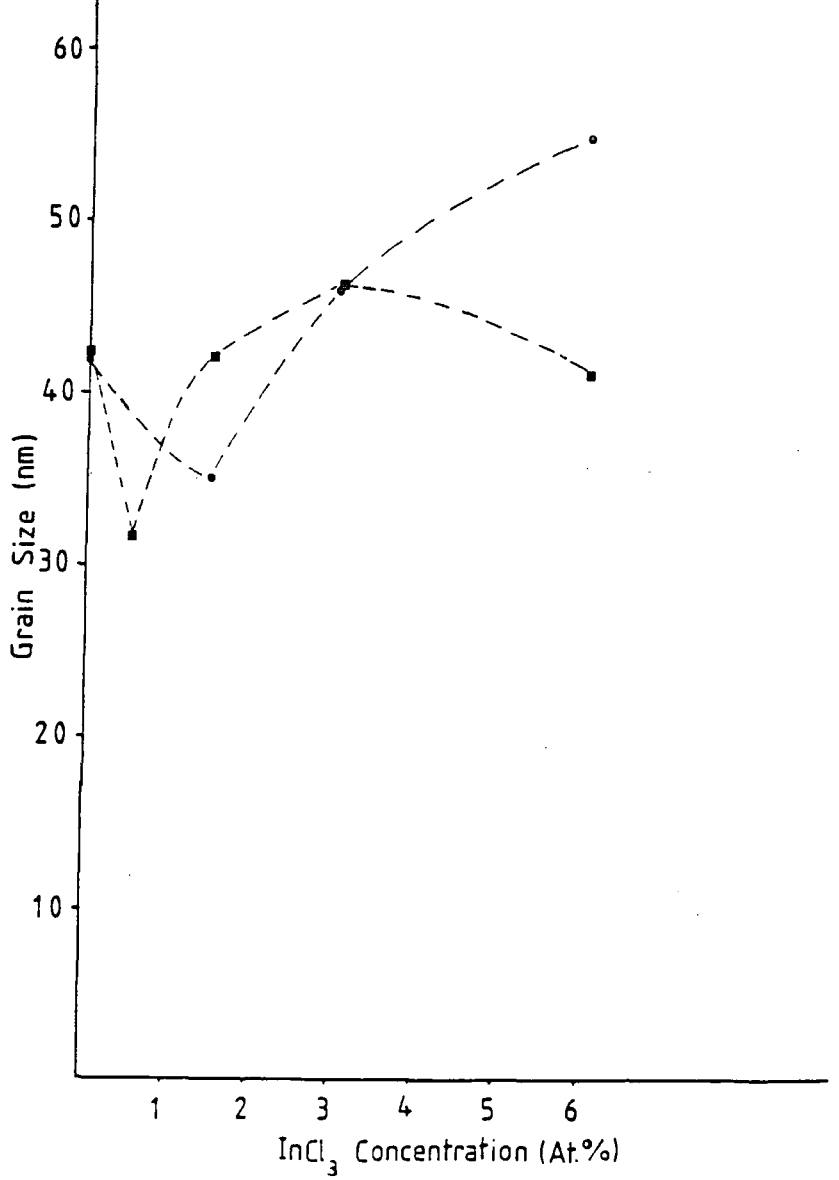

Figure 8.4. Variation of the grain size with $InCl_3$ solution concentration for film growth at 276°C (●) and 306°C (■) from 700 cm^3 of 0.1M $Zn(acac)_2.H_2O$.

Comparison of the preferred orientation of doped ZnO grown at 306°C				
Dopant concentration/(at.%)	Growth temperature	RHEED	XRD	TEM
0.5	306°C	$(11\bar{2}2)$	$(10\bar{1}1)/(11\bar{2}2)$	$(10\bar{1}0)/(10\bar{1}1)$
3.0	276°C	$(10\bar{1}1)/(10\bar{1}0)$	$(10\bar{1}1)$	$(10\bar{1}0)/(10\bar{1}1)$

Table 8.4. Summary of the preferred orientation in In-doped ZnO films by RHEED, XRD and TEM.

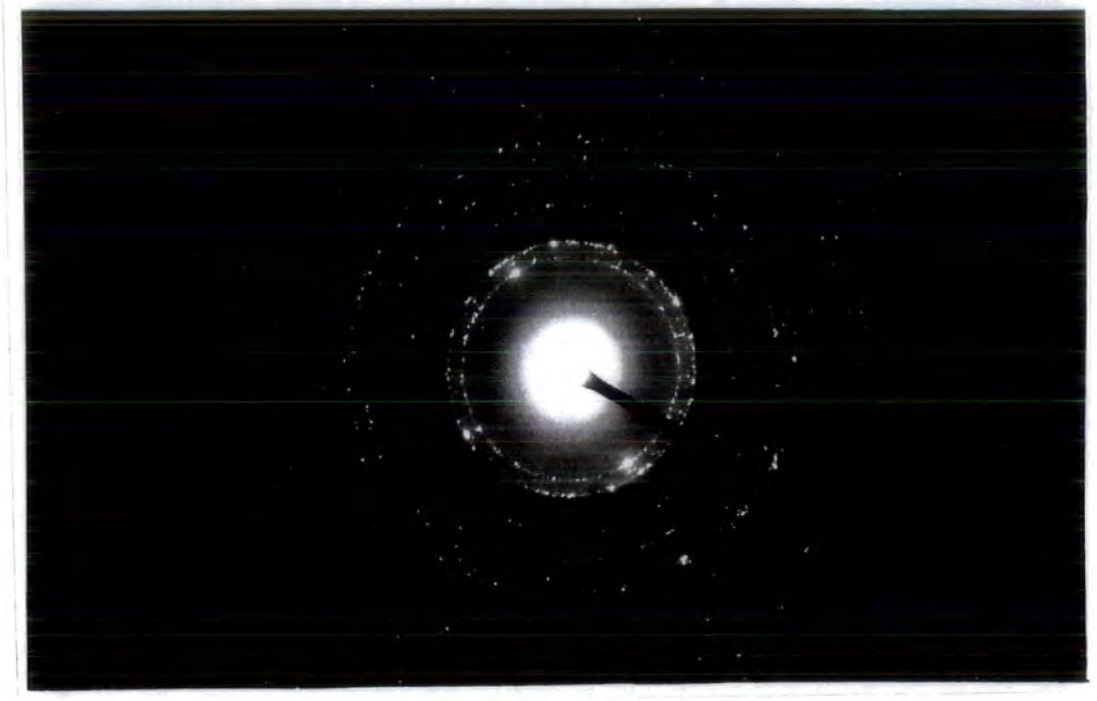

Figure 8.5. TEM diffraction pattern obtained from a film grown at 306°C from a 0.5 atomic percent doped solution.

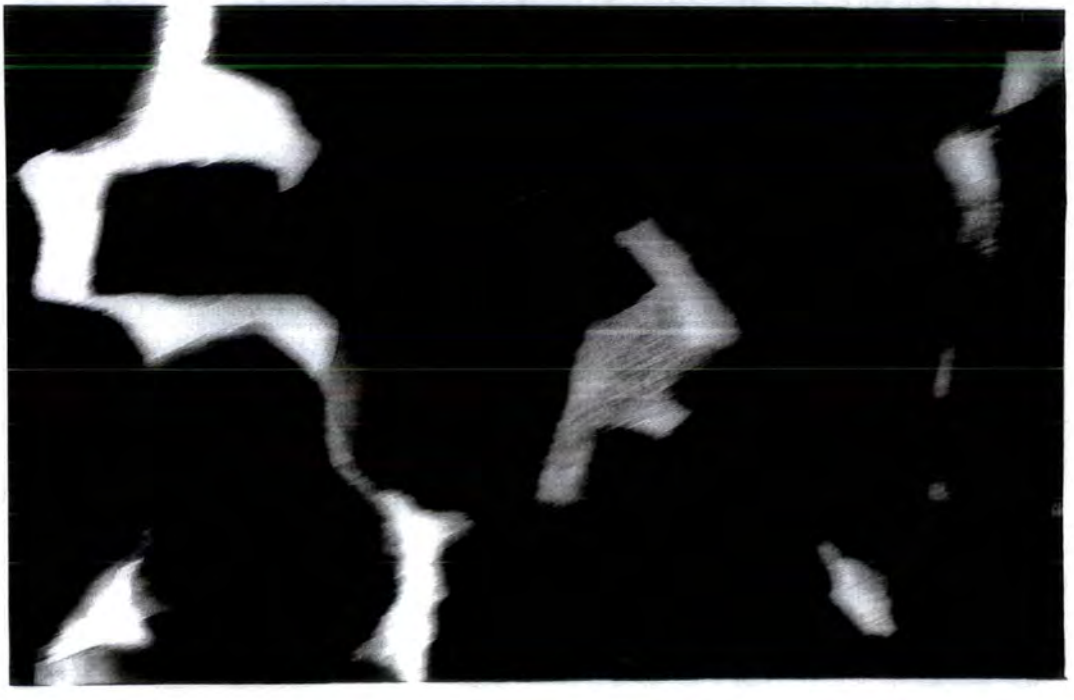

Figure 8.6. TEM micrograph obtained from a film grown at 306°C from a 0.5 atomic percent doped solution.

8.4. For the film grown at 306°C the preferred order was $(11\bar{2}2)$ from RHEED, and a mixture of $(10\bar{1}1)$ and $(11\bar{2}2)$ from XRD. Thus there is some agreement and overlap between the different techniques used for the film grown at higher temperature. For the film grown at 276°C, the preferred orientation was $(10\bar{1}1)$ by all three techniques with some $(10\bar{1}0)$ about the film normal, as is expected for a film having a preferred orientation. The film put down on rocksalt had the largest crystallites.

8.4 Discussion of Crystallinity, Preferred Orientation and Grain Size

The observed trend was that initially surface crystallinity was improved by the addition of small amounts of $InCl_3$ to the spray solution. However the further addition of dopant led to a degradation in the crystallite ordering in the films and to a randomisation of the structure when compared to an undoped control. This can be explained in terms of the growth suppression observed when small additions of dopant were added. This suppression (due to competition of the dopant species with the zinc species) causes the films to grow in a more ordered way, since in the initial stages of film growth the nuclei take longer to grow and therefore thermodynamic requirements rather than mass requirements control film growth. This can occur without any detrimental influence on the structure since the original dopant solution concentration is so low. In this situation the grain boundaries are more ordered and the order within grains and crystallites is good. However as the dopant concentration increases the disorder increases and this is probably due to a build up of dopant in the grains (manifesting themselves as defects at interstitials and substitutional positions) and at the intergranular boundaries. A build up of dopant atoms will destroy the relationship between grains and the crystalline perfection within grains. This has the effect of causing grains to be more randomly oriented. At the higher growth temperature of 306°C this is accentuated since the grains are irregularly shaped. At high dopant levels the relationship between grains is randomised, apparently at all stages of film growth, and again this probably occurs as a result of nuclei in the initial stages of growth grains being disordered relative to one another. This has the effect of changing the dominant driving force from one preferred

plane to several.

The XRD study on doped films grown at 276°C and 306°C indicates that the presence of the dopant did not interfere with the bulk film growth even though more indium was present in these lower temperature films. Therefore the presence of indium does not alter the factors that affect the development of preferred order in the film as it grows. In all films the bulk orientation was unchanged from that in the undoped layer i.e $(10\bar{1}1)$. Most of the film surfaces had some $(11\bar{2}2)$ preferred order and therefore shared much with the undoped films also grown at high temperature. Some also had some $(10\bar{1}1)$ surface preferred order indicating again that sometimes the bulk structure is not independent of the surface structure. However other planes which did not occur in undoped film growth were present and most have been solely due to the effect of $InCl_3$ (i.e $(11\bar{2}0)$ and $(10\bar{1}0)$). These occurred at the higher solution doping levels.

The influence of dopant would be to change the growth rate of different planes due to its effect on the probability of adsorption of precursor material. In addition a dopant atom would also change the interfacial energy of the plane and introduce distortion if it was either too large or too small for the site it was occupying. For indium the ion is slightly larger than the zinc ion, and if indium replaced zinc a lattice distortion would occur. The fact that indium dopant does change the preferred orientation in some circumstances points to such an influence being present. In previous work the preferred order of $InCl_3$ doped zinc oxide films grown at high temperature (400°C) was $(10\bar{1}1)$, as opposed to (0002) for an undoped film, with the $(11\bar{2}2)$ and the $(11\bar{2}0)$ orientations apparent in some of the films. This compares with the $(10\bar{1}1)$ and $(11\bar{2}2)$ preferred orientations seen in high temperature undoped films, and the same orientations obtained in lightly doped films, and in addition the $(10\bar{1}0)$ and $(11\bar{2}0)$ orientations obtained with doped films [1]. The $(11\bar{2}0)$ preferred order can also be obtained in undoped films when oriented substrates are used [2].

The grain sizes of these films varied from 32 nm to 55 nm at both growth temperatures, with larger sizes being obtained at the lower temperature by some 10 nm. When

a small addition of dopant was made to the spray solution a reduction in the grain size was immediately obvious. This occurred together with a suppression in the film growth rate and an improvement in the crystallinity. It is logical to assume that if the overall film growth rate is suppressed then the grain and crystallite growth rates will also be suppressed and the crystallinity will be improved.

8.5 Electrical Properties of $InCl_3$ Doped Zinc Oxide

Plots of film resistivity (at room temperature) versus dopant concentration for growth at 276°C and 306°C are shown in figure 8.7 where an undoped film grown at 306°C is shown as having a resistivity of 10 Ωm.

The room temperature resistivities of the doped films varied from 10 Ωm to 10^{-4}Ωm as the solution doping level was increased from zero to 6 atomic percent. The addition of 1.5 atomic percent of $InCl_3$ to the growth solution reduced the film resistivity by four orders of magnitude for a film grown at 276°C and by 5 orders of magnitude for a film grown at 306°C. These results suggest that although less indium is present in films grown at 306°C, more of it is present in an electrically active form.

A plot of the carrier concentration as a function of $InCl_3$ content in the precursor solution is shown in figure 8.8 for films grown at 306°C. The carrier concentration decreased slightly from 10^{26} m^{-3} at 1.5 atomic percent $InCl_3$ to 7.5×10^{25} m^{-3} at 6 atomic percent $InCl_3$. The resistivity of films grown from 0.5 atomic percent was too high to allow Hall measurements to be made. The maximum electrically active concentration of indium was incorporated when 1.5 atomic percent was used and this produced films with the lowest resistivity, 10^{-4}Ωm. The corresponding electron mobility was 5.8 cm^2 V^{-1} s^{-1}, very much less than the electron mobility in single crystal zinc oxide which is approximately 180 cm^2 V^{-1} s^{-1} [3]. In polycrystalline films grain boundaries reduce the mobility of free carriers.

The carrier concentrations in films grown at 276°C showed greater scatter but were generally of the order of 10^{25} m^{-3} corresponding to resistivities $\approx 10^{-3}$Ωm and mobilities similar to those in films grown at 306°C. The Hall measurements clearly demon-

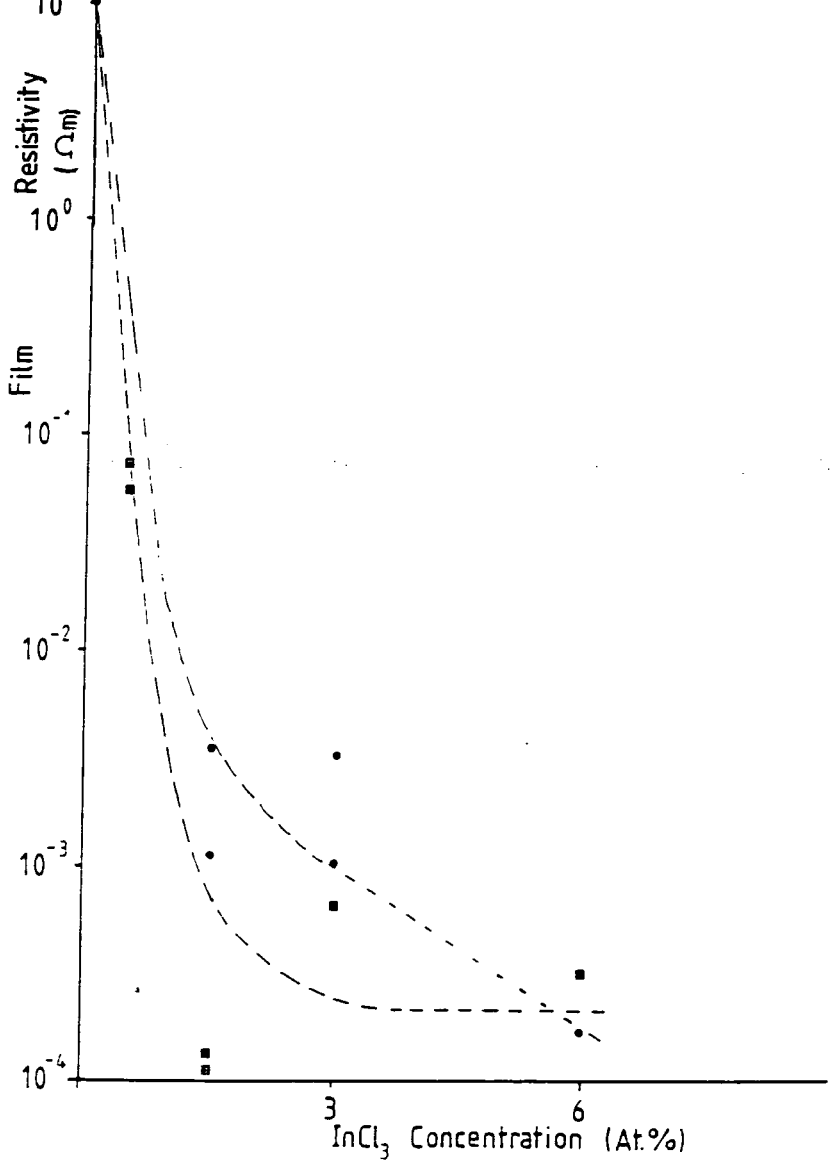

Figure 8.7. Variation of the film resistivity with $InCl_3$ solution concentration for film growth at 276°C (●) and 306°C (■).

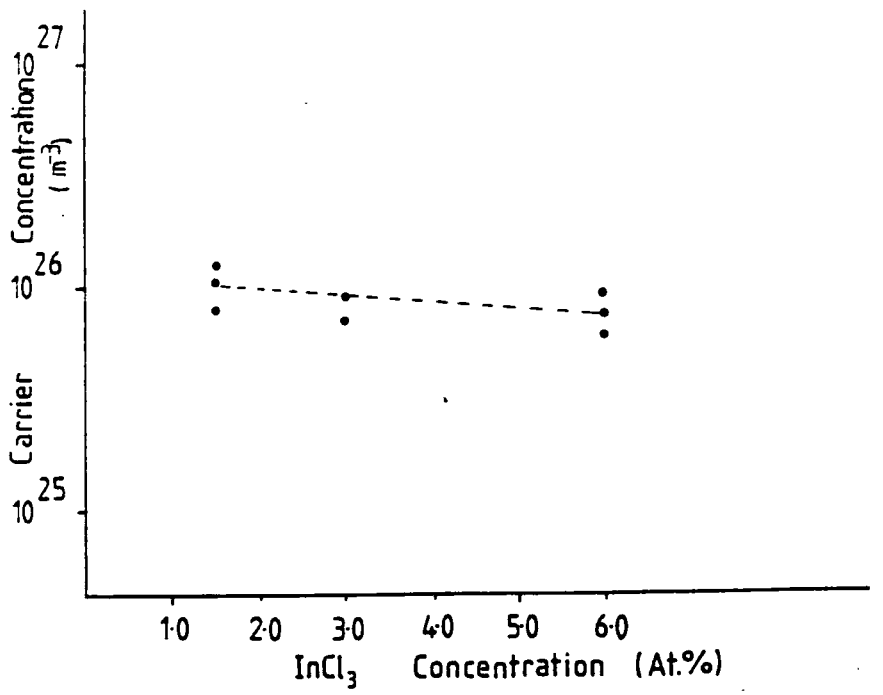

Figure 8.8. Variation of the carrier concentration versus $InCl_3$ solution concentration for film growth at 306°C.

strate that more electrically active indium is incorporated in films grown at 306°C. Temperature dependent measurements in figures 8.9 to 8.12 showed that the carrier concentration (figure 8.11) increased from 10^{24} m^{-3} to 7×10^{25} m^{-3} while resistivity was almost constant (figure 8.9) and electron mobility decreased from 5×10^{-3} m^2 V^{-1} s^{-1} to 3×10^{-4} m^2 V^{-1} s^{-1} (figure 8.12) with increasing temperature from 100K to 313K. The resistivity measurements indicate that the material is degenerate (i.e. that the Fermi level has entered the conduction band). The high carrier concentration also suggests that the material is degenerate. The mobility is proportional to reciprocal temperature suggesting metallic-like behaviour (at the highest temperatures R_H became too small to measure, as shown clearly in figure 8.10; these points were therefore not included in the curve fitting in figure 8.12) which is also consistent with a degenerate material. If we regard the carrier mobility as limited by scattering at oscillating atoms where Q is the scattering cross-section of an atom for an electron with the Fermi energy giving a mean free path of λ_F, then

$$\lambda_F NQ = 1 \tag{8.1}$$

where N = no. of atoms per unit volume. Therefore,

$$\lambda_F = \frac{1}{NQ} \tag{8.2}$$

But Q is proportional to $\langle x^2 \rangle$ where x is the amplitude of vibration. The potential energy of oscillation is given by

$$2\pi^2\nu^2 m\langle x^2\rangle = \frac{kT}{2} \tag{8.3}$$

Therefore,

$$\lambda_F \propto \frac{1}{Q} \propto \frac{1}{\langle x^2\rangle} = \frac{1}{T} \tag{8.4}$$

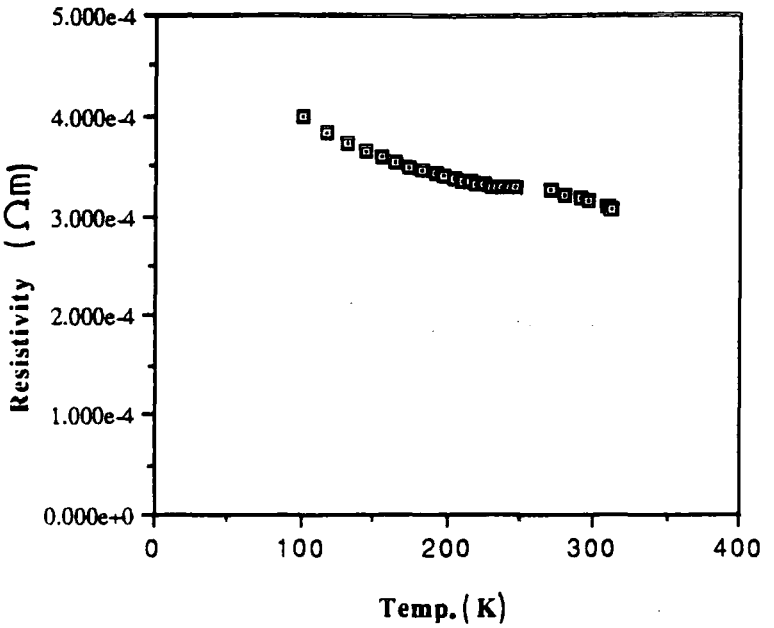

Figure 8.9 Variation of the resistivity with temperature for an indium doped film grown at 306°C.

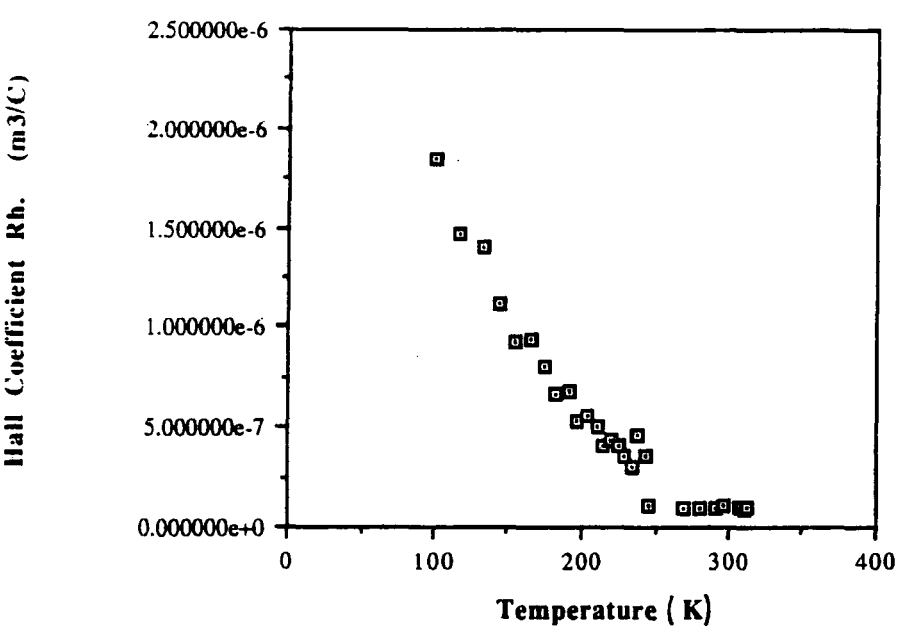

Figure 8.10 Variation of the Hall Coefficient with temperature for an indium doped film grown at 306 °C.

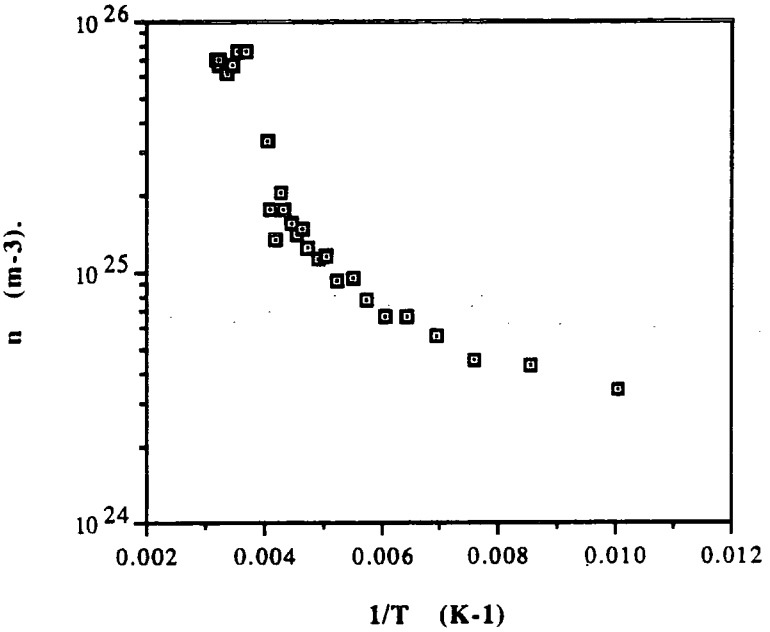

Figure 8.11 Variation of n (carrier concentration)(log scale) versus reciprocal Kelvin for an indium doped film grown at 306°C.

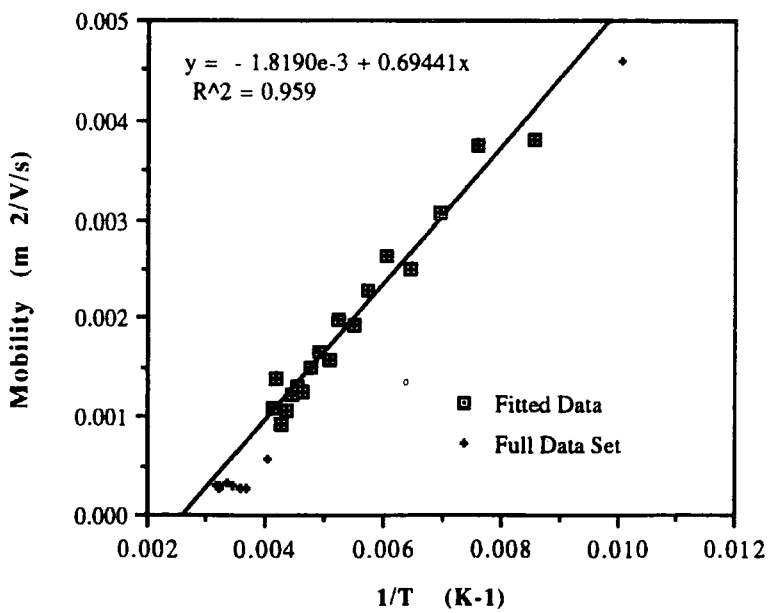

Figure 8.12 Variation of carrier mobility versus reciprocal temperature for an indium doped film grown at 306°C.

and since v_F (the velocity of electron at the Fermi surface) is independent of T it follows that

$$\mu = \frac{e\tau}{m} = \frac{e\lambda_F}{mv_F} \propto \lambda_F \propto \frac{1}{T} \tag{8.5}$$

where m is the effective mass of a free carrier and

$$\sigma = ne\mu \propto \frac{1}{T} \tag{8.6}$$

where σ is the conductivity.

For a metallic material n is independent of T but here n decreases with decreasing temperature, which is semiconductor-like behaviour, where freeze out of carriers occurs. However plots of $\log(nT^{-3/4})$ did not really show the straight line behaviour expected suggesting that the temperature dependence of carrier concentration was not soley related to carrier freeze out effects.

8.6 Optical Properties

The optical transmittance was measured for films grown at 276°C and 306°C from approximately 300 nm to 2500 nm and is plotted in figures 8.13 to 8.15. All films had negligible transmission at wavelengths of 300 nm and less. From 300 nm to 500 nm the transmittance increased sharply from 16 % to 92 % for doped films grown at 276°C (figure 8.13). The spectra are marked by interference fringes where the transmittance varied in a periodic way. Higher transmittances were recorded between 300 and 1000 nm but fell towards 2500 nm (2.5 μm). Generally film transmittance also decreased with increasing solution dopant concentration but this does not take into account the effect of film thickness, which also varied with dopant concentration. To summarise the films were highly transmitting between 300 nm and 1500 nm, but became increasingly absorbing or reflecting between 1500 nm and 2500 nm due to free carrier absorption. Of all the doped films the most lightly doped film had the highest overall transmittance (0 - 85 % near to the bandgap; and between 61 - 91 % at the minima and maxima of the interference fringes). This is to be compared with the undoped film grown at 306°C

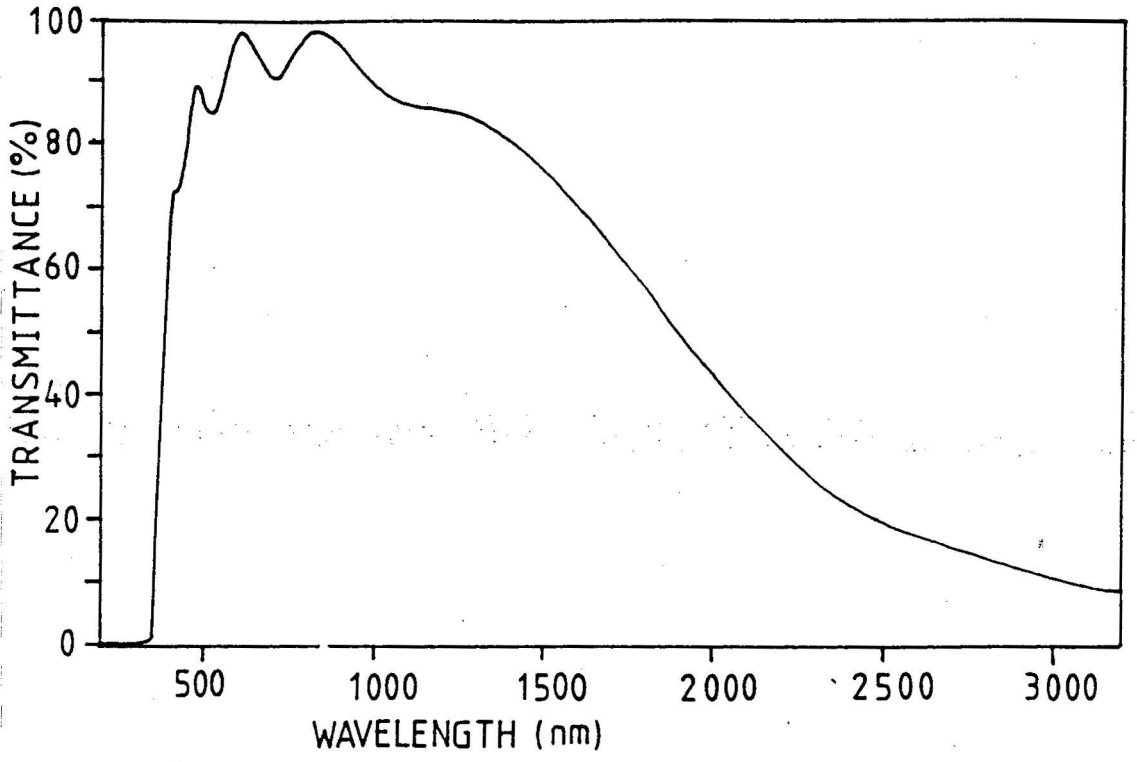

Figure 8.13 Variation of film transmittance versus wavelength for an In-doped (6 at.%) film grown at 276°C.

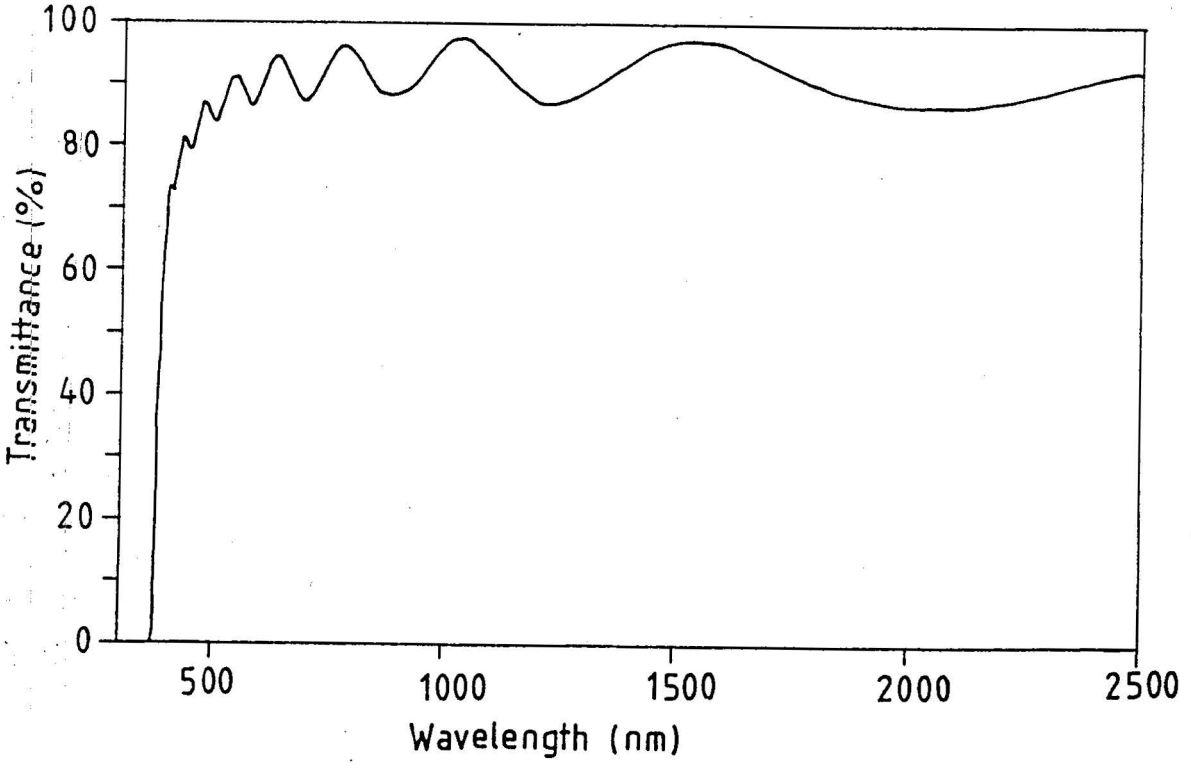

Figure 8.14 Variation of film transmittance versus wavelength for an undoped film grown at 306°C.

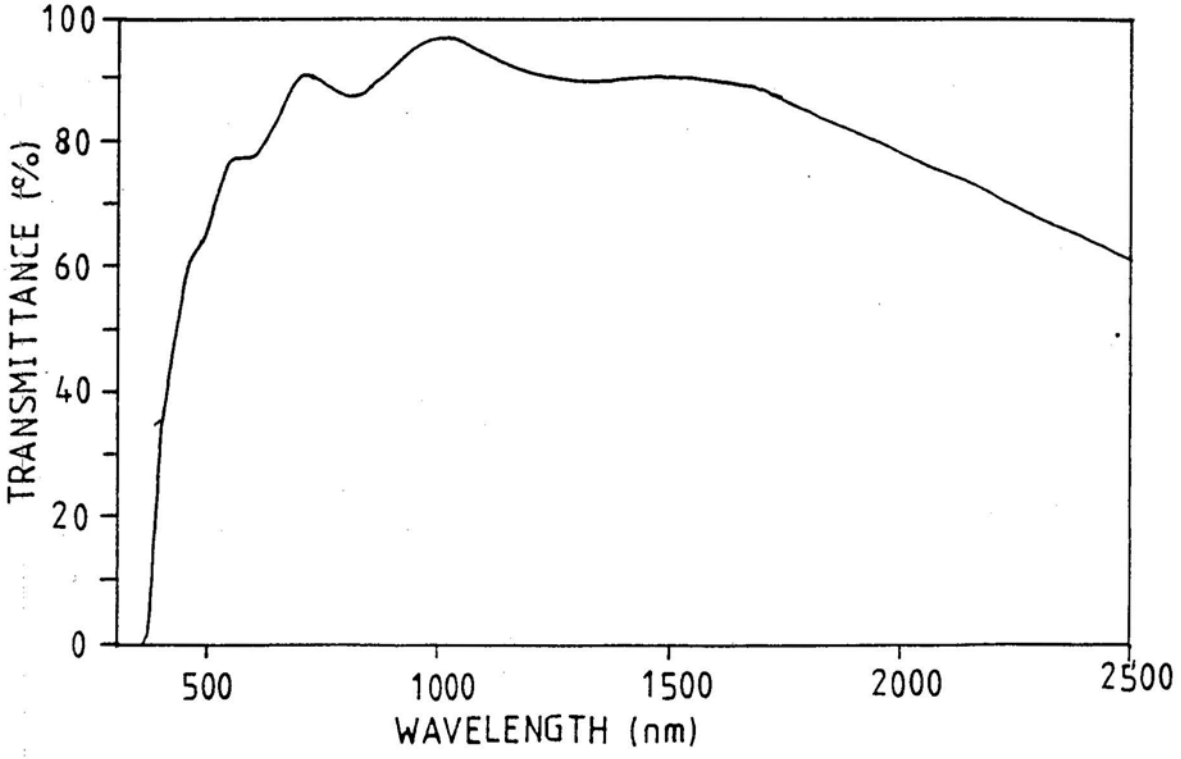

Figure 8.15 Variation of film transmittance versus wavelength for an In-doped (6 at.%) film grown at 306°C.

(figure 8.14) which had a transmission of between 0 to 96 % near to bandgap and 78 - 92 % away from the bandgap with no free carrier absorption.

Doped films grown at 306°C (figure 8.15) were similar and had transmissions between 55 % and 96 % away from bandgap. Generally speaking, doped films grown at 306°C were more transmitting (lower extinctions) than those grown at 276°C but were not as good as the undoped film. These results demonstrate the effect of growth temperature and dopant concentration on transmittance. At the slightly higher temperature the effect of dopant was marginal and the transmission was relatively uniform, whereas at 276°C the presence of dopant had a stronger influence on the film properties in reducing the transmittance especially at longer wavelengths.

The determination of the bandgap of an undoped film using the procedure described in appendix 2 led to a value of 3.27 eV. This was obtained from the intercept of the plot of α^2 versus photon energy shown in figure 8.16. The bandgap of an indium doped film calculated in a similar way from the plot of α^2 versus photon energy was 3.28 eV (see figure 8.17). The addition of the dopant did not change the optical bandgap significantly.

Plots of the refractive indices of the two films as a function of wavelength are shown in figures 8.18 and 8.19. The refractive index of both films increased with wavelength beyond 600 nm.

The analytical procedure for the optical transmission measurements also provided an estimate for the thickness of the ZnO layers. Comparison with the direct measurement using the α-step instrument generally gave values 8-14% less than those provided by the optical measurements. It is not clear why the discrepancy arose, but it is worth noting that the α-step measurements were made by etching a step in the film and this may have underestimated the thickness. The optical measurements are an average over the relatively large area of the beam (a few nm^2) and may be influenced by small undulations.

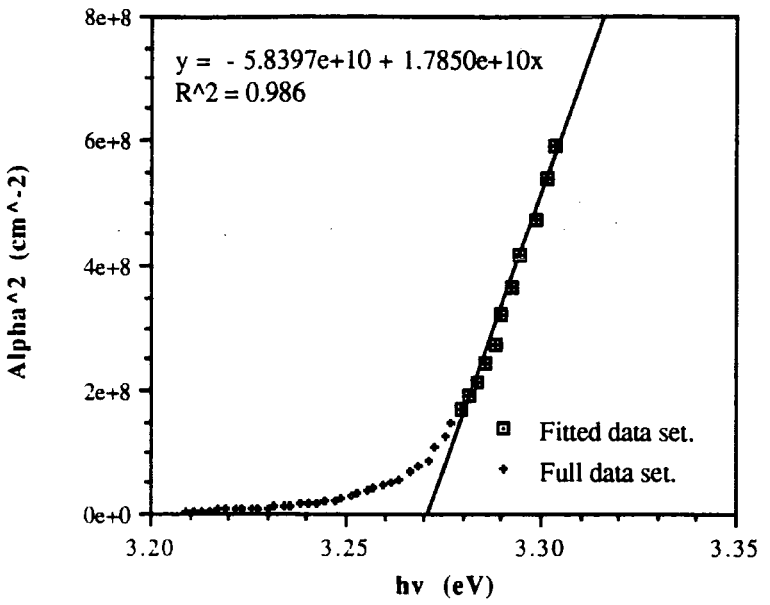

Figure 8.16 Plot of α^2 against photon energy for the determination of bandgap in an undoped film

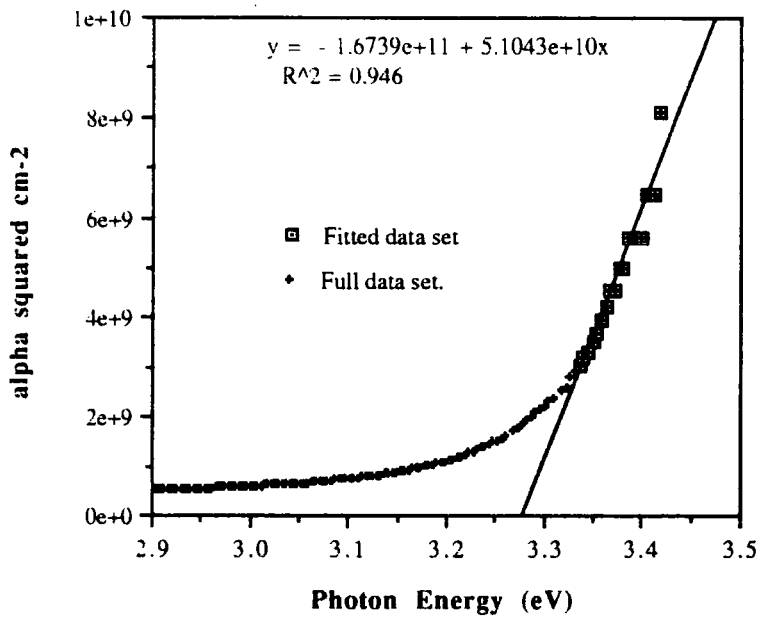

Figure 8.17 Plot of α^2 against photon energy for the determination of bandgap in an indium doped film.

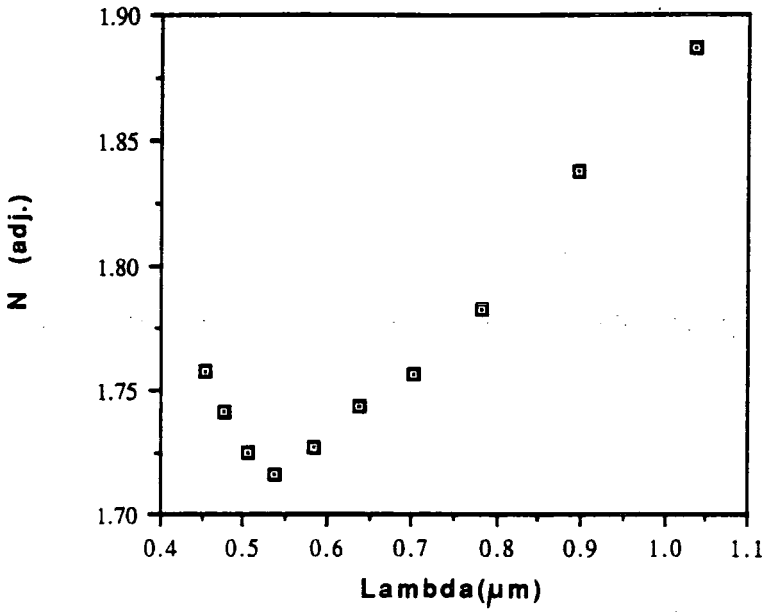

Figure 8.18 Plot of refractive index (n) versus wavelength for an undoped film.

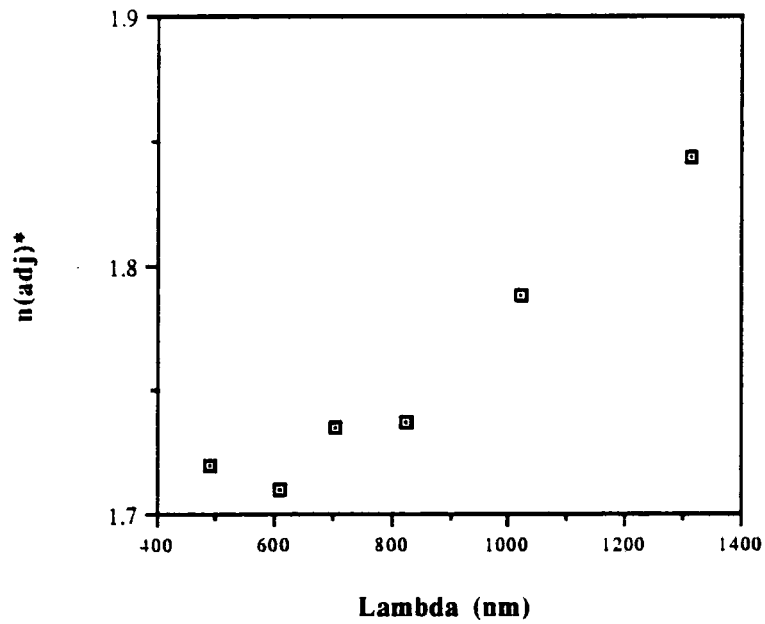

Figure 8.19 Plot of refractive index (n) versus the wavelength for an indium doped film.

8.7 Discussion of Electrical and Optical Properties

Doping ZnO with indium and chlorine results in the substitution of zinc atoms by indium atoms and oxygen atoms by chlorine atoms to form donors. Ionization of electrons from these donors leads to the formation of free carriers. When a proper doping process is employed indium exists in the lattice nominally as In^{2+} below the freeze out temperature, but on heating the loosely bound third valence electron is donated to the conduction band and the indium ion relaxes to the In^{3+}. Similarly chlorine will exist as Cl^{2-} at low temperature and as Cl^{-} at high temperature. Only a small thermal energy is necessary to excite electrons to the conduction band [1]. This is readily provided at room temperature. The result of growing doped films at 276°C and 306°C was to decrease the resistivity from approximately 10 Ωm to 10^{-4}Ωm and to increase the carrier concentration, which in some films saturated (10^{26} m^{-3}) when using the maximum doping levels. This situation was reached for both growth temperatures but with less dopant at the slightly higher temperature of 306°C. Therefore there was no difference in the degree to which the resistivity could be lowered in the range of dopant concentration studied, but only in the ease and efficiency per dopant molecule included in the spray solution. However the results of doping at 276°C suggested that the resistivity could be lowered by further additions, whereas at 306°C the limit on the resistivity appeared to be reached with a doping concentration of 1.5 atomic percent. Indeed the resistivity increased and the carrier concentration decreased with further addition perhaps indicating that the indium and chlorine were simply sitting in a nonactive form possibly as In_2O_3 and/or $InCl_3$ at the grain boundaries.

The results from elemental analysis (ESCA) show that more dopant was present in the film grown at 276°C, but from the electrical results it is clear that this is not in an active form. The gradual addition of dopant when growth was carried out at 276°C resulted in a gradual decrease in film resistivity, which speaks of incomplete pyrolysis of the dopant precursor with an increasing proportion contributing free carriers to the zinc oxide lattice (the inactive fraction might still be responsible for the enhancement

of grain size and effect on structural properties however).

At 306°C a concentration of 1.5 atomic percent In doping leads to the maximum concentration of free electrons. Therefore dopant precursor utilisation at 306°C outweighs that at 276°C in terms of conversion to an electrically active form in the lattice, even though the evaporation effects are also stronger. Structurally the two most conducting films were quite different. The first grown at 276°C had a grain size of 55 nm, a small degree of ordering, $(10\bar{1}1)$ bulk and $(11\bar{2}2)/(11\bar{2}0)$ surface orientation, but was otherwise random. The more lightly doped film grown at 306°C had a grain size of 32 nm and the same preferred orientations, but with generally better crystallite ordering. Overall these results suggest that a combination of large grain size and a high density of donors benefit film conductivity.

For comparison with other work it is worth reporting that high temperature spray pyrolysed $InCl_3$ doped zinc oxide grown using zinc acetate had resistivities of the order 10^{-4} - $10^{-5}\Omega$m without any heat treatment, whereas spray pyrolysis has yielded films with resistivities of the order $5\times10^{-6}\Omega$m to $7\times10^{-7}\Omega$m for ITO, $10^{-5}\Omega$m for indium oxide, 10^{-5} - $10^{-4}\Omega$m for undoped tin oxide, $10^{-5}\Omega$m for antimony doped tin oxide, and $5\times10^{-6}\Omega$m for fluorine doped tin oxide up to 1983 [4]. Also of interest is the sputtering of indium doped zinc oxide which had a resistivity of $8\times10^{-6}\Omega$m [5]. More recently spray pyrolysed ITO has yielded resistivities of $3\times10^{-6}\Omega$m [6] and fluorine doped In_2O_3:Sn grown by sputtering, $6\times10^{-6}\Omega$m [7]. Recent attempts to grow tin oxide by reactive sputtering have yielded films having resistivities of $9\times10^{-5}\Omega$m [8].

The results of optical calculations compares with the work of Major et al. [1] and Jin et al. [9] where the refractive index varied from 1.9 to 2.3 between bandgap and 1 μm.

8.8 Photoluminescence Measurements

The photoluminescence spectra of two films were measured, both grown at 306°C from 0.5 and 1.5 atomic percent $InCl_3$ doped solutions. Spectra were also taken from undoped films grown at 306°C under identical conditions, and at 276°C using the spray

kit before its modernisation. All the emission spectra were fairly broad and relatively featureless, extending throughout the visible from 410 to 700 nm. Maxima in the emission were detectable in the undoped film grown at 306°C where peaks occurred at about 480, 520 and 580 nm. The green (520 nm) and yellow (580 nm) bands have been observed previously by numerous investigators [10–14]. Films doped with $InCl_3$ had a rather similar, but weaker photoluminescence, with suggestions of maxima near 480, 520, and 560 nm. There was no clear cut indication of any direct influence of In or Cl.

8.9 Chapter Eight References

(1) Major S., Banerjee A. and Chopra K.L., *J Mater. Res., 1 (2)*, 300, (1986).

(2) Shimuzu M., Katayama T., Shiosaki T. and Kawabata A., *J. Cryst. Growth, 99*, 399, (1990).

(3) CRC Handbook of Chemistry and Physics, CRC Press, Inc., Ed. Robert C., Weast Ph.D, (1977-1978).

(4) Chopra K.L., Major S. and Pandya D.K., *Thin Sol. Films, 102*, 1, (1983).

(5) Minami T., Sato H., Nanto H., and Takata S., *Jpn. J. Appl. Phys. 24 (10)*, L781, (1985).

(6) Vasu V., Bubramanyham A., *Thin Sol. Films, 193/194* , 696, (1990)

(7) Geofrey C., Portier J., Campet G., Salardenne J., Couturier G., Bourrel M., Chabagno J.M., and Ferry D., *Thin Sol. Films, 202*, 77, (1991).

(8) Howson R.P, Barankova H., Spencer A.G., *Thin Sol. Films, 196*, 315, (1991).

(9) Jin Z.C., Hamberg I., and Granqvist C., *J. Appl. Phys. 64 (10)*, 5117, (1988).

(10) Hirschwald et al., ed. Kaldis E., Curr. Top. Mater. Sci., 7, 143, North-Holland Publishing Company, (1981).

(11) Falcony C., Ortiz A., Garcia M. and Helman J.S., *J. Appl. Phys., 63 (7)*, 2378, (1988).

(12) Falcony C., Ortiz A. and Garcia M., Priv. comm., (1991).

(13) Bushan S., Chukichev M.V., *J. Mat. Sci. Lett.*, 7, 319, (1988).

(14) Minami T., Nanto H. and Takata S., *J. Mat. Sci.*, *17*, 1364 , (1982).

Chapter Nine

Growth of Doped Zinc Oxide at High Temperature Using Alternative Aluminium, Indium and Gallium Precursors

9.1 Introduction

The experimental work described in the two preceding chapters was concerned with the use of $InCl_3$ as the dopant precursor. This was because that compound had proved to be the most effective in reducing the resistivity of the grown film while retaining a high degree of transparency. In the course of the work however, a variety of other dopant precursors were investigated, and the experiments carried out with these are described in this chapter. The properties of undoped films grown at 306°C in a wet ambient with in-flight heating were used as a control, since these were the best high temperature conditions for the growth of ZnO. They were also the conditions used in the majority of growth experiments to be described here. Comparison of the properties of the undoped film with doped films allowed the effectiveness of the doping procedure and the influence of the presence of dopant in the films to be determined.

9.2 Dopant Precursors

The dopant precursors examined are listed in table 9.1. $In(acac)_3$ has been used before as an indium source for the growth of In_2O_3 and ITO using the CVD technique [1] but only recently in spray pyrolysis [2] for applications in the electronics industry. For our work $In(acac)_3$ was prepared in the Chemistry Department.

The two indium precursors were chosen to test whether the presence of chloride had any influence on film conductivity or film structure. It was initially not clear whether the effects of adding $InCl_3$ were due to the indium or chlorine. Consequently a second Cl-free dopant was used to try to determine the role, if any, of the Cl.

$AlCl_3$ was used because it has been used as a dopant precursor to grow ZnO:Al and to deposit insulating films of Al_2O_3, [3] and $Al(OPr^i)_3$ was tried because it has been used in CVD processes to make films of Al_2O_3 for use in VLSI [4,5,6] and other device structures as insulating barrier layers [1]. Both aluminium compounds were

Dopant precursor used in high temperature growth		
Indium based	Aluminium based	Gallium based
$InCl_3.3H_2O$	$AlCl_3$	$Ga(acac)_3$
$In(acac)_3$	$Al(OPr^i)_3$	

Table 9.1. Summary of precursors used in doped ZnO film growth.

Melting points of dopant precursors compared with $Zn(acac)_2.H_2O$/(°C)					
$Zn(acac)_2.H_2O$	$InCl_3$	$In(acac)_3$	$Al(OPr^i)_3$	$AlCl_3$	$Ga(acac)_3$
138	586	≈ 300	119	100	195

Table 9.2. Summary of melting points of dopant precursors

investigated to make a comparison between an already established aluminium dopant for spray pyrolysis with a possible alternative.

$Ga(acac)_3$ is the least well established dopant material and is more stable than $GaCl_3$ which has been more commonly used.

The melting points of the compounds are set out in table 9.2. They show that $AlCl_3$ is the most volatile material. In order of increasing volatility $AlCl_3 \geq Al(OPr^i)_3 \geq Ga(acac)_3 \geq In(acac)_3 \geq InCl_3$.

9.3 Growth of Films with $In(acac)_3$ as the Dopant

Films were grown at 306°C using concentrations up to 3 atomic percent of indium tris-acetylacetonate as the dopant and 0.1M $Zn(acac)_2.H_2O$ as the zinc precursor.

All $In(acac)_3$ doped films were adherent to the substrate and varied from being colourless to clear green in transmission and were smooth with no surface speckle.

Figure 9.1 shows a plot of the film thickness versus the dopant concentration in the growth solution. The film thickness for the undoped film was 940 nm and the thickness fell to 250 nm with the addition of 0.5 atomic percent of $In(acac)_3$, increased again to 590 nm when a dopant concentration of 1.5 atomic percent was used and fell again to 370 nm when the maximum of 3 atomic percent was used. This is evidence that growth suppression occurred during film growth when this dopant was used.

At the lowest concentration of $In(acac)_3$ used (0.5 atomic percent) the suppression was the greatest suggesting that the exact concentration is not important. This suppression occurs through the blocking of active sites (open surface, kinks, ledges, holes) by a species with a stronger binding energy than the zinc. The effects of the blocking of these active sites result in the inhibition or suppression of growth (lateral or vertical) through deactivation by the dopant. It still might be possible for dopant related species to become activated after a time delay having occupied a native active site ; or it may be that the dopant related species may re - evaporate. $In(acac)_3$ is not very volatile and is a bulky molecule that would remain on the zinc oxide surface and influence growth. The steric influence of the $In(acac)_3$ molecule might be expected to prevent zinc from

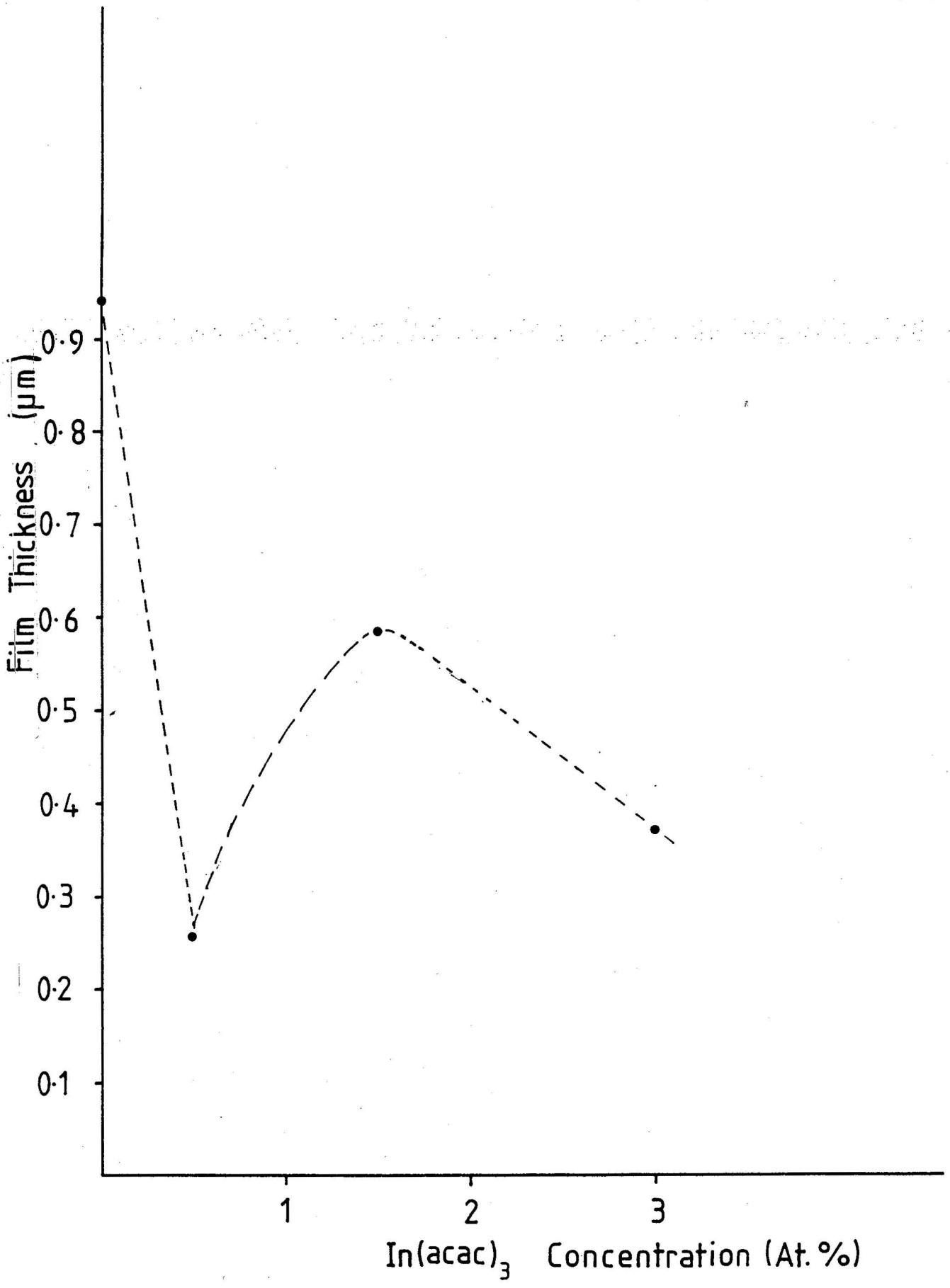

Figure 9.1. Variation of the film thickness with $In(acac)_3$ solution concentration.

becoming attached at suitable growth sites while the higher coordination number of the indium could lead to bonding by the indium through the oxygen. These effects would lead to a reduction in the ZnO growth rate observed.

9.3.1 Indium Concentration in $In(acac)_3$ Doped Zinc Oxide Films

The indium content as estimated by ESCA carried out at ICI Wilton for the three $In(acac)_3$ films is presented in table 9.3 and figure 9.2. The plot shows that the incorporation of indium in the film rises linearly with the concentration of indium in the starting solution, with an incorporation efficiency of 20% - 30%. The carbon concentration varied from 17% to 25% in these films which was not significantly different from the concentration of carbon in $InCl_3$ doped films. Its presence could be put down to the residual carbon in the ESCA instrumentation and the incomplete pyrolysis of the precursors.

9.3.2 Structural Characterisation

The films were characterised in the same way as before by RHEED and XRD and the orientations compared with the ASTM card for a random sample of polycrystalline ZnO powder. Table 9.4 lists the surface preferred orientations compared with the bulk preferred orientations.

The electron diffraction pattern in figure 9.3 is of a film with the addition of 0.5 atomic percent of $In(acac)_3$ to the growth solution. As well as reducing the growth rate, the indium changes the film structure markedly increasing the crystallite order due to the presence of the 0.1 - 0.2 atomic percent that becomes incorporated into the film. Indeed the pattern suggests that there is strong clustering of localised groups of crystals in this film along planes other than the preferred orientation. This film was only 250 nm thick and therefore the dopant must have exerted a strong influence.

For films grown from 1.5 atomic percent containing solutions the electron diffraction pattern reveals that crystallites grew along fewer planes and that there was more misorientation (i.e the arcs are longer), and so the main preferred orientation was relatively more dominant.

ESCA Analysis of $In(acac)_3$ doped ZnO films grown at 306°C					
$In(acac)_3$ solution	Film composition (1) at the surface				
	(2) after slight etching / (at.%)				
/(at.%)	Zinc	Indium	Oxygen	Carbon	Chlorine
0.5	(1) 35	0.1	44	20	0.9
	(2) 31	0.2	45	25	< 0.5
1.5	(1) 42	0.4	40	17	1.0
	(2) 38	0.4	44.5	17	< 0.5
	(1) 38	0.9	40	21	< 0.5
3.0	(2) 35	0.7	40	24.5	0.7

Table 9.3. Elemental composition of $In(acac)_3$ doped ZnO.

Comparison of the surface and bulk preferred order in doped ZnO films grown from $In(acac)_3$ containing solutions		
Dopant concentration/(at.%)	Surface preferred order	Bulk averaged preferred order
0	$(11\bar{2}2)$	$(10\bar{1}1)$
0.5	$(11\bar{2}2)$	$(10\bar{1}1)/(11\bar{2}0)$
1.5	$(11\bar{2}0)$	$(11\bar{2}0)/(10\bar{1}0)$
3.0	$(11\bar{2}0)$	$(10\bar{1}0)/(10\bar{1}1)$

Table 9.4. Summary and comparison of surface and preferred orientations for doped ZnO films grown from $In(acac)_3$ doped solutions.

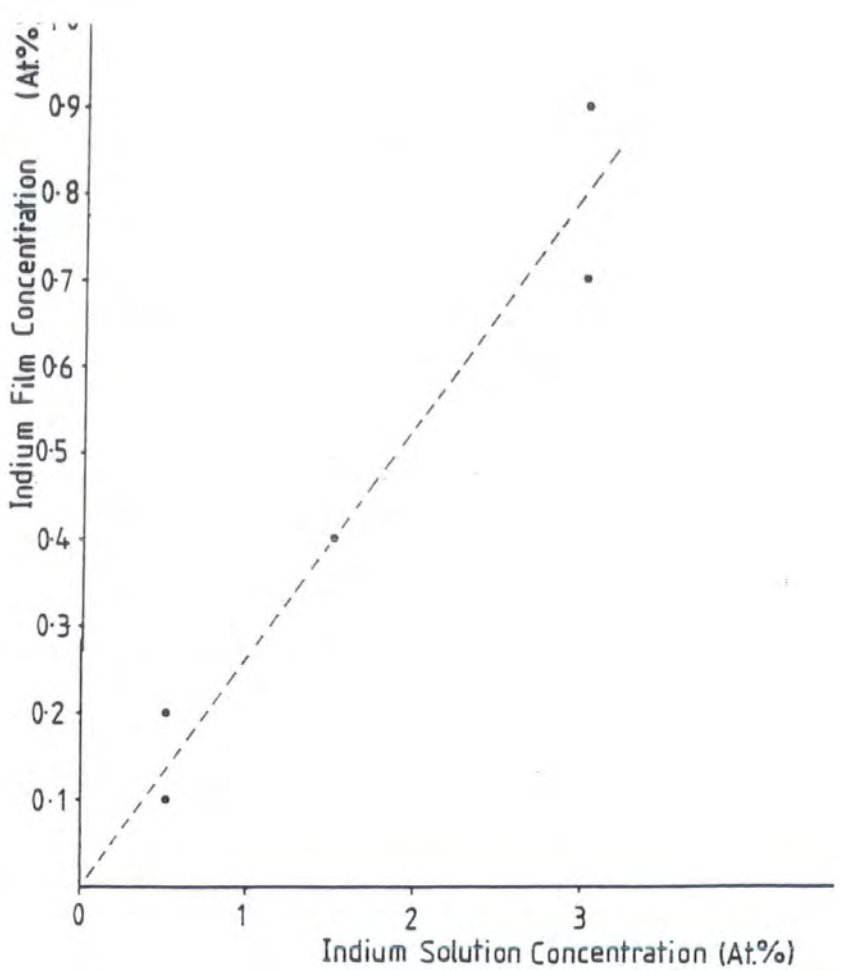

Figure 9.2. Variation of the Indium film concentration with $In(acac)_3$ solution concentration.

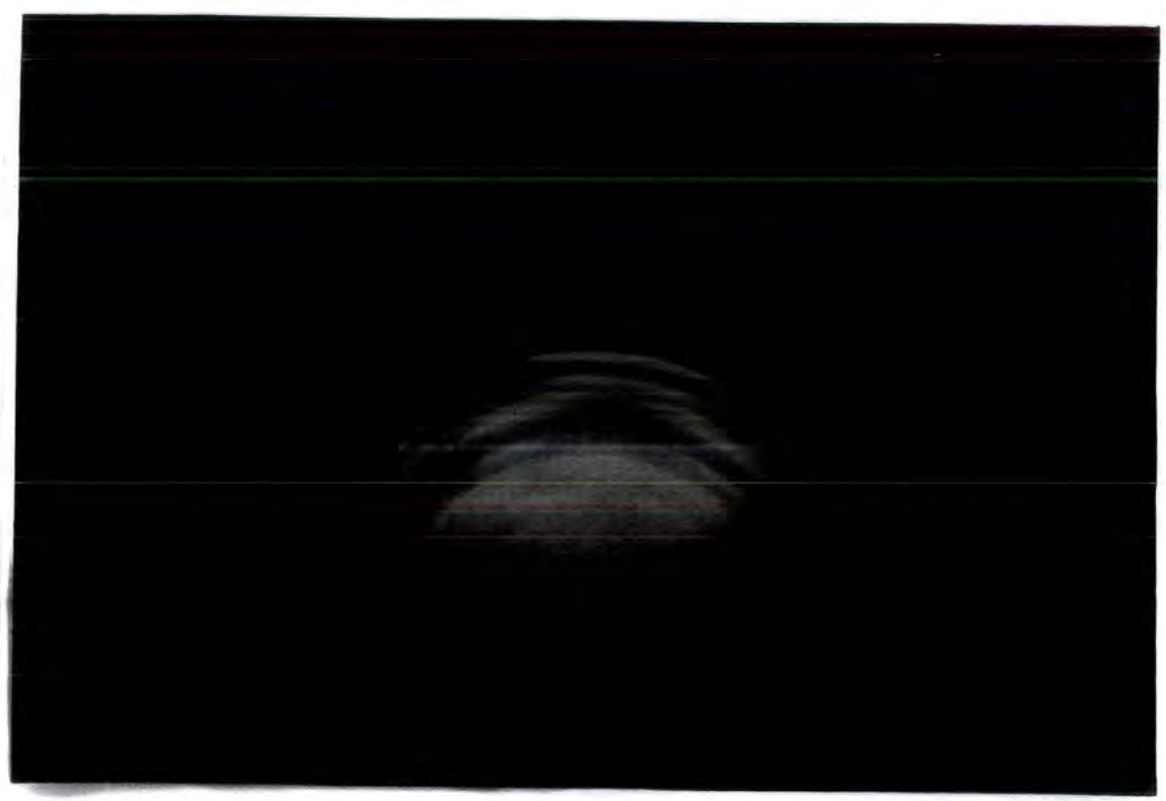

Figure 9.3. RHEED pattern taken from a doped ZnO film grown from a 0.5 atomic percent $In(acac)_3$ doped solution.

The film grown from a 3 atomic percent solution gave a pattern which consisted of longer arcs while still retaining a main preferred order, indicating that the effect of increasing the dopant concentration was to degrade the crystallite ordering. Small additions improved the crystallinity and degree of preferred orientation, but the effect of increasing the dopant concentration was to randomise crystallite ordering.

The preferred orientations of ZnO films doped with $In(acac)_3$, as determined by RHEED and XRD, are compared in table 9.4, while the XRD intensity data are summarised in table 9.5.

The bulk preferred order was $(10\bar{1}1)$ with some $(11\bar{2}0)$ when the dopant concentration was 0.5 atomic percent and this changed to $(11\bar{2}0)$ and some slight $(10\bar{1}0)$ (1.5 atomic percent) and eventually to predominantly $(10\bar{1}0)$ at the highest concentration used (3 atomic percent). This indicates that the adddition of small quantities of dopant changed the film growth and continued to do so with larger additions.

9.3.2.1 Grain Size

The grain sizes of films grown at 306°C from $In(acac)_3$ containing solutions were calculated using the full width half maximum of peaks corresponding to preferred orientations observed in XRD spectra, and are plotted in figure 9.4. They show that compared to an undoped film, the grain size fell from 42 nm to 30 nm for a film grown from a 0.5 atomic percent containing solution. As the solution dopant concentration was raised the grain size remained unchanged until with the highest dopant concentration used (3 atomic percent) a further decrease was recorded. Additions of $In(acac)_3$ dopant clearly led to an overall reduction in the grain size. This contrasts with the enhancement of grain growth which was found using $InCl_3$ thus promoting the role of chlorine in demonstrating diffusion.

9.3.3 Discussion of Structural Studies

The results obtained from the study of the electron diffraction patterns for $In(acac)_3$ doped films indicate that the lightly doped films initially became more ordered and with increased doping became more randomised. This would suggest that the indium was

	(a) Intensity data for polycrystalline zinc oxide							
Crystal plane	$(10\bar{1}0)$	(0002)	$(10\bar{1}1)$	$(10\bar{1}2)$	$(11\bar{2}0)$	$(10\bar{1}3)$	$(11\bar{2}2)$	Preferred order
D_{hkl}/Å	2.816	2.602	2.476	1.911	1.626	1.477	1.379	None : random
Peak intensities/(%)	71	56	**100**	29	40	35	28	polycrystalline
Dopant concentration/(at.%)	(b) Intensity data for films doped with $In(acac)_3$ and grown at 306°C							
0	12	35	**100**					$(10\bar{1}1)$
0.5		17	**100**		26	9	18	$(10\bar{1}1)/(11\bar{2}0)$
1.5	**100**	8	34		**66**			$(11\bar{2}0)/(10\bar{1}0)$
3.0	**95**	17	**100**		26			$(10\bar{1}0)/(10\bar{1}1)$

Table 9.5. Summary of the XRD intensity data for doped ZnO films grown from $In(acac)_3$ doped solutions.

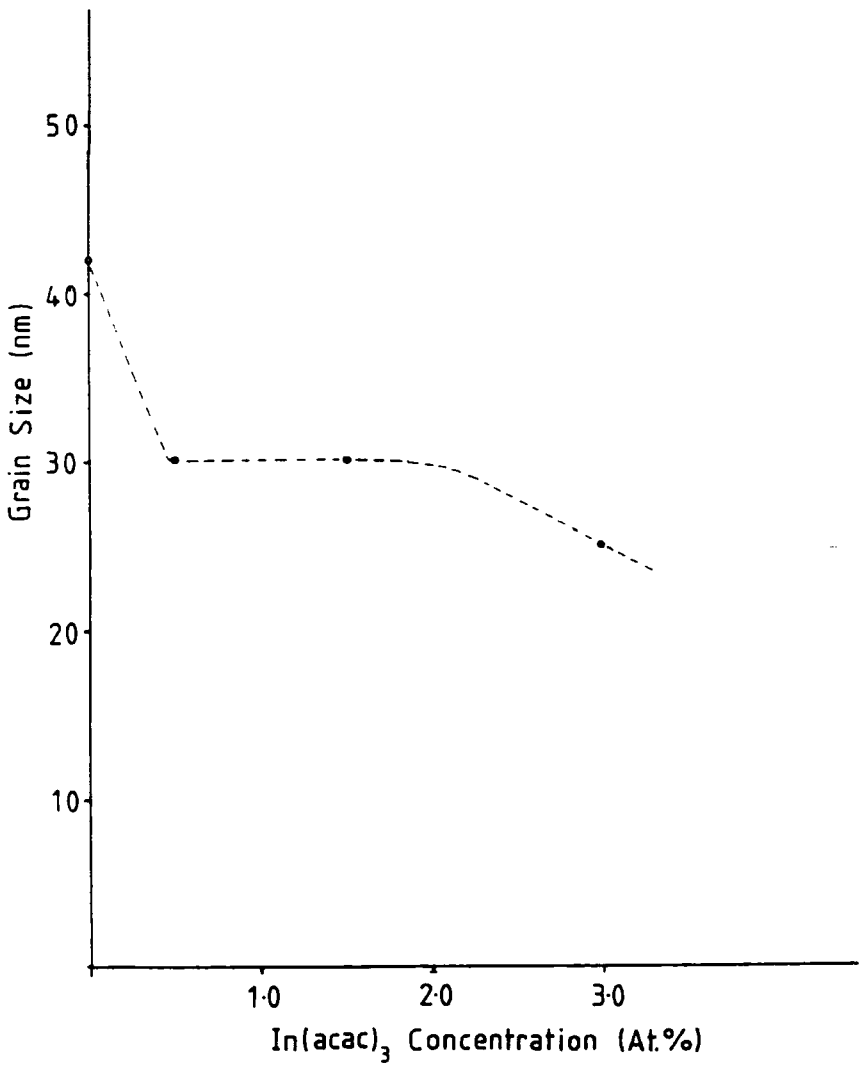

Figure 9.4. Variation of the ZnO grain size with $In(acac)_3$ solution concentration.

occupying sites in the film that affect film order. The initial improvement (0.5 atomic percent $In(acac)_3$ in solution was associated with a slower growth rate and as a result the energetics of film growth were biased toward film order rather than film thickness (i.e crystallite misorientation was restricted), with growth along several axes indicating that the film was in the initial stages of the development of a preferred order. However the addition of an increased amount of $In(acac)_3$ led to the formation of a film which had a dominant preferred orientation axis with hardly any growth off this main axis. Such films were more than twice as thick as the more lightly doped film and therefore there is reason to believe that the preferred orientation developed as the film with the lowest Gibbs free energy became dominant. The film grown from 0.5 atomic percent of $In(acac)_3$ possessed the best structure of the three. The main arc was spread out and therefore there was some slight misorientation. The film had better order than the undoped film and therefore the presence of dopant at these concentrations had a beneficial influence on film structure.

The most heavily doped film was thinner again and contained the most indium. The degree of order was undeveloped and the action of the dopant was to introduce disorder in and between crystallites and grains which would tend to destroy the relationship between them and prevent them growing along the same axis. Therefore indium is likely to sit on zinc sites and on interstitial positions in channels in the ZnO lattice causing distortion of equilibrium bond lengths and altering the potential energy. In addition it is possible that precipitation of indium occurred at grain boundaries or in more substantial intergranular phases. In the most extreme case, regions of the film could consist of amorphous ZnO where the difference in order within the grains was not substantially better than that of the intergranular phases. However the film structure was not appreciably worse than in the undoped film.

As stated previously the addition of 0.5 atomic percent of $In(acac)_3$ to the growth solution altered slightly the way the ZnO films grew, in that lightly doped films had the same surface preferred order as the undoped $(11\bar{2}2)$, and a similar bulk preferred order

$(10\bar{1}1)$ changing to $(10\bar{1}1)$ with some slight $(11\bar{2}0)$ with the addition of $In(acac)_3$ derived indium. Therefore the presence of indium in these quantities did not significantly change either the thermodynamics (Gibbs free or interfacial energy at grain boundaries) or the kinetics affecting the choice of crystal habit.

However with increasing $In(acac)_3$ derived indium the similarities with the undoped film ceased. The surface preferred order became $(11\bar{2}0)$ and the bulk preferred order a mixture of $(10\bar{1}0)$ and $(11\bar{2}0)$, pointing to similar film structure in the bulk and at the surface. Film structure overall is heavily influenced by the dopant. Therefore at these concentrations of indium the order of preference as to which is the fastest growing and energetically more favourable growth axis changes. At the highest dopant level the surface is still $(11\bar{2}0)$ oriented but the bulk shows some $(10\bar{1}1)$ order pointing to a possible return to undoped growth mechanisms. In all samples the growth appears to be modified as the ZnO grows on ZnO instead of on the substrate. The substrate surface is amorphous silica so the initial deposit will be random although a preferred order quickly develops as the film thickens and subsequent monolayers become better ordered and more crystalline. These results confirm that the $(11\bar{2}0)$ and the $(10\bar{1}0)$ orientations are related to the presence of indium.

The grain size data show that the grain size was depressed by the influence and presence of $In(acac)_3$ derived indium. This depression was constant up to 1.5 atomic percent above which a smaller fall was recorded. This points to a restriction on the growth rate of the grains that was not linked with the overall film growth rate or its mechanism. The decomposing precursor could be segregating out at grain boundaries and preventing the movement of grain boundaries (i.e the diffusion of interstitial zinc or oxygen vacancies). Thus these films are fine grained and consequently have more grain boundary area than films possessing larger grains. A small grain size also indicates that film growth is more vertical than horizontal.

9.3.4 Electrical Properties

The resistivities and transport properties of the $In(acac)_3$ doped films were measured at room temperature. Film resistivity varied from 10 Ωm to $1.3\times10^{-3}\Omega$m as the solution dopant concentration was increased from 0 to 3 atomic percent (0 to 0.8 atomic percent in the film) as shown in figure 9.5.

Initially with the addition of the smallest amount of $In(acac)_3$ the resistivity fell 100-fold. Further additions resulted in less dramatic lowering of film resistivity suggesting saturation in the doping efficiency. Clearly $In(acac)_3$ can act as a dopant precursor but lower resistivities were achieved using $InCl_3$ indicating that chlorine had also been incorporated.

The mobility and the concentration of free carriers in $In(acac)_3$ doped films were measured as a function of dopant concentration and the results are shown in figures 9.6 and 9.7. The mobilities varied from 5.8 $cm^2\ V^{-1}\ s^{-1}$ for the film grown from a 0.5 atomic percent doped solution, to 0.6 $cm^2\ V^{-1}\ s^{-1}$ from a 1.5 atomic percent doped solution, then up to 4 $cm^2\ V^{-1}\ s^{-1}$ from a 3 atomic percent doped solution. The mobility did not vary linearly with dopant concentration, but was higher when the film thickness was smaller (see figures 9.1 and 9.6), suggesting that mobility was inversely proportional to film thickness and that it was not influenced by dopant concentration.

The carrier concentration rose from $10^{23}\ m^{-3}$ to $6\times10^{24}\ m^{-3}$ as the solution doping level was increased from 0.5 atomic to 3 atomic percent. Saturation occurred at between 1.5 and 3 atomic percent. The electrical properties of doped ZnO films as represented by the the resistivity and carrier concentration show that $In(acac)_3$ as a dopant is less effective than $InCl_3$.

9.3.5 Optical Properties

The results of the determination of optical transmission in the wavelength range 300 nm to 2500 nm for $In(acac)_3$ doped films are outlined in table 9.6. Absorption coefficients (absorbance) were calculated from optical transmission. The typical transmittance and absorbance of an undoped film are also included. The undoped film had

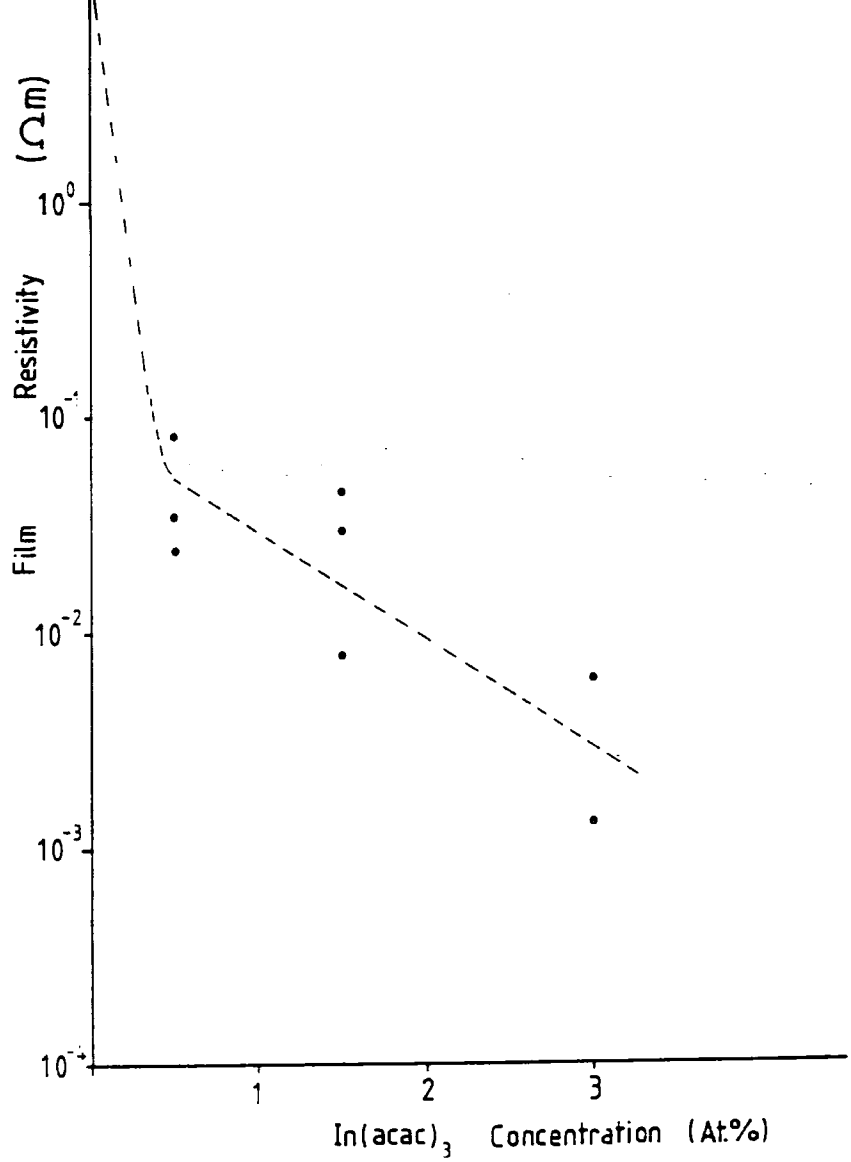

Figure 9.5. Variation of the ZnO film resistivity with $In(acac)_3$ solution concentration.

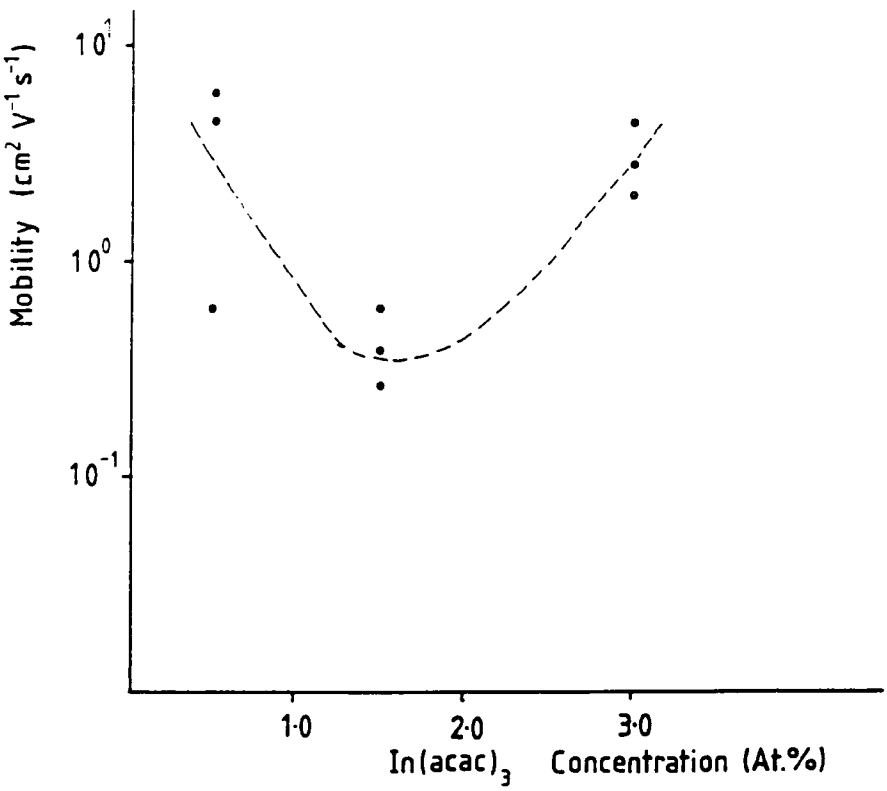

Figure 9.6. Variation of the carrier mobility in doped ZnO with $In(acac)_3$ solution concentration.

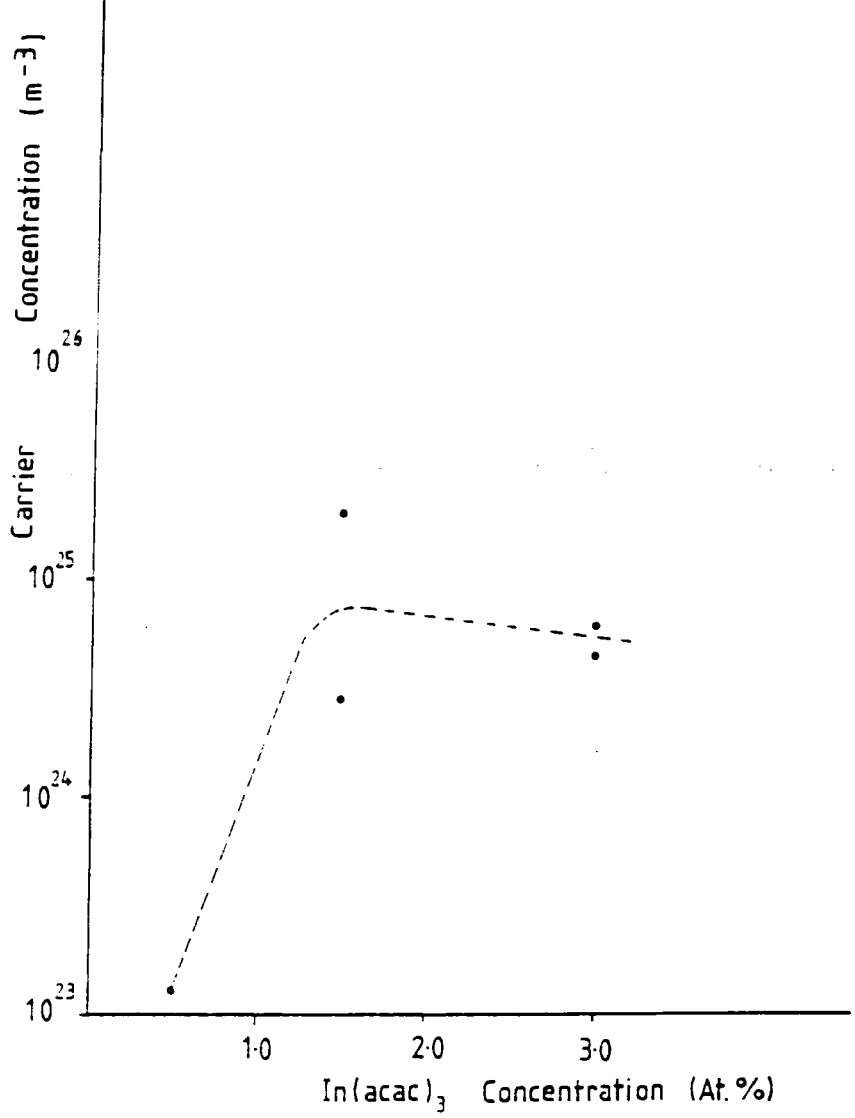

Figure 9.7. Variation of the carrier concentration in doped ZnO with $In(acac)_3$ solution concentration.

Transmission and absorbance of $In(acac)_3$ doped ZnO films grown at 306°C					
Wavelength ranges (nm)	300 -500	500 -1000	1000 - 1500	1500 - 2000	2000 -2500
$In(acac)_3$ Dopant concentration	(1) Transmittance % ; (2) Absorbance $/10^6$ m^{-1}				
0	(1) 0 - 86 (2) $\geq$ 0.16	78 - 95 0.05 - 0.26	82 - 91 0.1 - 0.2	80 - 92 0.09 - 0.24	81 - 92 0.09 - 0.22
0.5	(1) 0 - 99 (2) $\geq$ 0.04	81 - 99 0.04 - 0.84	89 - 97 0.12 - 0.46	87 - 89 0.47 - 0.56	88 - 90 0.42 - 0.51
1.5	(1) 0 - 80 (2) $\geq$ 0.38	82 - 96 0.07 - 0.34	82 - 86 0.26 - 0.36	86 - 89 0.2 - 0.26	84 - 85 0.3 - 0.28
3.0	(1) 0 - 97 (2) $\geq$ 0.08	84 - 99 0.03 - 0.47	94 - 97 0.08 - 0.17	86 - 91 0.25 - 0.4	85 - 86 0.41 - 0.44

Table 9.6. Summary of the transmittance and absorbance in In-doped ZnO films grown from $In(acac)_3$ doped solutions.

an average transmittance of 86% and an absorbance of 0.16×10^6 m^{-1} (a range of 0.05 - 0.26) across all wavelengths. For $In(acac)_3$ doped films the transmittance varied from 80% to 99% away from the absorption edge and the absorbance from 0.03 to 0.84×10^6 m^{-1}. Overall the most transmitting films were also the most lightly and the heavily doped with an average transmittance of 90% and absorbances of 0.47×10^6 m^{-1} and 0.28×10^6 m^{-1} away from the bandedge. The film with lowest average absorbance was grown from the intermediate solution, when the average transmittance was only 86%. The absorbance measurement takes the film thickness into account so that the films can be compared. Therefore even though the two thinnest films were more transmitting it was the film grown from a solution of an intermediate concentration that was the least absorbing per unit thickness indicating that the density of optically active centres was lower. The density of centres ought to have been at a maximum in the most heavily doped film and indeed the absorbance was higher at some wavelengths than in the other films.

Overall these films are extremely transmissive suggesting that processes such as absorption and reflection are very small.

9.3.6 Photoluminescence Measurements

Photoluminescence spectra for a film grown from a 1.5 atomic percent $In(acac)_3$ containing solution are shown in figures 9.8 and 9.9 (expanded). They show that there is a broad emission band at 577 nm (2.15 eV) with suggestions of other bands at 500 and 610 nm. Some of the peaks between 417 nm and 591 nm were approximately equally spaced (168 meV to 174 meV) and were located on either side of the principal peak maximum. In addition there was a group of peaks centred between 460 nm and 477 nm separated by 31 - 32 meV apart : at 476.6 nm (2.6 eV), 470.7 nm (2.633 eV), 465.2 nm (2.664 eV) and 459.8 nm (2.695 eV).

9.3.7 Conclusions

Incorporation of indium into the film using $In(acac)_3$ as a source was successful and therefore this dopant must be involatile enough and reactive enough to decompose

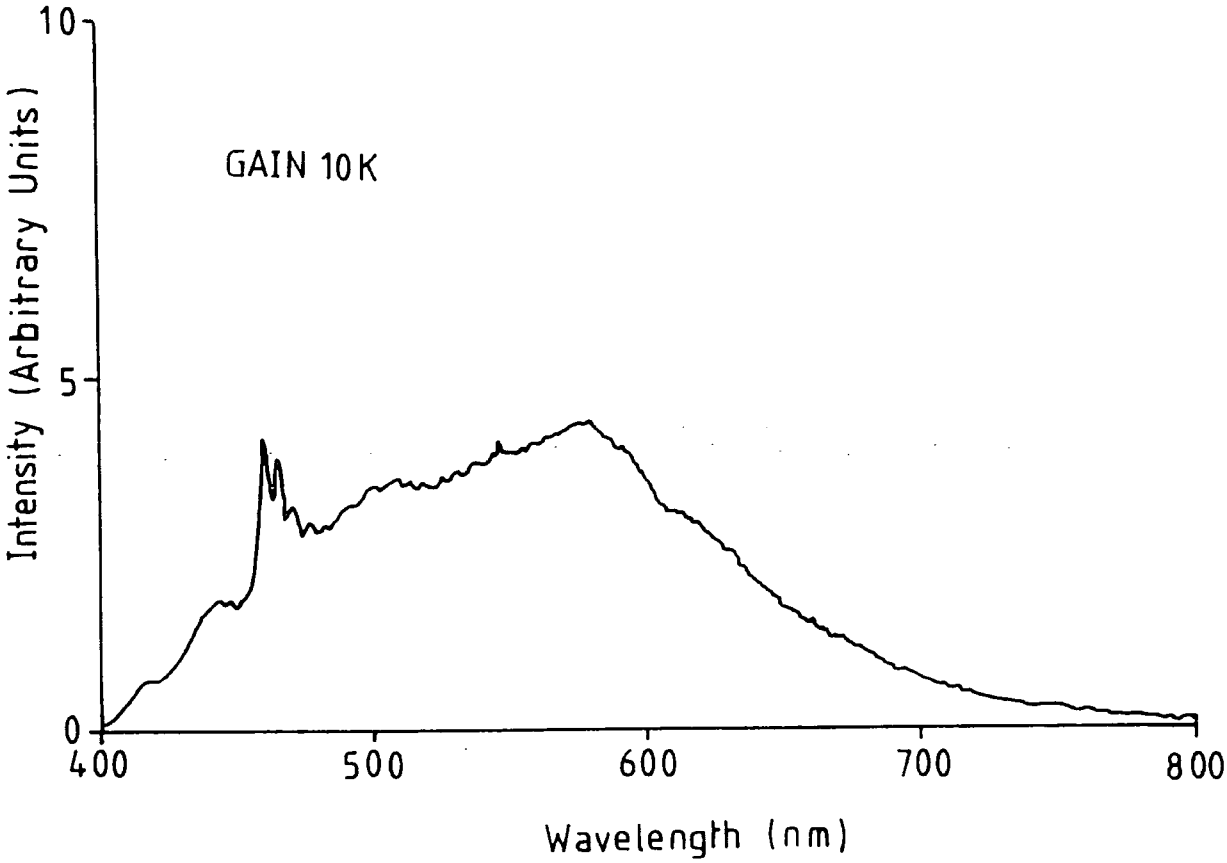

Figure 9.8. Photoluminescence spectrum of a ZnO film grown from 1.5 atomic percent $In(acac)_3$ doped solution.

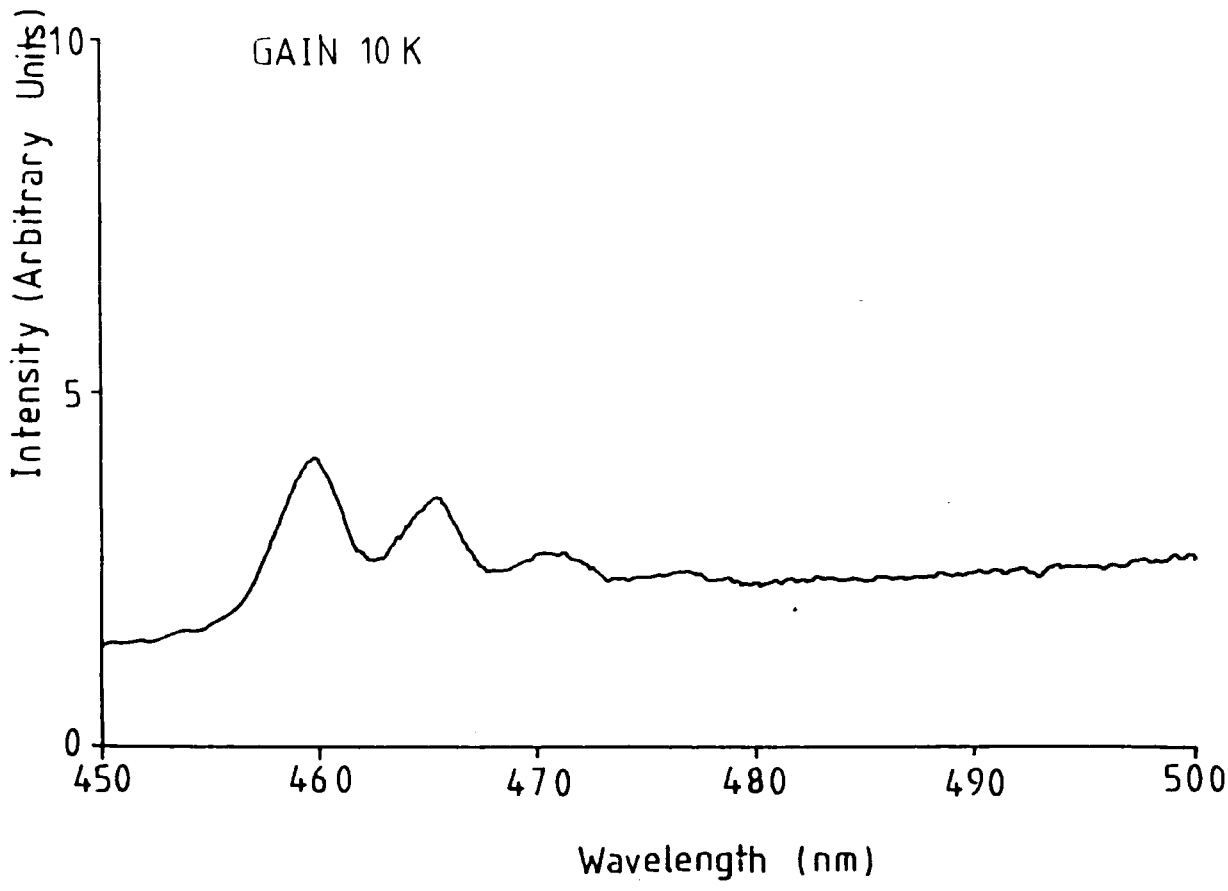

Figure 9.9. Expansion of figure 9.8 showing phonon satellites.

on the film surface. Bonding between the film and substrate and intra - film bonding was good. There was no evidence of pinholes, cracking, or voids. The films were clear, transparent and free from grain. Growth suppression occurred during film growth when using $In(acac)_3$, possibly due to binding between $In(acac)_3$ fragments and the surface, thus preventing binding by $Zn(acac)_2.H_2O$. Increasing additions of indium into the lattice resulted in an initial improvement and then a randomisation of the crystallite ordering. The preferred orientation was initially unchanged at the surface and slightly modified in the bulk, but was transformed with further additions of indium to $(11\bar{2}0)$ at the surface and a mixture of $(11\bar{2}0)$ and $(10\bar{1}0)$ in the bulk. Therefore the incorporation of indium was different from that of indium from $InCl_3$ in that the growth rate of certain zinc oxide planes was affected. The effect of $In(acac)_3$ was to reduce grain size relative to undoped zinc oxide, pointing to the importance of chlorine in grain growth enhancement when $InCl_3$ was used. Doping zinc oxide with $In(acac)_3$ reduced the film resistivity to $1.3\times10^{-3}\Omega m$ when the precursor solution doping level was 3 atomic percent. The small grain size may have limited the conductivity through carrier depletion by traps (section 2.5.2).

9.4 Growth of $Al(OPr^i)_3$, $AlCl_3$ and $Ga(acac)_3$ Doped ZnO

The results of experiments on the growth of aluminium doped ZnO and gallium doped ZnO using $Al(OPr^i)_3$, $AlCl_3$ and $Ga(acac)_3$ as dopants and 0.1M solutions of $Zn(acac)_2.H_2O$ are described in the following sections. The concentrations of $Al(OPr^i)_3$ used were 0.5, 1.5 and 3 atomic percent. This dopant has been used as a precursor for Al_2O_3 in VSLI fabrication and has a melting point of 194 °C. Aluminium doping was tried as an alternative to indium doping because of the lower cost and possibly lower toxicity. In addition two films were grown using $AlCl_3$ (m.pt. $\approx$ 100°C) doped solutions containing 0.5 atomic percent and 3 atomic percent.

Two other films were grown using $Ga(acac)_3$ at concentrations of 0.5 and 1.5 atomic percent. $Ga(acac)_3$ (m.pt. $\approx$ 194°C) has not been cited in the literature as having been used as a dopant precursor for zinc oxide. All films were grown at 306°C in a wet

ambient with in-flight heating for 14-15 minutes.

All $Al(OPr^i)_3$, $AlCl_3$ and $Ga(acac)_3$ doped films were adherent to their substrates. $Al(OPr^i)_3$ doped films grown from 0.5 atomic percent doped solutions were dark grey tinted, while those grown from the 1.5 atomic percent doped solution were pink or red in transmission. At the highest doping level (3 atomic percent) the films were again darkly tinted. $AlCl_3$ doped films were either green (the lightly doped film) or light brown (the more heavily doped film). The $Ga(acac)_3$ doped films were green to violet (the lightly doped film) and green (the heavily doped film). All films were smooth, transparent and free from visible grain.

The curves in figure 9.10 show the variation of the thicknesses of $Al(OPr^i)_3$, $AlCl_3$ and $Ga(acac)_3$ doped films. The thicknesses of all the films were reduced when the dopants were used, although ESCA measurements failed to reveal the presence of any aluminium or gallium.

9.4.1 Structural Characterisation

The results of the surface preferred orientation as determined by RHEED are compared with the results of the bulk averaged preferred orientation as determined by XRD in tables 9.7, 9.8 and 9.9.

Comparison of the RHEED patterns showed that the smallest addition of $Al(OPr^i)_3$ led to a big improvement in the degree of preferred order, and to a reduction in the grain size, as indicated by the reduction in the arc length and width and the disappearance of spots in the diffraction rings. As well as the main preferred orientation representing the axis about which the majority of crystallites were oriented there were also other but less favoured orientations representing planes in the unit cell of ZnO lying off at certain angles.

As the solution doping level was increased the film structure became more random as the arcs became longer and wider, pointing to an increase in crystallite disorder. Increasing the dopant concentration to 3 atomic percent led to films having a completely random structure.

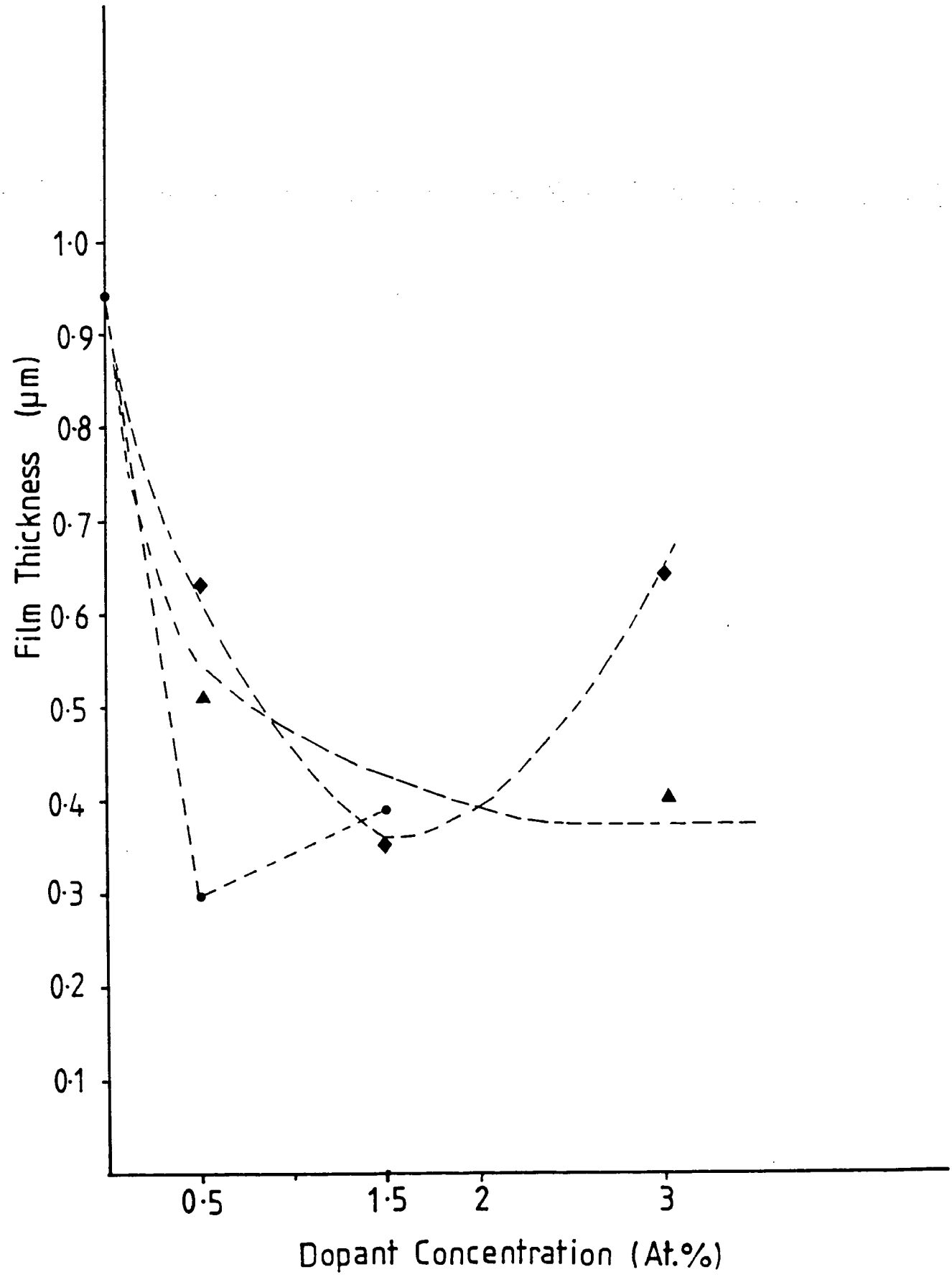

Figure 9.10. Variation of the doped ZnO film thickness versus the $Al(OPr^i)_3$ (◆), $AlCl_3$ (▲) and $Ga(acac)_3$ (●) solution concentrations.

Comparison of the surface and bulk preferred order in doped ZnO films grown at 306°C from $Al(OPr^i)_3$ containing solutions		
Dopant concentration/(at.%)	Surface preferred order	Bulk averaged preferred order
0	$(11\bar{2}2)$	$(10\bar{1}1)$
0.5	$(11\bar{2}2)$	$(10\bar{1}1)$
1.5	$(11\bar{2}2)$	$(10\bar{1}1)$
3.0	weak $(11\bar{2}0)$	$(11\bar{2}0)/(10\bar{1}1)/(10\bar{1}0)$

Table 9.7. Summary and comparison of the surface and bulk averaged preferred orientation in doped ZnO films grown from $Al(OPr^i)_3$ doped solutions.

Comparison of the surface and bulk preferred order in doped ZnO films grown at 306°C from $AlCl_3$ containing solutions		
Dopant concentration/(at.%)	Surface preferred order	Bulk averaged preferred order
0	$(11\bar{2}2)$	$(10\bar{1}1)$
0.5	$(11\bar{2}2)$	$(10\bar{1}1)/(11\bar{2}2)$
3.0	$(11\bar{2}2)$	$(10\bar{1}1)/(11\bar{2}2)$

Table 9.8. Summary and comparison of the surface and bulk averaged preferred orientation in doped ZnO films grown from $AlCl_3$ doped solutions.

Comparison of the surface and bulk averaged preferred order in doped ZnO films grown at 306°C from $Ga(acac)_3$ containing solutions		
Dopant concentration/(at.%)	Surface preferred order	Bulk preferred order
0	$(11\bar{2}2)$	$(10\bar{1}1)$
0.5	$(11\bar{2}2)$	$(10\bar{1}1)$
1.5	weak $(11\bar{2}2)$	$(10\bar{1}1)$

Table 9.9. Summary and comparison of the surface and bulk averaged preferred orientation in doped ZnO films grown from $Ga(acac)_3$ doped solutions.

The preferred orientations at the surface and in the bulk for $Al(OPr^i)_3$ doped ZnO are shown in table 9.7. For films grown from 0.5 and 1.5 atomic percent containing solutions the surface and bulk preferred orders were $(11\bar{2}2)$ and $(10\bar{1}1)$ respectively, and were therefore no different from the undoped film. However use of the highest doping level led to the formation of films having a $(11\bar{2}0)$ plane at the surface and a $(11\bar{2}0)$ and $(10\bar{1}1)$ preferred orientation in the bulk. Therefore $Al(OPr^i)_3$ as a dopant does not affect the film structure appreciably except when high concentrations are present in the spray solution.

The preferred order of the $AlCl_3$ doped films was virtually unchanged but did have some $(11\bar{2}2)$ orientation present in the bulk structure. The surface preferred order was $(11\bar{2}2)$ while the bulk average was $(10\bar{1}1)$. The use of $AlCl_3$ did affect film structure and there is a suggestion that there is some continuity between surface and bulk structure and the growth mechanism. The surface and bulk structure of $Ga(acac)_3$ doped films was no different from that of an undoped layer. This dopant therefore does not affect the film structure at all.

The grain sizes for $Al(OPr^i)_3$ doped films are set out in figure 9.11 as a function of the dopant concentration. Once again the grain size fell steadily from from 42 nm to 29 nm as the solution doping level was increased from 0 to 3 and 6 atomic percent.

With $AlCl_3$ the grain size was not much affected by the dopant concentration whereas with $Ga(acac)_3$ the more usual decrease in grain size was observed.

9.4.2 Discussion of Crystallographic Texture, Preferred Orientation and Grain Size Studies

The crystallinity and degree of preferred orientation improved (relative to undoped films) when dopant concentrations of 0.5 and 1.5 atomic percent of $Al(OPr^i)_3$ were used, while higher dopant concentrations resulted in the randomisation of the films. The same was true for $AlCl_3$ and $Ga(acac)_3$. As with indium doping, the initial improvement points to more ordered film growth which may be due to the depression of film growth rate (suggesting higher evaporation and diffusion rates) allowing the fastest

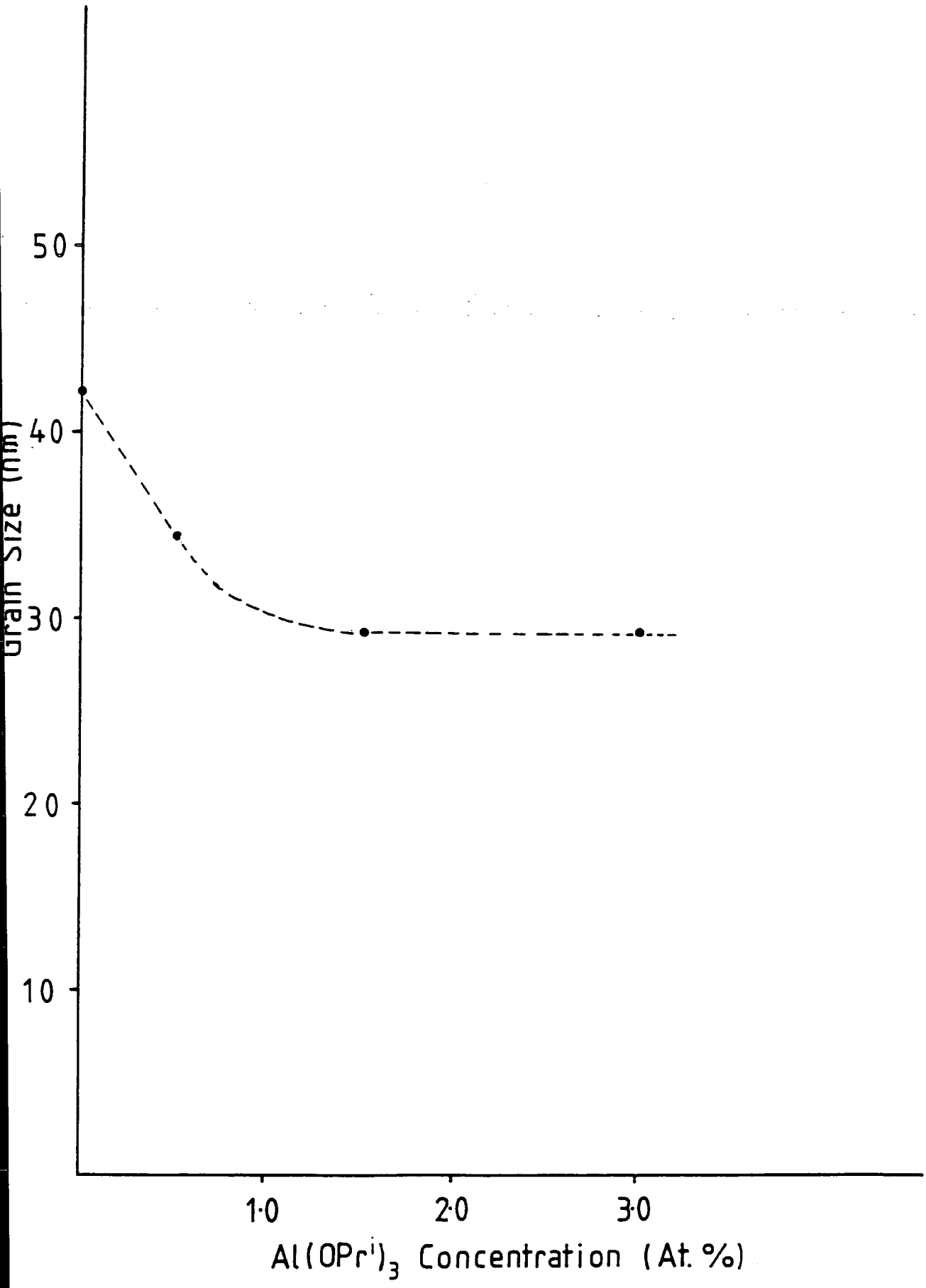

Figure 9.11. Variation of the grain size in doped ZnO with Al(OPr^i)$_3$ solution concentration.

growing planes to dominate. This may occur through the differential growth rates associated with particular planes leading to differing degrees of growth suppression (i.e. the dopant has more effect on the slower growing planes perhaps). On faster growing planes $Zn(acac)_2.H_2O$ will be able to compete more effectively, leading to a resolving of the growth rates of different planes when there is a smaller percentage of energy being taken up in the decomposition of $Zn(acac)_2.H_2O$ when the mass of zinc oxide being deposited is reduced. However as higher concentrations of dopant were used, film order was lost as a result of the influence of disorder within and between the grains. However since no aluminium or gallium was detected within the films the observed effects may have been due to the presence of dopants on the film surface during growth. The binding energy of aluminium to oxygen is 500 KJ mol^{-1} and therefore Al - O containing species will be more tightly bound than Zn - O species (bonding energy 276 KJ mol^{-1}). However Ga - O species perhaps will be the most weakly bound since this binding energy is 250 KJ mol^{-1}.

The use of high concentrations of $AlCl_3$ led to the formation of larger grains suggesting the chlorine enhanced the grain growth as with $InCl_3$.

The preferred orientation of $Al(OPr^i)_3$ doped films was unchanged from that of the undoped case with one exception. This suggests that the interaction of this dopant with the lattice was limited to the crystallinity and did not go as far as to change which plane was the fastest growing. The exception was the most heavily doped film where the surface orientation was $(11\bar{2}0)$ and the bulk averaged a mixture of $(11\bar{2}0)$, $(10\bar{1}0)$, and $(10\bar{1}1)$ pointing to a increase in the growth rate of the $(11\bar{2}0)$ and the $(10\bar{1}0)$ planes. Such an influence was also observed when $In(acac)_3$ was used. Therefore the action of aluminium on the growth rates of the planes of zinc oxide is similar (i.e. it enhances, relatively speaking, the growth rate and thermodynamic preference for nucleation along the $(11\bar{2}0)$ axis with respect to the other planes). This occurs at the highest doping level suggesting that groups of aluminium containing species are responsible. The ion size of Al^{3+} is of the order 40 - 50 pm and therefore much smaller than zinc (74 pm) whereas

the size of Ga^{3+} is 60 pm. It is likely that large groups of smaller sized ions are needed to influence the growth rate of different planes. The slight correspondence between the surface and the bulk preferred order of the most heavily doped film indicates that the overall structure is not dissimilar to the surface structure.

The films grown using $AlCl_3$ and $Ga(acac)_3$ indicate that these compounds and any group III metal ion derived from them did not exert any influence on the thermodynamics and kinetics of growth along ZnO planes (even though film growth rate suppression had occurred releasing energy for other processes).

Grain size measurements show that $Al(OPr^i)_3$ doping does not result in grain growth enhancement as with $AlCl_3$. Nor was any grain growth enhancement observed for $Ga(acac)_3$ doping. In all cases grain growth is supressed initially as is the film growth rate. This is likely to be due to the involatility of $M^{(III)}$ - O species with respect to $M^{(III)}$ - Cl species suggesting that the chloro species diffuse and evaporate more easily than the oxo species. The $M^{(III)}$ - Cl species are more weakly attached and evaporate more easily. With larger additions of dopant the difference is more obvious and while grain growth is enhanced (film growth rate approximately constant for $AlCl_3$ doping) the grain growth remains suppressed by a constant factor.

The volatility and reactivity of $AlCl_3(.xH_2O)$ (decomposition and melting point 100°C) outweigh those of either $Al(OPr^i)_3$ (melting point 119°C) or $Ga(acac)_3$ (melting point 194°C). The Al - O and Al - Cl bond strengths are approximately equal (500 KJ mol^{-1}) and greater than the Ga - O bond strength (250 KJ mol^{-1}).

9.5 Electrical Properties of Doped Zinc Oxide

The resistivities of films doped with $Al(OPr^i)_3$, $AlCl_3$ and $Ga(acac)_3$ and plots of film resistivity are shown in figure 9.12. All dopants reduced the resistivity but $Al(OPr^i)_3$ was more effective than $AlCl_3$. However the lowest value achieved with $Al(OPr^i)_3$ was $10^{-2}\Omega m$ with a correspondingly low carrier concentration for the heavily doped film of 5×10^{23} m^{-3}. The resistivities of films grown from 0.5 and 3 atomic percent $AlCl_3$ doped solutions varied from $4\times10^{-1}\Omega m$ to $4\times10^{-2}\Omega m$. $Ga(acac)_3$ doped films

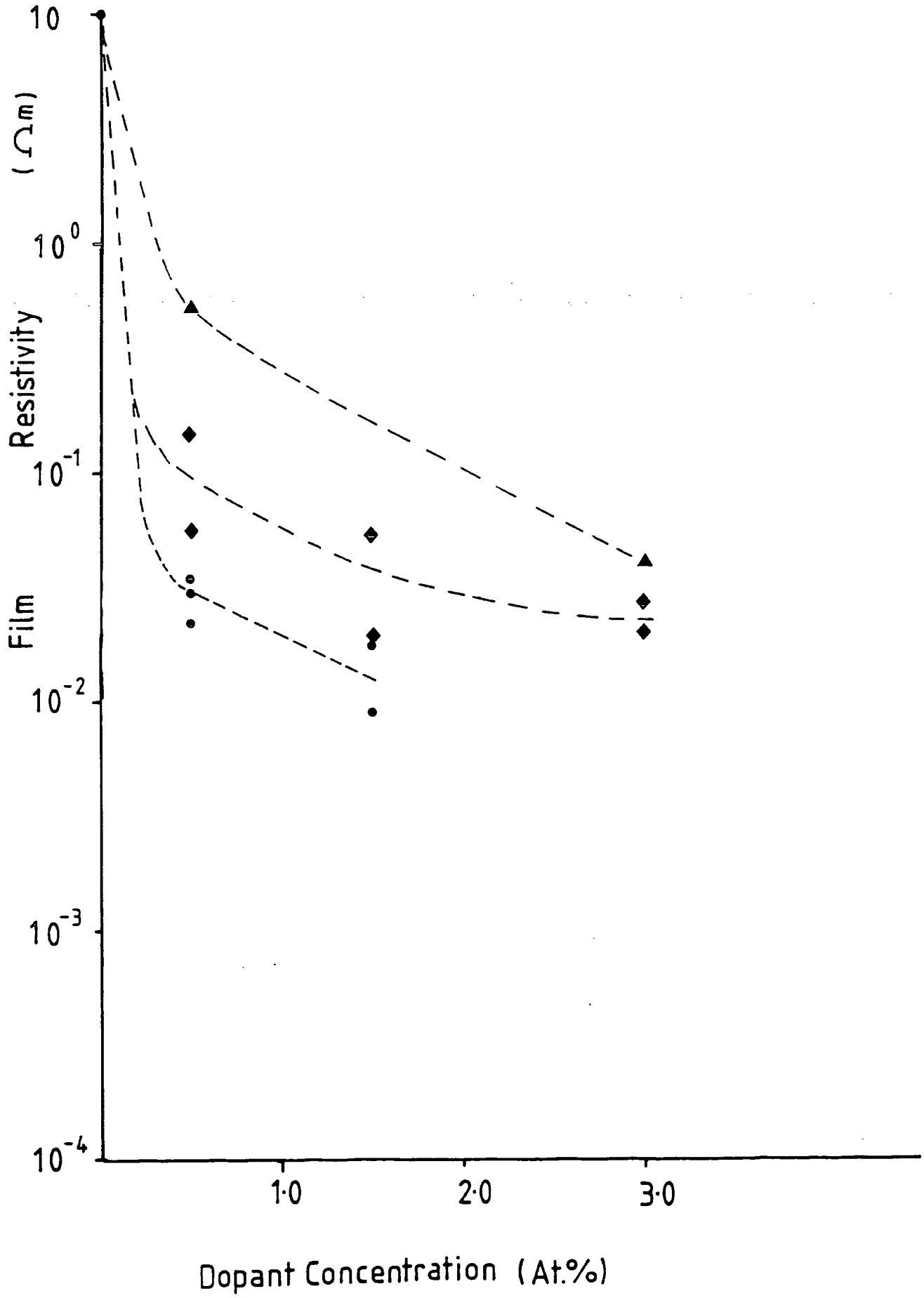

Figure 9.12. Variation of the doped ZnO film resistivity with $Al(OPr^i)_3$ (◆), $AlCl_3$ (▲), and $Ga(acac)_3$ (●), solution concentrations.

had resistivities of the order of 1.3 - 3 $\times 10^{-2}\Omega$m. Both $AlCl_3$ and $Ga(acac)_3$ might be able to reduce the resistivity further if higher levels were used. Clearly all three precursors reduced the resistivity even though their concentrations incorporated in the film were less than 0.5 atomic percent. Clearly the problem was to grow the group III element into the film. None of these precursors led to films with resistivities lower than $10^{-2}\Omega$m.

9.6 Optical Properties of $Al(OPr^i)_3$, $AlCl_3$ and $Ga(acac)_3$ Doped Zinc Oxide

The results of the measurement of optical transmittance for $Al(OPr^i)_3$ doped films are shown in table 9.10 and compared with that of an undoped film. The transmittance varied from 82% to 99% (the fluctuations being due to interference fringes) and the absorbances from 0.02×10^6 m^{-1} to 0.46×10^6 m^{-1}. These films are highly transmitting from the bandedge to the infrared. The film grown with the lowest dopant concentration (0.5 at.%) had the highest average transmittance, 92% and the lowest overall extinction (0.14×10^6 m^{-1}). Films grown using $AlCl_3$ and $Ga(acac)_3$ had similar transmissions.

The photoluminescence spectra taken from films grown using $Al(OPr^i)_3$ (1.5 at.%), $AlCl_3$ (3 at.%), and $Ga(acac)_3$ (1.5 at.%) as dopants are shown in figures 9.13, 9.14 and 9.15. The emission of the film grown using $Al(OPr^i)_3$ shows one principal peak at 466 nm (2.450 eV) with a suspicion of a second band at 554 nm (2.156 eV) (figure 9.13).

The emission spectrum from a film grown using $AlCl_3$ as a dopant is shown in figure 9.14. Here there is a main peak 570 nm (2.18 eV) with a smaller peak at 496 nm (2.5 eV). The most intense emission occurs at a different wavelength when the aluminium precursor is changed from $Al(OPr^i)_3$ to $AlCl_3$ suggesting that chlorine plays a significant role in the 570 nm luminescence. The spectrum of a film grown from $Ga(acac)_3$ containing solution (figure 9.15) also had two peaks of low intensity at 507 nm (2.44 eV) and 575 nm (2.15 eV).

9.7 Discussion of Electrical and Optical Properties

The electrical measurements demonstrate that the dopants discussed in this chapter were not as efficient as $InCl_3$ as figure 9.16 shows, which summarises the resistivities

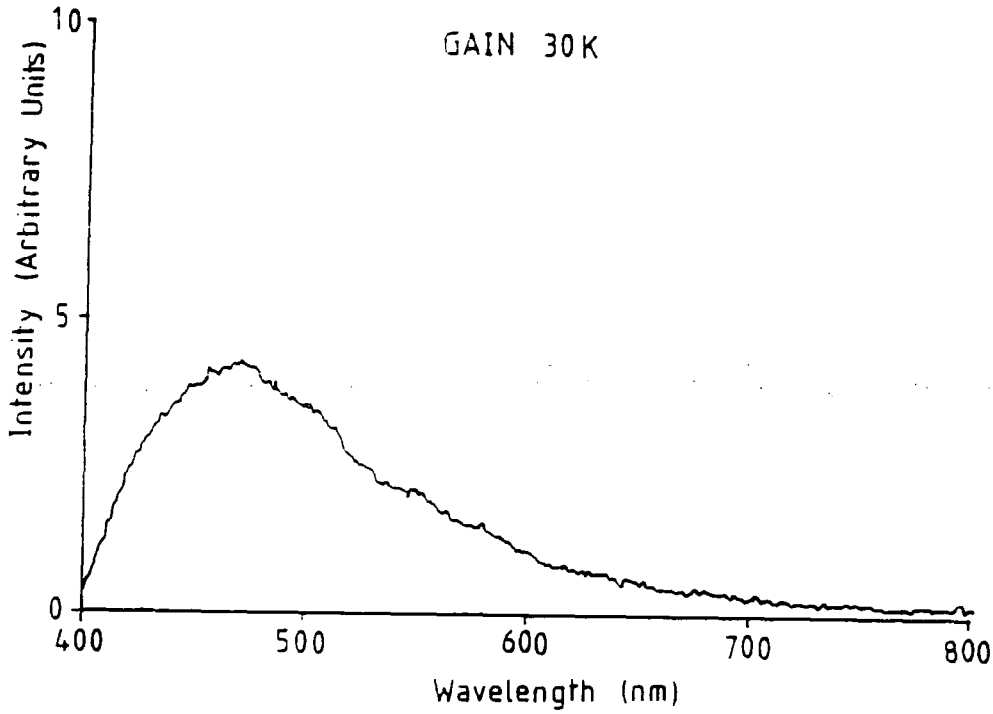

Figure 9.13. Photoluminescence spectra of the doped ZnO film grown from a 1.5 atomic percent $Al(OPr^i)_3$ doped solution.

Transmission and absorbance of ZnO films grown at 306°C using $Al(OPr^i)_3$ as a dopant						
Wavelength ranges (nm)		300 - 500	500 - 1000	1000 - 1500	1500 - 2000	2000 - 2500
$Al(OPr^i)_3$ Dopant concentration/(at.%)		(1) Transmittance / % (2) Absorbance / 10^6 m^{-1}				
0	(1)	0 - 86	78 - 95	82 - 91	80 - 92	81 - 92
	(2)	$\geq$ 0.16	0.05 - 0.26	0.1 - 0.2	0.1 - 0.24	0.1 - 0.22
0.5	(1)	0 - 80	85 - 99	85 - 96	89 - 92	92 - 94
	(2)	$\geq$ 0.35	0.02 - 0.26	0.06 - 0.25	0.13 - 0.18	0.10 - 0.14
1.5	(1)	0 - 94	85 - 97	97 - 99	89 - 92	87 - 88
	(2)	$\geq$ 0.18	0.09 - 0.46	0.03 - 0.09	0.23 - 0.33	0.37 - 0.4
3.0	(1)	0 - 89	84 - 96	82 - 85	89 - 92	88 - 89
	(2)	$\geq$ 0.18	0.07 - 0.28	0.26 - 0.31	0.13 - 0.19	0.19 - 0.2

Table 9.10. Summary of the transmittance and absorbance of doped ZnO films grown from $Al(OPr^i)_3$ doped solutions.

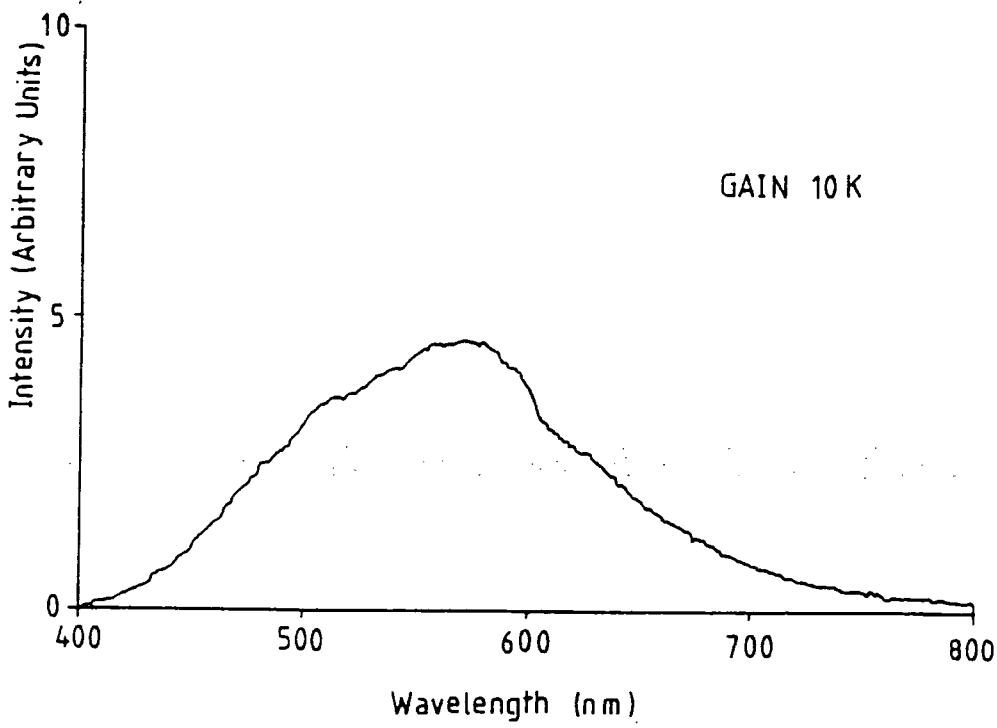

Figure 9.14. Photoluminescence spectra of the doped ZnO film grown from a 3 atomic percent $AlCl_3$ doped solution.

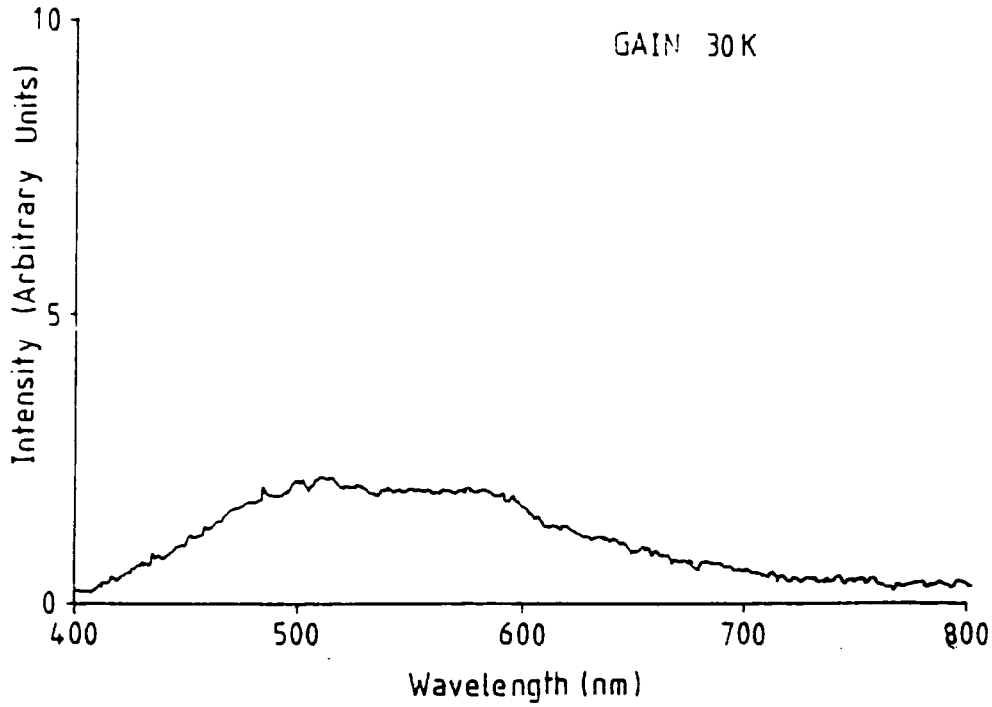

Figure 9.15. Photoluminescence spectra of the doped ZnO film grown from a 1.5 atomic percent $Ga(acac)_3$ doped solution.

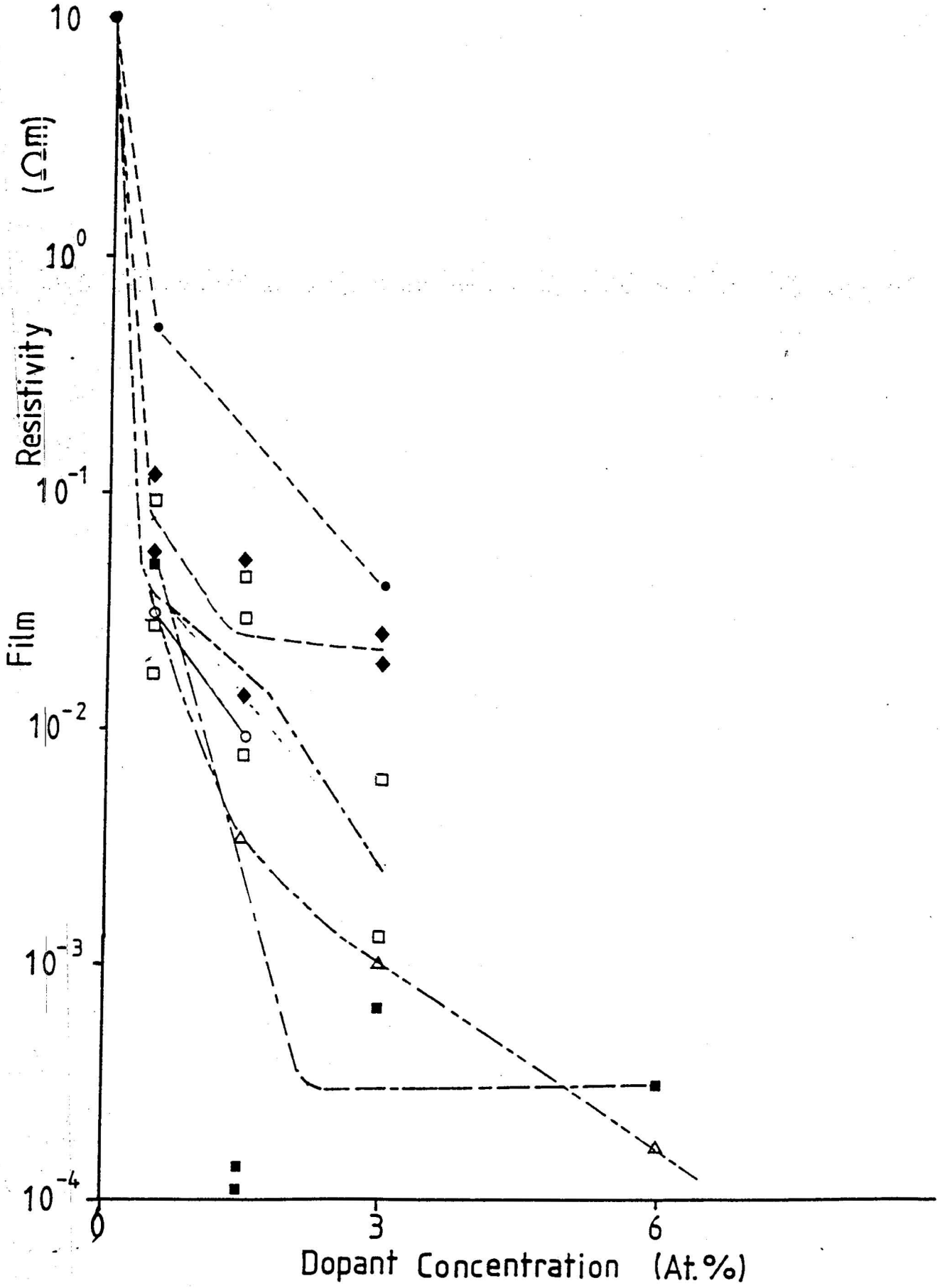

Figure 9.16. Summary of the film resistivities from a variety of dopants versus the solution concentration. Symbols : ◆ = film growth from $Al(OPr^i)_3$ doped solutions ; ● = film growth from $AlCl_3$ doped solutions ; ○ = film growth from $Ga(acac)_3$ doped solutions ; △ = film growth from $InCl_3$ doped solutions (276°C) ; ■ = film growth from $InCl_3$ doped solutions (306°C) ; □ = film growth from $In(acac)_3$ doped solutions.

of all the films grown at high temperature. The ESCA studies found less than 0.5 atomic percent of aluminium or gallium in the films, although structural disorder was still observed, indicating that dopant was present in the lattice and/or or at grain boundaries. The reduced resistivities of doped samples confirm that dopants were incorporated at concentrations below the detectivity of ESCA. Saturation of the film resistivity occurred when using $Al(OPr^i)_3$ at levels above 0.5 - 1.5 atomic percent which was not observed with either $AlCl_3$ or $Ga(acac)_3$ over the ranges studied and might indicate that the use of higher concentrations of $AlCl_3$ and $Ga(acac)_3$ would give lower resistivities. Gallium is an oxygen getter (i.e it catalytically removes oxygen), which indium and aluminium are not, so that it might produce zinc excess and subsequently free carriers in gallium doped films. Overall $Ga(acac)_3$ was more efficient than the aluminium precursors and gave film resistivities at a 1.5 atomic percent level that were superior to film resistivities that were obtained using $Al(OPr^i)_3$ or $AlCl_3$ at doping levels of up to 3 atomic percent.

The well known green emission band (507 nm) characteristic of zinc oxide (due to either zinc or oxygen vacancies) was found in the $Ga(acac)_3$ doped film only, while emission peaks at slightly shorter wavelengths (i.e 466 nm and 496 nm) were found in the aluminium doped films which might suggest that these are associated with aluminium related defects (Al_{Zn}).

Peaks near the yellow band (which normally occurs at 590 nm) were also observed with a possible shift to shorter wavelengths as the dopant was changed from $Ga(acac)_3$ to $AlCl_3$, then to $Al(OPr^i)_3$. This therefore might possibly be related to a defect influenced by a group III metal ion. This suggests that $Al(OPr^i)_3$ has the greatest effect on the electro - optical properties of the film.

9.8 Conclusions

Growth suppression was observed with the additions of (1) $Al(OPr^i)_3$, (2) $AlCl_3$ and (3) $Ga(acac)_3$ to $Zn(acac)_2.H_2O$ even though the incorporation efficiency of these dopants was below 0.5 atomic percent possibly due to evaporation or volatility ((1),(2))

or high thermal stability (3).

The structure of the films was initially improved with small additions of dopant but randomised again when higher levels were used. The preferred orientation was only affected for a film heavily doped with $Al(OPr^i)_3$, indicating that this group of dopants did not interact with the growing film planes to a significant degree.

Grain sizes were suppressed on adding dopant except with $AlCl_3$ doped films where the presence of chlorine counteracted the effects of the aluminium due to a diffusion process involving chlorine.

Film resistivity was lowered with all three dopants. $Al(OPr^i)_3$ was more efficient than $AlCl_3$ over the range studied, but at higher doping levels $AlCl_3$ would give better results. Overall, $Ga(acac)_3$ gave the most promising results with a steeper decline in the film resistivity as the doping level was increased. However none of these dopant precursors was as efficient as $InCl_3$ or $In(acac)_3$. The optical transmission was good and broad featureless photoluminescence bands were observed in the green and yellow.

9.9 Chapter Nine References

(1) Ryabova L.A., ed. Kaldis E., Curr. Top. Mat. Sci., 7 (5), 589, North-Holland Publishing Company, (1981).

(2) Tiburcio - Silver A., Joubert J.C., Labeau M., *Thin Sol. Films, 197*, 195, (1991)

(3) Cossement D., Streydio J.M., *J. Cryst. Growth, 72*, 57, (1985).

(4) Mutoh H., Mizokami Y., Matsui H., Hagiwara S., Ino M., *J. Electrochem. Soc., 122 (7)*, 987, (1975).

(5) Duffy M.T., Revesz A.G., *J. Electrochem. Soc. 117 (3)*, 372, (1970).

(6) Aboaf J.A., *J. Electrochem. Soc., 114 (9)*, 948, (1967).

Chapter Ten

Summary and Conclusions

The original objective of this project was to produce transparent conducting films of ZnO by spray pyrolysis at a temperature low enough ($\leq$ 200°C) to permit successful deposition on plastic. Earlier work in this project had concentrated on the use of zinc acetate as a precursor. For this, substrate temperatures in excess of 250°C were required, so that clearly a different precursor was necessary if conducting films were to be prepared on plastic. In a cooperative programme with P. Coates and A.J. Banister in the Chemistry Department, University of Durham, a range of precursors were prepared and tested. $Zn(acac)_2.H_2O$ turned out to be the best. In the early part of the work effort was concentrated on an extensive investigation of the growth and properties of undoped films grown from $Zn(acac)_2.H_2O$ under a wide range of conditions. The effects of adding a variety of donor impurities were then examined and $InCl_3$ proved to be the most effective donor precursor. The lowest resistivity films grown at low temperatures were those where a dry ambient and substrate heating only were used. In contrast, the lowest resistivities in films grown at higher temperatures required the use of wet ambient and in-flight heating.

10.1 The Growth of Undoped Layers

For undoped film growth of ZnO from $Zn(acac)_2.H_2O$ the growth rate was heavily influenced by the growth temperature and other conditions. There was an important discontinuity in the film properties at a growth temperature of 200°C. From 96°C - 200°C the thickness of the films decreased with increasing substrate temperature, but above 200°C the thicknesses were relatively constant. Below 200°C crystallinity, adhesion, and optical properties were poor. The film resistivity was very high at low temperature but a minimum was observed when a growth temperature of 300°C was used. Undoped films grown below 200°C (when 0.1M solutions of $Zn(acac)_2.H_2O$ were used) had a different preferred order from those grown above 200°C. Films grown below 100°C were random polycrystalline. In many cases the preferred orientation of the

undoped films improved during growth and only the early stages were more random.

The grain size in undoped films was temperature activated and increased with increasing growth temperature. The inclusion of water during growth increased (i) the polycrystallinity, and (ii) the film resistivity markedly when growth was carried out below 200°C but decreased it when growth was carried out above 200°C. The best high temperature conditions for the deposition of undoped conducting adherent ZnO were in the region 276 - 336°C in a wet ambient with in-flight heating. The best low temperature conditions for the deposition of undoped conducting adherent ZnO were in the region of 216°C in a dry ambient with no in-flight heating. The lowest resistivity for undoped films was $3\times10^{-2}\Omega$m for growth at 300°C in a wet ambient. This was reduced to $2\times10^{-4}\Omega$m after annealing at 375°C in a reducing mixture of hydrogen and nitrogen.

A study of the decomposition of $Zn(acac)_2.H_2O$ to ZnO indicated that this can occur by at least four different routes. These were : (a) the *intra*molecular route, a low temperature route where the coordinated water is responsible for the hydrolysis of $Zn(acac)_2.H_2O$; the mechanism is exothermic ; (b) the thermolysis mechanism, a high temperature route where the only means of decomposition are by the cleavage of bonds through the concentration of energy ; this is likely to be aided by a high collision frequency among precursor molecules ; (c) the *inter*molecular mechanism, a low temperature mechanism where the hydrolysing agent is external ; (d) an unknown mechanism or mechanisms dependent on the onset of thermolysis and therefore aided by the water hydrolysis lessening the reliance on thermal activation. The overall controlling factor was re-evaporation from the substrate across the temperature range studied. Mixing of the characteristics of all the decomposition mechanisms with the evaporation characteristics for the zinc precursor and solvent results in the original curves shown in figures 1 and 2 of section 5.3. In the low temperature (in a dry ambient) growth of undoped ZnO the *intra*molecular mechanism operates, whereas at high temperature the *inter*molecular and the thermolysis mechanisms operate. When water is present

inter- and *intra-*molecular mechanisms operate when low temperatures are used to grow undoped ZnO , but at high temperatures these, the thermolysis, and other mechanisms including the a hydro-thermolysis mechanisms operate as well.

10.2 Doping at Low Temperatures

The use of $InCl_3$ as a dopant precursor led to better quality films especially those grown at low temperature from lower concentrations of precursor. Most of the films were highly transmitting in the visible and near infrared region. The low temperature growth (175-200°C) of doped ZnO produced films with resistivities of the order $10^{-5}\Omega$m and visible transmittances of 80%. These values compare favourably with those for ZnO:Al and SnO_2. Relatively large grain sizes (60-80 nm) and a relatively high degree of preferred order were also obtained in the most conducting films, but were not a necessary requirement for good conduction. The doping level is the dominant factor.

Thinner films were only slightly less conductive and had a random structure , whereas thicker films were more ordered due to the survival of the fastest growing planes.

The deposition behaviour between 175°C and 200°C was invariant and led to films having similar and ideal properties for a transparent conducting oxide. Doped ZnO was also grown on a plastic substrate resulting in a film which was slightly less conductive ($5\times10^{-5}\Omega$m) than on glass and had a different structure and significantly larger grain size. This is attributed to substrate effects in that the plastic used had a crystalline oriented surface while the glass did not. Our primary objective of growing on a substrate that can withstand high temperatures was therefore achieved.

Growth below 175°C resulted in the formation of inferior ZnO films. These had higher resistivities and lower transmittances than required for transparent conducting coating but were still however adherent to their substrate and might find a use as antistatic coatings.

10.3 Doping at High Temperatures

A number of films were grown at higher temperatures using $InCl_3$, $In(acac)_3$,

$Al(OPr^i)_3$, $AlCl_3$ and $Ga(acac)_3$ as dopant precursors. The growth rate was reduced when $InCl_3$ was used. The crystallinity of the films was improved by small additions of $InCl_3$ but randomised by further additions up to 6 atomic percent. When light $InCl_3$ doping was employed, the preferred growth axis was unchanged from that of the corresponding undoped ZnO film on the surface and in the bulk. The grain size was initially reduced when the doping was light but increased when heavy doping and higher temperatures were used. The resistivity was reduced by the addition of $InCl_3$ and the lowest value obtained was $10^{-4}\Omega$m. The films were all luminescent with broad green and yellow emission bands. The spectra of undoped films contained a greater diversity of emission peaks.

For films grown from different sprayed volumes doped with $InCl_3$ the degree of preferred orientation improved as the films thickened.

Growth suppression also occurred when using $In(acac)_3$, possibly due to binding between $In(acac)_3$ fragments and the surface preventing binding to the surface by $Zn(acac)_2.H_2O$. Incorporation of indium in the film using $In(acac)_3$ was successful as evidenced by ESCA and demonstrates that this dopant must be involatile and reactive enough to decompose on the film surface. Increasing additions of indium into the lattice resulted in an initial improvement and then a randomisation of the crystallite ordering. The preferred orientation was initially unchanged at the surface and slightly modified in the bulk but was transformed with further additions of indium to $(11\bar{2}0)$ at the surface and a mixture of $(11\bar{2}0)$ and $(10\bar{1}0)$ in the bulk. The incorporation of indium from $In(acac)_3$ was different from that of indium from $InCl_3$ in that the growth rates of various ZnO planes were affected. The effect of $In(acac)_3$ was to reduce the grain size relative to that in undoped ZnO, pointing to the importance of chlorine in grain growth enhancement when $InCl_3$ was used. The lowest resistivity for films grown using $In(acac)_3$ was $1.3\times10^{-3}\Omega$m which was higher than that when $InCl_3$ was used, which suggests that both the In and the Cl formed shallow donors.

The growth rate was also reduced when (1) $Al(OPr^i)_3$, (2) $AlCl_3$ and (3) $Ga(acac)_3$

were used as donor precursors.

The incorporation efficiency of these dopants was below 0.5 atomic percent due to evaporation or volatility or high thermal stability. The structure of the doped ZnO films was initially improved with small additions of dopant but randomised again with high dopant levels. In only one film was the preferred orientation altered from that expected for undoped films indicating that this group of dopants do not interact with the growing film planes to any significant degree. Grain sizes were reduced on adding dopant except with $AlCl_3$ where the grain size was approximately constant. This was probably due to the opposite effect of a diffusion process involving chlorine. Film resistivities were lowered by the use of all three dopants. $Al(OPr^i)_3$ was more efficient than $AlCl_3$ over the range studied. Overall, $Ga(acac)_3$ gave the most promising results with a steeper decline in the film resistivity as the dopant concentration was increased ($\approx 10^{-2}\Omega m$). In most films the optical bandgap was unchanged and, where measured, the film transmittance was high (80% - 99%).

10.4 Summary and Suggestion for Further Work

This work has demonstrated the existence of the common features of the growth of undoped and doped ZnO by spray pyrolysis. Particularly novel are the dopant effects which are the growth rate suppression, the effect of dopant on the grain growth, and the conversion efficiency of the dopant precursor (a function of the physico-chemical properties of the precursor, its volatility, decomposition temperatures and reaction pathways and ionic radius, bond strengths, surface bonding and dopant solvation and atomic diffusion rates) into an electrically active form in the lattice. The presence of different dopants during film growth leads to different types of growth behaviour with different resultant properties of the films (i.e the chloro-dopants showed a lower degree of film growth rate suppression on average than the acetyacetonato dopants, and the rate of grain growth was larger with chloro-dopants).

In industrial - academic liaisons of this kind it is vital that an understanding of the basic processes is established while working in parallel to develop a product through

the arm of scientific research that is attractive to industry so that neither aspect is neglected. This project did yield some insight and understanding and the data to go with it. The present work has illustrated some of the uncertainties and unknowns in the growth of undoped and doped ZnO films and it is hoped that future work will be carried out in this and the following areas :

(1) The use of $Zn(acac)_2.H_2O$ in a CVD or some other semiconductor deposition system (MOMBE) for the production of zinc containing materials in the form of single crystal or highly ordered microcrystalline thin films on a small pilot scale.

(2) The use of $Zn(acac)_2.H_2O$ as a precursor in spray pyrolysis in the production of ZnO films (and the recycling of ZnO powder for use in the ceramic powder industry) in conjunction with an electrostatic control and ultrasonic rather than pneumatic or centrifugal atomisation on a small pilot scale.

(3) The search for novel aluminium or other dopants that are as efficient as indium dopants for the production of conducting transparent doped ZnO.

(4) The comparison of ITO, SnO_2, and ZnO grown using a standard deposition system on a pilot scale along with other less well known transparent conducting oxides.

(5) The search for new precursors, native and dopant, designed for the production of chemically pure, highly oriented ZnO microcrystalline films in order to replace established precursors that are involatile and thermally stable and which do not lend themselves to low temperature growth of thin films.

Appendix 1
Summary of the Materials Grown in Thin Film Form by Spray Pyrolysis

Film material	Precursor	Solvent	Growth temperature/(°C)	Reference
Pd	palladium acetylacetonate	butanol	300 - 350	(1,2)
Ru	ruthenium acetylacetonate	butanol	380 - 400	(1,2)
Pt	platinum acetylacetonate	butanol	340 - 380	(1,2)
VC	vanadium dichloride		1000	(3)
SnO_2	tin tetrachloride	water-hydrochl-oric acid		(4)
SnO_2	tin tetrachloride	water hydrochl-oric acid	500	(5)
SnO_2	tin tetrabromide	water hydrobro-mic acid		(3)
SnO_2	ammonium hexa-chlorostannate	water		(6)

Film material	Precursor	Solvent	Growth temperature/(°C)	Reference
SnO_2	tin diacetate-dichloride	ethyl-acetate		(6)
SnO_2	tin dichloride	ethanol		(7)
SnO_2	tin tetrachloride	alcohol		
SnO_2:Sb	(a) tin tetrachloride (b) antimony trichloride	ethanol-water	380	(8)
SnO_2	(a) tin tetrachloride	alcohol	220 - 520	(9)
SnO_2:Sb	(a) tin dichloride (b) tin tetrachloride (c) antimony trichloride	alcohol	340 - 450	(10)
SnO_2:Sb	(a) tin tetrachloride (b) antimony trichloride	butyl acetate	300 - 540	(11)

Film material	Precursor	Solvent	Growth temperature/(°C)	Reference
SnO_2	tin dibutyl diacetate	butanol	400 - 600	(12)
SnO_2:F	(a) tin tetrachloride (b) ammonium fluoride	alcohol	400 - 450	(13)
SnO_2:F	(a) tin tetrachloride (b) ammonium fluoride	ethanol-water	380	(8)
SnO_2:F	(a) tin tetrachloride (b) ammonium fluoride	water alcohol	300 - 600	(14)
SnO_2:F	(a) tin tetrachloride (b) ammonium fluoride	ethanol-water	400	(15)
SnO_2	tin dichloride	alcohol	450	(16)
In_2O_3	indium trichloride	alcohol -water	500	(17)
In_2O_3	indium trichloride	butyl acetate/ butanol		(17)

Film material	Precursor	Solvent	Growth temperature/(°C)	Reference
In_2O_3	indium acetylacetonate	acetyl-acetone	480	(1)
In_2O_3	indium trichloride	ethanol-water methanol-water		(18)
ITO	(a) indium trichloride (b) tin tetrachloride	butyl acetate	300 - 450	(11)
ITO	(a) indium trichloride (b) tin tetrachloride	butyl-acetate	500	(19)
ITO	(a) indium trichloride (b) tin tetrachloride	hydrochl-oric acid + water		(20)
ITO	(a) indium trichloride (b) tin tetrachloride	ethanol-water-hydrochl-oric acid	450 - 510	

Film material	Precursor	Solvent	Growth temperature/(°C)	Reference
ITO	(a) indium trichloride (b) tin chloride	butyl acetate	580	(21)
ZnO	zinc acetate	water	500	(22)
ZnO	zinc chloride	water	360 - 460	(23)
ZnO	zinc nitrate	water	380 - 480	(24)
ZnO	zinc acetate	water	360 - 460	(25,26,27)
ZnO:In	zinc acetate (+indium trichloride)	water	250 - 500	-
ZnO:In	zinc chloride (+ indium trichloride)	water/ ethanol	375 - 525	(28)
ZnO:Al	zinc chloride (+ aluminium trichloride)	water/ ethanol	375 - 525	(28)
ZnO:Al	zinc acetate (+ aluminium trichloride)	water/ propanol	300 - 500	(29)
PbO	lead dichloride	water	-	(7)

Film material	Precursor	Solvent	Growth temperature/(°C)	Reference
B_2O_3	boron trichloride	water		(7)
Al_2O_3	aluminium trichloride			(7)
CdO	cadmium dichloride		500	(7)
Cr_2O_3	chromium acetylacetonate	butanol	520 - 560	(1.2)
Fe_2O_3	iron acetylacetonate	butanol	400 - 550	(1.2)
V_2O_3	vanadium acetylacetonate	butanol	450 - 510	(1.2)
VO_2	vanadium acetylacetonate	butanol	360	(1.2)
Al_2O_3	aluminium acetylacetonate	butanol	480	(1.2)
Al_2O_3	alumunium isopropoxide	butanol	420 - 650	(1.2)
Y_2O_3	yttrium acetylacetonate	butanol	300 - 360	(1.2)

Film material	Precursor	Solvent	Growth temperature /°C)	Reference
Ti_2O_3	butyl orthotitanate	butanol acetyla-cetonate	400	(1,2)
ZrO_2	butyl orthozirconate	butanol	450	(1,2)
Cu_2S	(a) copper acetate (b) thiourea	water		(31)
CdS	(a) cadmium dichloride (b) thiourea		300 - 510	(32)
CdS	(a) cadmium dichloride (b) ammonium thiocyanate (c) urea			(33)
CdS	(a) cadmium dichloride (b) cadmium acetate (c) thiourea		380	(34)
CdS	(a) cadmium dichloride (b) thiourea		450	(35)

Film material	Precursor	Solvent	Growth temperature/(°C)	Reference
CdS	(a) cadmium dichloride (b) thiourea		340	(36)
CdS	(a) cadmium dichloride (b) thiourea		440	(36)
CdS	(a) cadmium dichloride (b) thiourea		230 - 400	(37)
CdS	(a) cadmium dichloride (b) N,N Dimethyl thiourea (c) thiourea		300 - 500	(14)
CdS:Cu	(a) cadmium dichloride (b) thiourea		320 - 380	(38)
CdS:Al/Cu	(a) cadmium dichloride (b) thiourea		250	(39)
CdS:In	(a) cadmium dichloride (b) thiourea		320	(40)

Film material	Precursor	Solvent	Growth temperature/(°C)	Reference
ZnS/ZnSe	(a) zinc acetate (b) zinc chloride (c) thiourea (d) N,N dimethyl selenourea		450	(41)
CdSe	(a) cadmium dichloride (b) N,N dimethyl selenourea			(42)
CdSe	(a) cadmium dichloride (b) ammonium selenate (c) N,N dimethyl selenourea		250 - 280	(33)
CdSe	(a) cadmium dichloride (b) N,N dimethyl selenourea		235	(43)
CdSe	(a) cadmium dichloride (b) selenourea			(14)

Film material	Precursor	Solvent	Growth temperature/(°C)	Reference
CdTe	(a) cadmium dichloride (b) ammonium tellurocyanate			(33)
PbS	(a) lead acetate (b) lead dichloride (c) lead nitrate (d) thiourea		100 - 400	(44)
$CuInS_2$	(a) copper (I) chloride (b) N,N dimethyl thiourea (c) indium trichloride		350	(45)
$CuInS_2$	(a) copper (I) chloride (b) N,N dimethyl thiourea (c) indium trichloride		180 - 350	(46)
$CuInS_2$	(a) copper (II) acetate (b) thiourea (c) indium trichloride		200 - 500	(47,48)

Film material	Precursor	Solvent	Growth temperature/(°C)	Reference
$CuInS_2$	(a) copper (I) chloride (b) thiourea (c) indium trichloride		300	(47,48)
$CuInSe_2$	(a) copper (I) chloride (b) N,N, dimethyl selenourea (c) indium trichloride		200 - 600	(45)
$CuInSe_2$	(a) copper (I) chloride (b) N,N dimethyl selenourea (c) indium trichloride		175 - 275	(49)
$CuInSe_2$	(a) copper (I) chloride (b) N,N dimethyl selenourea (c) indium trichloride		260	(50,51)

Film material	Precursor	Solvent	Growth temperature/(°C)	Reference
$CuGaS_2$	(a) copper (I), (II) chlorides (b) gallium trichloride (c) N,N dimethyl thiourea			(52)
$CuGaSe_2$	(a) copper (I), (II) chlorides (b) N,N dimethyl selenourea			(53,54)
$CuIn(S_{1-x}Se_x)_2$	(a) copper (I) chloride (b) indium trichloride (c) N,N dimethyl thiourea (d) N,N dimethyl selenourea	water	280	(55)
$CuIn(S_{1-x}Se_x)_2$	(a) copper (I) chloride (b) indium trichloride (c) N,N dimethyl thiourea (d) N,N dimethyl selenourea	water	330	(56)

Film material	Precursor	Solvent	Growth temperature/(°C)	Reference
CdS_x-Se_{1-x}	(a) cadmium dichloride (b) thiourea (c) N,N dimethyl		450	(57)
CdS_x-Se_{1-x}	(a) cadmium dichloride (b) N,N dimethyl thiourea (c) N,N dimethyl selenourea			(14)
Cd_{1-x}-Zn_xS	(a) cadmium dichloride (b) zinc dichloride		400	(57)
Cd_{1-x}-Zn_xS	(a) cadmium dichloride (b) zinc nitrate (c) thiourea		250 - 400	(58)
Cd_{1-x}-Zn_xS	(a) cadmium dichloride (b) zinc dichloride (c) thiourea		300 - 500	(59)

Film material	Precursor	Solvent	Growth temperature/(°C)	Reference
Cd_{1-x}-Zn_xS	(a) cadmium dichloride (b) zinc dichloride (c) thiourea		400	(60)
Cd_{1-x}-Zn_xS:In	(a) cadmium dichloride (b) zinc dichloride (c) thiourea		350	(61)
Bi_2Cd-S_4	(a) bismuth nitrate (b) cadmium dichloride		250 - 300	(62)
$CdSnO_3$ Cd_2-SnO_4	(a) cadmium dichloride (b) tin tetrachloride			(63)
YBa_2-Cu_3-O_{7-x}	(a) yttrium nitrate (b) barium nitrate (c) copper nitrate	water, water-glycerol	300	(64)

Appendix 1 References

(1) Viguie J.C., Spitz J., *J. Electrochem. Soc., 122* , 585, (1975).

(2) Blandenet G., Court M. and Legarde Y., *Thin Solid Films, 77*, 91, (1981).

(3) Chopra K.L., Kainthla R.C., Pandya D.K. and Thakoor A.P., *Physics of Thin Films, 12*, 167, (1982).

(4) Kim H., Laitinen H.A., *J. Ceram. Soc., 58(1-2)*, 23, (1975).

(5) Manifacier J.C., *Thin Sol. Films, 90*, 297, (1982).

(6) Pink H., Treitinger L., *J. Jpn Appl. Phys..19(3)*, 513, (1980).

(7) Semenov V.N., Barenkov Y.E., Anakhun V.Z., Averbakh E.M. and Mittova I.Y., *Inorg. Mater..14(2)*, 193, (1978).

(8) Islam M.N., Hakim M.O., *J. Phys. Chem., 46(3)*, 339, (1985).

(9) Constantino C., Jousse D., *J. Appl. Phys., 54*, 431, (1983).

(10) Vincent C.A., Weston D.G., *J. Electrochem. Soc., 116*, 518 , (1972).

(11) Siefert W., *Thin Sol. Films, 120*, 267, (1984).

(12) Caillard F., Smith A. and Baumard J.F., *Thin Sol. Films, 208* ,4 ,(1992).

(13) Aboaf J.A., Marcotte V.C. and Chou N.J., *J. Electrochem. Soc. 118*, 701, (1973).

(14) Tomar M.S., Garcia F.J., *Prog. Cryst. Growth Chara., 4*, 221, (1981).

(15) Mohammed M.T., Abass A.K., *Phys. Stat. Sol.(a)*, 83, 681, (1984).

(16) Krishnakumev R., Ramakrishran K., Suryanarayana C.V., Lakshaman and A.K. and Subramaian V., *Bull. Electrochem., 1*, 185, (1985).

(17) Muranoi T., Funukoshi M., *Thin Sol. Films. 48*, 309, (1975).

(17) Groth R., *Phys. Stat. Sol.(a), 14*, 69, (1966).

(18) Pommier R., Gril C. and Marucchi J., *Thin Sol. Films, 77*, 91, (1981).

(19) Kostlin H., Lewis W. and Jost R., *Phys. Stat. Sol., 29*, 87, (1975).

(20) Manifacier J.C., Szepessy L., Bresse J.F. and Perotin M., *Mater. Res. Bull., 14*, 109, (1979).

(21) Haitjema H., Elich J.J.Ph., *Thin Sol. Films, 205*, 93, (1991).

(22) Nobbs J., Gillespie F.C., J. Phys. Chem. Solid. 31(10), 2353, (1970).

(23) Aranovich J., Ortiz A., and Bube R.H., *J. Vac. Sci. Technol.,16(4)*, 994, (1979).

(24) Bahadur L., Hamdani M., Koenig J.K. and Chartier P., *Solar Energy Mater., 14*, 107, (1986).

(25) Major S., Banerjee A. and Chopra K.L., *Thin Sol. Films, 108*, 333, (1983).

(26) Major S., Banerjee A. and Chopra K.L., *Thin Sol. Films, 143,* 19, (1986).

(27) Major S., Banerjee A. and Chopra K.L. *J. Mater. Res., 1(2),* 300, (1986).

(28) Streydio J.M., Cossment D., *J. Cryst. Growth, 72,* 57, (1985).

(29) *Thin Sol. Films, 198,* 67, (1991).

(31) Marucchi J., Perotin M., 13^th IEEE Photovoltaic Specialists Conf., Washington D.C., Piscataway. N.J., 298, (1978).

(32) Ma Y., Bube R.H., *J. Electrochem. Soc., 124,* 74, (1977).

(33) Chen S.N., McDonough, *J. Electrochem. Soc., Extended Abstract 79-2,* 1603, (1973).

(34) *Top. Appl. Phys., 31,* 224, (1979), Springer-Verlag, ed. B.O. Seraphin.

(35) Tsou C.C., Cleveland J.R.,*J. Appl. Phys., 51,* 455, (1980).

(36) Shirreffs B.F., Geib K. and Jones K.A., *J. Electrochem. Soc., 131* , (1984).

(37) Escosura H., Garcia - Camerero E., Arjona F. and Rueda R., *Sol. Cells, 11,* 211, (1984).

(38) Chamberlain R.R., Skarman J.S.,*J. Electrochem. Soc., 113,* 86, (1966).

(39) Jordan J.F.,*Proc. int. Conf. Solar Energy, CNRS, Toulouse,* 57, (1976).

(40) Krishnakumar R., Ramprakash Y., Subramanian V., Chanarasekara and Pillar A.S., *Proc. SPIE 29^th annual int. technical symposium on optical and electrooptical engineering, San Diego. California* ,569, (1985).

(41) Semenov V.N., Averbakh C.M.,*Inorg. Mater. (USSR), 14(8),* 1196, (1978).

(42) Tsuik M., Minoura H., Nakamura T. and Veno Y., *J. Appl. Electrochem., 8,* 523, (1978).

(43) Chin Hsin, Liu J., Olsen J., Saunders J.R. and Wang J.H., *J. Electrochem. Soc., 128,* 1224, (1981).

(44) Semenov V.N., Averbakh E.M. and Ugai Y.A., *Zh. Prikl. Khim., 53(1),* 39, (1980).

(45) Pamplin B., Feigelson R.S., *Thin Sol. Films, 60,* 141, (1979)

(46) Gorska M., Beaulieu R., Loferski J.J. and Rosseler B., *Sol. Energ. Mater., 1,* 313, (1979).

(47) Rajaram P., Thangaraj R., Sharma A.K. and Agnihotri O.P., *Sol. Cells, 14,* 123, (1985).

(48) Rajaram P., Thangaraj R. and Sharma A.K.,*Thin Sol. Films, 100,* (1983).

(49) Gorska M., Beaulieu R. and Loferski J.J., *Sol. Energ. Mater., 2,* 343, (1980).

(50) Gordon F., Gomer W.P. and Dekeyser W., *Photovoltaic And Photoelectrochemical Solar Energy Conversion,* 194, Plenum Press, 194, (1981).

(51) Bates C.W., Nelson K.F., Raza S.A., Mooney J.B., Recktenwald J.M., Mackintosh L. and Lamoreaux R., *Thin Sol. Films, 88,* 279, (1982).

(52) Pamplin B.R., *Prog. Cryst. Growth Chara., 1(4),* 395, (1979)

(53) Pamplin B.R., Feigelson R.S., *Mater. Res. Bull., 14(1)*, 1, (1979).

(54) Pamplin B.R., Feigelson R.S., *Thin Sol. Films, 60(2)*, 141, (1979).

(55) Subbaramaiah K., Raga Sundara V., *Thin Sol. Films, 208*, 247, (1992).

(56) Subbaramaiah K., Raga Sundara V., *Thin Sol. Films, 207*, 6, (1992).

(57) Feigelson R.S., Abdourahin, Diaz N., Shaim-Yih, and Bube R.H., *J. Appl. Phys., 48*, 3162, (1977).

(58) Banerjee A., Nath P., Venker V.D. and Chopra K.L., *Phys. Stat. Sol.(a)*, 46, 723, (1978).

(59) Uplane M.D., Pawar S.H., *Sol. Cells, 10*, 177, (1983).

(60) Uplane M.D., Pawar S.H., *Mater. Chem. Phys., 10*, 465, (1984).

(61) Pamplin B.R., Feigelson R.S., *Mater. Res. Bull., 14*, 1, (1979).

(62) Pawar S.H., Tamhankar S.P. and Lockhande C.D., *J. Electrochem. Soc., 132*, 261, (1985).

(63) Ortiz A., *J. Vac. Sci. Technol., 20(1)*, 7. (1982).

(64) Arya S.P.S., Hinterman H.E., *Thin Solid Films, 193/194*, 841, (1990).

Appendix 2

Determination of Optical Constants

This section describes the method for determining the optical constants of zinc oxide films, which in turn are used in the measurement of optical bandgap. The technique, based on the work of Swanepoel [1], relies on the envelopes of the maxima and minima of the interference fringes in the transmission spectrum of a thin film.

The transmittance T of a thin film of thickness d on a thick transparent substrate of refractive index s is a function of several variables (λ, s, n, d, α) where n and α are the refractive index and absorption coefficient of the layer. In the non-absorbing (transparent) part of the transmission spectrum where $\alpha \longrightarrow 0$ the transmittance T can be expressed as:

$$T = \frac{Ax}{B - Cxcos\phi + Dx^2} \qquad (A2.1)$$

where

$$x = exp(\alpha d) \qquad (A2.2)$$

$$A = 16n^2s \qquad (A2.3)$$

$$B = (n+1)^3(n+s^2) \qquad (A2.4)$$

$$C = 2(n^2-1)(n^2-s^2) \qquad (A2.5)$$

$$D = (n-1)^3(n-s^2) \qquad (A2.6)$$

$$\phi = 4\pi nd/\lambda \qquad (A2.7)$$

The minima (T_m) and maxima (T_M) in the transmission spectrum occur when $\cos\phi = \pm 1$ giving

$$T_M = \frac{Ax}{B - Cx + Dx^2} \qquad (A2.8)$$

$$T_m = \frac{Ax}{B + Cx + Dx^2} \qquad (A2.9)$$

Equations (A2.8) and (A2.9) effectively describe the envelope functions of the maxima and minima and may be combined to eliminate the unknown x giving a single expression for the refractive index :

$$n = [N + [N^2 - s^2]^{1/2}]^{1/2} \qquad (A2.10)$$

where

$$N = \frac{2s(T_M - T_m)}{T_M T_m} + \frac{s^2 + 1}{2} \qquad (A2.11)$$

However, T_m and T_M are strictly only defined at extrema in the transmission spectrum and thus (A2.10) may only be evaluated at these wavelengths.

Therefore measurements of T_M and T_m at each extremum may be used to calculate a value of the refractive index ($n(\lambda)$). The conditions for a maximum or minimum in the transmission spectrum are given simply by :

$$2nd = m\lambda \qquad (A2.12)$$

where m is the fringe order (integer for a maximum, half integer for a minimum). In the transmission spectrum m is unknown, but may be determined from a simple graphical procedure, as follows. If the order of a given fringe extremum is m_i, then the order of its neighbouring extrema will be $m_i \pm 1/2$, the next nearest $m_i \pm 1$ and so on. Thus selecting the longest wavelength fringe extremum in the spectrum as the starting point, (i.e m_i) equation (A2.12) may be written as :

$$2nd = (m_i - (l/2))\lambda \qquad (A2.13)$$

$$\frac{l}{2} = m_i - 2d(\frac{n}{\lambda}) \qquad (A2.14)$$

which is a straight line with slope equal to twice the layer thickness and an intercept corresponding to the fringe order of the initial fringe. A typical example of this is shown in figure A2.1. Since m_2 must be an integer or half integer the intercept may be forced to the nearest integer/half integer value and equation (A2.1) used to correct the values of n obtained from (A2.10) which will be subject to error. Importantly this procedure provides a reliable estimate for the average film thickness, d. Once n and d are known then α may be determined from [1]

$$x = exp(-\alpha d) = \frac{(n+1)^3(n+s^2)T}{16n^2s} \qquad (A2.15)$$

The extinction coefficient k is related to α by :

$$k = \frac{\alpha\lambda}{4\pi} \qquad (A2.16)$$

The above procedure provides values of n and k for the transparent region of the films spectrum only. Accurate values of α in the bandedge region cannot be obtained from transmission alone unless n is known. However extrapolated values of n in the bandedge region may be obtained by realising that the dispersion of n is well described by the Cauchy relation :

$$n = \frac{a}{\lambda^2} + b \qquad (A2.17)$$

The constants a and b may be determined from fitting equation (A2.17) to n in the transparent region. A straightline relationship is obtained by simply re-writing (A2.17) as :

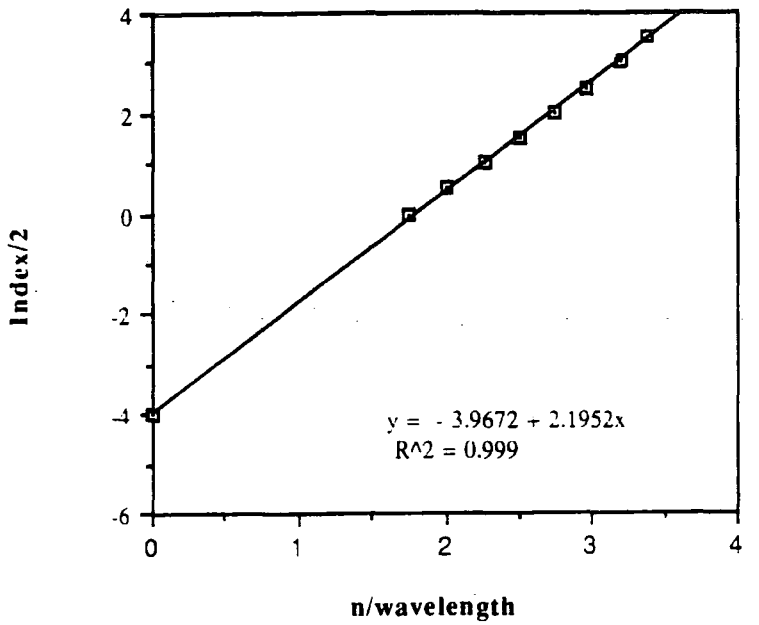

Figure A2.1 Variation of (l/2) versus (n/λ) for the determination of fringe order and film thickness.

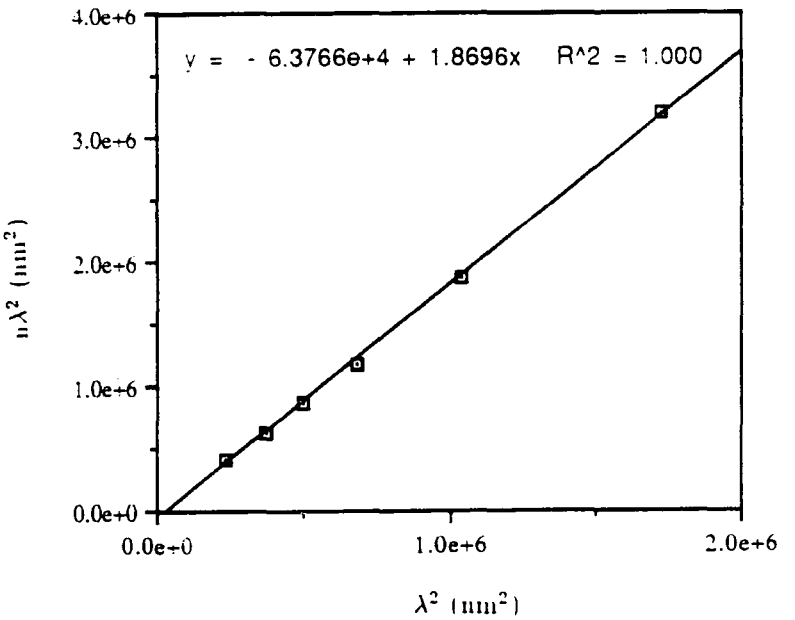

Figure A2.2 Variation of $n\lambda^2$ versus λ^2.

$$n\lambda^2 = a + b\lambda^2 \qquad (A2.18)$$

A typical example of this is given in figure A2.2. Once a and b have been determined equation (A2.17) is used to extrapolate values of n in the bandedge region. These, in turn, are used in equation (A2.15) to obtain values of α. Finally a plot of α^2 versus photon energy in the bandedge region will yield an estimate for the optical bandgap from the extrapolated intercept on the energy axis.

Appendix 2 References

(1) Swanepoel R.,*J. Phys. E.: Sci. Instrum.*, *17*, 896, (1984).

My thanks to the sponsoring organisation for financial support,

training, good food, excellent

hospitality and friendship

Sponsors : ICI Ltd (Paints and Films Groups)

Richard Marbrow

Jonathon Lloyd

Ed West

Eric Nield